

# รายงานวิจัยฉบับสมบูรณ์

## การพัฒนาวิธีการประเมินค่าความเค้นภายในไม้ ระหว่างและหลังการอบแบบใหม่ชนิดเรียลไทม์

โดย รองศาสตราจารย์ ดร.นิรันดร มาแทนและคณะ
ศูนย์วิจัยความเป็นเลิศด้านวิทยาศาสตร์และวิศวกรรมไม้
สำนักวิชาวิศวกรรมศาสตร์และทรัพยากร
มหาวิทยาลัยวลัยลักษณ์ จังหวัดนครศรีธรรมราช

เมษายน 2561





## รายงานวิจัยฉบับสมบูรณ์

## การพัฒนาวิธีการประเมินค่าความเค้นภายในไม้ ระหว่างและหลังการอบแบบใหม่ชนิดเรียลไทม์

โดย รองศาสตราจารย์ ดร.นิรันดร มาแทนและคณะ
ศูนย์วิจัยความเป็นเลิศด้านวิทยาศาสตร์และวิศวกรรมไม้
สำนักวิชาวิศวกรรมศาสตร์และทรัพยากร
มหาวิทยาลัยวลัยลักษณ์ จังหวัดนครศรีธรรมราช

เมษายน 2561

## รายงานวิจัยฉบับสมบูรณ์

## การพัฒนาวิธีการประเมินค่าความเค้นภายในไม้ ระหว่างและหลังการอบแบบใหม่ชนิดเรียลไทม์

## คณะผู้วิจัย

รองศาสตราจารย์ ดร.นิรันดร มาแทน	หัวหน้าโครงการ
ผู้ช่วยศาสตราจารย์ ดร.สถาพร จันทวี	นักวิจัย
ผู้ช่วยศาสตราจารย์ สัจจพันธ์ ลีละตานนท์	นักวิจัย
นายใจเพ็ชร โต๊ะหมาด	ผู้ช่วยวิจัย

ศูนย์วิจัยความเป็นเลิศด้านวิทยาศาสตร์และวิศวกรรมไม้ สำนักวิชาวิศวกรรมศาสตร์และทรัพยากร มหาวิทยาลัยวลัยลักษณ์ อำเภอท่าศาลา จังหวัดนครศรีธรรมราช

สนับสนุนโดยสำนักงานกองทุนสนับสนุนการวิจัย
และมหาวิทยาลัยวลัยลักษณ์
(ความเห็นในรายงานนี้เป็นของผู้วิจัย สกว. และมหาวิทยาลัยวลัยลักษณ์
ไม่จำเป็นต้องเห็นด้วยเสมอไป)

### กิตติกรรมประกาศ (Acknowledgements)

คณะผู้วิจัยใคร่ขอขอบคุณทุนพัฒนานักวิจัยเรื่องการพัฒนาวิธีการประเมินค่าความเค้นภายในไม้ ระหว่างและหลังการอบแบบใหม่ชนิดเรียลไทม์ (Grant No. RSA5880025) จากสำนักงานกองทุนสนับสนุน การวิจัย (สกว.) และมหาวิทยาลัยวลัยลักษณ์ ประจำปังบประมาณ 2558

ขอขอบคุณคณะกรรมการพิจารณาจัดสรรทุนวิจัยทุกท่านที่เล็งเห็นความสำคัญพร้อมทั้งให้โอกาส นักวิจัยได้ดำเนินการพัฒนางานอย่างต่อเนื่อง พร้อมทั้งให้คำแนะนำที่เป็นประโยชน์ต่อการพัฒนางานวิจัยนี้ เป็นอย่างมาก

ขอขอบคุณ คุณเจษฎา อังวิทยาธร กรรมการผู้จัดการบริษัทนครศรีพาราวู้ดจำกัด อำเภอเมือง จังหวัด นครศรีธรรมราช คุณสุทิน พรชัยสุรีย์ กรรมการผู้จัดการบริษัทเขามหาชัยพาราวู้ดจำกัด อำเภอเมือง จังหวัด นครศรีธรรมราช คุณชัชชม เหล่าฤทธิไกร กรรมการผู้จัดการบริษัทเอเซียแปซิฟิคพาราวู้ดจำกัด อำเภอเมือง จังหวัดตรัง และคุณศุภวิทย์ นุกิจรังสรรค์ กรรมการผู้จัดการบริษัททุ่งหลวงวู้ดอินดัสตรี้ส์ จำกัด อำเภอเวียง สระ จังหวัดสุราษฎร์ธานี สำหรับการอนุเคราะห์ไม้ยางพาราอบแห้งขนาดต่างๆที่ใช้ในงานวิจัยนี้

#### บทคัดย่อ

รหัสโครงการ: RSA5880025

**โครงการ:** การพัฒนาวิธีการประเมินค่าความเค้นภายในไม้ระหว่างและหลังการอบแบบใหม่ชนิด

เรียลไทม์

นักวิจัย: นิรันดร มาแทนและคณะ สำนักวิชาวิศวกรรมศาสตร์และทรัพยากร มหาวิทยาลัยวลัยลักษณ์

E-mail Address: mnirundo@wu.ac.th, mnirundo@yahoo.com

ระยะเวลาโครงการ: 3 ปี จาก 1 กรกฎาคม 2558 ถึง 30 มิถุนายน 2561

เนื่องจากความยุ่งยากในการวัดค่ามอดูลัสของไม้ จึงทำให้การตรวจสอบความเค้นภายในไม้แปร รูปทั้งระหว่างและหลังการอบแห้งในอุตสาหกรรมโดยทั่วไปจึงมีการรายงานเฉพาะค่าความเครียดหรือค่า การโก่งเนื่องจากการคลายตัวของความเค้นภายในชิ้นไม้ตัวอย่างที่ถูกตัดเท่านั้น เพื่อที่จะประเมินขนาด ของความเค้นภายในไม้แปรรูปโดยตรง ผู้วิจัยได้นำเสนอเทคนิคใหม่โดยได้ออกแบบและสร้างเครื่องมือ สำหรับการวัดแรงคืนตัวของชิ้นไม้ที่ถูกผ่าครึ่ง พร้อมทั้งได้หาเงื่อนไขการติดตั้งที่เหมาะสมประกอบด้วย จากการทดลองพบว่าแรงคืนตัวที่วัดได้มีค่าเปลี่ยนแปลงตามความยาวของการผ่าและขนาดของชิ้นไม้ ตัวอย่าง ผู้วิจัยประสบความสำเร็จในการพัฒนาแบบจำลองทางคณิตศาสตร์โดยอาศัยทฤษฎีคานยื่น แบบยืดหยุ่นเพื่ออธิบายพฤติกรรมของแรงคืนตัวในขอบเขตของการดัด โดยอาศัยค่าตัวแปรรูปร่างที่ คำนวณได้ ขนาดของความเค้นสูงสุดภายใน  $\sigma_{\!_{
m m}}$  ในด้านกว้างของไม้แปรรูปสามารถหาได้โดยไม่ จำเป็นต้องทราบค่ามอดูลัสของไม้ (Chapter 4, Paper I) สำหรับในไม้แปรรูปที่มีองค์ประกอบของความ เค้นภายในหลายทิศทาง แบบจำลองได้ถูกปรับปรุงเพื่อที่จะแยกผลของความเค้นในทิศอื่น ๆในรูปของ แรงคงค้าง  $P_o$  เพื่อให้สามารถประมาณค่า $\sigma_{
m m}$  ได้ดียิ่งขึ้น (Chapter 5) ผู้วิจัยได้ออกแบบแผนภาพระหว่าง แรงคืนตัวและความเค้นภายในเพื่อหาค่า $\sigma_{\scriptscriptstyle
m m}$  และ  $P_o$  โดยตรงจากค่าแรงคืนตัวที่วัดได้จากชิ้นไม้ตัวอย่าง ทั้งนี้เพื่อความสะดวกในการใช้งานในอุตสาหกรรม นอกจากนี้ผู้วิจัยได้ใช้การวิเคราะห์เชิงตัวเลข แบบจำลองไฟในต์อีลีเมนต์เพื่อคำนวณหาค่าตัวแปรรูปร่างนอกขอบเขตของการดัดสำหรับไม้แปรรูป ขนาดต่างๆ (Chapter 6) โดยพบว่าเทคนิคการวัดแรงคืนตัวที่นำเสนอนี้ให้ค่าที่สอดคล้องกับการวัดโดยใช้ เทคนิคดั้งเดิมของการผ่าและการทดสอบมาตรฐาน (Chapter 7, Paper II) สุดท้ายเทคนิคการวัดแรงคืนตัว ได้ถูกนำมาใช้ในการติดตามการเกิดความเค้นในไม้ยางพาราที่ตำแหน่งต่างๆในลำตันในระหว่างการอบ อย่างต่อเนื่อง โดยพบว่าการกลับทิศของแรงคืนตัวที่วัดได้ซึ่งประกอบด้วยจุดต่ำสุดสองจุดนั้นเกิดขึ้นช้า กว่าในส่วนของไม้อายุน้อยด้านในเมื่อเทียบกับไม้เต็มวัยที่ด้านนอก ทั้งนี้จุดต่ำสุดลำดับที่สองจะค่อย ๆ หายไปเมื่อนำไม้แปรรูปไปแช่ในน้ำก่อนทำการอบ (Chapter 8, Paper III) ในโครงการพัฒนานักวิจัยของ สกว. ในระยะ 3 ปีข้างหน้า ผู้วิจัยจะใช้เทคนิคการวัดแรงคืนตัวที่พัฒนาขึ้นนี้ศึกษากลไกทางอุณหพล ศาสตร์และจลนศาสตร์ของการเกิดความเค้นในไม้ในระหว่างการอบต่อไป

คำสำคัญ: ความเค้นภายใน, การวัดความเค้น, การอบไม้, ไม้ยางพารา

#### **Abstract**

Project Code: RSA5880025

Project Title: Development of a new method for real time assessment of internal stress in

lumber during and after kiln drying

Investigator: Nirundorn Matan, School of Engineering and Resources, Walailak University

E-mail Address: mnirundo@wu.ac.th, mnirundo@yahoo.com

**Project Period:** 3 years from 1<sup>st</sup> July 2015 to 30<sup>th</sup> June 2018

Due to difficulties in determining modulus of elasticity of wood, only strain or deflection profiles caused by relaxation of internal stress are normally evaluated for industrial kiln-dried lumber. To directly assess the level of internal stress within the lumber, a new technique of measuring the restoring force on a half-split specimen has been presented and the corresponding device has been designed and constructed (Chapter 3, Paper I). The measured restoring force varies with half-split length and specimen dimension. A mathematical model based on an elastic cantilever beam theory has been successfully developed to describe the restoring force behavior in a flexural response regime. By means of the calculated shape factor, the magnitude of the maximum linearly averaged internal stress  $\sigma_{\scriptscriptstyle m}$  in the width direction can be derived without prior knowledge of the modulus of elasticity of wood (Chapter 4, Paper I). In the specimens containing other stress components, the model has been modified to separate the effects of other stress components in term of a remnant force  $P_0$  for a better estimation of  $\sigma_{\rm m}$  (Chapter 5). For a use in the lumber industry, a restoring force-internal stress chart has been designed to deduce both  $\sigma_{\rm m}$  and  $P_{\rm 0}$  directly from the measured restoring force profile. Outside the flexural response range, a numerical analysis based on finite element model has been employed to determine the shape factor for various dimensions of lumber (Chapter 6). The proposed restoring force technique has been found to be quantitatively consistent with the conventional McMillen slice test and the standard case-hardening test (Chapter 7, Paper II). Finally the restoring force measurement has been adopted to monitor in real-time a generation of drying stress within the lumber from different rubber tree trunk locations. The detected restoring force profiles, consisting of two negative force maxima, appears to proceed slower in the inner juvenile wood than in the outer mature wood. The second negative force maximum gradually disappears upon water immersion of the specimens (Chapter 8, Paper III). The restoring force technique will be employed to investigate complex thermodynamic and kinetic mechanisms of internal stress generation within lumber during kiln drying in the next 3-year program of the TRF Research Career Development Grant.

Keywords: Internal stress, stress measurement, wood drying, rubberwood

### บทสรุปสำหรับผู้บริหาร (Executive Summary)

### 1. รายละเอียดเกี่ยวกับโครงการวิจัย / แผนงานวิจัย

#### 1.1 ชื่อเรื่อง

ชื่อโครงการ (ภาษาไทย) การพัฒนาวิธีการประเมินค่าความเค้นภายในไม้ระหว่างและหลัง การอบแบบใหม่ชนิดเรียลไทม์

(ภาษาอังกฤษ) Development of a new method for real time assessment of internal stress in lumber during and after kiln drying

### 1.2 ชื่อคณะคณะผู้วิจัย

รองศาสตราจารย์ ดร.นิรันดร มาแทน หัวหน้าโครงการ
 ผู้ช่วยศาสตราจารย์ ดร.สถาพร จันทวี นักวิจัย
 ผู้ช่วยศาสตราจารย์ สัจจพันธ์ ลีละตานนท์ นักวิจัย
 นายใจเพ็ชร โต๊ะหมาด ผู้ช่วยวิจัย

ศูนย์วิจัยความเป็นเลิศด้านวิทยาศาสตร์และวิศวกรรมไม้ มหาวิทยาลัยวลัยลักษณ์ อำเภอท่าศาลา จังหวัดนครศรีธรรมราช 80160 โทร 075-673671 โทรสาร 075-672399

1.3 งบประมาณและระยะเวลาทำวิจัย
 ได้รับทุนอุดหนุนการวิจัยประจำปี 2558 เป็นจำนวนเงิน 1,500,000 บาท
 ระยะเวลาทำการวิจัย 3 ปี ตั้งแต่ 1 กรกฎาคม 2558 ถึง 30 มิถุนายน 2561

### 2. สรุปโครงการวิจัย

#### ความสำคัญและที่มาของปัญหา

Without a proper assessment of internal stress (IS) developed within lumber during drying, up to 7% of kiln dried rubberwood lumber is normally rejected as a result of severe drying defects and distortions. Because of the interrupted and destructive nature of all available standard tests which rely primarily on measurements of strain related behavior, it is almost impossible to adapt those techniques for a real-time IS measurement. A new concept of measuring a restoring force of a "half-split" specimen has been proposed by the author. However, there is a need to design the restoring force device and to generalize the equation used to convert the measured restoring force to IS for various sizes of lumber commercially kiln dried in the industries

#### วัตถุประสงค์

The objectives of the research are to (i) design and construct the device for detecting the restoring force for practical uses in lumber industries, (ii) propose the practical equations for evaluation of internal stresses developed within different sizes of rubberwood lumber using the restoring force measured and (iii) develop the online restoring force measurement technique to study variability of internal stress within a rubber tree trunk.

#### ระเบียบวิธีวิจัย/ผลการวิจัยของโครงการ

A new force based technique for a direct assessment of internal stress within lumber has been presented and the corresponding device has been designed and constructed (Chapter 3, Paper I). Optimal set up of the apparatus was also demonstrated. The measured restoring force appears to vary with half-split length and specimen thickness. A mathematical model based on an elastic cantilever beam theory has been successfully developed to describe the restoring force behavior in a flexural response regime. By means of the calculated geometrical shape factor, the magnitude of the maximum linearly averaged internal stress  $\sigma_{_{\mathrm{m}}}$  in the width direction can be derived without prior knowledge of the modulus of elasticity of wood (Chapter 4, Paper I). In the specimens containing other internal stress components, the model has been modified to successfully separate the effects of other stress components in term of remnant force  $P_0$  for a better estimation of the main internal stress  $\sigma_{\rm m}$  (Chapter 5). In addition, the restoring forceinternal stress chart has been improved to be more universal for investigating the internal drying stress. No matter whether the other stress components exist or not, the chart is able to determine the stress in any pieces of kiln-dried lumber. For a practical use in the lumber industry, a restoring force-internal stress chart has also been proposed to deduce both  $\sigma_{\rm m}$  and  $P_{\rm 0}$  directly from the restoring force profile. Outside the flexural response range, a numerical analysis based on finite element model has been successfully employed to determine the geometrical shape factor for various dimensions of lumber (Chapter 6). A comparison of the restoring force technique has been made against the conventional McMillen slice test and the standard case-hardening test. The measured restoring forces for each lumber's size are quantitatively consistent with the released strain data measured by the McMillan slice test and the casehardening test values (Chapter 7, Paper II). Finally the restoring force measurement has been adopted to monitor in real-time a generation of drying stress within the lumber from different rubber tree trunk locations. The restoring force profiles, consists of two negative force maxima, appears to proceed slower in the inner juvenile wood than in the outer mature wood. The second negative force maximum gradually disappears upon water immersion of the specimens. It is proposed that variability of the internal stress within the trunk of a rubber tree originates from the role of cell wall amorphous constituents and cell wall extractives on creep property and the movement of bound water within the wood cell wall during drying (Chapter 8, Paper III). The proposed restoring force technique has potential to be an alternative method to the existing techniques for a reliable and meaningful assessment of drying stress within industrial kiln-dried lumber both during and after kiln-drying.

#### ข้อเสนอแนะจากการวิจัย

The proposed restoring force technique will be employed to investigate complex thermodynamic and kinetic mechanisms of internal stress generation within lumber during kiln drying in the next 3-year program of the TRF Research Career Development Grant.

#### การนำไปใช้ประโยชน์

A new force based technique for a reliable assessment of internal stress within lumber, which has overcome many difficulties of the conventional methods especially in determining modulus of elasticity of wood, has been published in prestigious journal in a field of wood science and technology (Wood Science and Technology Journal). The author convinces that this technique will be accepted by the international community of wood science and technology as an alternative standard method for an assessment of internal stress within lumber to be used worldwide.

## <u>สารบัญ</u>

	หน้า
กิตติกรรมประกาศ	iii
บทคัดย่อ	iv
Abstract	V
บทสรุปสำหรับผู้บริหาร	vi
สารบัญ	∨iii
Chapter 1 Introduction	1 (3)
1.1 Research problem and its significance	1-1
1.2 Objectives	1-2
1.3 Scope of research	1-2
References	1-3
Chapter 2 Literature review	2 (12)
2.1 Generation of internal stress within lumber during drying	2-1
2.2 The existing internal stress measurement techniques	2-2
References	2-11
Chapter 3 Design and construction of the restoring force apparatus	3 (18)
3.1 Introduction	3-1
3.2 Materials and methods	3-1
3.3 Results and discussions	3-8
3.4 Conclusions	3-17
References	3-18
Chapter 4 Quantification of internal stress within lumber using a beam theory	4 (16)
4.1 Introduction	4-1
4.2 Materials and methods	4-1
4.3 Results and discussions	4-3
4.4 Conclusions	4-15
References	4-16
Chapter 5 Interpretation of restoring force of lumber with several stress compon	nents 5 (21)
5.1 Introduction	5-1
5.2 Materials and methods	5-2
5.3 Results and discussions	5-5
5.4 Conclusions	5-19
References	5-20
Chapter 6 Interpretation of the restoring force of lumber at various thicknesses	6 (16)
6.1 Introduction	6-1
6.2 Materials and methods	6-1
6.3 Results and discussions	6-4
6.4 Conclusions	6-15
References	6-16

Chapter 7 Comparison of the restoring force against the standard techniques	
7.1 Introduction	7-1
7.2 Background	7-2
7.3 Materials and methods	7-3
7.4 Results and discussions	7-6
7.5 Conclusions	7-17
References	7-18
Chapter 8 Within-tree variability of internal stress generated during drying of lumber	8 (19)
8.1 Introduction	8-1
8.2 Materials and methods	8-2
8.3 Results and discussions	8-5
8.4 Conclusions	8-15
References	8-16
Chapter 9 Outputs from this project	9 (2)
Appendix:	A (52)
Paper I: A new assessment of internal stress within kiln-dried lumber	
using a restoring force technique on a half-split specimen	
Paper II: Comparison of techniques for quantification of internal stress	
within industrial kiln-dried timber	A2
Paper III: Within-tree variability of internal stress generated	
during drying of rubberwood lumber	A3
International conferences	A4
Article for press release	A5

### Chapter 1

#### Introduction

#### 1.1 Research problem and its significance

In industrial lumber drying, the difficulty experienced during the process is the tendency of the wood defects and distortions. Without a proper control of the drying process, up to 7% of kiln dried rubberwood lumber is normally rejected as a result of severe drying defects and distortions (Angvitayatorn 2014, Luengworaphan 2014). Defects generated during drying are mainly caused by a high perpendicular to grain internal stress (IS) developed within the lumber as a result of differential shrinkage between the surface and the core sections (Simpson 1991, Perré and Passard, 2007). This IS generated during drying is influenced by temperature, relative humidity and air flow inside the kiln (Simpson 1991, Tarvainen et al. 2006, Pang 2004). If IS is ignored, or is not properly accounted for, an attempt to reduce drying time and energy by simply accelerating the drying rate could easily result in creating various defects e.g. warps, internal splitting, surface checking and end checking. Average moisture content, traditionally utilized to progress the drying schedule to a more severe condition, is not a proper indication of the development of the internal stress and as a consequence is not appropriate for kiln schedule control (McMillen 1963, Fuller 2000).

To evaluate IS within lumber during or after kiln drying, many standard techniques such as the McMillen slice test (McMillen 1963), the prong test (Simpson 1991) and the cup test (the European Committee for Standardization 2002) are generally employed. However, because of the interrupted and destructive nature of the tests, it is almost impossible to adapt such techniques for a real-time IS measurement. In addition, all standard tests mentioned rely primarily on measurements of deformation or strain related behavior rather than direct measurements of force or stress. Modulus of elasticity, depending on several factors such as moisture content, density and orientation of wood (Matan and Kyokong 2003), can complicate the interpretation of the IS levels from the magnitude of the strain values obtained. As a result, the prong test, widely used to quantify the amount of residual IS left within lumber after drying, was reported to potentially provide an ambiguous reading on the level of the IS (Fuller and Hart 1994).

A research team at the Center of Excellence in Wood Science and Engineering, Walailak University originally invented a new technique which was able to detect the IS behavior by monitoring the restoring force of a so called "half-sawn" specimen which can be measured during drying in a real time mode (Diawanich et al. 2010, Tomad et al., 2012) or after drying in an interrupted mode (Diawanich et al. 2012). In addition, the resultant force obtained has been verified with differential released strains obtained from the interrupted McMillen's slice test. An equation has also been proposed to interpret the restoring force in terms of ISs. However, the device built and the calculation of IS have been restricted to the 30mm thick and 80mm wide rubberwood lumber.

There is a need to redesign the restoring force device and to generalize the equation used to convert the measured restoring force to IS for various sizes of lumber commercially kiln dried in the industries worldwide. The finite element (FE) method has been employed in this research as a tool to generate numerical models with necessary parameters and to predict the ISs in rubberwood lumber. An attempt has been also be made to find a closed-form expression for the shape factor used to derive IS from the measured restoring force for various sizes of lumber.

#### 1.2 Objectives

The objectives of the research are to

- 1. Design and construct the device for detecting the restoring force for practical uses in lumber industries.
- 2. Propose the practical equations for evaluation of internal stresses developed within different sizes of rubberwood lumber using the restoring force measured.
- 3. Develop a physically based model for describing the restoring force in a real-time mode.

#### 1.3 Scope of research

Various sizes of rubberwood lumber available in the industries have been used throughout this research. Finite element analysis has been performed to simulate the restoring force measured. Once the model has been validated, the correction factor which is dependent on size of the lumber has been deduced for the calculation of the internal stress.

#### References

- 1. Angvitayatorn, J. (2014). Nakornsri Parawood Co., Ltd., Private Communication.
- 2. Diawanich, P., Matan, N. and Kyokong, B. (2010). Evolution of internal stress during drying, cooling and conditioning of rubberwood lumber. European Journal of Wood and Wood Products 68: 1-12.
- 3. Diawanich, P., Tomad, S., Matan, N. and Kyokong, B. (2012). Novel assessment of casehardening in kiln-dried lumber. Wood Science and Technology 46: 101-114.
- 4. European Committee for Standardization (2002) Sawn timber Method for assessment of case-hardening. CEN standard ENV 14464.
- 5. Fuller, J. (2000). Determining the source of changing shrinkage during kiln drying. Drying Technology 18(1&2): 261–278.
- 6. Fuller, J., Hart C.A. (1994). Factors that influence the prong test. In Proceedings of the 4th IUFRO International Wood Drying Conference, Rotorua, New Zealand, pp 313-320.
- 7. Luengworaphan, M. (2014). Thainakorn Parawood Co., Ltd., Private Communication.
- 8. Matan N., Kyokong, B. (2003). Effect of moisture content on some physical and mechanical properties of juvenile rubberwood. Songklanakarin Journal of Science and Technology 25(3): 327-340.
- 9. McMillen, J. (1963). Stresses in wood during drying. Report 1651, US Department of Agriculture, Wisconsin, USA.
- 10. Pang, S. (2004). Airflow reversals for kiln drying of softwood lumber: application of a kiln-wide drying model and a stress model. Proc 14<sup>th</sup> International Drying Symposium, Sao Paulo, Brazil, B: 1369-1376.
- 11. Perré, P., Passard, J. (2007). Stress development. In: Fundamentals of wood drying. Ed. Perré, P. European COST A.R.BO.LOR., Nancy, France, pp 243-271.
- 12. Simpson, W.T. (1991). Dry kiln operator's manual. Agric.Handbook AH-188. US Department of Agriculture, Wisconsin, USA.
- 13. Tarvainen, V., Ranta-Maunus, A., Hanhijarvi, A. (2006). The effect of drying and storage conditions on case hardening of Scots pine and Norway spruce timber. Maderas Cienc. Tecnol. 8(1):3-14.
- 14. Tomad, S., Matan, N., Diwanich, P. and Kyokong, B. (2013). Internal stress measurement during drying of rubberwood lumber: effects of wet-bulb temperature in various drying strategies. Holzforschung 66: 645-654.

## Chapter 2

#### Literature review

#### 2.1 Generation of internal stress within lumber during drying

At the beginning of the drying period, moisture content of a whole piece of lumber is still above the fiber saturation point at which cell walls are completely saturated by water and no free water in cell cavities. Changes of lumber dimensions are vanished and internal stresses do not exist at this phase. Whenever the moisture content at the outer layer is below the fiber saturation point while the inner one is still saturated, the differential shrinkage is turned out as a result of the restraint between the dry exterior and the wet interior. At this point, the incompatible deformation induces a tensile stress in the exterior of a lumber in which counterbalances a compressive stress in the interior layer (Figure 2.1a). Undesired surface and end checking of a lumber may come up if the tensile stress perpendicular to the grain exceeds its strength during the early period. As the drying process carries on, the surface and the core are dried under tensile stress the compressive stress, respectively, as a result of time dependent behavior, i.e. viscoelastic and machano-sorptive creep. The internal stress at the surface layer then reverse from tensile to compressive stress, and compressive stress in the core layers also inverts to tensile stress in the meanwhile (Figure 2.1b). Then, unwanted core splitting may show up at the end of the drying process. This mechanical response is also known as casehardening (Perré and Passard 2007, Moutee et al. 2007).

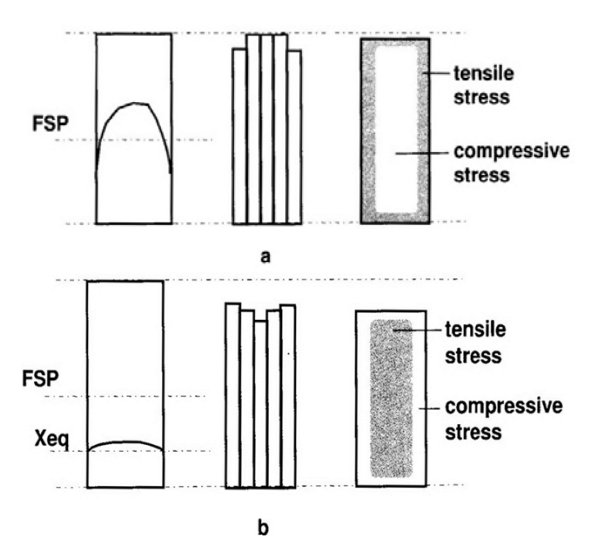


**Figure 2.1** Internal stress generation within lumber during (a) the first and (b) second stages of drying (Perré and Passard, 2007).

#### 2.2 Internal stress measurement techniques

#### 2.2.1 The McMillen slicing technique

According to the McMillen slicing technique (McMillen, 1963), the lumber is first cut to the specimen with a 30mm section along the grain. While still in the complete section, the specimen is pre-marked across the thickness in to many equaled slices. The width of each slice is measured. As each slice is cut free, it contracts or elongates depending on whether the wood of the slice was under tension or compression. After cutting into many equaled slices, width of each slide was immediately measured (Figure 2.2). Elastic strain of each slice is then calculated using the width measured before and after slicing.

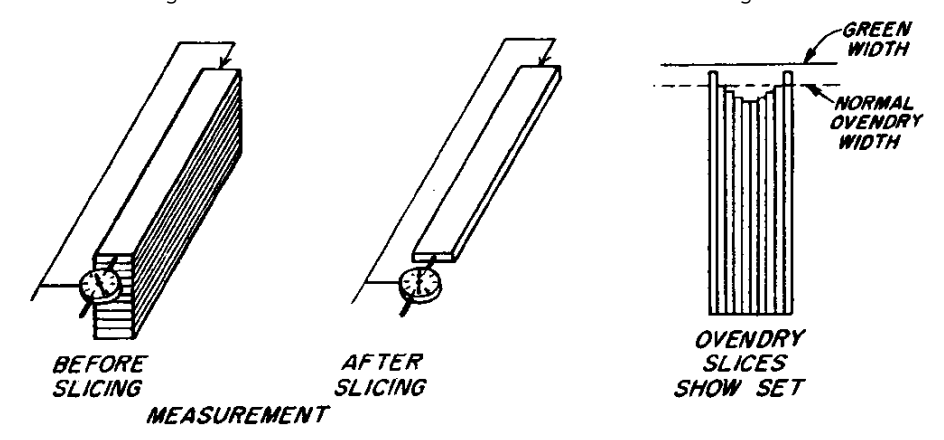
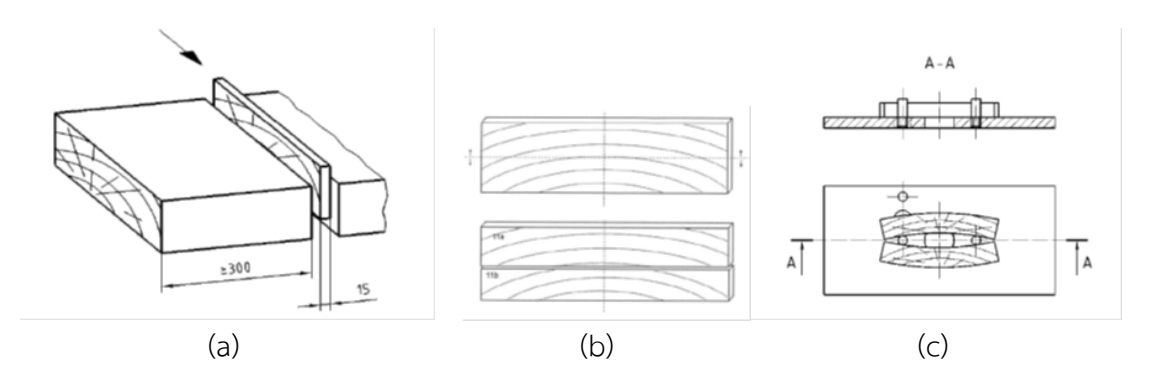


Figure 2.2 The McMillen slicing technique (McMillen, 1963).

#### 2.2.2 The cup test

Assessment of IS according to the cup test (European Committee for Standardization, 2010) is shown in Figure 2.3. The specimen, full cross section with 15 mm long, is cut into two half of equal thickness. The distance between the two test pieces at mid-point is recorded on the test jig. That distance is then subtracted with diameter of test jig pins to obtain the actual distance between two pieces of specimens and multiplied by a factor of 1.78 to obtain the CEN value (European Committee for Standardization, 2010).



**Figure 2.3** Method for assessment of the cup test (a) preparation of the test slice from lumber, (b) marking and cutting of the test slice and (c) evaluation of IS with the test jig (European Committee for Standardization, 2010).

#### 2.2.3 The prong test

The prong test (Figure 2.4) is commonly used by industry as part of quality control program to assess the stress state in lumber (Simpson, 1991). Lumber is usually cut into three prongs, and the middle prong is removed. To indicate stress level, Fuller (1995) proposed the prong response, PR = (W-W')/2 where W is the precut prong tip distance, W' is the release prong tip distance, and L is the prong length.

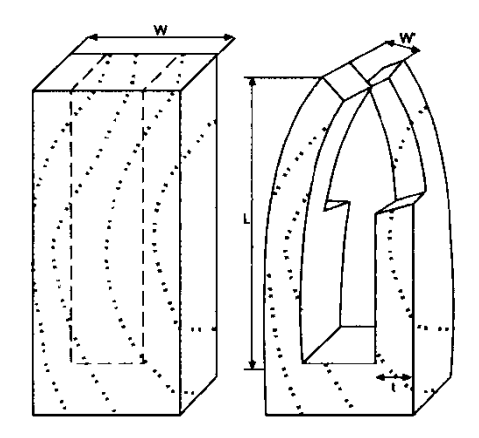


Figure 2.4 Prong test geometry and recorded measurements (Fuller, 1995).

#### 2.2.4 The Flying-wood test

The Flying-wood test was proposed to monitor the development of IS in real time during drying (Figure 2.5). A specimen with five insulated faces is dried so that the moisture can migrate only through the free face. The irregular moisture profiles produce a stress field whose torque is not balanced. This stress field bends the sample section. Such deformation reflects the IS within wood (Allegretti and Perre, 2000).

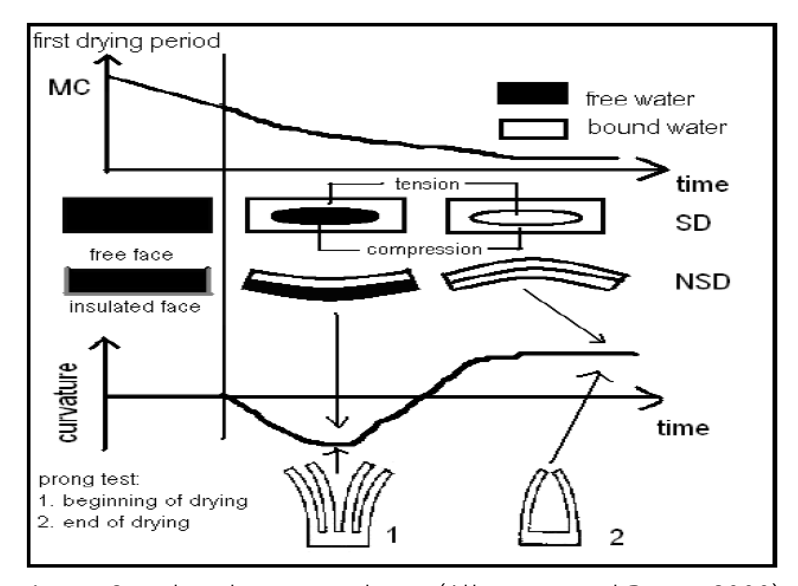
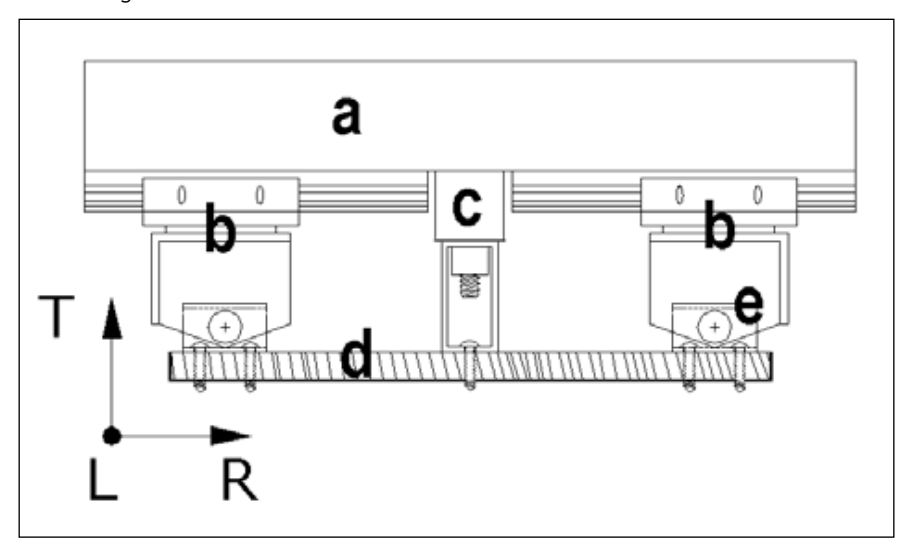


Figure 2.5 The Flying-wood test (Allegretti and Perre, 2000).

#### 2.2.5 The Flying-wood test with fixed displacement

The Flying-wood test was further developed by Allegretti (2004) to investigate force required to keep the board flat during drying using the three dot-shaped devices (Figure 2.6). The bending curvature is constrained by the load cell which can measure the correspondent tensile or compressive force according to the potential cupping direction. Evolution of the measured forces during drying of beech wood at 5, 10 and 15 mm thick at 45°C, 65°C and 85°C are shown in Figure 2.7.



**Figure 2.6** The device for measuring forces required to keep the flying-wood specimen flat during drying: a) stiff bar, b) lateral supports screwed to the board, c) load cell measuring forces in T direction, d) wooden board with five insulated faces and e) sliding blocks and hinges that can move in R direction and rotate around the L axis (Allegretti, 2004).

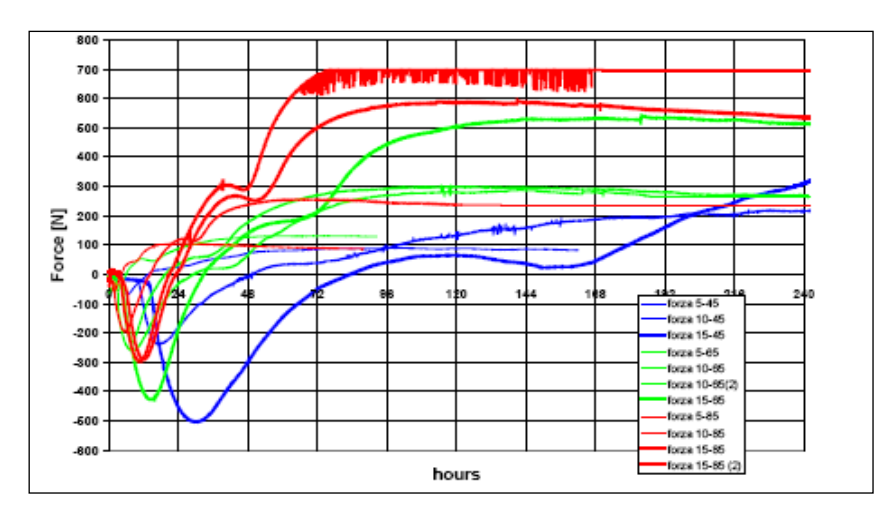


**Figure 2.7** Forces required to keep the flying-wood specimen flat during drying of beech wood at 5, 10 and 15 mm thick at 45°C, 65°C and 85°C (Allegretti, 2004).

#### 2.2.6 A sensor to measure wood stress during drying process

Allegretti and Ferrari (2008) developed a force sensor to measure the magnitude of IS at specific location in lumber during drying. The sensor has been designed using a silicon micromachined pressure gage insert in a Teflon shell. Teflon works as a medium between the gauge and wood (Figure 2.8). The force sensor is inserted in the hole of the board in the longitudinal direction. From the measurement signals shown in Figure 2.9, compressive force was applied at (A) to keep the sensor contact with the wood.

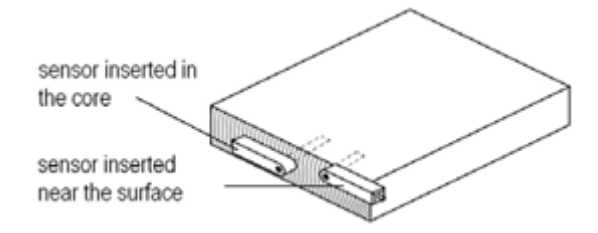


**Figure 2.8** A force sensor used to measure IS at specific location in wood during drying (Allegretti and Ferrari, 2008).

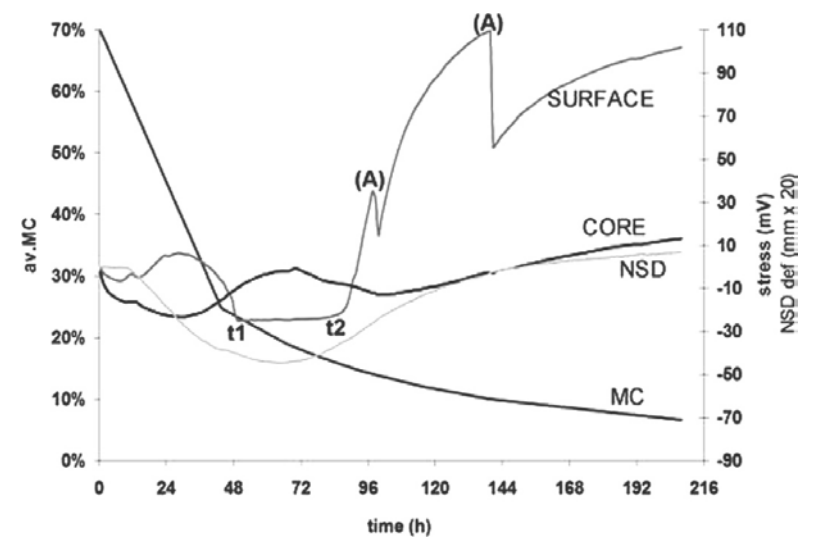
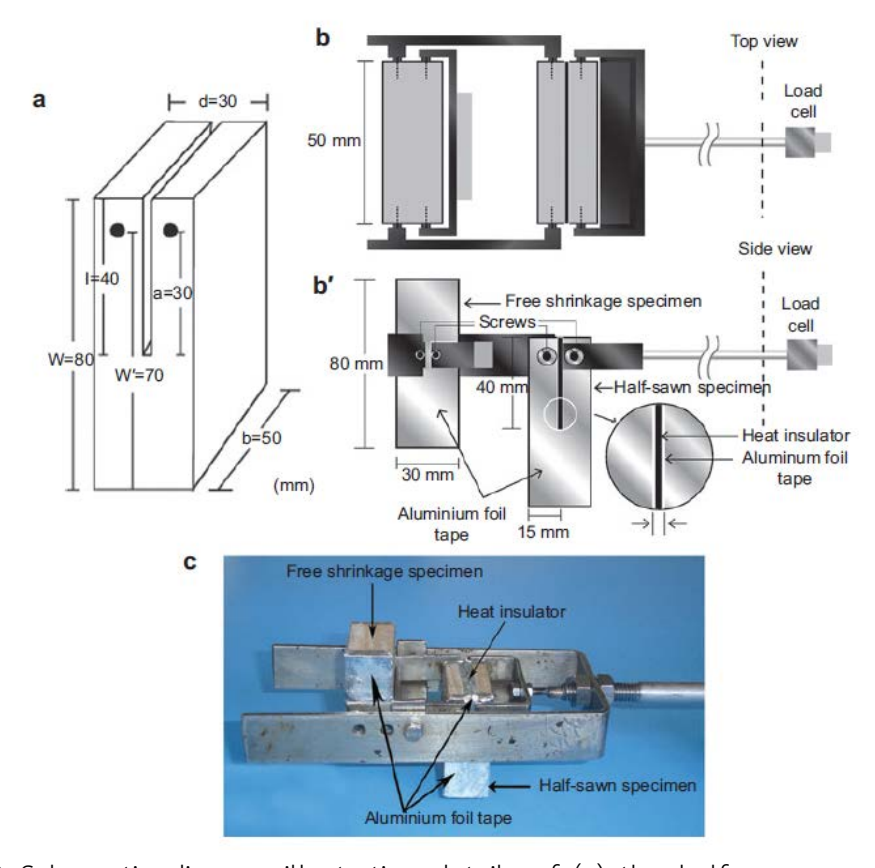


Figure 2.9 Measurement signals obtained from the force sensor (Allegretti and Ferrari, 2008).

#### 2.2.7 The restoring force measurement technique

The restoring force required to restrain a so-called "half-sawn" specimen (Figure 2.10a) straight during drying is measured via a load cell (Diawanich et al. 2010). The halfsawn specimen is prepared from fresh lumber of dimensions 30mm (thickness in radial direction)×80mm(width in tangential direction)×50mm (length in longitudinal direction) sawn in the tangential direction by a half width (40mm) in order to divide the thickness into half (15mm). The saw line is 2mm wide. Longitudinal surfaces and the half-sawn faces are then sealed with thin aluminium tape to prevent moisture loss, before inserting a thin piece of heat insulation into the saw line to prevent direct heat transfer into the core of the specimen. Force generated as a result of the half-sawn specimen's shrinkage has to be compensated for by adding a "free shrinkage" specimen of the same dimensions (Diawanich et al. 2010, Tomad, et al. 2012). The restoring force measuring device equipped on both the half-sawn and the free shrinkage specimens is shown in Figures 2.10b and 2.10c.



**Figure 2.10** Schematic diagram illustrating details of (a) the half-sawn specimen, (b) the restoring force measuring device equipped with the half-sawn and the free shrinkage specimens and (c) photograph of the device with an inset showing installation of the device inside the lumber stack in the drying kiln (Tomad, et al. 2012).

Diawanich et al. 2010 demonstrated that the technique could be used to monitor the evolution of internal stress from the beginning until after the end of drying (Figure 2.11). The measured restoring force remains at zero at the beginning of drying before taking a negative value, corresponding to a net tensile force in the half-sawn specimen. After attaining a maximum value, the amount of tensile force swiftly decreases and changes its sign to a positive one, corresponding to a net compressive force on the half-sawn specimen. The compressive force is continuously increasing and reaches a maximum before slightly declining up until the end of the drying process. Apart from being able to detect the internal stress evolution during drying, cooling and conditioning, the device was also able to detect internal stress changes after conditioning when the kiln door was opened and the lumber was exposed to the ambient atmosphere outside the kiln. A sharp drop of force after conditioning period was expected to cause by temperature difference between the surface

and the core layers. This sharp drop in force was only temporary, after the whole specimen was cooled down, the force raised back close to the original value after conditioning. After drying and conditioning, the internal stress within the kiln dried lumber still evolved in the ambient atmosphere outside the kiln. Compressive force detected increase during the night due to moisture absorption of the specimen surface layer caused by relatively high humidity. This force decreased during the day as a result of moisture desorption caused by relatively low humidity of surrounding air. The compressive force amplitude on the second day was lower than that of the first day and continued to decrease for the following days.

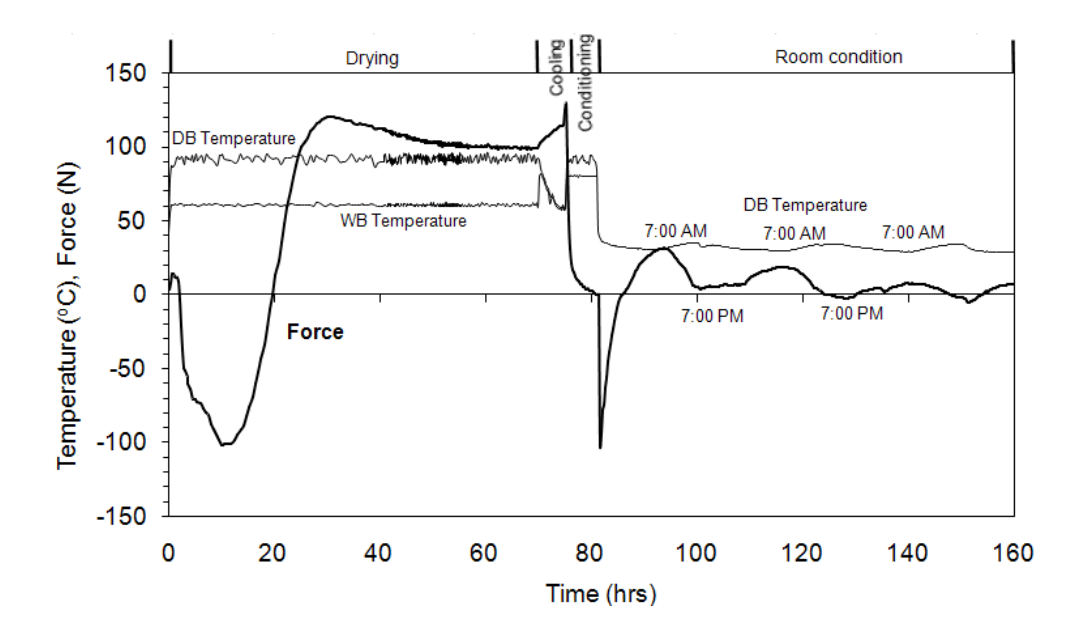


**Figure 2.11** Evolution of the restoring force during drying, conditioning and after exposing to room condition of rubberwood (Diawanich et al. 2010).

Tomad et al. (2012) used the restoring force measuring device to improve a twostep drying schedule of rubberwood lumber. The results obtained are shown in Figure 2.12. Two extreme single-step drying conditions designated as "severe" and "conservative" at wetbulb temperatures of 40 °C and 80 °C, respectively, were applied as control drying. According to the two-step drying strategy, when the time of abrupt wet-bulb temperature change from conservative to severe drying conditions is extended up to the time of stress reversal, the force detected after stress reversal decreases from the level of severe drying to that of conservative drying. Once the time of stress reversal is exceeded, the force profile is largely unaffected by the parameters of the severe drying condition. Gradual reduction in

wet-bulb temperature beyond the time of peak stress also reduces the force detected later after stress reversal under severe drying conditions.

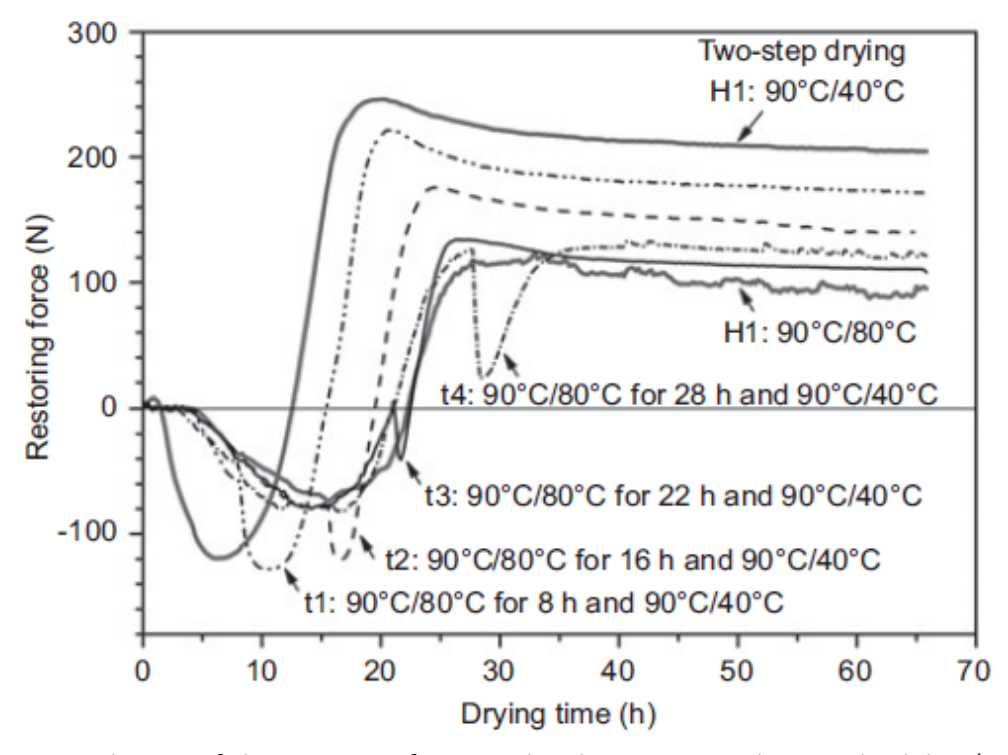


**Figure 2.12** Evolution of the restoring force under the two-step drying schedules (Tomad et al. 2012).

Diawanich et al. 2012 and Tomad et al. 2012 also calculated the magnitude of IS using the restoring force data obtained. The amount of stress generated within the specimen can be estimated from the restoring force, P, required to pull the half-sawn specimen, having change in mouth opening  $\Delta\delta$  after sawing, back to its original thickness, d, via an equation (Lados and Apelian 2006):

$$P = \frac{E.\Delta \delta.b}{m\left(\frac{a}{W'}\right)} \tag{2.1}$$

where 
$$\frac{a}{W'} = 1.0012 - 4.9165u + 23.057u^2 - 323.91u^3 + 1798.3u^4 - 3513.2u^5$$

$$u = \frac{1}{\sqrt{m\left(\frac{a}{W'}\right)} + 1}$$

E is Young's modulus, a and W' are the half-sawn length and the width of specimen measured from a point where the force was applied and b is a section length (Figure 2.9a).

To a first approximation, by assuming that the internal stress varies linearly over the half-thickness of the half-sawn specimen, an average magnitude of maximum stress at the surface and the core layers,  $\sigma_m$ , can be expressed as (Walton 2002):

$$\sigma_m = \frac{E.\Delta\delta.d}{4I^2} \tag{2.2}$$

where d and l are the thickness and the sawn length of the half-sawn specimen (Figure 2.10a). Combining the equations 2.1 and 2.2, it can be shown that

$$\sigma_m = \frac{m\left(\frac{a}{W'}\right)d}{4hl^2}P\tag{2.3}$$

According to equation 2.3, the magnitude of IS can be calculated from the restoring force P without a requirement of Young modulus of the lumber. This is a major advantage of this technique over traditional techniques which rely on measurements of deformation or strain related behavior such as the McMillen's slice test, the cup test and the prong test. However, one should expect the value of  $m \left( \frac{a}{W'} \right)$  in the equation 2.3 is dependent on specimen size. This value should be deduced for various sizes of lumber which has been performed in this project.

#### References

- 1. Allegretti, O. and Perré, P. (2000). The Flying wood test used to study the variability of drying behavior of oak. In 2<sup>nd</sup> Workshop of COST Actions E 15, "Quality Drying of Hardwood". Hungary: Sopron.
- 2. Allegretti, O. (2004). Non symmetrical tests-experimental results for free and constrained samples of Beech wood. Ex proceeding: COST E15 conference, (pp. 22-24), Greece: Athens.
- 3. Allegretti, O., Ferrari S. (2008). A sensor for direct measurement of internal stress in wood during drying: Experimental tests towards the industrial application, Drying Technology Journal 26: 1150-1154.
- 4. Angvitayatorn, J. (2014). Nakornsri Parawood Co., Ltd., Private Communication.
- 5. Diawanich, P., Matan, N. and Kyokong, B. (2010). Evolution of internal stress during drying, cooling and conditioning of rubberwood lumber. European Journal of Wood and Wood Products 68: 1-12.
- 6. Diawanich, P., Tomad, S., Matan, N. and Kyokong, B. (2012). Novel assessment of casehardening in kiln-dried lumber. Wood Science and Technology 46: 101-114.
- 7. European Committee for Standardization (2002) Sawn timber Method for assessment of case-hardening. CEN standard ENV 14464.
- 8. Fuller, J. (2000). Determining the source of changing shrinkage during kiln drying. Drying Technology 18(1&2): 261–278.
- 9. Fuller, J., Hart C.A. (1994). Factors that influence the prong test. In Proceedings of the 4th IUFRO International Wood Drying Conference, Rotorua, New Zealand, pp 313-320.
- Fuller, J. (1995). Modeling prong test response during Conditioning of red Oak lumber.
   Res. Pap. FPL-RP-537. Madison, WI: U.S. Department of Agriculture, Forest Service,
   Forest Products Laboratory.
- 11. Lados, D.A., Apelian, D. (2006). The effect of residual stress on the fatigue crack growth behavior of Al-Si-Mg cast alloys-Mechanisms and corrective mathematical models. Metallurgical and Materials Transactions A 37:133-145.
- 12. Luengworaphan, M. (2014). Thainakorn Parawood Co., Ltd., Private Communication.
- 13. Matan N., Kyokong, B. (2003). Effect of moisture content on some physical and mechanical properties of juvenile rubberwood. Songklanakarin Journal of Science and Technology 25(3):327-340.

- 14. McMillen, J. (1963). Stresses in wood during drying. Report 1651, US Department of Agriculture, Wisconsin, USA.
- 15. Moutee, M., Fortin, Y., Fafard, M. (2007). A rheological model of wood cantilever as applied to wood drying. Wood Science and Technology 41: 209-234.
- 16. Moutee, M., Fortin, Y., Laghdir, A., Fafard, M. (2010). Cantilever experimental setup forrheological parameter identification in relation to wood drying. Wood Science and Technology 44: 31-49.
- 17. Pang, S. (2004). Airflow reversals for kiln drying of softwood lumber: application of a kiln-wide drying model and a stress model. Proc 14<sup>th</sup> International Drying Symposium, Sao Paulo, Brazil, B: 1369-1376.
- 18. Perré, P., Passard, J. (2007). Stress development. In: Fundamentals of wood drying. Ed. Perré, P. European COST A.R.BO.LOR., Nancy, France, pp 243-271.
- 19. Simpson, W.T. (1991). Dry kiln operator's manual. Agric.Handbook AH-188. US Department of Agriculture, Wisconsin, USA.
- 20. Tarvainen, V., Ranta-Maunus, A., Hanhijarvi, A. (2006). The effect of drying and storage conditions on case hardening of Scots pine and Norway spruce timber. Maderas Cienc. Tecnol. 8(1):3-14.
- 21. Tomad, S., Matan, N., Diwanich, P. and Kyokong, B. (2013). Internal stress measurement during drying of rubberwood lumber: effects of wet-bulb temperature in various drying strategies. Holzforschung 66: 645-654.
- 22. Walton, H.W. (2002). Deflection methods to estimate residual stress. In Handbook of Residual Stress and Deformation of Steel; Totten, G., Howes, M., Inoue, T., Eds.; ASM International, Ohio, pp89-98.

## Chapter 3

### Design and construction of a restoring force apparatus

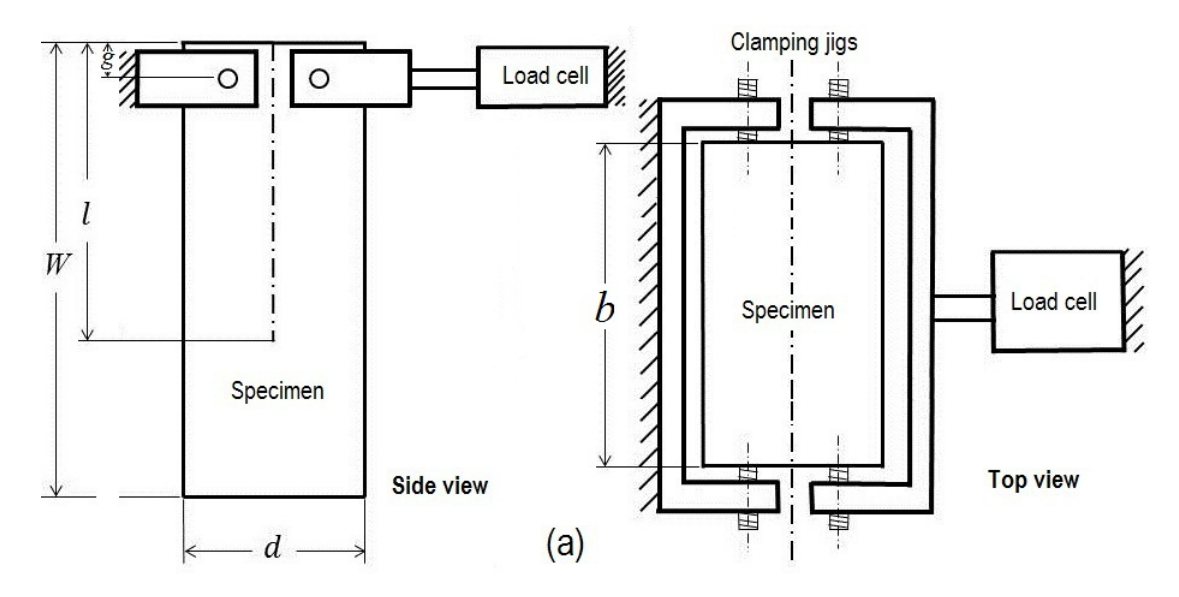
#### 3.1 Introduction

A new approach of a restoring force measurement on "half-split" specimens has been proposed by Diawanich et al. (2012). This idea has been extended to monitor in real-time the internal stress during drying, conditioning and storage of lumber (Diawanich et al. 2010 and Tomad et al. 2012). In their work, the width of lumber was sawed at half thickness by a half-length before being transferred to a device attached to the universal testing machine to measure the force required to restore the specimen back to its initial configuration. But just a small error in the thickness measurement during restraining of the half-split specimen to its original configuration could lead to a large variation in the measured force. Therefore, further improvement to this technique is required. In this chapter, a restoring force measuring apparatus suitable to be used in the lumber industry is designed and constructed. The equipment and the wood specimen are tested and optimized to obtain a repeatable and reliable measurement of the restoring force.

#### 3.2 Materials and methods

#### 3.2.1 Design of restoring force measuring apparatus

The principle of restoring force measurement on half-split specimen was based on the concept proposed by Diawanich et al. (2012). The equipment (Figure 3.1a and 3.1b) consists mainly of a relatively stiff steel frame, two 56 mm wide clamping jigs and a load cell (Cooper Instrument, USA). One jig was fixed to the steel frame and another was attached to a steel rod connected to the load cell.



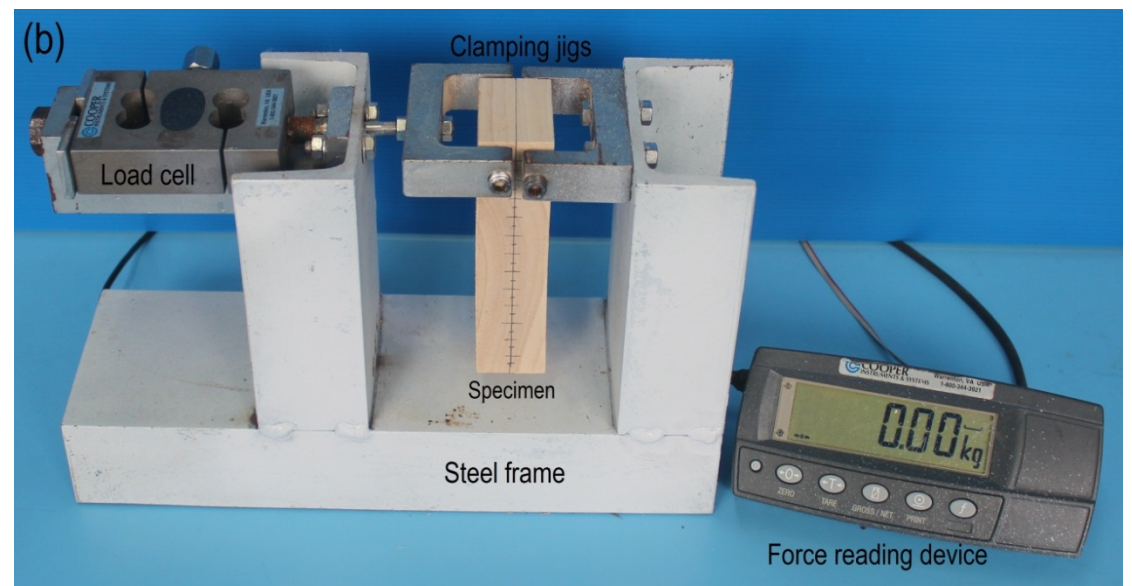


**Figure 3.1** (a) Schematic diagram of the restoring force measuring apparatus and (b) photograph of the wood specimen installed in the device before half-split sawing.

Industrial kiln-dried rubberwood lumber obtained from a local sawmill in Nakhon Si Thammarat, Thailand was used in this study. The flat-sawn lumber was 130 mm wide (W) in the tangential (T) direction and approximately 1 m long in the longitudinal (L) direction (Figure 3.2a). A wood specimen cut to a length (b) of 50 mm (Figure 3.2b) was clamped onto the jigs at a distance (g) of 10 mm away from the top end (Figure 3.1b).

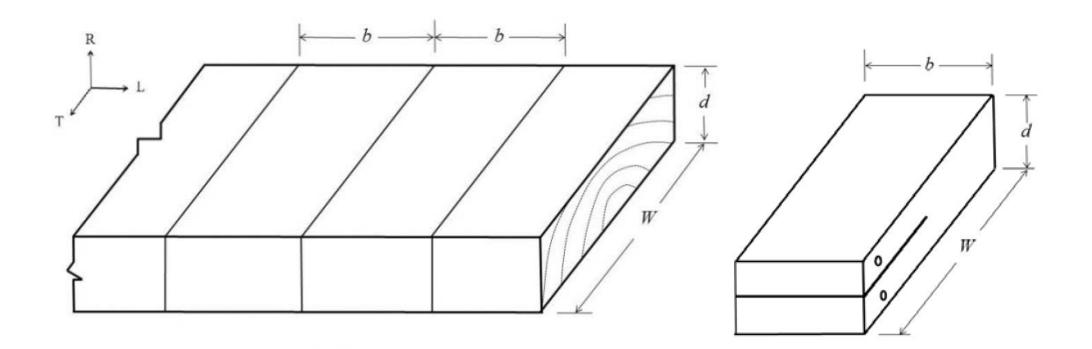
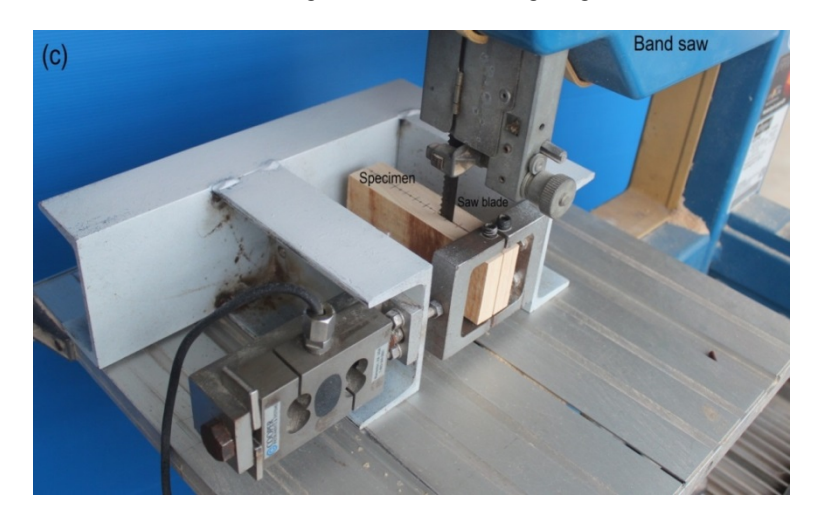


Figure 3.2 Sample layouts of (a) the test specimens cut from the lumber and (b) the half-split specimen for the restoring force measurement.

The restoring force was measured as a function of the half-split length (*l*) for thicknesses (*d*) in the radial (R) direction. While being clamped to the frame, the specimen was half-split at half the thickness for a required length (*l*). The apparatus was designed so that the width of the specimen clamped to the frame can be sawed with a band saw (Figure 3.3). The kerf from the saw was 2 mm wide. Without restraining the specimen, the relaxation of internal stress would cause the two legs of the half-split specimen to be deformed inward or outward. Since the specimen is restrained to the frame and to a steel rod connected to the load cell, the net force generated as a result of internal stress relaxation within the half-split specimen was transferred to the load cell. The sign and magnitude of the force, displayed on the force reading device (Figure 3.4), was recorded and transferred to the computer in real time mode during and after cutting (Figure 3.5).



**Figure 3.3** Photograph of the wood specimen installed in the device during half-split sawing using a band saw.



Figure 3.4 Photograph of the wood specimen installed in the device after half-split sawing.

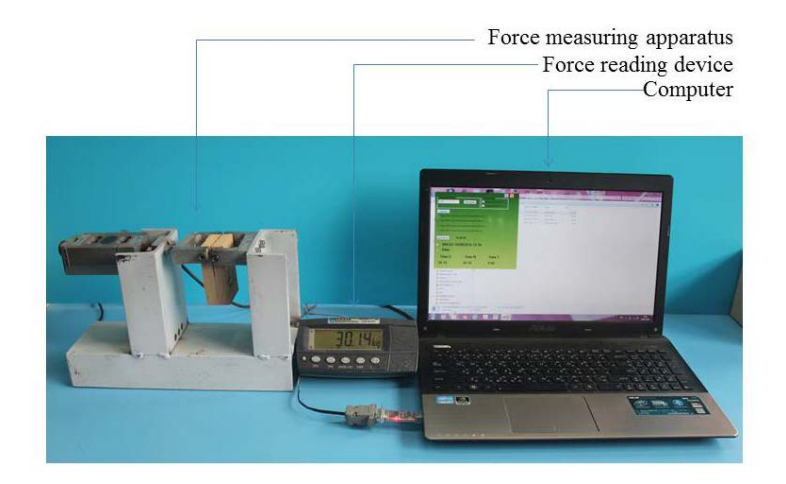


**Figure 3.5** Photograph of the restoring force measuring apparatus and the data recording system.

#### 3.2.2 Optimization of torque on screws to hold the specimen to the apparatus

Effect of torque applied on screws to fix the wood specimen to the restoring force apparatus was investigated. Defect free kiln-dried rubberwood specimens with dimensions of 30 mm thick (*d*), 80 mm wide (*W*) and 50 mm long (*b*) were prepared. The specimen was then fixed to the restoring force measuring device with four screws (Figure 3.1a). Each screw has pressing contact area of 24 mm<sup>2</sup>. Various levels of torque i.e. 0.5, 1.0, 1.5, 2.0, 3.0 and 4.0 N·m were applied to each screw (Figure 3.6). The specimen clamped to the frame was half-split at a half thickness for a length (*l*) of 40 mm and the magnitude of the restoring force was recorded.

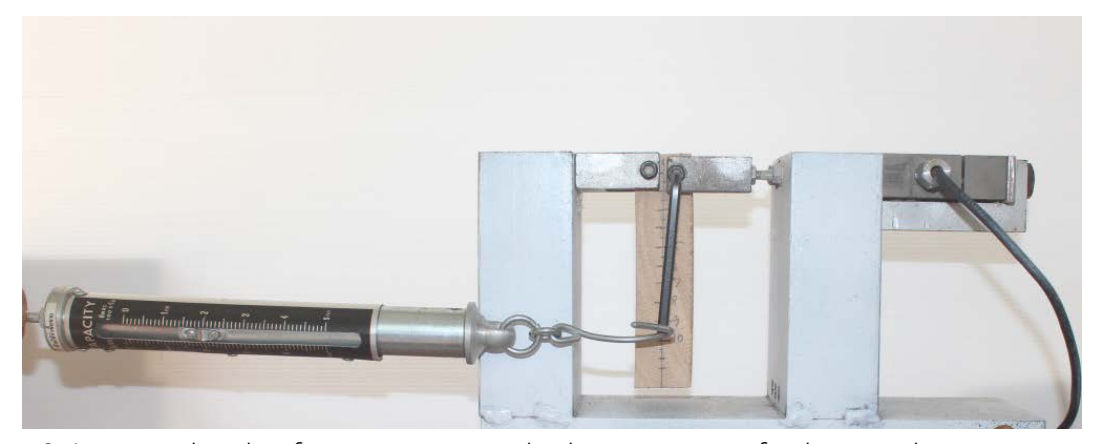


**Figure 3.6** Various levels of torque were applied on screws to fix the wood specimen to the restoring force apparatus.

#### 3.2.3 Effect of screw contact area on measured restoring force

Examination of different contact areas of screw used to fix the wood specimen to the apparatus on the measured restoring force was carried out. Three replicates of defect free kiln-dried rubberwood specimens with dimensions of 30 mm thick (*d*), 130 mm wide (*W*) and 50 mm long (*b*) were prepared from a single piece of lumber. The specimen was fixed to the restoring force measuring device with four screws using applied torque of 2 N·m. Three levels of screw contact area i.e. 3, 13 and 24 mm<sup>2</sup> were used (Figure 3.7). The specimen clamped to the frame was then half-split at a half thickness for a length (*l*) from 10 mm to 110 mm at 5 mm intervals. The magnitude of the restoring force was then recorded.



**Figure 3.7** Three levels of screw contact area (3 mm<sup>2</sup>, 13 mm<sup>2</sup> and 24 mm<sup>2</sup>) used in this study.

#### 3.2.4 Effect of specimen length on measured restoring force

Ten pieces of kiln-dried rubberwood lumber (30 mm thick, 100 mm wide and  $\sim$ 1 m long) were used. For each piece of lumber, defect free wood specimens having various lengths (*b*) of 40 mm, 50 mm, 60 mm, 70 mm and 80 mm were prepared (Figure 3.8). The specimen was clamped to the restoring force measuring device by using four screws having contact area of 24 mm<sup>2</sup> and applied torque of 2 Nm. The specimen was half-split at a half thickness for a length (*l*) of 50 mm and the magnitude of the restoring force was recorded.



Figure 3.8 Wood specimens having various lengths for the restoring force measurement.

#### 3.2.5 Effect of unsplit length on measured restoring force

Three pieces of kiln-dried rubberwood lumber (30 mm thick, 100 mm wide and  $\sim$ 1 m long) were used. Eight 50 mm long wood specimens which were free from any defects were cut from each piece of lumber. The specimens' widths (W) were reduced to 30 mm, 40 mm, 50 mm, 60 mm, 70 mm 80 mm 90 mm and 100 mm (Figure 3.9a-c). Each specimen was clamped to the restoring force measuring device by using four screws having contact area of 24 mm<sup>2</sup> and applied torque of 2 N·m. Various unsplit lengths of the half-split specimens (5 mm, 15 mm, 25 mm, 35 mm, 45 mm 55 mm 65 mm and 75 mm) were obtained by half-splitting the specimen for a length (l) of 25 mm. The magnitude of the restoring force was recorded.

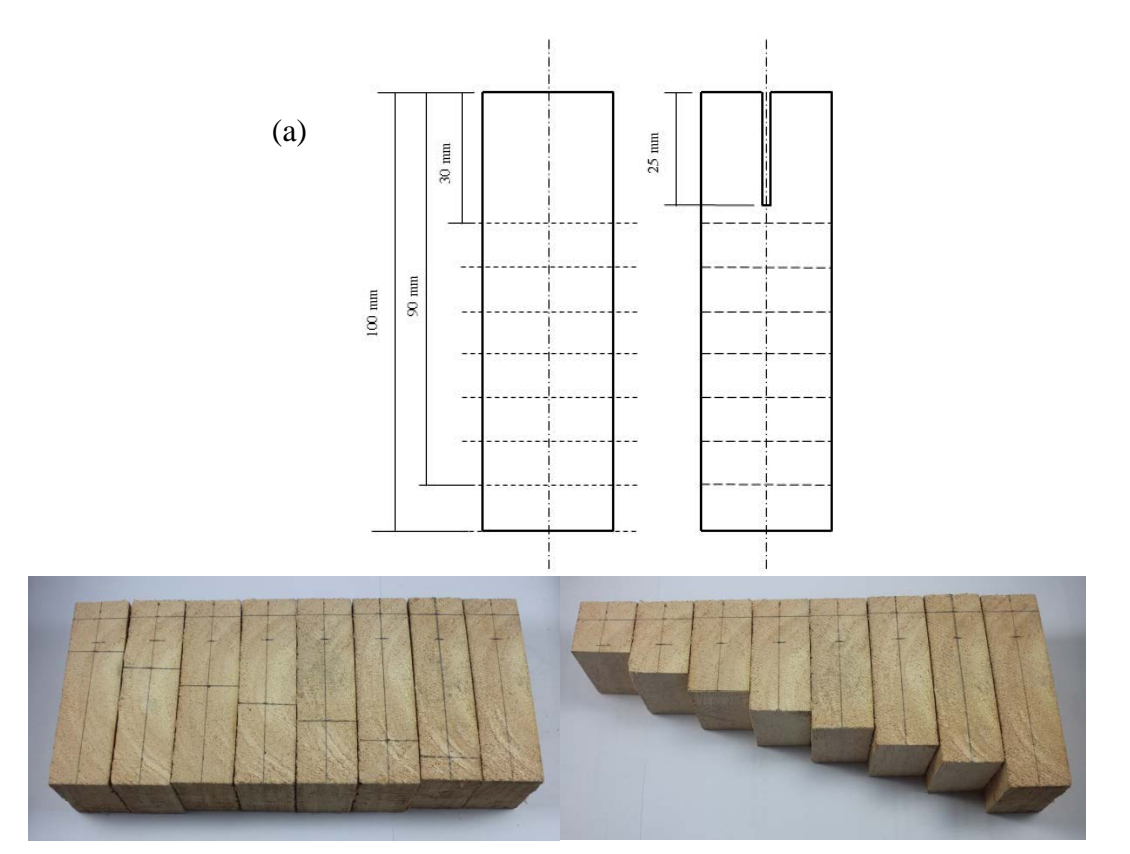


Figure 3.9 (a) Schematic diagram showing the layout of the specimens having different unsplit lengths, (b) pre-marked specimens before cutting to different widths and (c) specimens after cutting to different widths.

3.2.6 Effects of distance and angular deviations from the half-split line on the measured restoring force

Influences of distance and angular deviations of sawing away from the half-split line on the measured restoring force were investigated. Two sets of defect free kiln-dried rubberwood specimens of dimensions 30 mm thick (*d*), 105 mm wide (*W*), and 50 mm long (*b*) were prepared. Three replicates for each set were cut from a single piece of lumber. While being clamped to the restoring force apparatus by using four screws having contact area of 24 mm<sup>2</sup> and applied torque of 2 N·m, the first set of specimens was sawed in a wide direction at various distances away from a half thickness line at 0 mm, 1 mm, 2mm and 3mm (Figure 3.10a). The second set of specimens were sawed at various angles away from the half thickness line at 0°, 1°, 2° and 3° (Figure 3.10b). Sawing of both sets of specimens was performed at 5 mm interval from 10 mm to 100 mm away from the top end. The magnitude of the restoring force was detected during sawing.



**Figure 3.10** Pre-marked specimens showing (a) distance and (b) angular deviations away from the half thickness line.

#### 3.2.7 Repeatability of the restoring force measurement

By using the suitable parameters obtained from all previous sections, the apparatus was tested for the repeatability of the restoring force measurement. Five defect free wood specimens of dimensions 30 mm thick (*d*), 130 mm wide (*W*) and 50 mm long (*b*) cut from a single piece of kiln-dried lumber were prepared. Each specimen was pre-marked at 5 mm interval along a half thickness line. Then the specimen was fixed to the restoring force measuring device by using four screws having contact area of 24 mm<sup>2</sup> and applied torque of 2 N·m. The restoring force was measured during sawing at the half thickness line using a band saw.

#### 3.3 Results and discussions

#### 3.3.1 Restoring force measurement on half-split specimens

Internal compressive and tensile stresses often remain in both an outer layer and an inner core of lumber after kiln drying (McMillen 1958; Simpson 1999). A resultant force generated due to relaxation of these internal stresses tends to bend the two legs of the half-split specimen inward. This behavior is similar to the prong response of kiln-dried lumber that is commonly observed in sawmill industry; however, the deflection degree of half-split specimens is relatively small. According to the prong test, the central portion accounting for about one third of the thickness is generally removed (Simpson 1999) so that the deflection of the two legs could be easily measured. But removing a bigger central portion of lumber would lead to a larger error in quantifying the internal stress level because the degree of prong deflection is only caused by redistribution of the internal

stresses within the remaining portion of lumber. Fuller and Hart (1994) also reported an ambiguous reading on the internal stress level of the prong test as a result of the amount of the wood removed.

Within this work, the apparatus was designed to hold the half-split specimen to the initial position at the clamping points. As a result, a tensile (positive) restoring force was detected on the load cell. Figure 3.11 shows typical evolution of the force value reading on the load cell before, during and after half-split sawing. Before cutting, the force was set to zero. The force increased during the sawing to a required length. A slight fluctuation in the force value as a result of saw blade vibration can be observed. An instantaneous elastic response of the restoring force was recorded immediately after half-splitting the specimen to the required length and removing the specimen from the saw blade. Thereafter, the force value slightly increased with time as a result of viscoelastic creep. Mechano-sorptive creep should also play a role over time as moisture could easily diffuse into or out of the inner section of the specimen via the saw kerf. Creep response of the specimen could affect the measured values of the restoring force when multiple sawing at various half-split lengths was performed (Figure 3.12). To minimize such an effect from creep to less than 3 %, the multiple sawing on each specimen was completed in a short time of less than 3 minutes. Detailed analysis of the creep response is beyond the scope of the present thesis and should be explored in the future.

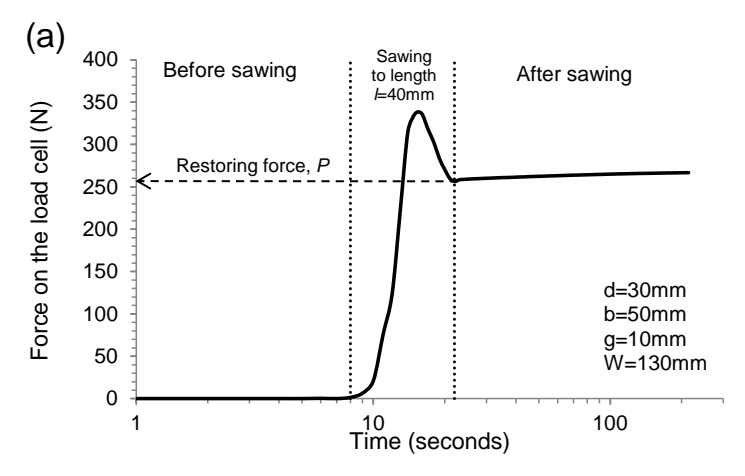


**Figure 3.11** Typical evolution of the detected force on the load cell before, during and after half-split sawing of the specimen fixed to the restoring force measuring device using a single sawing at 40 mm.

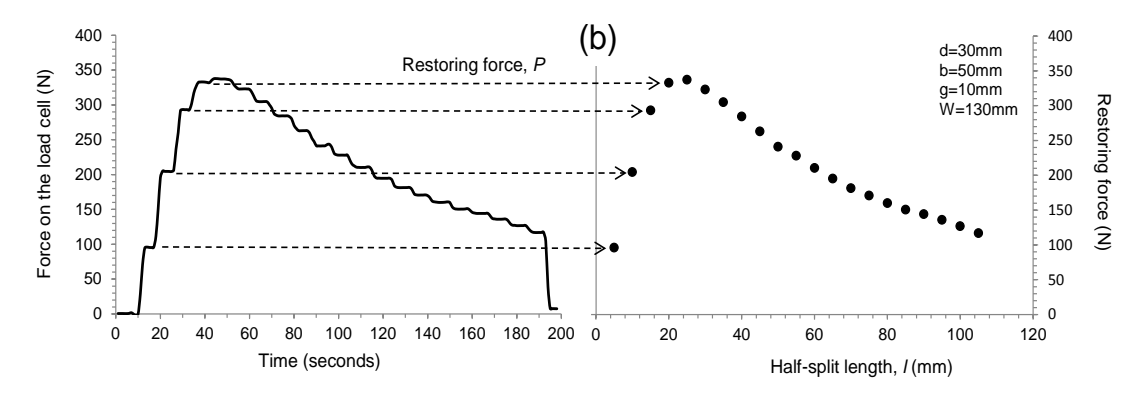


**Figure 3.12** Multiple sawing at 5 mm intervals. Some values of the derived restoring force are also indicated in the graphs.

#### 3.3.2 Optimization of torque on screws to hold the specimen to the apparatus

Figure 3.13 shows the measured restoring force plotted against the level of torque applied on each screw. The pressing contact area between the screw and the wood specimen was 24 mm<sup>2</sup>. The measured restoring force first increases with applied torque up to 2 N·m. Once this torque level is exceeded, the measured restoring force becomes largely unaffected by the applied torque. Therefore, the minimum torque of 2 N·m is required to hold the wood specimen to the apparatus. Using higher level of torque is also possible. However, if the magnitude of applied torque is too high of up to 4 N·m, it was observed that cracks were developed in some specimens. It is suggested that the optimum level of applied torque lies from 2-3 N·m.

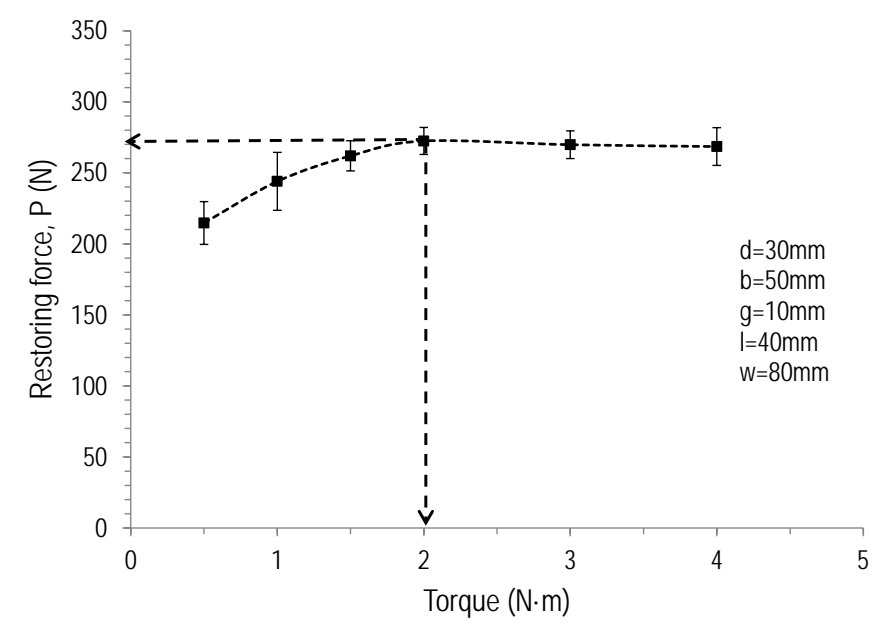


**Figure 3.13** Influence of applied torque to hold the wood specimen to the restoring force apparatus on the magnitude of the measured restoring force.

#### 3.3.3 Effect of screw contact area on measured restoring force

Figure 3.14 shows the measured restoring force plotted against the half-split length at various contact areas of screws and the wood specimen. It is obvious that the restoring force profiles obtained from the test using screws having contact areas from 3 mm<sup>2</sup> to 24 mm<sup>2</sup> do fall into a single curve. The contact area of screws used within this range therefore does not affect the value of the measured restoring force. However, to reduce the value of stress intensity in the vicinity of the clamping area that might induce crack in the specimen, the maximum contact area examined of 24 mm<sup>2</sup> is chosen for the restoring force measurement.

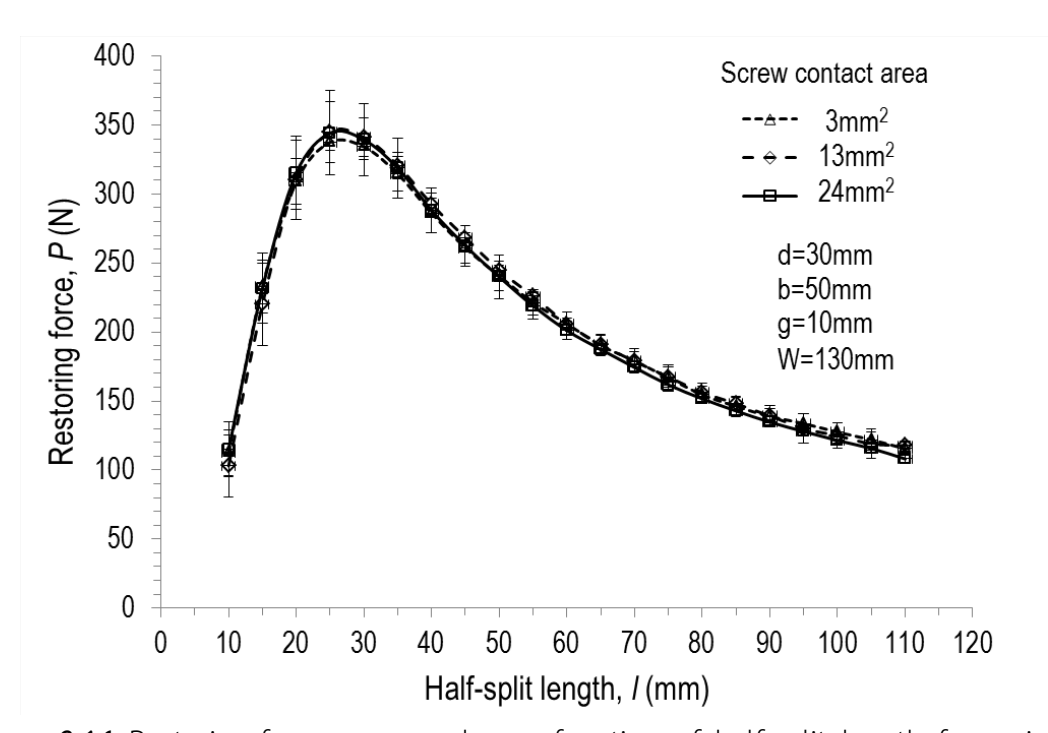


Figure 3.14 Restoring force measured as a function of half-split length for various screw contact areas of 3 mm<sup>2</sup>, 13 mm<sup>2</sup> and 24 mm<sup>2</sup>.

#### 3.3.4 Effect of specimen length on measured restoring force

Figure 3.15 shows the effect of specimen length (*b*) on the measured restoring force of the wood specimens prepared from the same piece of lumber. The magnitude of the restoring force is proportional to length of the specimen. According to Lados and Apelian (2006), the restoring force required to push the half-cut specimen containing internal residual stress back to initial configuration prior to cutting follows

$$P = \frac{E \cdot \Delta \delta \cdot b}{S} \tag{3.1}$$

where E,  $\Delta\delta$  and S are Young's modulus, mouth opening and geometrical shape factor, respectively. Within this study, the specimen's length is constant at 50 mm.

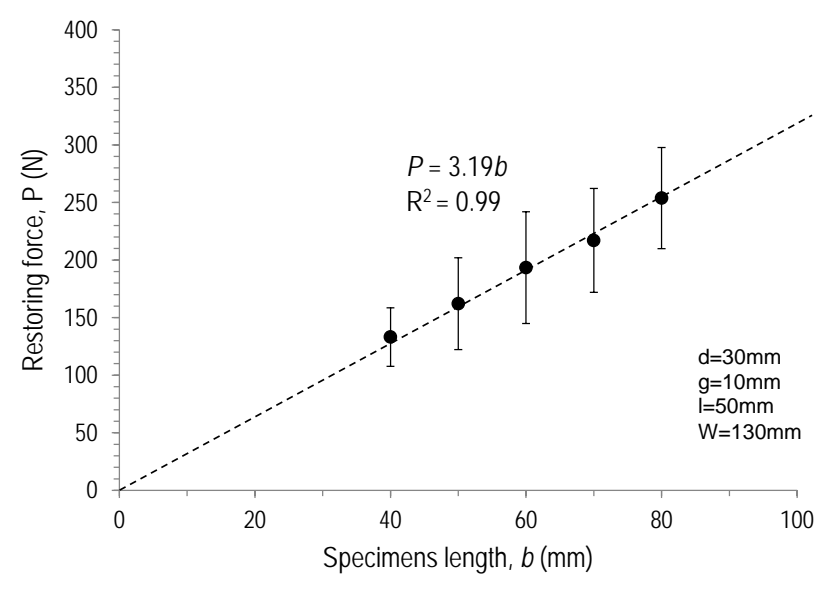


**Figure 3.15** A linear relationship between measured restoring force and length of wood specimen.

# 3.3.5 Effect of unsplit length on measured restoring force

Figure 3.16 shows the measured restoring force plotted against the unsplit length of the wood specimen. For the specimens having the unsplit length greater than 25 mm, the measured values of the restoring force are constant. The restoring force values dramatically decrease if the remaining unsplit section is less than 25 mm. For a relatively wide specimen, the stress field altered by the presence of the saw kerf is not influenced by the specimen end. Each leg of the half-split specimen behaves like a beam with one end rigidly attached to a fixed support (relatively large unsplit section of the specimen). However in a relatively narrow specimen, relaxation of stress in the form of strain takes place at the end of the specimen width. In this case, the leg of the half-split specimen cannot be thought as if one end is attached to a fixed support. Therefore lesser magnitude of the restoring force is required to restrain the legs at the clamping points.

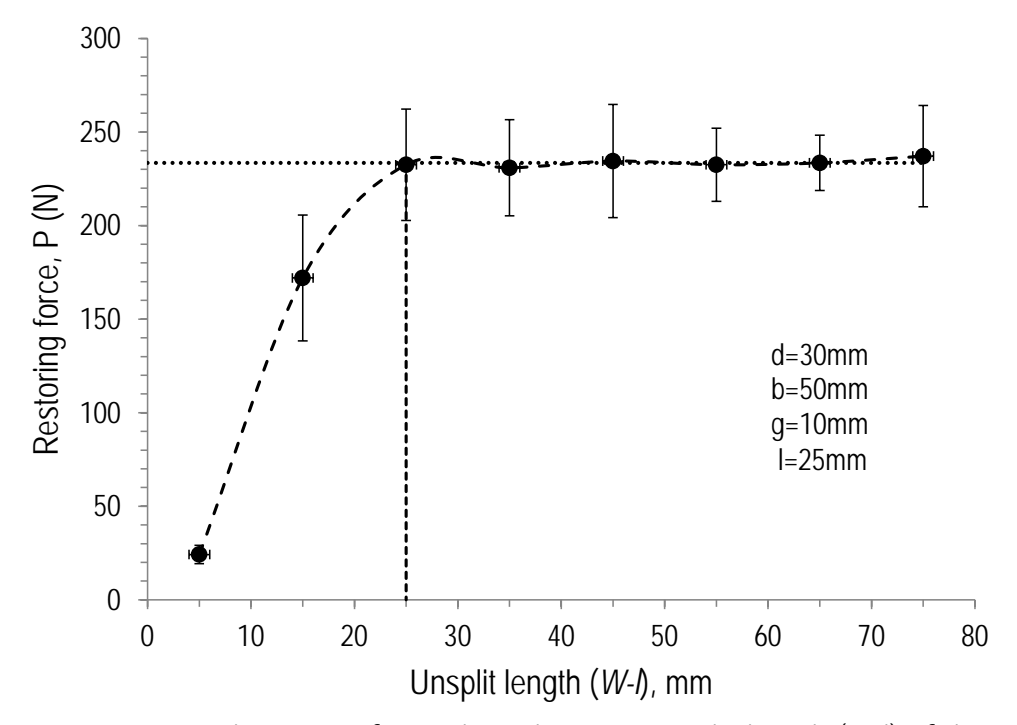
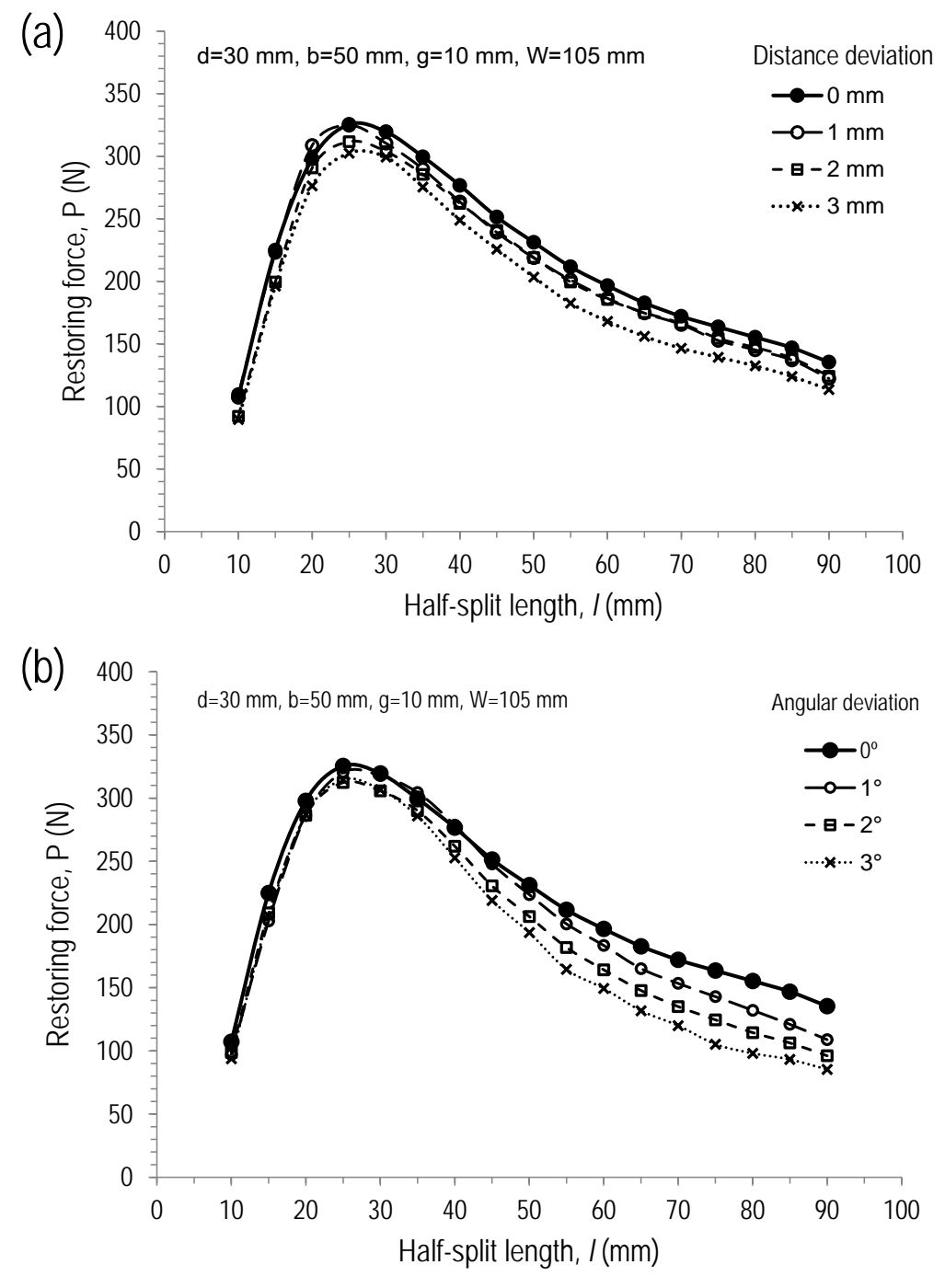


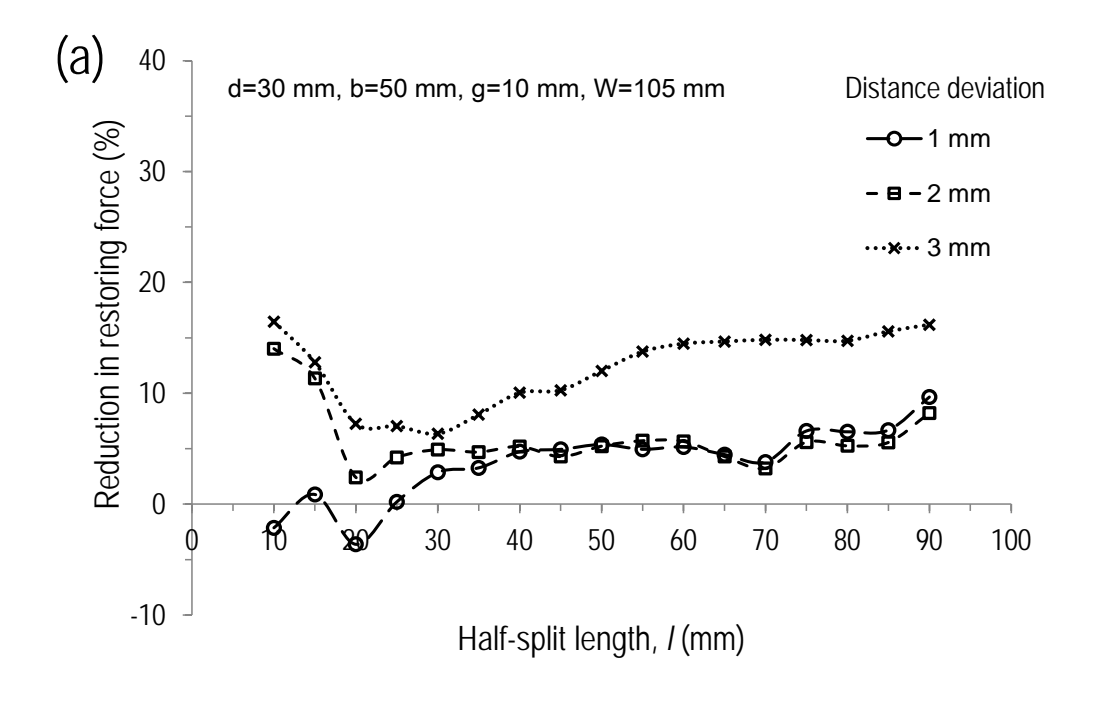
Figure 3.16 Measured restoring force plotted against unsplit length (*W-l*) of the 30 mm thick wood specimens having various width (*W*) and constant half-split length (*l*) of 25 mm.

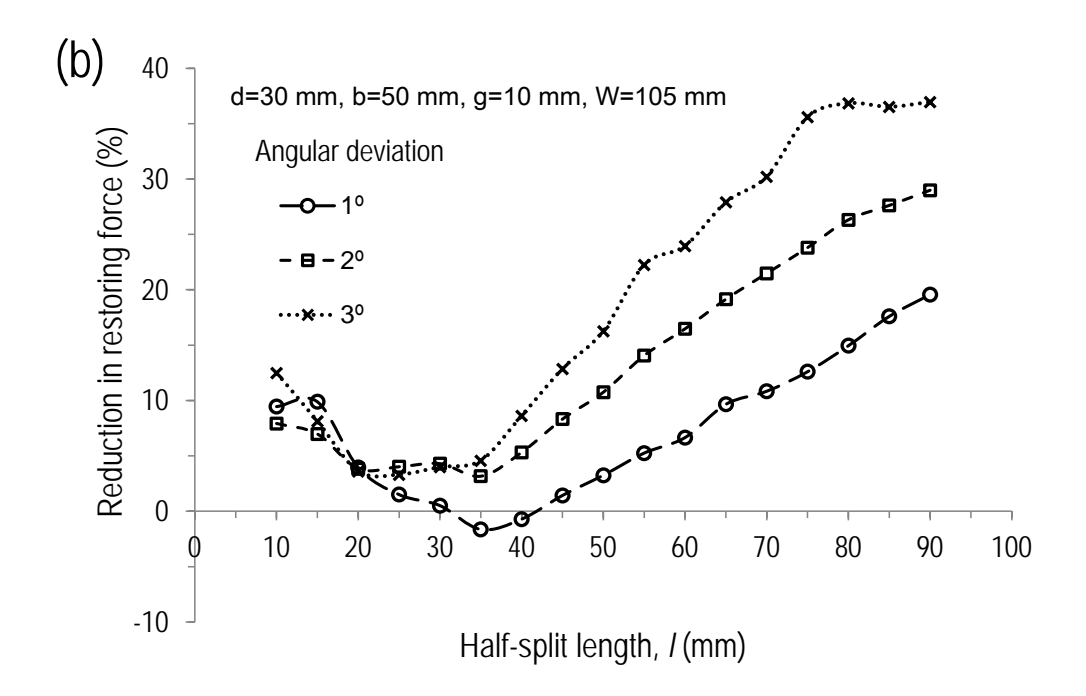
3.3.6 Effects of distance and angular deviations from the half-split line on the measured restoring force

During half-splitting of the specimen, a slight deviation of cutting from the half-split line might happen in practice. Figure 3.17a and 3.17b show effect of distance and angular deviations, respectively, of cutting from the half-split line on the measured restoring force. Both distance and angular deviations of cutting from the half-split line cause a reduction in the measured restoring force. Distance deviation seems to cause a reduction in the measured restoring force of about 3% to 12% for distance deviations of 1 mm to 3 mm from the half-split line (Figure 3.18a). The percentage in a reduction of the measured restoring force is roughly independent of the half-split length. On the other hand, angular deviation causes a reduction in the measured restoring force which is more pronounce at a longer half-split length (Figure 3.18b). This is because angular deviation causes larger distance deviation from the half-split line at a longer half-split length. At the half-split length of 90 mm, angular deviations of 1°, 2° and 3° cause a reduction in the measured storing force of 20%, 29% and 37%, respectively. It is easily achievable in practice to keep distance deviation to within 1 mm from the half-split line at any half-split length so that an error caused by a reduction in the measured restoring force would be less than 5%.



**Figure 3.17** Measured restoring force plotted as a function of half-split length for various (a) distance and (b) angular deviations from the half-split line.

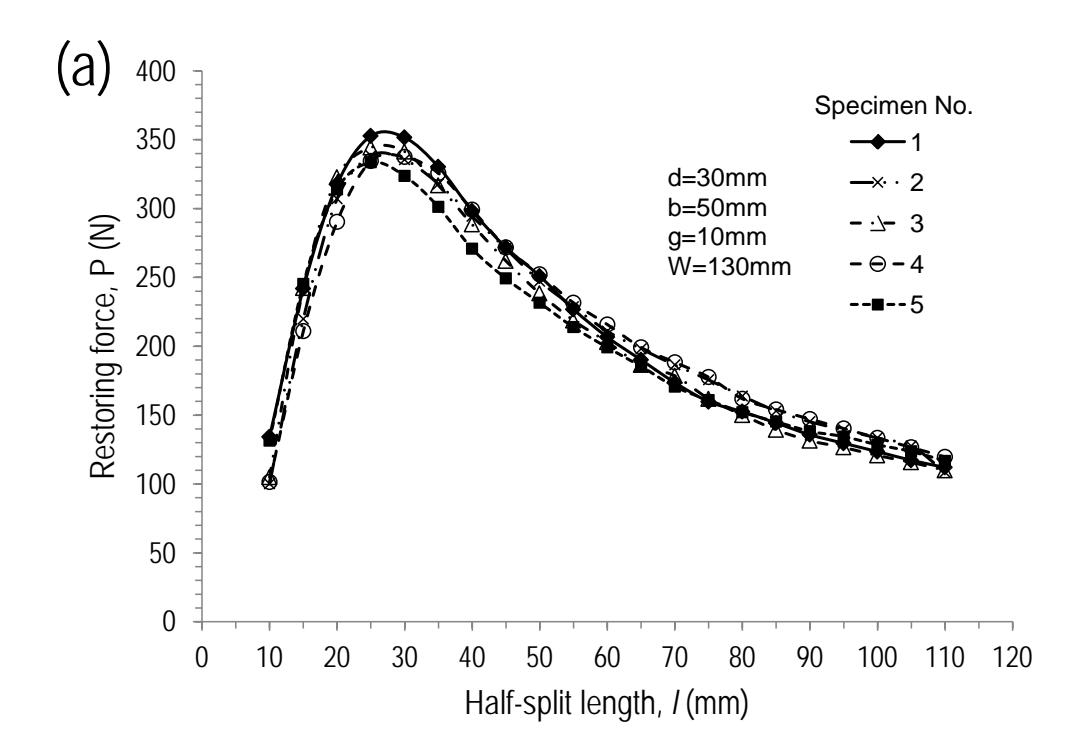




**Figure 3.18** Reduction in measured restoring force plotted as a function of half-split length for various (a) distance and (b) angular deviations from the half-split line.

# 3.3.7 Repeatability of the restoring force measurement

It is important to examine the repeatability of the proposed restoring force measurement technique. The technique should consistently produce the same measurement. Four screws, having contact area of 24 mm² with an applied torque of 2 N·m on each screw, were used to hold the wood specimens to the restoring force apparatus. The distance deviation from the half-split line was kept to within 1 mm during half-splitting. Results of the restoring force measurement from five wood specimens prepared from a single piece of kiln-dried lumber are shown in Figure 3.19a. All restoring force data from the five measurements seems to fall into a single curve. Average and standard deviation values of the restoring force were calculated and plotted against half-split length in Figure 3.19b. Coefficient of variation (CV) of five measurement data is only 4.5%. And it should be noted that variation observed in the measured restoring force is not solely caused by the measurement technique but could also arise from variability in the wood specimens. Therefore the restoring force measurement technique developed and the corresponding device designed and constructed produce a repeatable measurement of the restoring force at various half-split lengths.



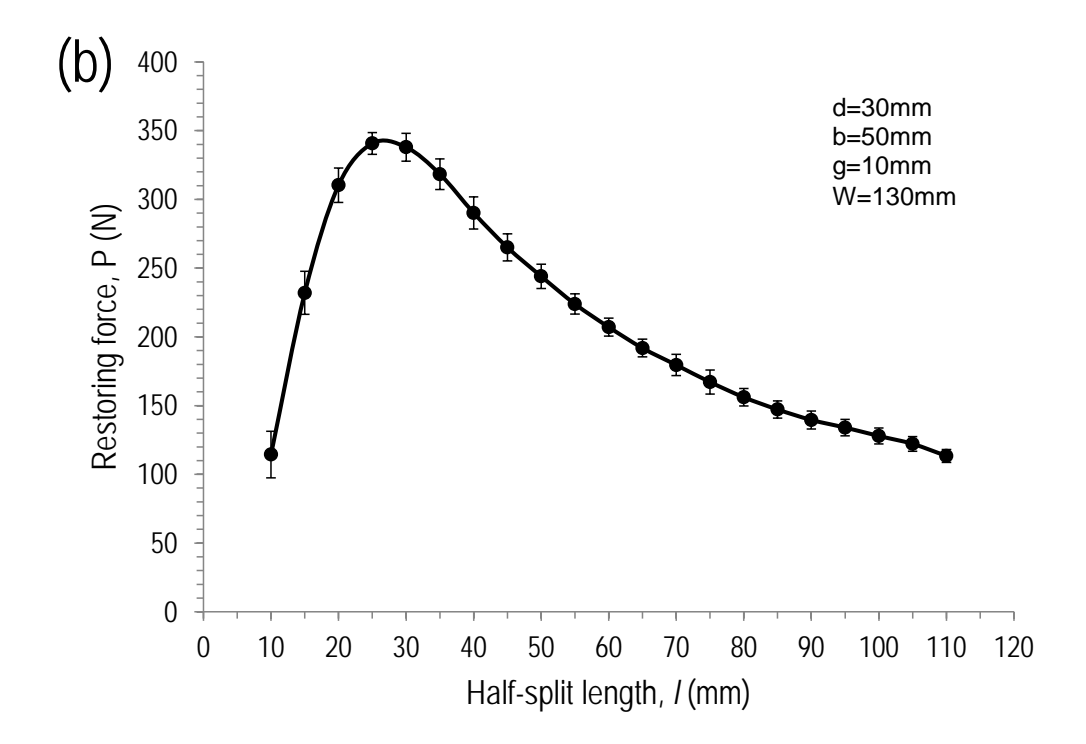


Figure 3.19 (a) Measured restoring force of five wood specimens prepared from a single piece of lumber and (b) average values with error bars of the data in (a) plotted against half-split length.

## 3.4 Conclusions

The following conclusions can be drawn from this chapter:

- 1. A novel technique for an assessment of internal stress within kiln-dried lumber by measuring the restoring force has been presented. The restoring force on the restrained half-split specimens can be measured online both in a single sawing mode at a particular half-split length and a multiple sawing mode at various half-split lengths.
- 2. Screw contact area of 24 mm<sup>2</sup> with an optimal applied torque on each screw of 2-3 N·m is suitable to hold the specimen to the apparatus. Cracks could be developed in the specimen if the screw contact area is too small or the applied torque is too high.
- 3. The magnitude of the restoring force is proportional to length of the specimen. At a particular half-split length of the 30 mm thick specimen, the measured restoring force is constant for the lumber having the remaining unsplit length greater than 25mm. The measured restoring force dramatically decreases below this value.
- 5. Both distance and angular deviations of cutting away from the half-split line reduce the measured restoring force value. By keeping the distance deviation away from the

half-split line to within 1 mm, an error resulting in a reduction in the measured restoring force is less than 5%.

6. The proposed restoring force measuring apparatus together with a suitable set up of the half-split specimen is proved to provide a repeatable measurement of the restoring force of the kiln-dried lumber at various half-split lengths.

#### References

- 1. Diawanich P, Matan N, Kyokong B (2010) Evolution of internal stress during drying, cooling and conditioning of rubberwood lumber. Eur J Wood Prod 68(1):1–12
- 2. Diawanich P,Tomad S, Matan N, Kyokong B (2012) Novel assessment of casehardening in kiln-dried lumber. Wood Sci Technol 46: 101-114
- 3. Fuller J, Hart CA (1994) Factors that influence the prong test. In: Proceedings of the 4th IUFRO international wood drying conference. Rotorua, pp 313–320
- 4. McMillen JM (1958) Stresses in wood during drying (Report 1652). Department of Agriculture, Forest Service, Forest Products Laboratory, Madison
- 5. Perré P, Passard J (2007) Stress development. In: Perré P (ed) Fundamentals of wood drying, European COST A.R.BO.LOR., Nancy, pp 243-271
- Schajer GS, Ruud CO (2013) Overview of residual stresses and their measurement. In: Schajer GS (ed) Practical Residual Stress Measurement Methods, John Wiley & Sons, West Sussex, pp1-27
- 7. Simpson WT (1999) Drying and control of moisture content and dimensional changes. In: Wood handbook (Wood as an Engineering Material). Department of Agriculture, Forest Service, Forest Products Laboratory, Madison
- 8. Tomad S, Matan N, Diawanich P, Kyokong B (2012) Internal stress measurement during drying of rubberwood lumber: effects of wet-bulb temperature in various drying strategies. Holzforschung 66: 645-654

# Chapter 4

# Quantification of internal stress within lumber using a beam theory

#### 4.1 Introduction

Since elastic modulus of wood changes with its moisture content and specific gravity (Bodig and Jayne 1982; Matan and Kyokong 2003; Sonderegger et al. 2013), therefore it is not practical to determine internal stress within kiln-dried lumber by analyzing strain or deflection that accompany the stress redistribution that occurs when internal stresses are elastically released by sectioning or splitting. The restoring force measuring technique developed in chapter 3 should allow, in principle, an assessment of internal stress without the use of the wood modulus data. In this chapter, mathematical calculation of the internal stress from the measured restoring force is developed. The derived internal stress is compared with one of the traditional slicing techniques. A chart for converting the restoring force to the internal stress is proposed for convenience in the industry. Demonstration of the technique is performed to follow the evolution of internal stress during the conditioning and storage stages of kiln-dried rubberwood lumber.

#### 4.2 Materials and Methods

# 4.2.1 Restoring force and slice test measurements

Six pieces of industrial kiln-dried rubberwood obtained from a local sawmill in Nakhon Si Thammarat, Thailand were used in this study. The restoring force was measured as a function of the half-split length (1) for thicknesses (d) of 30 mm and 50 mm (three replicates for each size) in the radial (R) direction. The flat-sawn lumber was 130 mm wide (W) in the tangential (T) direction and approximately 1m long in the longitudinal (L) direction. For each piece of lumber, two sets of specimens with relatively high levels of internal stress (HS) and low levels of internal stress (LS) were prepared. All specimens were free from defects such as knots and spiral grain. The HS specimens were tested immediately after kiln drying while the LS specimens were left in ambient air (28±2 °C and 75±6 % RH) for 3 weeks prior to testing. The specimens were cut to a length (b) of 50 mm (Figure 4.1a) and marked into a half thickness line at 5 mm intervals (Figure 4.1b) and also marked by divided lines so they could be cut into slices of 5 mm thick according to the McMillen slice test (McMillen, 1958) (Figure 1c). The initial width of each pre-marked slice  $(W_b)$  was measured by calipers to an accuracy of 0.01 mm. Specimens were then assembled into the restoring force measuring apparatus and were cut through the pre-marked half thickness line. The restoring force was monitored at 5 mm intervals up to 125 mm using a procedure described in

section 3.2.1. They were then cut into slices along the pre-marked lines and the width  $(W_o)$  of each slice was immediately measured.

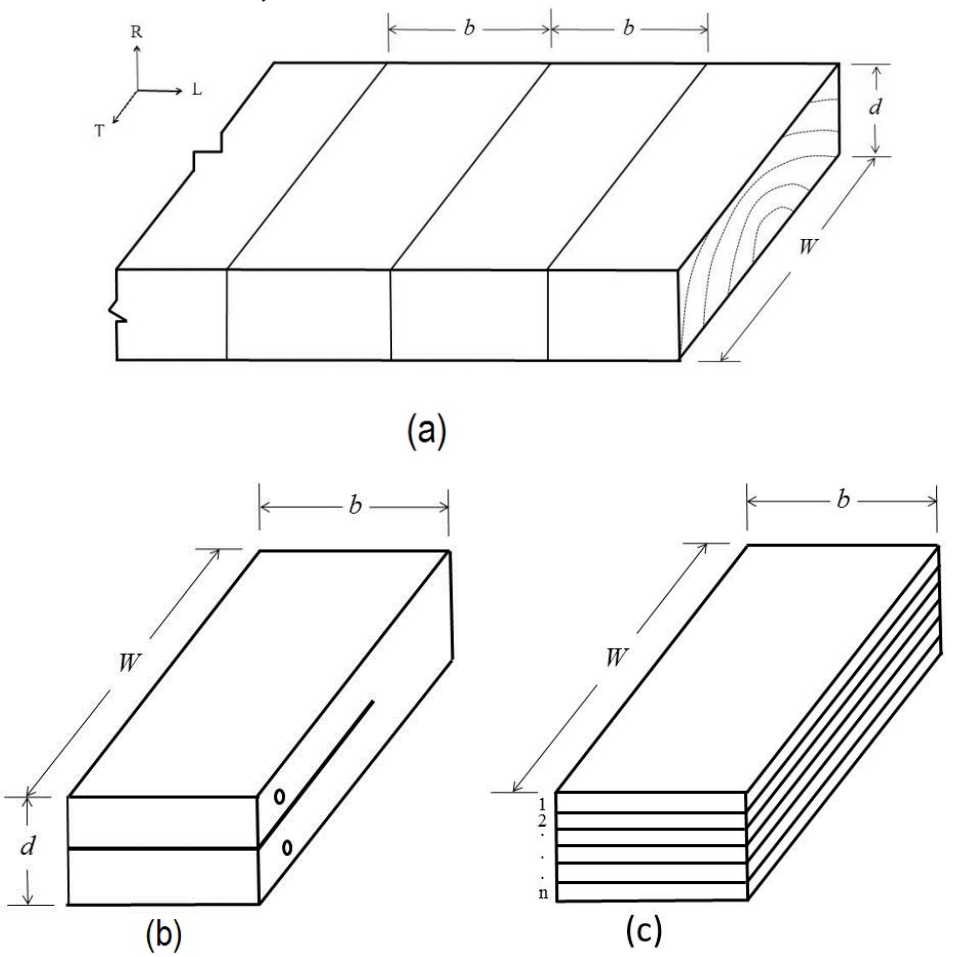


**Figure 4.1** Sample layouts of (a) the test specimens cut from the lumber, (b) the half-split specimen for the restoring force measurement and (c) the specimen for the McMillen slice test.

The released strain of each slice ( $\mathcal{E}$ ) was calculated according to  $\mathcal{E} = \frac{W_a - W_b}{W_b}$  . Each

slice was then subjected to a tensile test using a universal testing machine (Lloyd 150kN, UK) equipped with a strain gauge (Epsilon Technology, USA) to determine the value of Young's modulus in the tangential direction. After testing, a section of each slice was weighted both before and after oven-drying at 104 °C for 24 hours to determine its moisture content.

# 4.2.2 Internal stress relaxation of kiln-dried rubberwood lumber

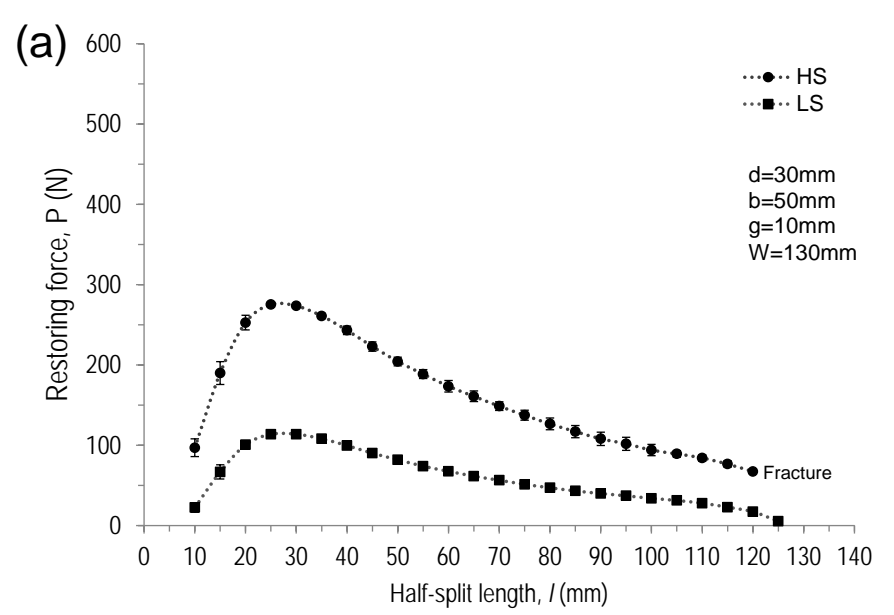
Six pieces of kiln-dried rubberwood lumber (30 mm thick, 130 mm wide and approximately 1 m long) were taken from a local sawmill in Nakhon Si Thammarat, Thailand. The ring orientation was selected such that normal to the growth ring aligned parallel to the thickness of the lumber. Defect-free specimens measuring 50 mm long were cut at least 50 mm from the end of each lumber. Restoring force measurement was then carried out on

the half-split specimens at cutting lengths from 60 mm to 100 mm. The remaining pieces of lumber were coated with aluminum paint at both ends. Three pieces of lumber were placed in a conditioning chamber (Binder, Germany) at 85  $^{\circ}$ C and 80  $^{\circ}$ RH. Another three pieces were left in ambient air at 28±2  $^{\circ}$ C and 75±6  $^{\circ}$ RH. Assessments of internal stress were later performed after 30 minutes and 90 minutes of conditioning and at 10 days and 20 days of storage, respectively.

#### 4.3 Results and discussions

# 4.3.1 Experimental restoring force profile

The curves of the restoring force as a function of half-split length obtained from the 30 mm and 50 mm thick specimens are shown in Figure 4.2a and Figure 4.2b respectively. For the 50 mm thick HS specimens, measurements could be made up to the half-split length of 100 mm (Figure 4.2b) because of the presence of cracks at the tip of the kerf. For both lumber thickness sizes, the magnitude of the restoring force varied with the half-split length.



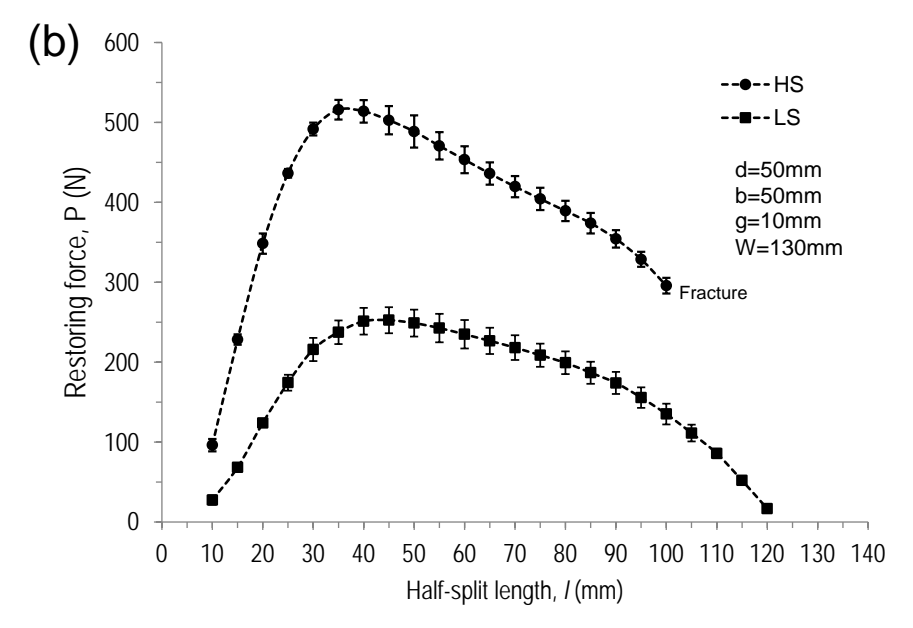


Figure 4.2 Experimental restoring force profiles as a function of half-split length of (a) the 30 mm and (b) the 50 mm thick kiln-dried rubberwood specimens with widths of 130 mm and lengths of 50 mm containing high levels (HS) and low levels (LS) of internal stress.

The restoring force first abruptly increased and reached the maximum values at the half-split lengths of around 25 mm for the 30 mm thick specimens and around 35-45 mm for the 50 mm thick specimens. After exceeding the maximum value, the restoring force gradually decreased with the increase of the half-split length. The magnitude of the restoring force appears to reflect the internal stress level within the specimen. And the restoring forces of the HS specimens are clearly higher than those of the LS specimens. However, the observed force values should also be influenced by the specimen's geometry. According to the Figure 4.2, higher restoring force levels were detected in the thicker specimens. In the following section, an attempt was made to relate the magnitudes of the restoring force to the level of the internal stress within the lumber.

#### 4.3.2 Estimation of the internal stress

By assuming a linear distribution of internal stress across half thickness of lumber (Figure 4.3a), the maximum linearly averaged internal stress  $\sigma_{\rm m}$  was assumed to be equal at the outer surface and at the inner core. This can be calculated by a deflection of the half-split specimen (Figure 4.3b) as expressed by

$$\sigma_m = \frac{E \cdot \Delta \delta \cdot d}{4l^2} \tag{4.1}$$

where E,  $\Delta\delta$ , d and l are Young's modulus in the tangential (T) direction, mouth opening, thickness and sawed depth of the specimen, respectively (Walton 2002).

A restoring force (P) is applied at distance a away from the end of the kerf (or at distance g away from the specimen end) to keep the half-split specimen in the original configuration prior to sawing (Figure 4.3c). According to Lados and Apelian (2006), the restoring force (P) can then be expressed as

$$P = \frac{E \cdot \Delta \delta \cdot b}{S} \tag{4.2}$$

where b is the sample length and S is the geometrical shape factor.

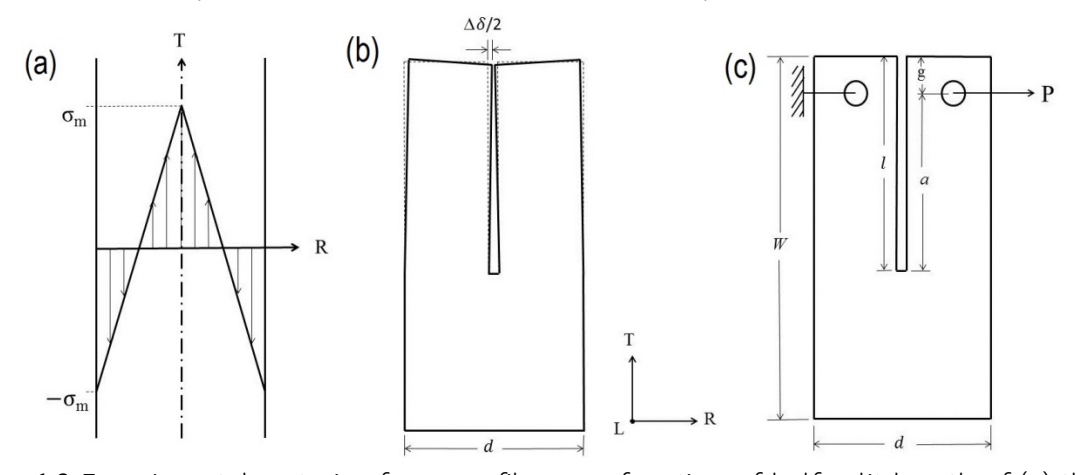


Figure 4.3 Experimental restoring force profiles as a function of half-split length of (a) the 30 mm and (b) the 50 mm thick kiln-dried rubberwood specimens with widths of 130 mm and lengths of 50 mm containing high levels (HS) and low levels (LS) of internal stress.

It can be considered that each leg of the half-split specimen acts as a cantilever beam that is rigidly fixed at one end and free at the other end. Also, it is assumed that the internal stress is fully relaxed across the thickness of the specimen and the effects of other stress components (including stresses in the thickness and the length directions, shear stresses and stress concentration around the end of the kerf) are negligible. The restoring force (*P*) is calculated using the cantilever beam equation (Hibbeler 2012) according to

$$P = \frac{6EI}{a^{2}(3l-a)} \frac{\Delta \delta}{2} = \frac{6EI}{(l-g)^{2}(2l+g)} \frac{\Delta \delta}{2}$$
 (4.3)

where I is the second moment of area which is equal to  $\frac{bd^3}{96}$ . By combining equations (4.1), (4.2) and (4.3), the restoring force P can be expressed as

$$P = \frac{4bl^2}{Sd}\sigma_{\rm m} \tag{4.4}$$

where the geometrical factor is  $S=\frac{32(l-g)^2(2l+g)}{d^3}$ . It should be emphasized that according to equation (4.4), the magnitude  $\sigma_{\rm m}$  can be straightforwardly calculated from the measured restoring force without prior knowledge of the Young's modulus E of the wood.

By plotting the restoring force (P) against the term  $\frac{4bl^2}{Sd}$ , the value of  $\sigma_{\rm m}$  can then be deduced from the slope of the graph. It appears that the model well describes the experimental restoring data at relatively small values of  $\frac{4bl^2}{Sd}$ . In this flexural response regime, the restoring force is proportional to the term  $\frac{4bl^2}{Sd}$  (Figure 4.4a-b).

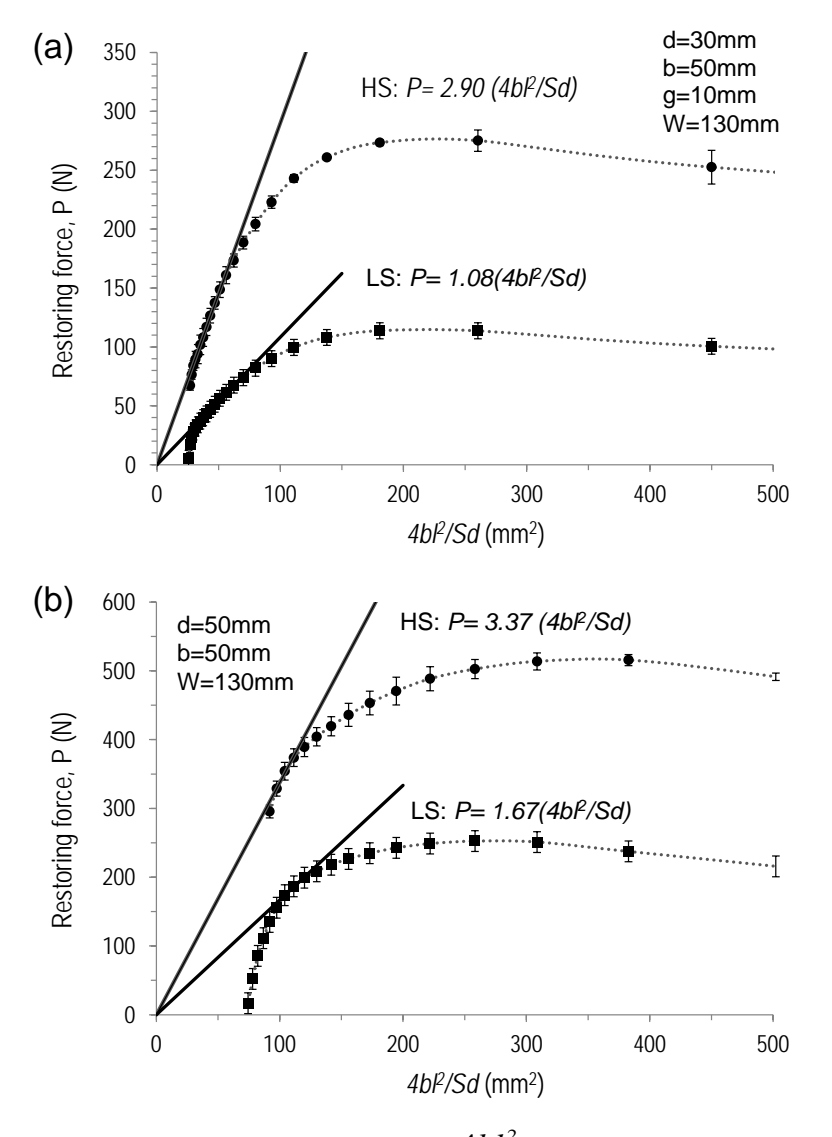
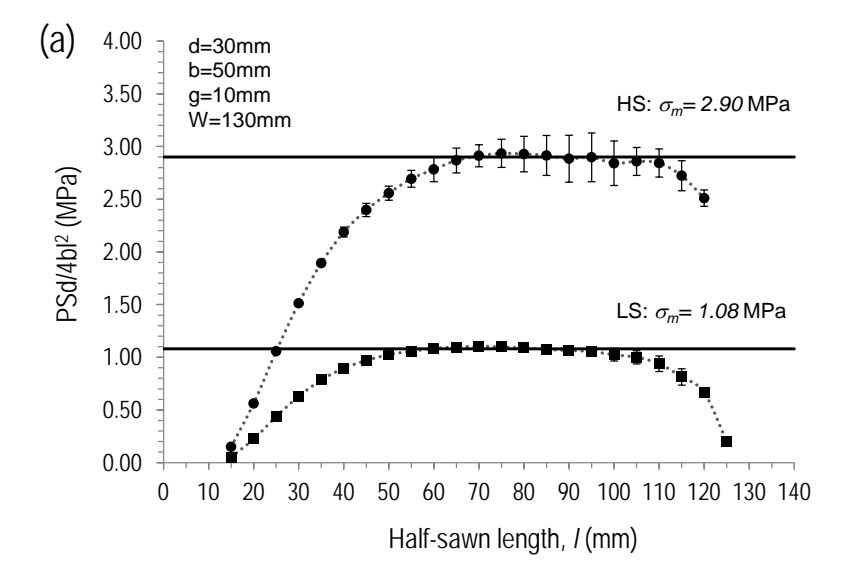


Figure 4.4 Plots of the restoring force versus  $\frac{4bl^2}{Sd}$  for (a) the 30 mm and (b) the 50 mm thick half-split rubberwood specimens.

Alternatively, one could plot the term  $\frac{PSd}{4bl^2}$  against the half-split length (*l*) and the maximum and constant value of the term  $\frac{PSd}{4bl^2}$  is the value of  $\sigma_{\rm m}$  (Figure 4.5 a-b).



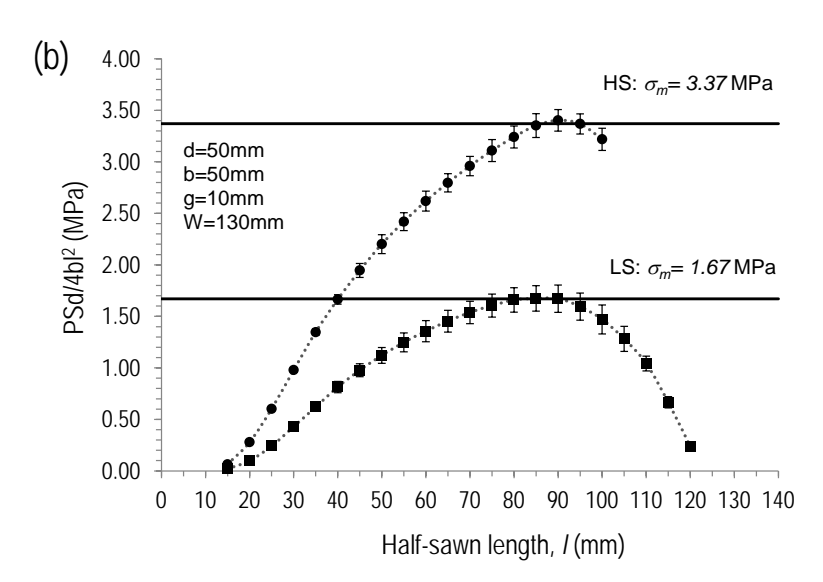
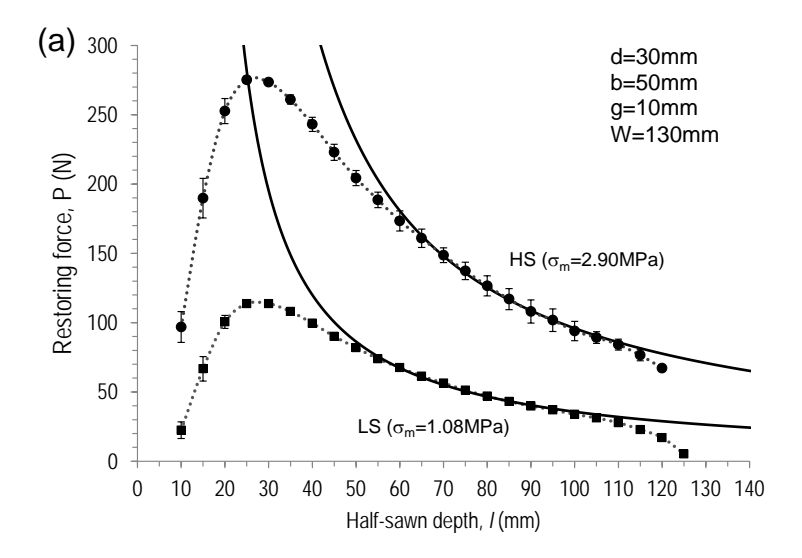


Figure 4.5 Plots of  $\frac{PSd}{4bl^2}$  versus the half-split length for (a) the 30 mm and (b) the 50 mm thick half-split rubberwood specimens containing relatively high (HS) and low (LS) levels of internal stress. Solid lines represent the best fits to the experimental data in the flexural response regime.

The magnitudes of  $\sigma_{\rm m}$  derived from the graphs are 2.90MPa and 1.08MPa for the 30 mm thick HS and LS specimens, respectively (Figure 4.4a and Figure 4.5a) and are 3.37MPa and 1.67MPa for the 50 mm thick HS and LS specimens, respectively (Figure 4.4b and Figure 4.5b). It should be noted that the presence of other stress components especially in the

thickness direction could also affect the measured restoring force value. For the purpose of this study, all pieces of flat-sawn lumber were selected such that stresses in thickness direction were relatively small compared to those in the direction of width. In the future, the effects of other stress components could be included in the calculations.

According to equation (4.4), the calculated restoring forces at those magnitudes of  $\sigma_{
m m}$  derived are compared with the experimental values in Figure 4.6a-b. As expected, a good agreement between the calculated and the measured restoring force values is obtained in the flexural response regime between the half-split lengths from 60 mm to 100 mm in the 30 mm thick and 130 mm wide specimens (Figure 4.6a). Outside this range, the calculated restoring forces overestimate the experimental values. At half-split lengths less than 60 mm, it is expected that the internal stress was not fully relaxed across the whole specimen thickness and the presence of stress field around the tip of the kerf had not yet been taken into account in the calculation. At the half-split lengths more than 100 mm, stress field generated by the deep kerf should have covered across the end of specimen with a width of 130 mm. Therefore, one end of a half-split specimen leg cannot be considered to be fixed to a rigid support. A modification of equation (4) to cope with such behaviors outside the flexural response regime warrants further investigation and is a subject of future work. This is crucial for thicker lumber such as the 50mm thick specimens where the flexural response range was rather small of 80-95 mm (Figure 4.6b). Estimation of the internal stress within thicker lumber using the purely flexural model proposed is still possible but might be no longer appropriate.



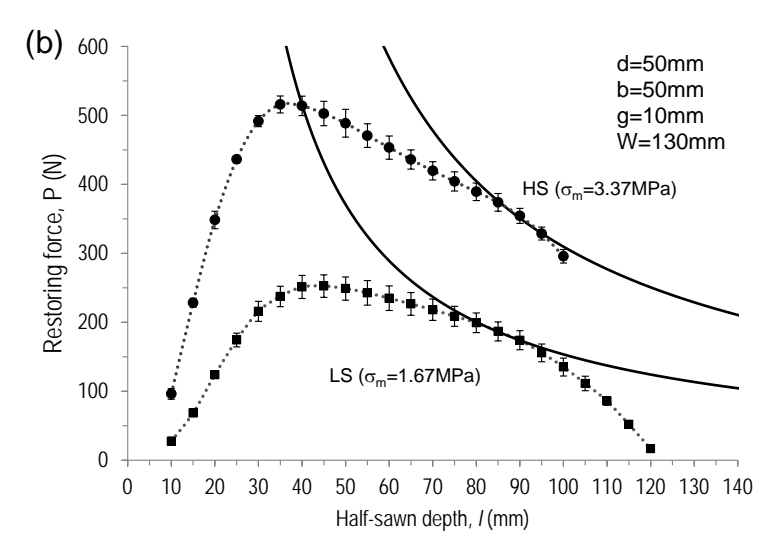


Figure 4.6 Comparison of experimental (symbols) and calculated restoring force (solid lines) profiles of the (a) 30 mm and (b) 50 mm thick half-split rubberwood specimens containing relatively high (HS) and low (LS) levels of internal stress at various half-split lengths.

# 4.3.3 Validation of $\sigma_{\scriptscriptstyle m}$ derived from the restoring force technique

The released strain and Young's modulus in the tangential direction plus moisture content distributions within the 30 mm and 50 mm thick HS and LS specimens obtained from the McMillen's slice test are shown in Figure 4.7 - 4.9. The elastic strains due to the release of internal stresses of both 30 mm and 50 mm were not uniform (Figure 4.7a-b). After slicing of the surface layer, lengthening with a positive value of released strain indicates that the wood in this layer was under compressive internal stress before being sliced. On the other hand, a negative released strain observed at the core layer indicates a tensile internal stress. This behavior has been reported for casehardening of kiln-dried lumber by various authors (McMillen 1958; Simpson 1999). Within the 30 mm thick specimens, moisture content was approximately uniform across the lumber thickness with the average values of 6.2±0.4 % and 10.2±0.5 % in the HS and LS specimens, respectively (Figure 4.8a). Larger variation of moisture content was observed in the 50 mm thick specimens with the average values of 6.9±1.2 % and 9.0±0.9 % in the HS and LS specimens, respectively (Figure 4.8b). Since moisture contents were lower in the HS specimens therefore Young's modulus in these specimens (585±112 MPa in the 30 mm thick and 657±116 MPa in the 50 mm thick specimens) were higher than those in the LS specimens (477±91 MPa in the 30 mm thick and 611±145 MPa in the 50 mm thick specimens) (Figure 4.9a-b).

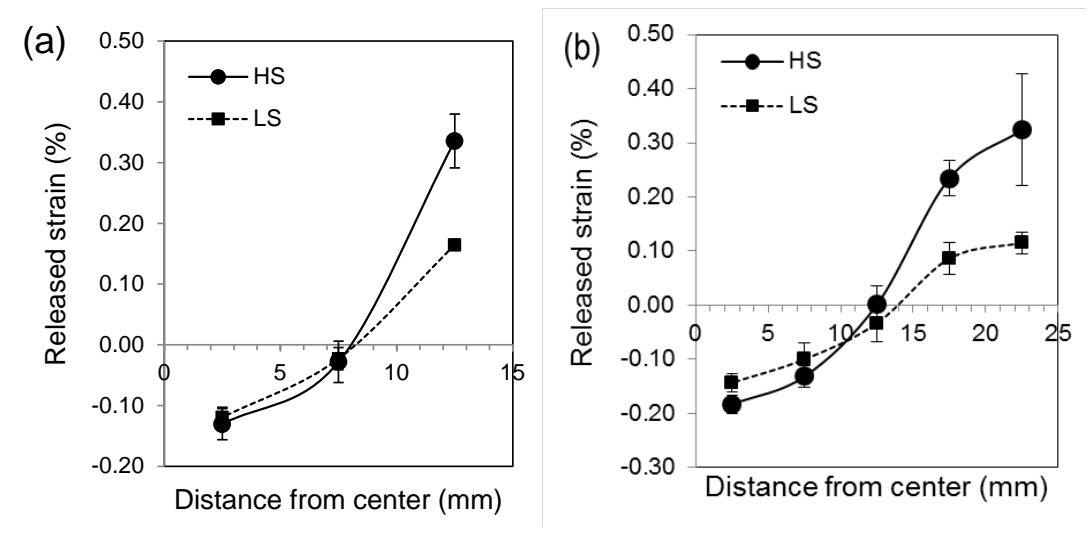
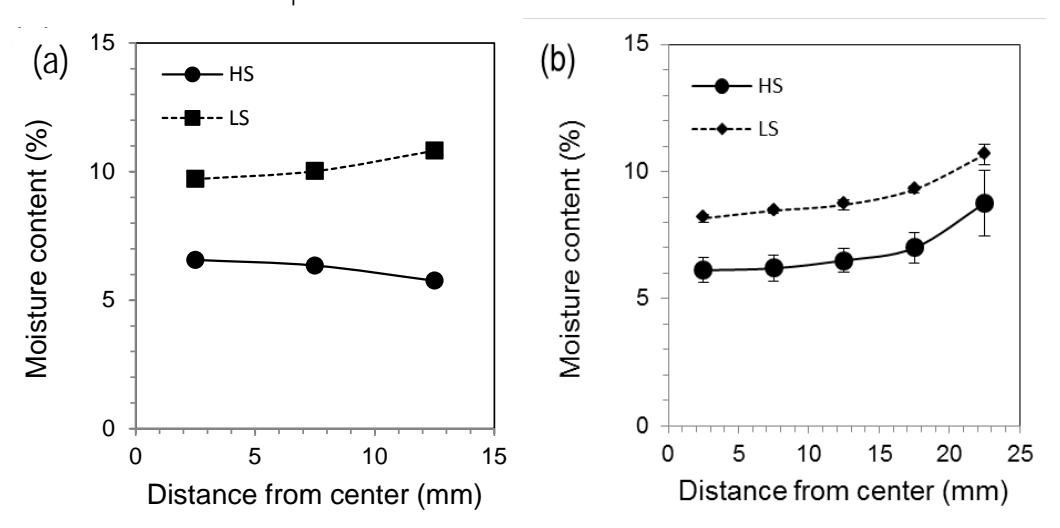
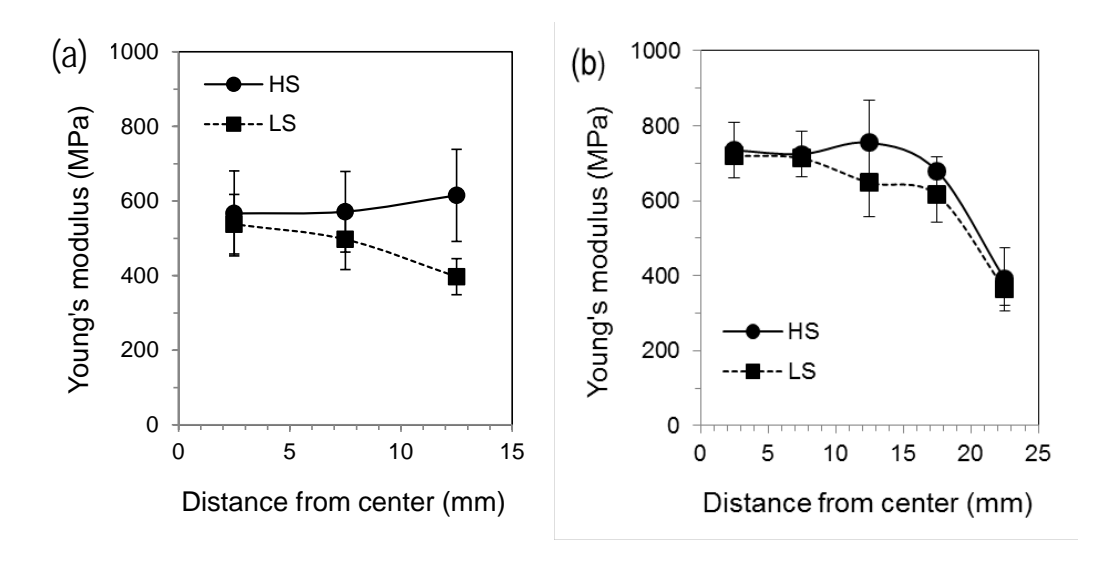


Figure 4.7 Distributions of released elastic strain within the (a) 30 mm and (b) 50 mm thick HS and LS specimens.

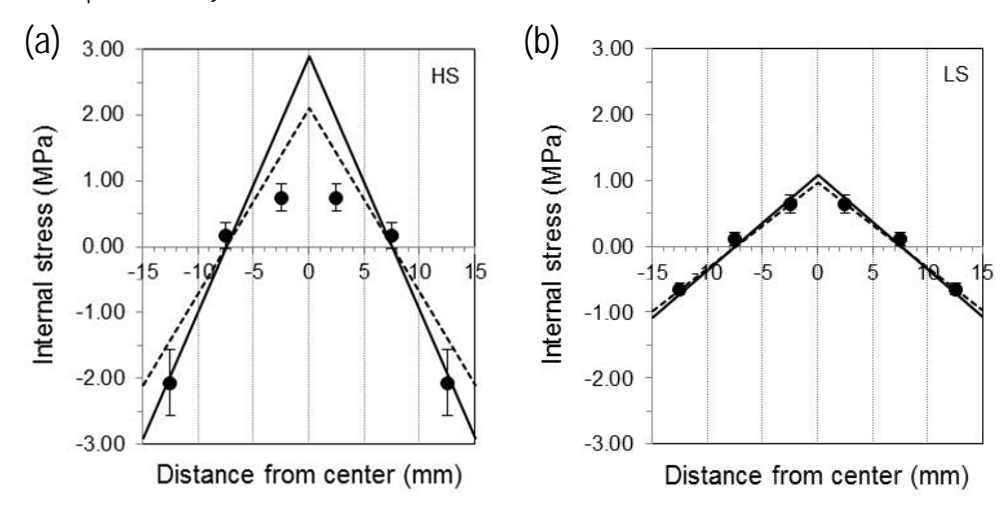


**Figure 4.8** Distributions of moisture content within the (a) 30 mm and (b) 50 mm thick HS and LS specimens.



**Figure 4.9** Distributions of Young's modulus within the (a) 30 mm and (b) 50 mm thick HS and LS specimens.

Corresponding internal stress profiles, product of the released strain and the Young's modulus for each slice, are shown in Figure 4.10a-d. The Poisson's ratio effect is assumed to be negligible. A linear average to the stress data was performed across the thickness. Corresponding maximum stresses  $\sigma_{\mathrm{m}}$  obtained were 2.10 MPa and 0.97 MPa for the 30 mm thick HS and LS specimens and 1.94 MPa and 1.04 MPa for the 50 mm thick HS and LS specimens, respectively. These values are in general agreement with those derived from the restoring force technique of 2.90 MPa and 1.08 MPa for the 30 mm thick HS and LS specimens and 3.37 MPa and 1.67 MPa for the 50 mm thick HS and LS specimens, respectively. A very close agreement is observed in the LS specimens where the internal stress profile is relatively low and roughly linear (Figure 4.10b and Figure 4.10d). At higher levels of internal stress, the stress profile deviates from the linear distribution. The maximum stresses at the surface and the core layer are different. Values of  $\sigma_{\scriptscriptstyle \rm m}$  both underestimate and overestimate the maximum compressive stress at the surface layer and the maximum tensile stress at the core layers, respectively (Figure 4.10a and Figure 4.10c). Nevertheless, a single value of  $\sigma_{
m m}$ , representing the average maximum magnitude of the internal stress within the kiln-dried lumber, should be a simple and convenient stress indicator to be used in lumber industry. Validation of  $\sigma_{
m m}$  obtained from the restoring force technique should be performed against other well-developed internal stress measurement techniques (Schajer and Ruud 2013) in the future.



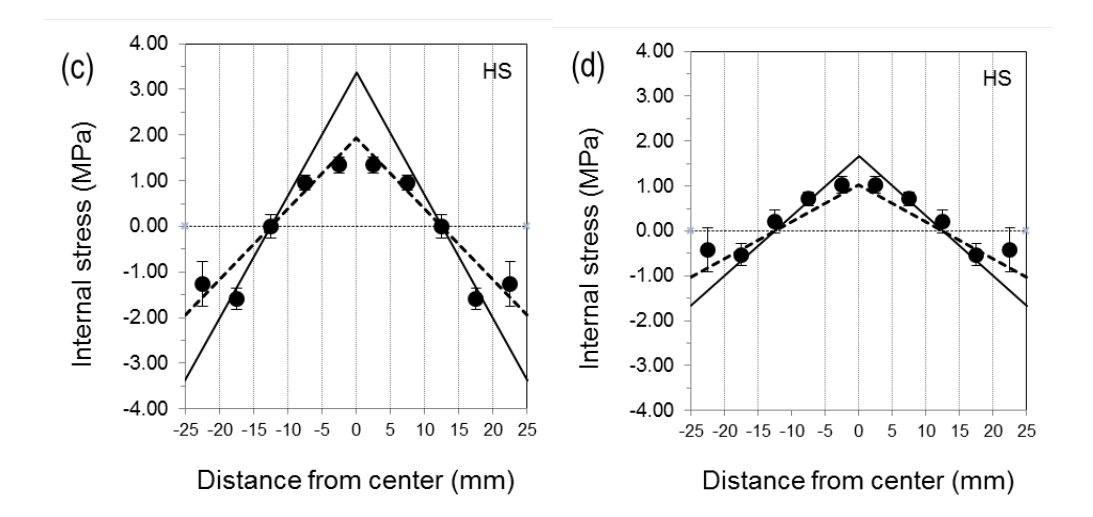


Figure 4.10 Distributions of the calculated internal stresses within (a) the 30 mm thick HS, (b) the 30 mm thick LS, (c) the 50 mm thick HS and (d) the 50 mm thick LS, specimens. Linearly averaged internal stress profiles obtained from the slice test (dashed lines) and the proposed restoring force technique (solid lines) are also displayed for comparison.

# 4.3.4 The restoring force-internal stress chart

Intended for practical use in the lumber industry, the chart of restoring force versus half-split length plotted at different levels of internal stress is created in Figure 4.11 – Figure 4.12. The demonstration was made in this work for 30 mm thick lumber with length in the longitudinal direction of 50 mm and the restraining point at 10 mm from the top end. Two sets of three 30 mm thick industrial kiln-dried rubberwood lumber were used. Stress relaxation of the kiln-dried lumber during conditioning at 85 °C and 80 % RH inside the conditioning chamber and during storage in ambient air at  $28\pm2$  °C and  $75\pm6$  % RH was investigated using the chart. The half-split length employed was from 60 mm to 100 mm, a suitable range as mentioned in section 4.3.2.

The measured restoring forces obtained from each group of lumber roughly follow a particular stress level line. The magnitude of  $\sigma_{\rm m}$  can be directly assessed through the chart. It can be seen in Figure 4.11 that after kiln drying,  $\sigma_{\rm m}$  was 3.3 MPa and after conditioning for 30 minutes and 90 minutes, it was reduced to 1.5 MPa and 0.6 MPa, respectively. For the second set of kiln-dried lumber, storage in ambient air for 10 days and 20 days reduced  $\sigma_{\rm m}$  to 1.8 MPa to 1.0 MPa, respectively (Figure 4.12).

The restoring force measurement on the half-split specimens together with the use of the proposed restoring force-internal stress chart should be a useful tool in estimating the magnitude of internal stress within industrial kiln-dried lumber. This technique should give a reliable and meaningful stress measurement and is easy to perform. Ongoing research focuses on determining  $\sigma_{\rm m}$  outside the flexural response regime, which is not covered by this model especially with relatively narrow (W < 90 mm) or thick (d > 30 mm) lumber.

Finite element analysis will be employed to study the complex stress behavior outside the flexural response regime.

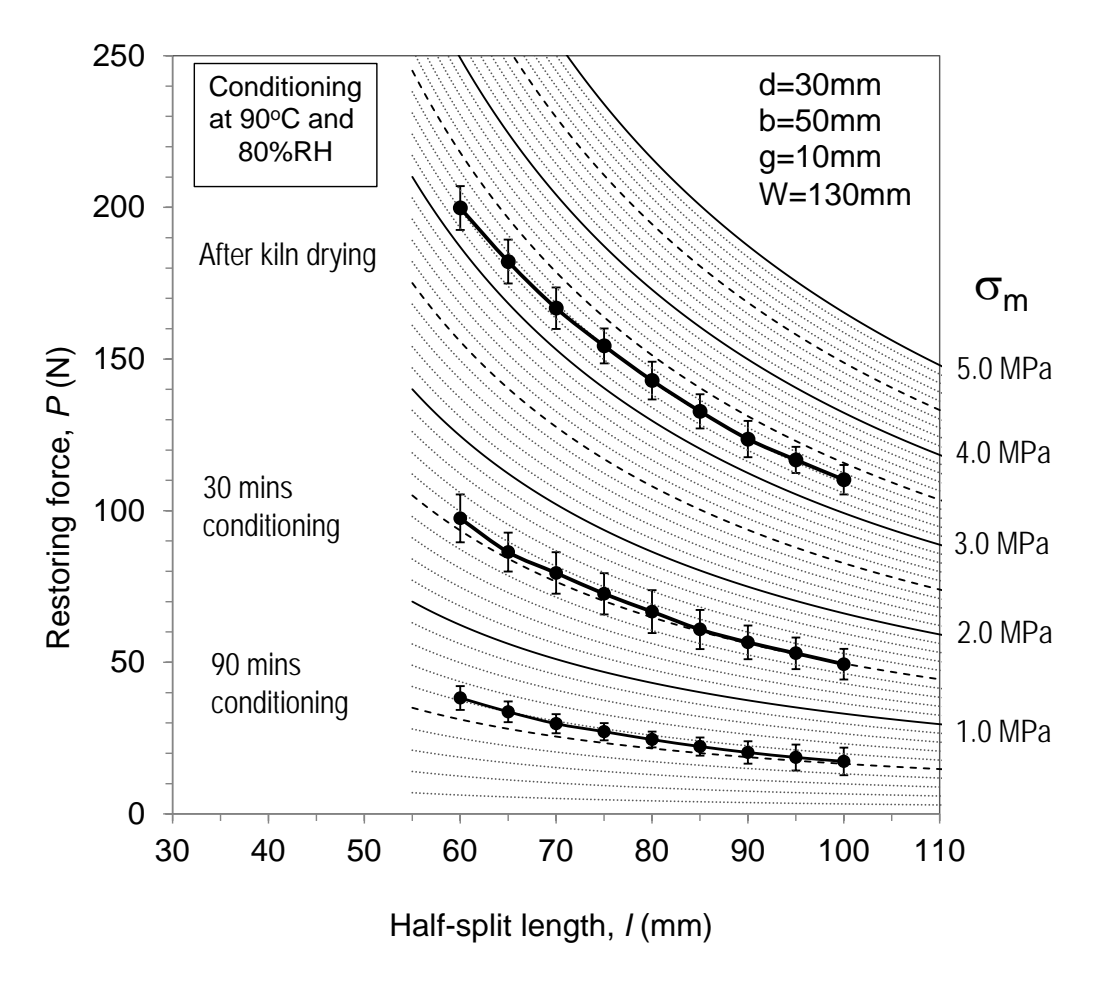


Figure 4.11 Determination of  $\sigma_{\rm m}$  using the restoring force-internal stress chart by plotting the measured values of the restoring force as a function of the half-split length of the 30 mm thick and 130 mm wide kiln-dried lumber during conditioning at 85 °C and 80 % RH.

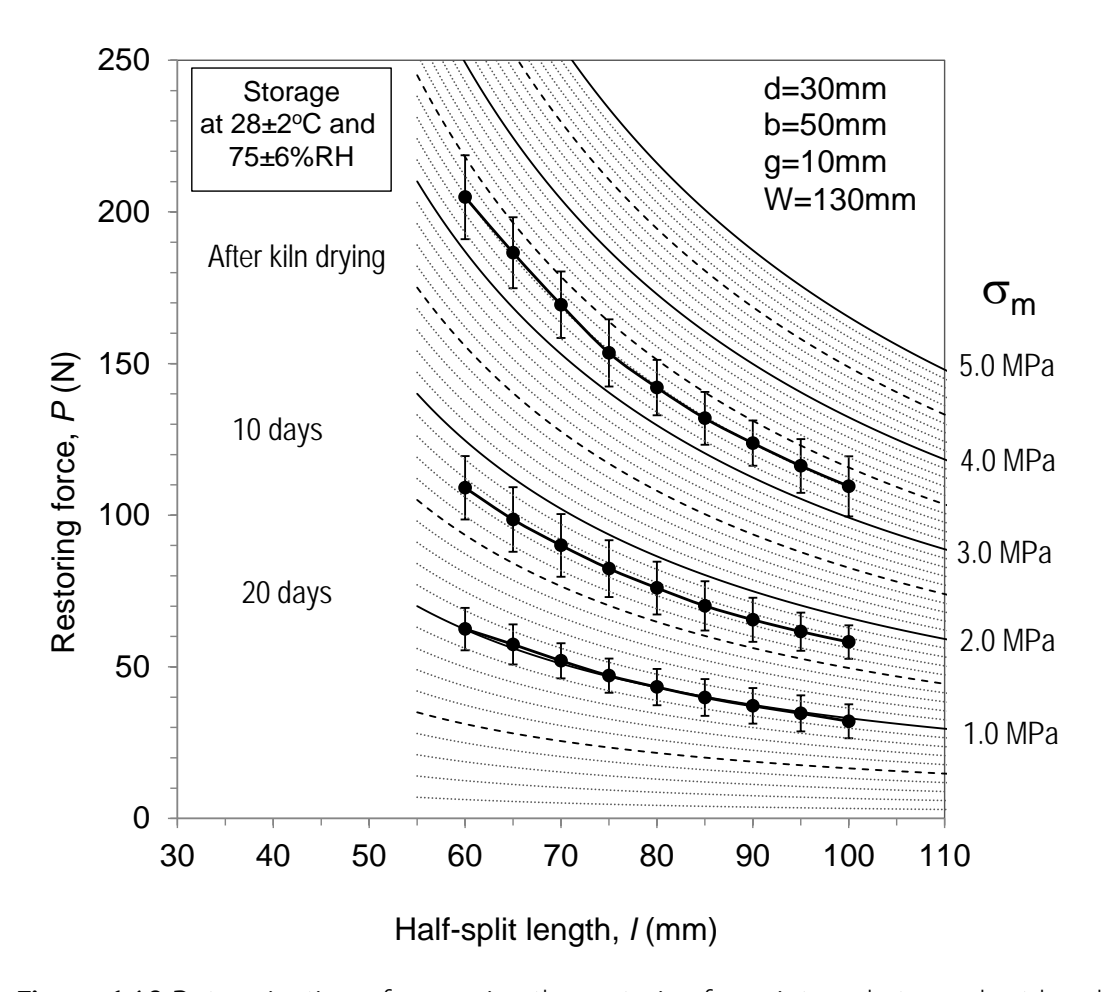


Figure 4.12 Determination of  $\sigma_{\rm m}$  using the restoring force-internal stress chart by plotting the measured values of the restoring force as a function of the half-split length of the 30 mm thick and 130 mm wide kiln-dried lumber during storage in ambient air at 28±2 °C and 75±6 % RH.

#### 4.4 Conclusions

The following conclusions can be drawn from this chapter:

- 1. The magnitude of the restoring force is dependent on the half-split length and thickness of the specimens. With increased half-split length, the restoring force sharply increases, reaches the maximum value and then gradually decreases. Higher restoring force is obtained in the thicker lumber.
- 2. The model based on an elastic cantilever beam theory has been successfully developed to directly deduce the maximum linearly averaged internal stress from the measured restoring force data within the flexural response regime. No information on the modulus of wood is required in the calculation. In the 30 mm thick lumber, the flexural range is between the half-split lengths from 60 to 100 mm. This flexural range becomes smaller in the thicker lumber.

- 3. General agreement is found between the magnitudes of the maximum linearly averaged internal stress derived from the restoring force technique and the conventional McMillen slice technique, especially in the specimens having a relatively low and roughly linear stress profile.
- 4. The restoring force-internal stress chart has been proposed for a practical use in the lumber industry. A demonstration was carried out to follow stress relaxation during conditioning and during storage of industrial kiln-dried rubberwood lumber.

## References

- 1. Bodig J, Jayne BA (1982) Mechanics of wood and wood composites. Van Nostrand Reinhold Company, New York
- 2. Hibbeler RC (2012) Structural analysis. Prentice Hall, New Jersey
- 3. Lados DA, Apelian D (2006) The effect of residual stress on the fatigue crack growth behavior of Al-Si-Mg cast alloys-mechanisms and corrective mathematical models. Metall Mater Trans A 37:133–145
- 4. McMillen JM (1958) Stresses in wood during drying (Report 1652). Department of Agriculture, Forest Service, Forest Products Laboratory, Madison
- 5. Matan N, Kyokong B (2003) Effect of moisture content on some physical and mechanical properties of juvenile rubberwood. Songklanakarin J Sci Technol 25(3):327–340
- 6. Simpson WT (1999) Chapter 12: drying and control of moisture content and dimensional changes. In: Wood handbook (Wood as an Engineering Material). Department of Agriculture, Forest Service, Forest Products Laboratory, Madison
- 7. Sonderegger W, Martienssen A, Nitsche C, Ozyhar T, Kaliske M, Niemz P (2013) Investigations on the physical and mechanical behavior of sycamore maple (*Acer pseudoplatanus* L.) Eur J Wood Prod 71:91–99
- 8. Walton HW (2002) Deflection methods to estimate residual stress. In: Totten G, Howes M, Inoue T (eds) Handbook of residual stress and deformation of steel. ASM International, Ohio, pp 89–98

# Chapter 5

# Interpretation of restoring force of lumber with several stress components

## 5.1 Introduction

Internal stress is always created within a piece of lumber during kiln drying as a result of the presence of moisture gradient which induces differential shrinkage between the outer and the inner core sections (McMillen 1958, Perre´ and Passard 2007). Even after the lumber is dried, residual compressive and tensile stresses continue to exist in the outer and the inner core layers, respectively (McMillen 1958; Simpson 1999). Remanufacturing of the stress-containing lumber can lead to a significant increase in losses due to distortion (Wengert 1992; Cai and Oliveira 2004). A reliable quantitative assessment of the residual stress is therefore crucial for a successful quality control (Welling 1994) and a development of effective stress relief procedure (Wengert 1992; Pang et al. 2001) of kiln-dried lumber.

To evaluate the internal stress remained within a piece of lumber, several stress relaxing techniques have been proposed since 1950s. The McMillen slice test (McMillen 1958) has been traditionally employed to assess the stress level within a kiln-dried lumber. This method determines the mechanical response of stress relaxation within slices cut from a lumber board. The released strain in each slice can be calculated by measured deformation. By knowing the modulus of elasticity, the released stress in each slice can then be calculated from the measured strain. Because of difficulties in measuring relatively small released strain of several wood slices, the later proposed prong test (Simpson 1991) and the case-hardening test (European Committed for Standardization 2010) performed by measuring a deflection caused by removing some sections or splitting of the lumber instead, have been commonly employed by kiln operators in sawmills. In all cases, the modulus of elasticity, depending on multiple influences including moisture, specific gravity, grain direction, temperature and so on (Bodig and Jayne 1982; Matan and Kyokong 2003; Kretschmann 2010; Sonderegger et al. 2013), is needed to relate measured strain or deflection profiles and IS.

To directly assess the magnitude of the internal stress without a requirement of the modulus data of the wood, a novel force based approach of measuring a restoring force on a so called "half-split" specimen has been first proposed by Diawanich et al. (2012). The deformed specimen sawn at half thickness was installed onto the universal testing machine and the force required for stretching back the specimen to the initial shape was measured. However, the position of returning the shape back to the initial configuration was ambiguous because the deformation was small, so the error depended on judgment of the tester. Jantawee et al. (2016) later improved the measurement technique by inventing a new

apparatus to restrain the specimen to the rigid steel frame while being cut by using a band saw. The net force caused by the stress relaxation within the half-split specimen at any cutting lengths was directly transferred to the steel rod connected the load cell. Direct interpretation of the internal stress from the measured restoring force data has also been developed by Jantawee et al. (2016) through the use of the geometrical shape factor derived by using an elastic cantilever beam theory. In addition, the stress chart related to the measured restoring force has been constructed for convenient use in the lumber industry.

However, there still exist two important limitations in Jantawee et al. (2016) calculations. First, only stress component in the width direction was taken into account. The effects of other stress components including stresses in the thickness and the length directions were assumed to be negligible. The flat-sawn lumber used in Jantawee et al. (2016) were selected such that stresses in thickness and length directions were relatively small compared to those in the direction of width. Second, the model based on an elastic cantilever beam theory was not valid outside the flexural response range especially at relatively short half-split length in the narrow piece of lumber. The main objective of this work is to tackle these two limitations. Some adjustments to the calculations and the restoring force-internal stress chart are made to separate the effects of other stress components for a better estimation of the main internal stress in the width direction. Finite element analysis is employed to validate and gain more understanding of the internal stress behavior for an entire range of half-split length. Emphasis is placed on investigation of the 30mm thick kiln-dried rubberwood lumber.

#### 5.2 Materials and method

#### 5.2.1 Measurements of the restoring force and the released strain

Thirty pieces of flat-sawn industrial kiln-dried rubberwood lumber were taken from a local sawmill in Nakhon Si Thammarat, Thailand. The lumber was 30 mm thick (d) in the radial direction, 100-130 mm wide (W) in the tangential direction and approximately 1 m long in the longitudinal direction. They were separated into two sets. The first set ( $P_0\sim0$ ) was specially selected to meet a requirement stated by Jantawee et al. (2016) that the internal stress mainly exists in the direction of width and other stress components such as in the thickness and length directions are negligible. Since the lumber was rare, so only a single piece of lumber was used. The second set ( $P_0\neq0$ ) was randomly taken for 15 pieces. A piece of wood was removed at approximately 50 mm away from the end of each lumber before making six wood specimens of 50 mm long (b) (Figure 5.1a). Two adjacent specimens were used for measurements of the restoring force according to Jantawee et al. (2016) and the released strain according to the McMillen slice test (McMillen 1958). Therefore, there were

three replicates for both the restoring force and the slice test measurements for each lumber. All prepared specimens were free from defects such as knots and spiral grain. The measurements were performed at two levels of internal stress i.e. at high internal stress (HS) and low internal stress (LS). Assessment of HS was immediately performed on the day the lumber obtained. The remaining pieces of lumber were capped with aluminum foil at both ends and were kept in the conditioning chamber at 20°C and 65%RH for 4 weeks. Then assessment of LS was again performed after the internal stress was partially relaxed to the lower level.

The restoring force measurement was performed using the device (Figure 5.1b) described by Jantawee et al. (2016), the specimen was clamped onto the steel frame by the screws at a distance (g) of 10 mm from the top surface. Small torque, 2-3 N·m, was applied to hold the specimen in place with a contact screw area of 24 mm<sup>2</sup> without damaging wood tissue (Jantawee, 2016). While being clamped to the frame, the specimen was cut at half thickness in a wide direction along a half-split length (I). The restoring force was then recorded at 5 mm intervals. For the McMillen slice test, the specimen surfaces in the thickness direction were first slightly planned to remove irregularities to obtain a relatively smooth surface before being marked by divided lines so it could be cut into six equal slices. The initial width of each pre-marked slice  $(W_b)$  was measured by calipers having a precision of 0.01 mm. Measurement positions on each slice were marked so that the following width measurements after slicing could be performed at the same positions. The specimens were then cut into slices along the pre-marked lines. Each slice was subsequently pressed flat before its width,  $W_a$ , was measured. Care was also taken to ensure that about the same force was applied on the caliper for every measurement. The released strain of each slice was calculated according to  $\varepsilon=\frac{W_a-W_b}{W}$  . All slices were tested to determine the Young's modulus in the tangential direction ( $E_T$ ) using a universal testing machine (Lloyd 150kN, UK) equipped with a strain gauge (Epsilon Technology, USA). A section of each slice was also weighted before and after oven-drying at 103±2°C for 24 hours to determine its moisture content.

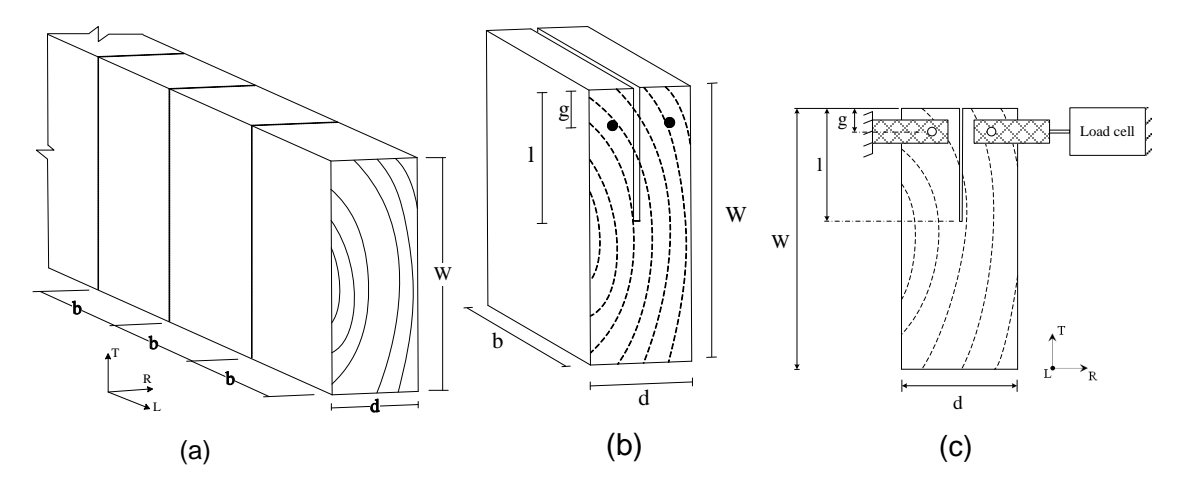


**Figure 5.1** (a) The test specimen cut from the lumber board, (b) the half-split specimen for the restoring force measurement and (c) diagram of the restoring force measuring apparatus.

# 5.2.2 Finite element analysis of the restoring force technique

To validate the mechanical response of the restrained half-split specimen, the three-dimensional finite element (FE) model was generated using SOLID186 elements in ANSYS v12. The constitutive model of linearly elastic three mutually orthogonal materials was given into the computational process. According to Bodig and Janye (1982), all moduli were determined as ratios of the measured modulus of elasticity in the tangential direction ( $E_L$ :  $E_R$ :  $E_T$  = 20 : 1.6 : 1,  $G_{LR}$ :  $G_{LT}$ :  $G_{RT}$  = 10 : 9.4 : 1 and  $E_L$ :  $G_{LR}$  = 14 : 1). Three Poisson's ratios were estimated to be  $\mu_{RL}$  = 0.02,  $\mu_{LT}$  = 0.02 and  $\mu_{RT}$  = 0.35 (Bodig and Jayne 1982; Kretschmann 2010). Since the specimen had two planes of symmetry, only a quarter of specimen was constructed (Figure 5.2) to reduce computational time in the solving process. Two planes of symmetry (LT and RT) were fixed in the R- and L-directions, respectively. All nodes in the clamping (screw) area were restrained in the R-direction to deduce the calculated restoring force,  $P_{col}$ . The released strain and Young's modulus data of the  $P_o \sim 0$  and  $P_o \neq 0$  sets of lumber determined by the McMillan slice test were applied to the layers corresponded to the tests.

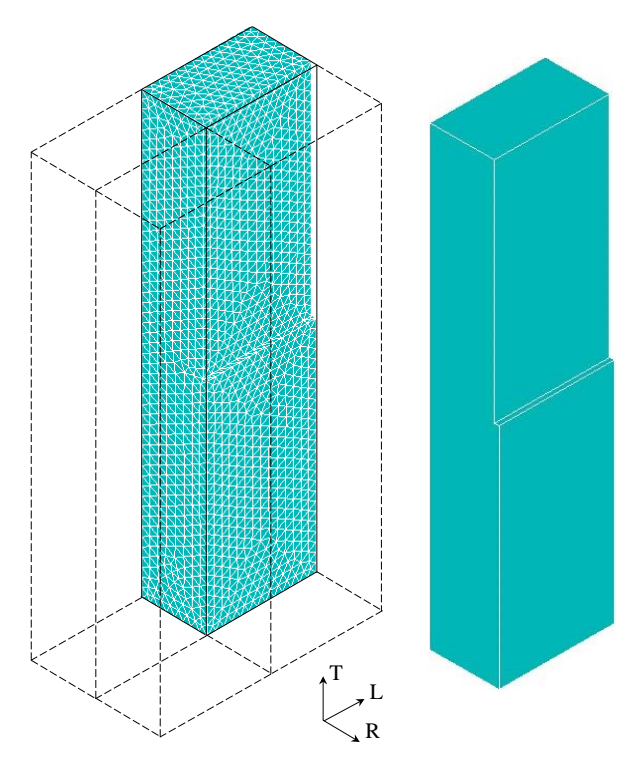


Figure 5.2 The 3D mesh for a quarter of the specimen used in finite element simulation.

# 5.2.3 Internal stress relaxation of kiln-dried rubberwood lumber

Three pieces of about 1 m long kiln-dried rubberwood lumber ( $P_o \ne 0$ ) were randomly selected from a local sawmill in Nakhon Si Thammarat, Thailand. Pieces of lumber had the thickness of 30 mm (d) and the width of 130 mm (W) Care was taken to ensure that the lumber thickness aligned in the radial direction. Three defect-free specimens were cut at about 50 mm away from the end of each lumber to the length of 50 mm (b). The residual stress in the half-split specimens was determined by using the restoring force measuring device at cutting length from 60 mm to 100 mm (in the flexural range) at every 5 mm intervals. The remaining pieces of lumber were coated with aluminum foil at both ends and stored in the conditioning chamber at 20°C and 65%RH. Every subsequent week up to 3 weeks, the stored pieces of lumber were taken for evaluating the restoring force.

#### 5.3 Results and discussion

5.3.1 Analytical calculation of internal stress in the presence of other stress components

For a piece of lumber which is half-split at a particular length l, the value of the restoring force P is proportional to the maximum internal stress in the width direction  $\sigma_{\rm m}$ , assumed to linearly vary from the outer surface through the inner core, according to

$$P = \frac{4bl^2}{Sd}\sigma_{\rm m} \tag{5.1}$$

$$S = \frac{32(l-g)^2(2l+g)}{d^3}$$
 (5.2)

where S is the geometrical factor (Jantawee et al. 2016). The value of P has been shown to be proportional to the term  $\frac{4bl^2}{Sd}$  with zero intercept at relatively low value of  $\frac{4bl^2}{Sd}$  or at relatively long half-split length in a so-called the flexural response regime. Consequently, the magnitude of  $\sigma_{\rm m}$  in the width direction can be directly obtained from the slope of the graph plotted between P and the term  $\frac{4bl^2}{Sd}$ . Effect of other stress components has been neglected in the above calculation and all lumber boards examined in Jantawee et al. (2016) were selected to contain relatively low level of stress in the other directions. This is the case for the Po~0 set of specimens shown in Figure 5.3a in which the magnitudes of  $\sigma_{\rm m}$  derived from the graphs are 2.62 MPa for the HS specimens and 1.02 MPa for the LS specimens, respectively.

The above limitation has been lifted within this work. All flat-sawn boards ( $P_o \neq 0$ ) have been randomly selected without any restrictions. Typical plots of P against the term  $\frac{4bl^2}{Sd}$  are shown in Figure 5.3b. Linear relationship between P and  $\frac{4bl^2}{Sd}$  is still observed in the flexural response regime but with a particular value of a positive y-intercept. Therefore, equation (5.1) has been modified to be

$$P = \frac{4bl^2}{Sd}\sigma_{\rm m} + P_o \tag{5.3}$$

where  $P_o$ , the y-intercept, is the remnant restoring force value where the term  $\frac{4bl^2}{Sd}$  is equal zero. This restoring force remains when the half-split length approaches infinity. The magnitudes of  $\sigma_m$  and  $P_o$  derived from the graphs are 2.46 MPa and 77.61 N for the HS specimens and 0.71 MPa and 56.42 N for the LS specimens, respectively (Figure 5.3b). According to equation (5.3), the calculated restoring forces at those magnitudes of  $\sigma_m$  and  $P_o$  derived are compared with the experimental values in Figure 5.4a-b. An excellent agreement between the calculated and the measured restoring force values can be observed in the flexural response regime between the half-split lengths from 45 mm to 110 mm in the HS specimens and from 60 mm to 110 mm in the LS specimens. During conditioning of the specimens at 20°C and 65%RH, the magnitudes of  $\sigma_m$  reduces by 71% from 2.46 MPa to 0.71 MPa while the values of  $P_o$  reduces by 27% from 77.61 N to 56.42 N.

The plots of P against  $\frac{4bl^2}{Sd}$  of other lumber boards randomly selected (14 boards) also show similar behavior and are governed by equation (5.3) (data shown in supplement material). Therefore the equation (5.3) must be universal to any pieces of lumber. The first term in equation (5.3) is the restoring force caused by the flexural response of the internal

stress relaxation in the width (tangential) direction after half-splitting as mentioned in Jantawee et al. (2016). The presence of  $P_o$  is expected to be caused by relaxation of other stress components especially in the thickness and the length directions which are irrelevant to bending of the half-specimen's legs. Investigation on the possible origin of  $P_o$  using the finite element model is described in the previous sections.

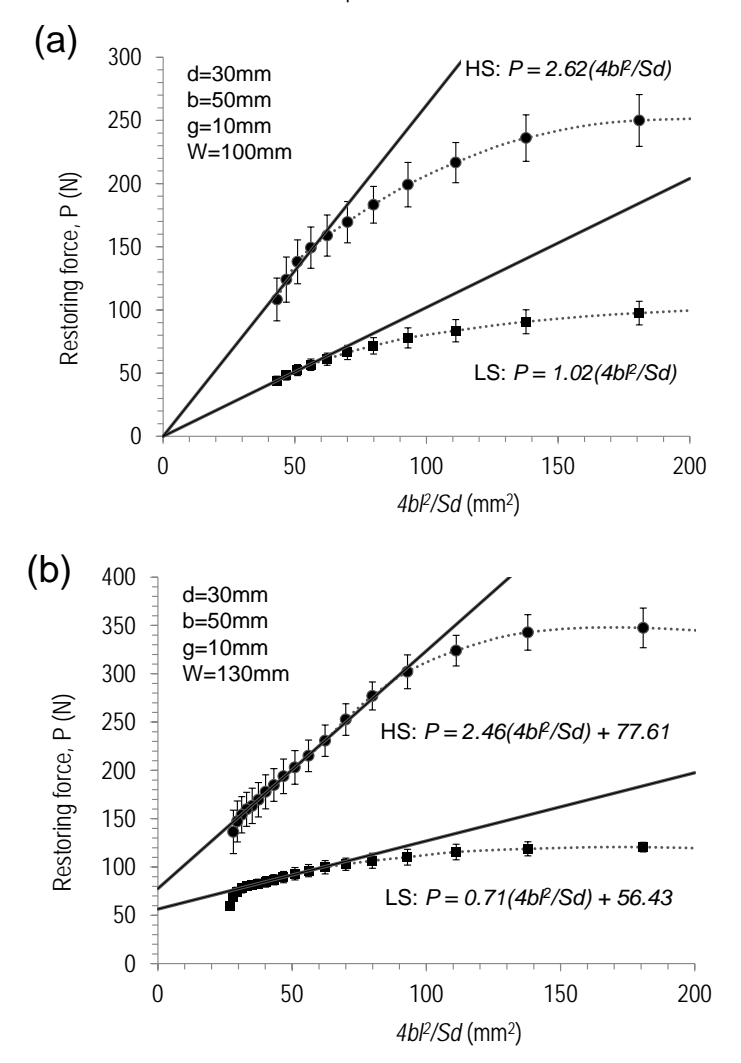


Figure 5.3 Plots of the restoring force versus  $\frac{4bl^2}{Sd}$  for the 30 mm thick half-split (a)  $P_o \sim 0$  and (b)  $P_o \neq 0$  rubberwood specimens containing relatively high (HS) and low (LS) levels of internal stress. Solid lines represent the best fits to the experimental data in the flexural response regime.

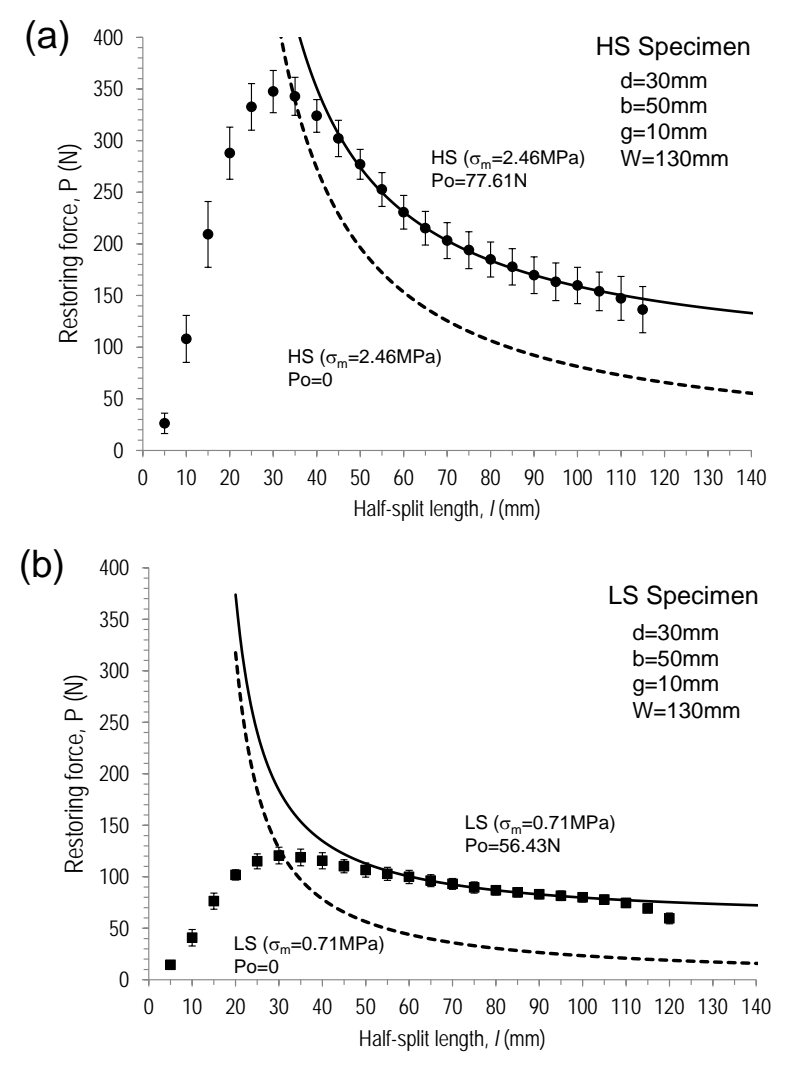
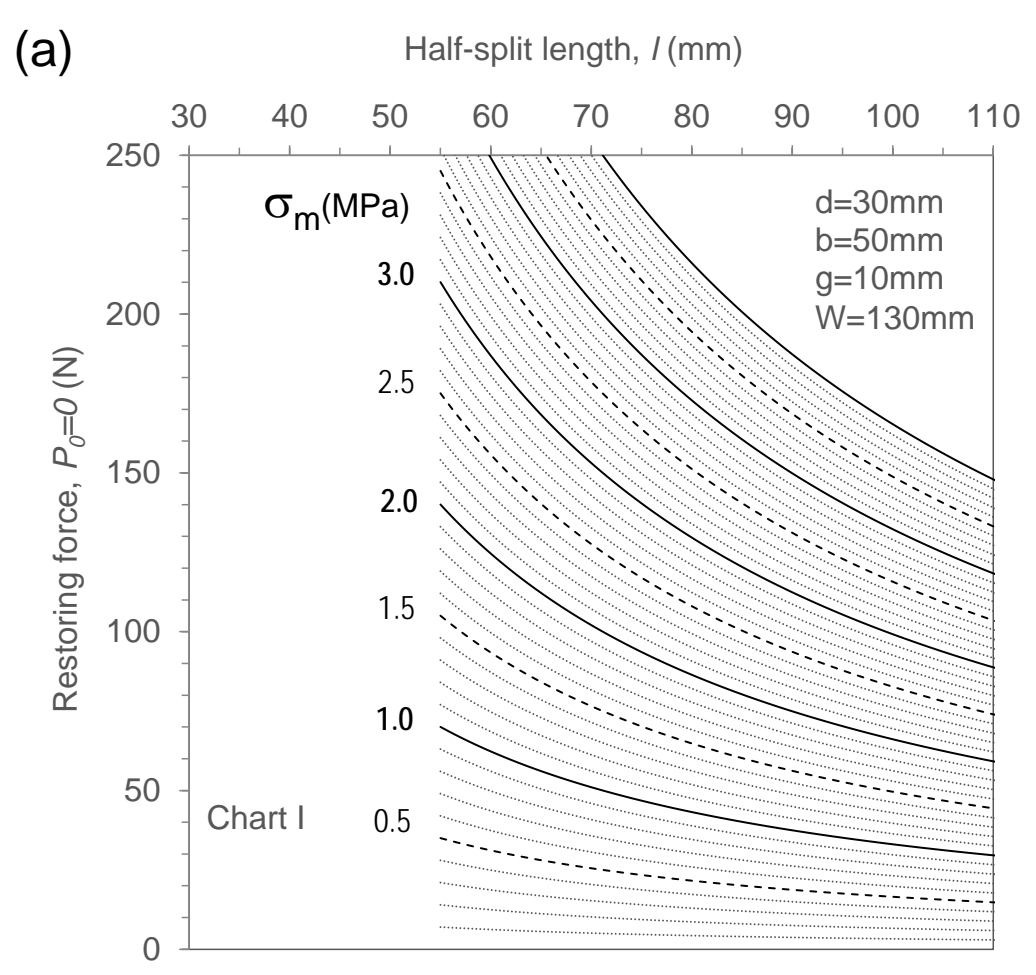


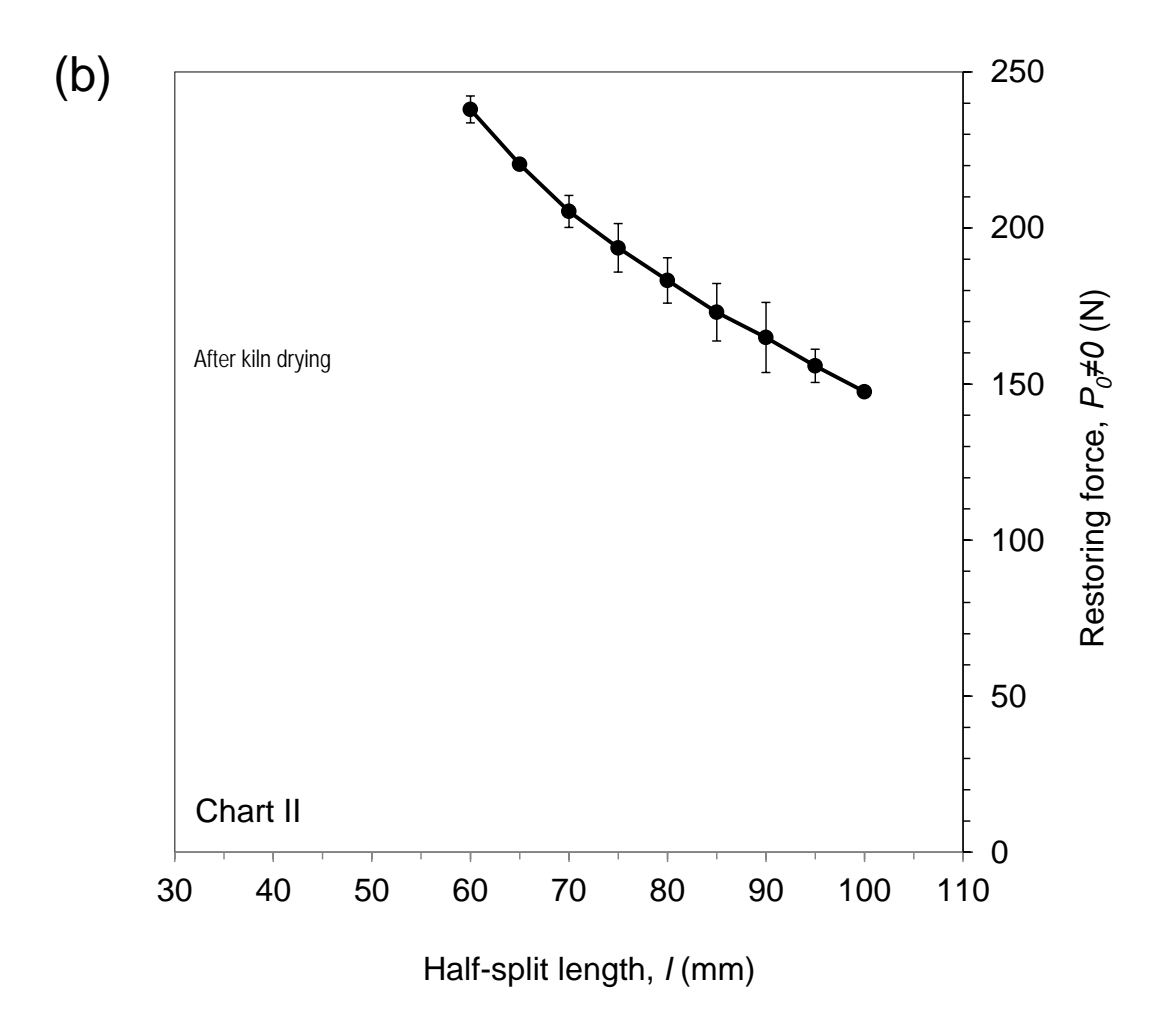
Figure 5.4 Comparison of experimental (symbols) and calculated restoring force (solid lines) profiles of the 30 mm thick half-split  $P_o \ne 0$  rubberwood specimens containing relatively (a) high (HS) and (b) low (LS) levels of internal stress at various half-split lengths. The calculated restoring force profiles without  $P_o$  (dash lines) are also shown for comparison.

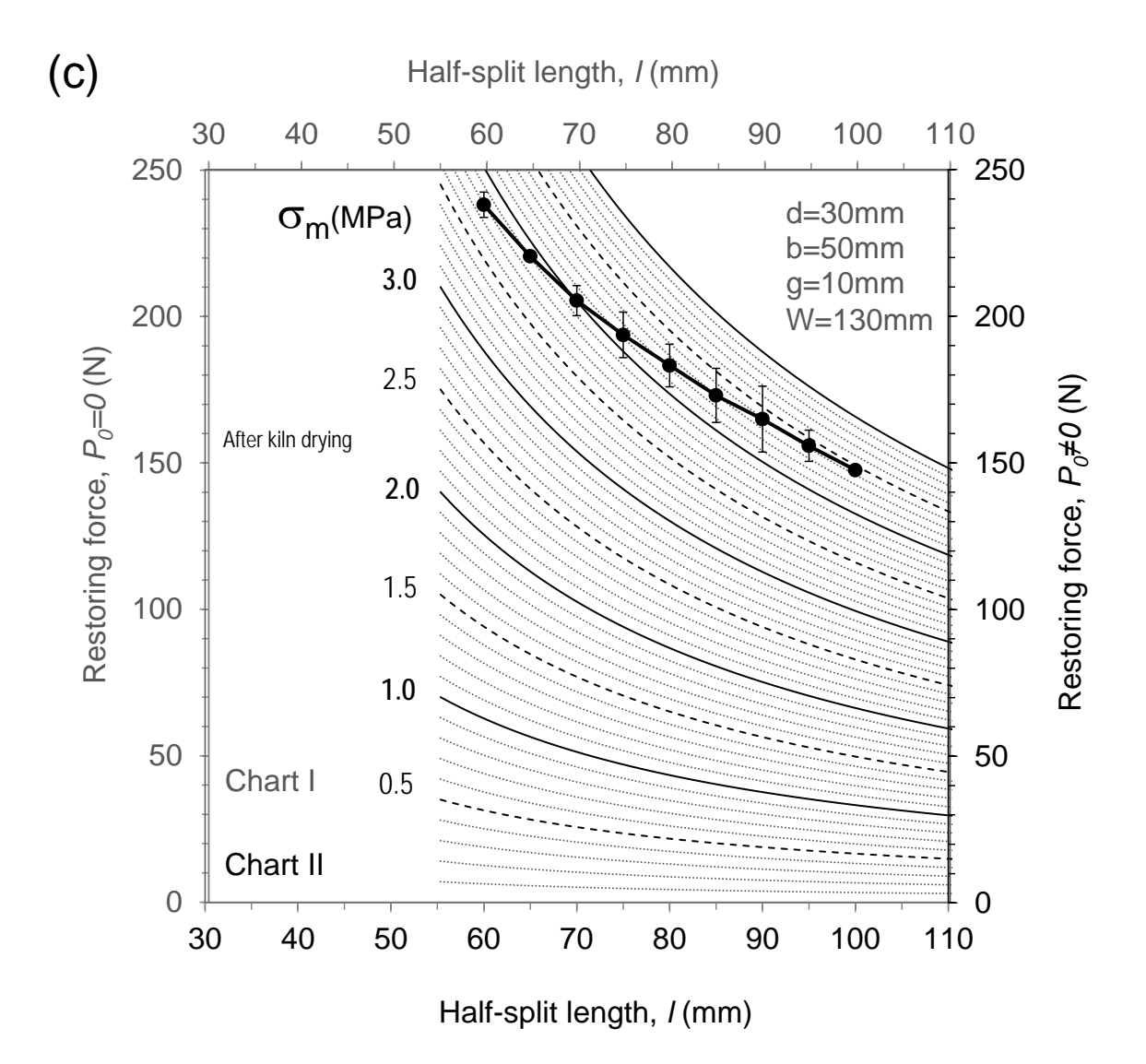
# 3.2 The universal restoring force-internal stress chart

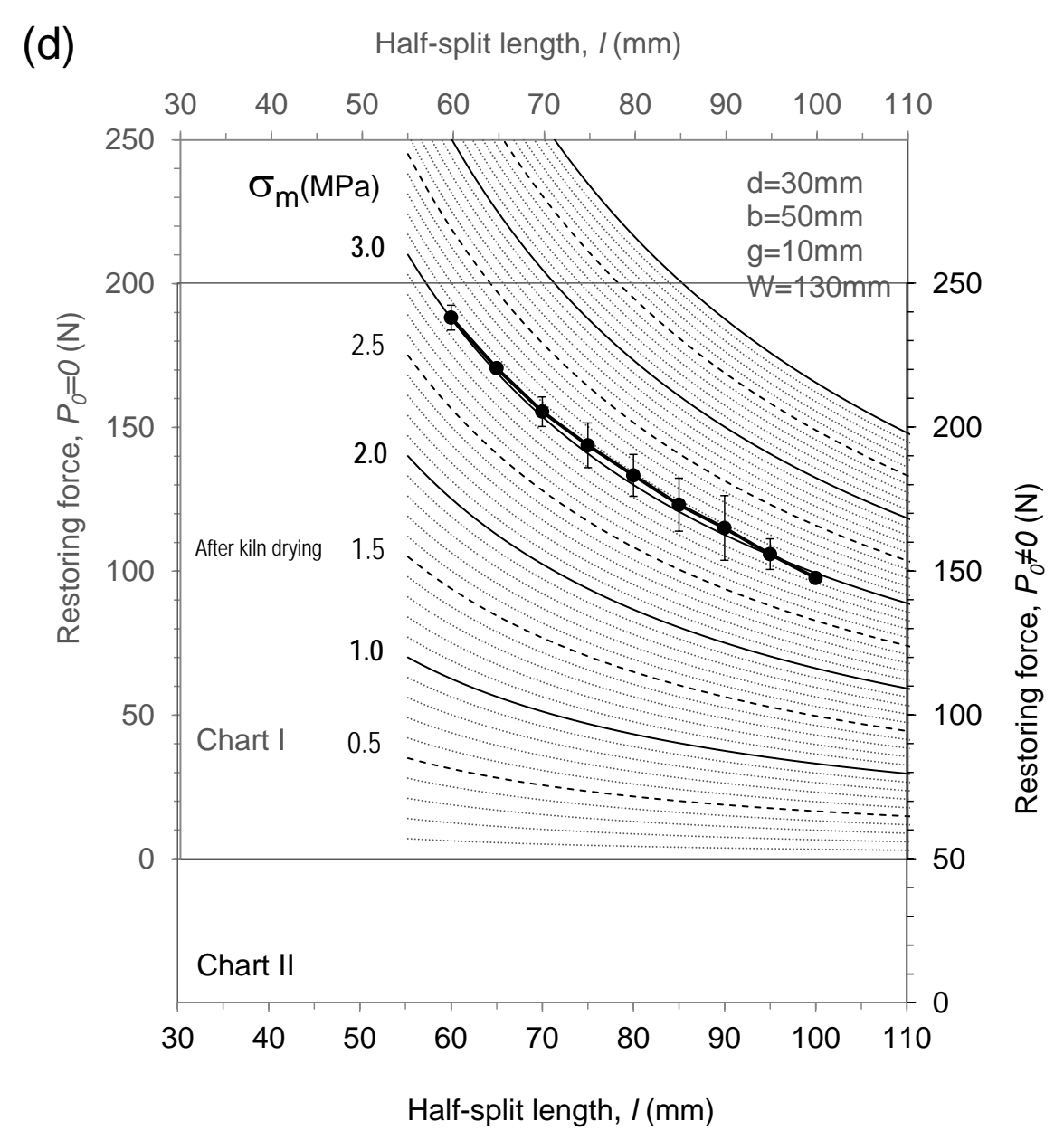
For practical use in the lumber industry, Jantawee et al. (2016) developed the restoring force-internal stress chart for the half-split specimen in which only the internal stress in the width (tangential) direction is assumed to dominate. The chart proposed by Jantawee et al. (2016) is successfully described the restoring force profiles of the  $P_o\sim0$  specimens. Within this work, the chart is improved in order to deduce both values of  $\sigma_m$  and  $P_o$  from the restoring force profile obtained from the  $P_o\neq0$  half-split specimens. A demonstration was performed to investigate the relaxation of internal stress during the conditioning of kiln-dried rubberwood lumber at 20°C and 65%RH. Figure 5.5a (Chart I) shows the restoring force-internal stress chart at  $P_o=0$  for the specimen with dimension similar to that reported by Jantawee et al. (2016). The restoring force profile as a function of the half-

split length of the industrial kiln-dried rubberwood lumber just after kiln drying is shown in Figure 5.5b (Chart II). Overlaying of Chart II on Chart I is displayed in Figure 5.5c. It is clear that because of the presence of  $P_o$ , the restoring force profile on Chart II does not follow any stress level lines on Chart I. By moving Chart I and Chart II in the vertical direction relative to one another, the restoring force profile does match a particular stress level line (Figure 5.5d). The magnitude of  $\sigma_m$ , caused by the flexural response of the internal stress relaxation in the width direction after half-splitting, can be read through Chart I at 3.0 MPa. The chart displacement in the vertical direction is the value of  $P_o$  which is 50 N. After conditioning at 20°C and 65%RH for 7 days and 21 days, the value of  $\sigma_m$  reduces to 2.1 MPa and 1.4 MPa, respectively, and the value of  $P_o$  reduces to 28 N and 10 N, respectively (Figure 5.6a-b). Therefore, the proposed procedure should be a convenient means in estimating the magnitudes of  $\sigma_m$  and  $P_o$  in the lumber factory.

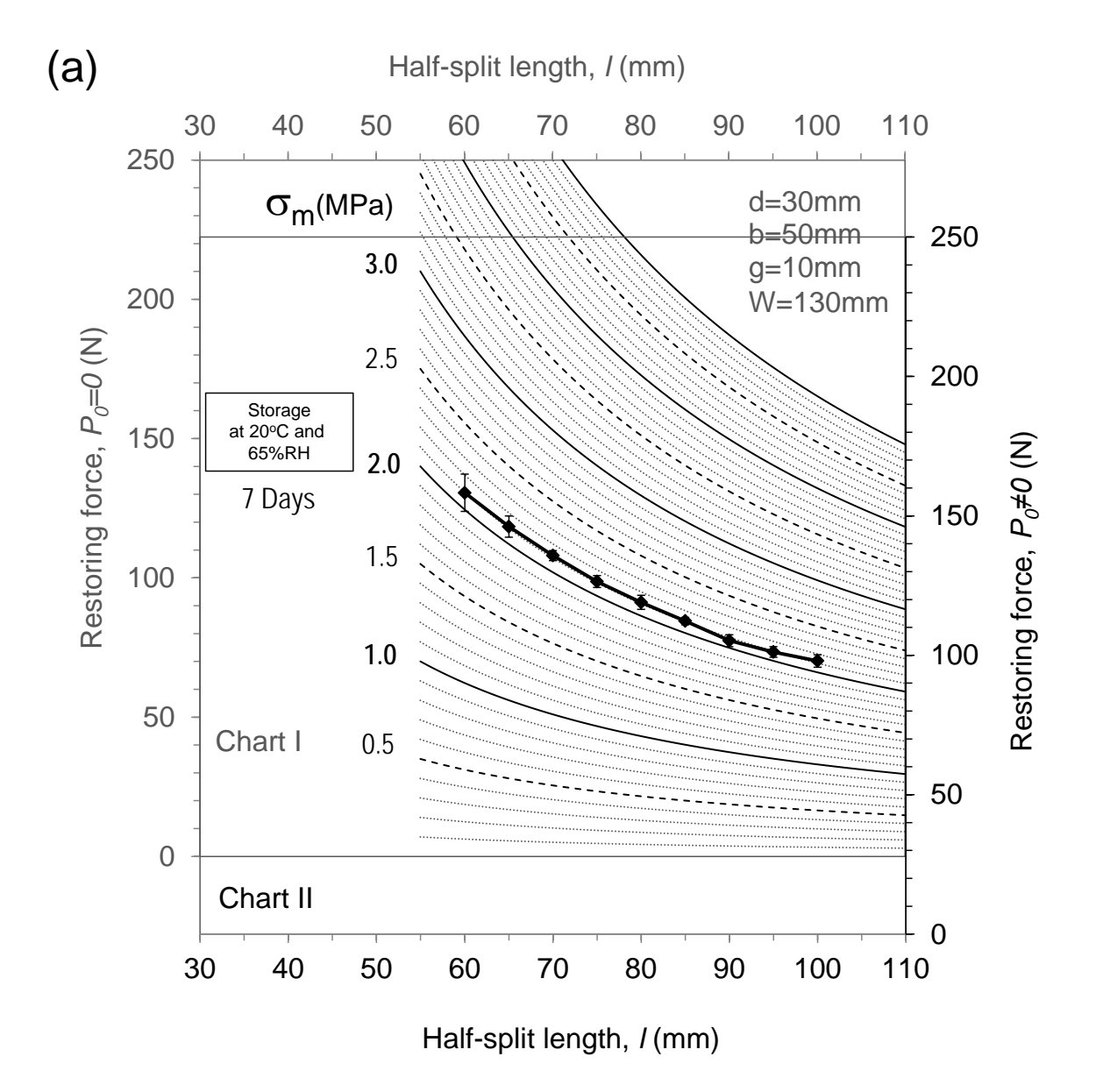








**Figure 5.5** Determination of  $\sigma_m$  and  $P_o$  of the 30 mm thick and 130 mm wide kiln-dried rubberwood lumber ( $P_o \neq 0$ ) just after drying, (a) The restoring force-internal stress chart at  $P_o = 0$  (Chart I), (b) the restoring force profile at  $P_o \neq 0$  (Chart II), (c) overlaying of Chart II on Chart I and (d) determination of  $\sigma_m$  and  $P_o$  by vertically moving Chart II with respect to Chart I.



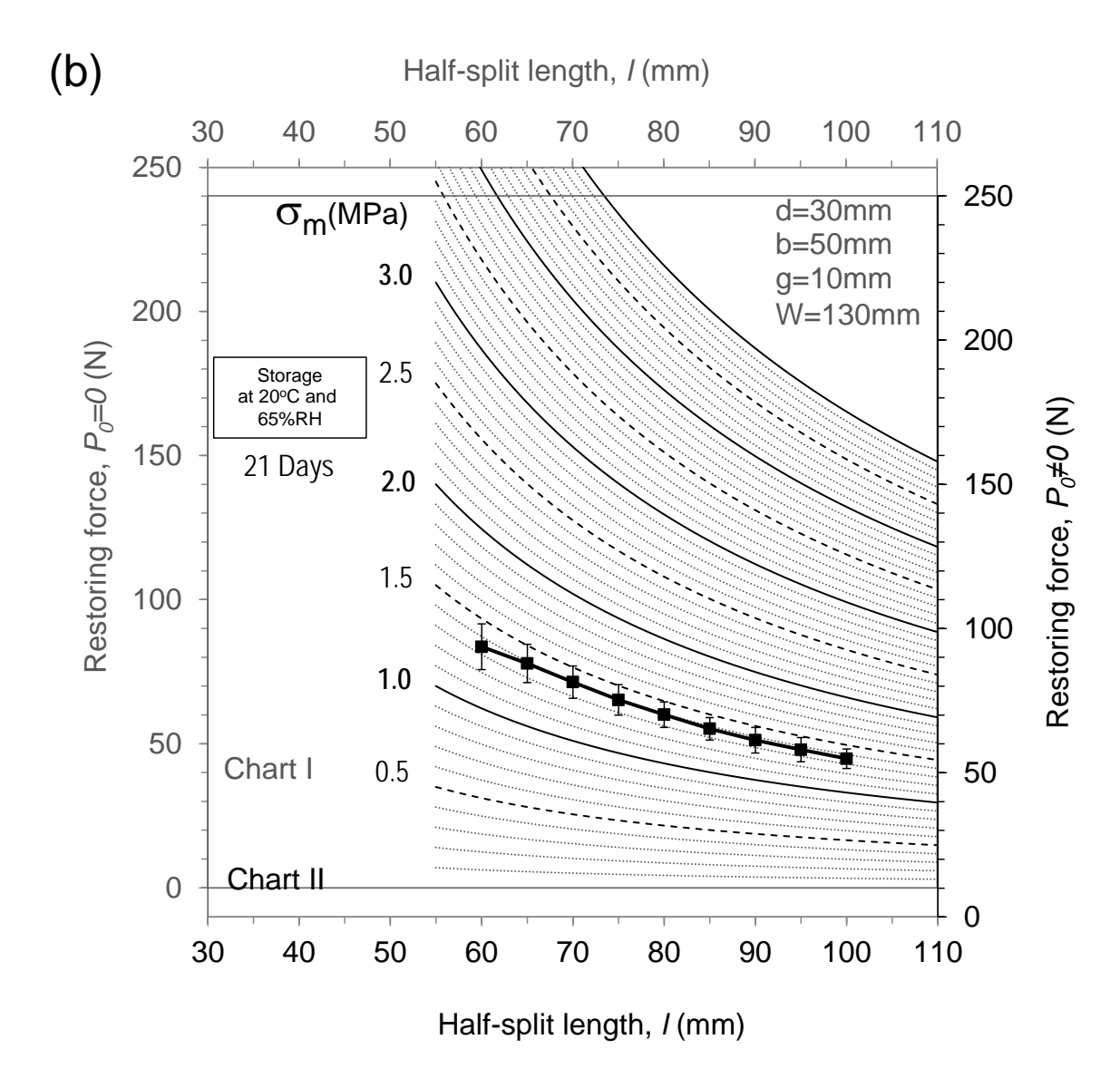


**Figure 5.6** Determination of  $\sigma_{\rm m}$  and  $P_{\rm o}$  of the 30 mm thick and 130 mm wide kiln-dried rubberwood lumber ( $P_{\rm o} \neq 0$ ) after conditioning at 20°C and 65 % RH for (a) 7 days and (b) 21 days.

# 5.3.3 FE analysis of restoring force of lumber containing main internal stress ( $P_0 \sim 0$ )

The FE model was first employed to describe the restoring force profiles of the HS and LS specimens prepared from the  $P_o\sim0$  type of lumber similar to those reported by Jantawee et al. (2016) in which the internal stress in the direction of width (tangential direction) mainly exists in the lumber. Effects of other stress components including stresses in the thickness (radial) and the length (longitudinal) directions on the restoring force are assumed to be negligible. Used as initial inputs for the FE model, the released strain and Young's modulus data across specimen thickness prior to half-splitting obtained by the McMillan slice test of the  $P_o\sim0$  sets of kiln-dried rubberwood lumber at two levels of internal stress (HS and LS) are listed in Table 1. As expected for the case-hardened kiln-dried

lumber, the negative and positive released strain values observed in the inner and outer sections of lumber after slicing, respectively, are caused by the tensile and compressive stresses remaining within the inner and outer sections, respectively (McMillen 1958). The magnitudes of Young's modulus across the thickness of all specimens examined are roughly uniform. The values are within the standard deviation. However, Young's modulus in the HS specimens is higher than that in the LS specimens because of lower moisture content prior to conditioning of the HS specimens.

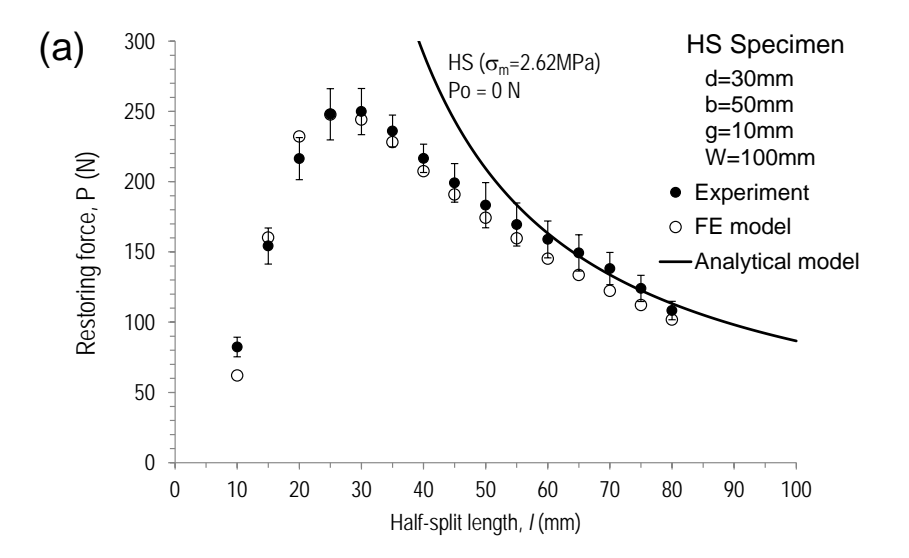
**Table 8.1** Released strain and Young's modulus data in the tangential direction of the  $P_o \sim 0$  and  $P_o \neq 0$  sets of kiln-dried rubberwood lumber at two levels of internal stress (HS and LS) used in the finite element calculations. Moisture contents across the thickness are also shown.

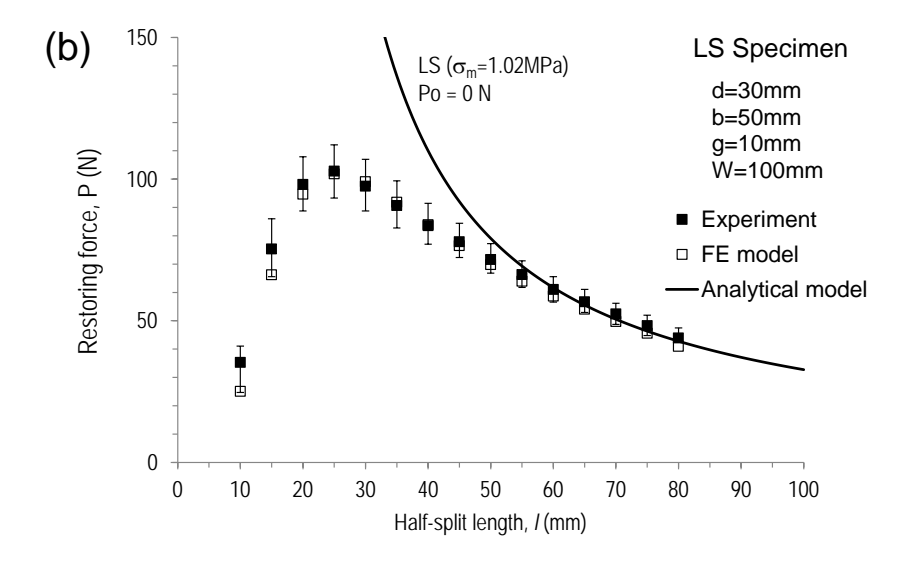
Type of lumber	Input	Stress level	Distance from the center in thickness direction		
			(mm)		
			2.5	7.5	12.5
P <sub>o</sub> ~0	Released strain, $\varepsilon$ (%)	HS	-0.19 (0.03)	-0.06	+0.28
				(0.03)	(0.06)
		LS	-0.10 (0.02)	-0.01	+0.12
				(0.03)	(0.02)
	Young's modulus, $E_T$ (MPa)	HS	543	555	588
			(64)	(49)	(54)
		LS	467	487	427
			(48)	(54)	(51)
	Moisture content (%)	HS	6.2	5.9	5.4
			(0.4)	(0.4)	(0.4)
		LS	10.7	10.9	11.4
			(0.2)	(0.2)	(0.3)
P₀≠0	Released strain, $\varepsilon$ (%)	HS	-0.15	0.03	+0.50
			(0.05)	(0.07)	(0.12)
		LS	-0.16	-0.07	+0.11
			(0.05)	(0.03)	(0.08)
	Young's modulus, $E_T$ (MPa)	HS	808	825	847
			(19)	(20)	(20)
		LS	633	622	594
			(23)	(26)	(23)
	Moisture content (%)	HS	5.6	5.5	5.0
			(0.2)	(0.1)	(0.3)
		LS	10.2	11.5	13.1
			(0.4)	(0.7)	(0.5)

Note: Numbers in the parenthesis are the standard deviation (SD).

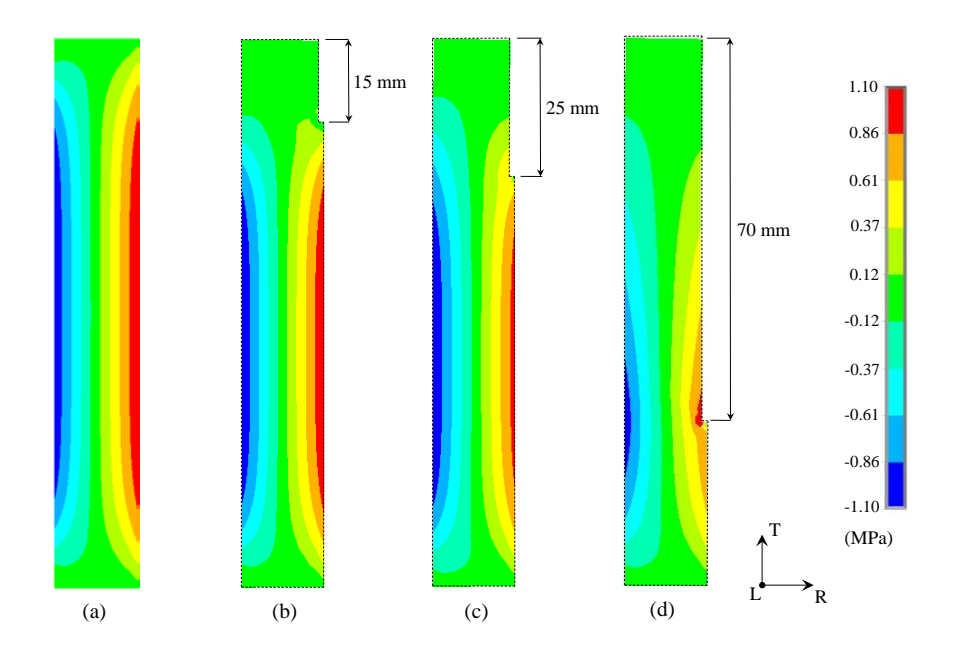
A reasonable agreement between the FE simulated ( $P_{cal}$ ) and the measured restoring force patterns is obtained for the entire profiles as shown in Figure 5.7. Good agreement is also observed in the flexural response regime together with the calculated restoring force values according to the analytical model based on an elastic beam theory. However, the FE model appears to capture the restoring force behavior at relatively short half-split lengths

outside the flexural range where the analytical model has failed (Jantawee et al. 2016). Detailed analysis of the transverse internal stress distribution of the LS specimen after halfsplitting and restraining at various half-split lengths as predicted by the FE model reveals different states of mechanical stress (Figure 5.8). In an uncut specimen (Figure 5.8a), internal stress linearly varies from compressive stress at the inner core to tensile stress at the outer surface. However, in the vicinity of the specimen ends of less than ~15mm, a half of specimen thickness  $(\frac{d}{2})$ , the magnitude of internal stress decreases due to stress relaxation at the edge (Figure 5.8a). As a result, within the half-split length I of less than 25 mm, a distance of half thickness away from the clamping positions  $(g + \frac{d}{2})$ , the restoring force at the clamping points increases with increasing half-split length (Figure 5.8b). And the restoring force reaches its maximum value when the half-split length I reaches the distance of ~25mm  $(g + \frac{d}{2})$  (Figure 5.8c). Once exceeding this value, a flexural response of the halfsplit specimen is more influential (Figure 5.8d). Each leg of the half-split specimen acts as a cantilever beam that is rigidly fixed at one end and free at the other end. Increasing halfsplit length, therefore, causes a reduction of the restoring force at the clamping points. Eventually at a relatively long half-split length, the restoring force profile can be described using a simple cantilever elastic beam equation (Hibbeler 2012) as described by Jantawee et al. (2016).





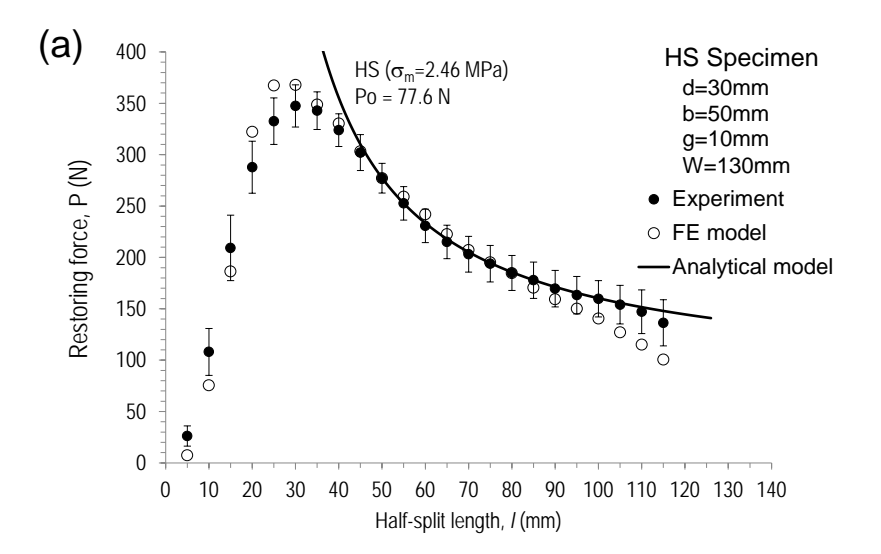
**Figure 5.7** Comparison of experimental (filled symbols) and FE simulated restoring force (open symbols) profiles of the 30mm thick  $P_o\sim0$  half-split (a) HS and (b) LS rubberwood specimens as a function of the half-split length. Profiles of the calculated restoring forces based on an elastic cantilever beam theory (solid lines) with  $P_o=0$  are also plotted for comparison.



**Figure 5.8** Contour plots of transverse internal stress predicted across the thickness of one quarter of the 30mm thick  $P_o \sim 0$  LS specimen at (a) initial configuration and after half-splitting at cutting lengths of (b) 15mm, (c) 25mm and (d) 70mm with the restoring force applied at 10mm away from the top surface.

5.3.4 Finite element (FE) analysis of restoring force of lumber containing other stress components ( $P_0 \neq 0$ )

Using the released strain and the Young's modulus data in the width (tangential) direction for the P₀≠0 set of specimens shown in Table 1, the FE simulated and measured restoring force profiles of the HS and LS specimens are plotted in Figures 5.9a-b, respectively. Although the magnitude of the simulated restoring force is, on average, at the same level as the measured one but the restoring force profiles as a function of the halfsplit length are clearly inconsistent. The difference manifests itself in the LS specimens containing relatively low level of the internal stress especially at relatively long half split length (Figure 5.9b). It is assumed in the FE model that the relaxed stress components, obtained from the McMillen slice test, is only in the width (tangential) direction. As a result, the FE simulated restoring force profile roughly conforms the pattern of Po=0 similar to those in Figure 5.7a-b. This indicates that relaxation of some other internal stress components which should exist within the lumber have not yet been accounted for in the FE model. In addition, the amount of the released strain measured using the McMillen slice test, used as inputs in the FE model, should have been affected by the internal stress relaxation in other orthogonal directions (Bodig and Janye 1982) especially in the thickness direction. The situation is rather complex and is required a full investigation of internal stress relaxation in all three main orthogonal directions (tangential, radial and longitudinal) and this is a subject of the future work.



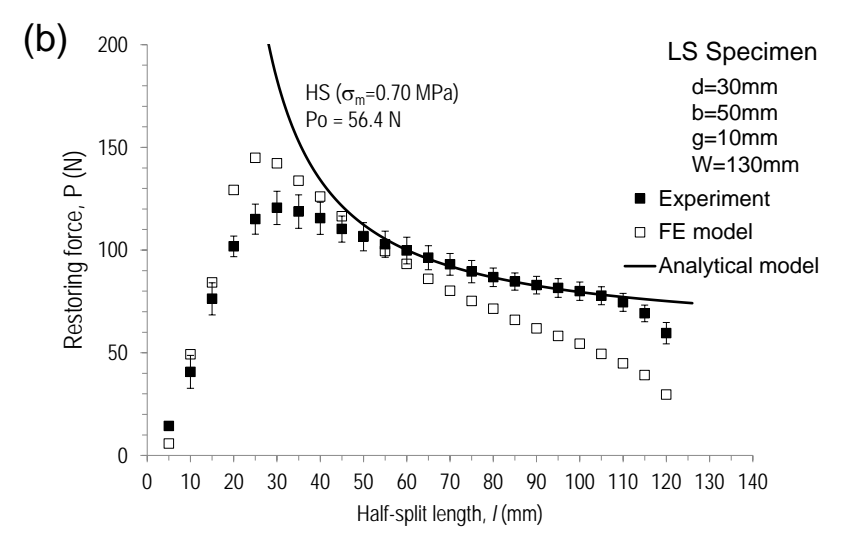


**Figure 5.9** Comparison of experimental (filled symbols) and FE simulated restoring force (open symbols) profiles of the 30mm thick  $P_o \neq 0$  half-split (a) HS and (b) LS rubberwood specimens as a function of the half-split length. Profiles of the calculated restoring forces based on an elastic cantilever beam theory (solid lines) with  $P_o \neq 0$  are also plotted for comparison.

#### 5.4 Conclusions

The following conclusions can be drawn from this work:

- 1) A general form of the analytical model based on an elastic cantilever beam theory has been successfully developed to directly quantify the main internal drying stress in the width direction within kiln-dried lumber which could also contain other stress components. The restoring force measured on a half-split specimen can be separated into two independent terms of a flexural force caused by relaxation of the main internal drying stress and a remnant force caused by relaxation of other stress components.
- 2) The universal restoring force-internal stress chart has been improved for a convenient use in the lumber industry. The magnitude of the internal drying stress within any pieces of kiln-dried lumber can be determined even in the presence of other stress components. A demonstration has been performed to monitor internal stress relaxation during conditioning of industrial kiln-dried rubberwood lumber.
- 3) With little effect from other internal stress components, by using the released strain and Young's modulus data in the width (tangential) direction obtained from the McMillen slice test, a numerical model based on finite element analysis successfully simulates the restoring force profile for an entire range of half-split

- length. This includes the restoring force profile at relatively short half-split length where the model based on an elastic cantilever beam theory fails.
- 4) In the presence of other stress components, only the released strain and Young's modulus data in the width (tangential) direction are insufficient to describe the restoring force behavior for the entire half-split length. The finite element model must be improved to incorporate some missing stress components.

### References

- 1. Bodig J, Jayne BA (1982) Mechanics of wood and wood composites. Van Nostrand Reinhold Company, New York
- 2. Cai L, Oliveira LC (2004) Equalizing and conditioning spruce-pine-subalpine fir lumber. Forest Prod J 54: 126-131
- 3. Diawanich P,Tomad S, Matan N, Kyokong B (2012) Novel assessment of casehardening in kiln-dried lumber. Wood Sci Technol 46: 101-114
- 4. European Committee for Standardization (2010) Sawn timber-method for assessment of case-hardening. CEN standard ENV 14464
- 5. Hibbeler RC (2012) Structural analysis. *Prentice Hall*, New Jersey
- 6. Jantawee S, (2016) Assessment of internal stress within kiln-dried lumber using a restoring force technique on a half-split specimen, PhD thesis, School of Engineering and Resources, Walailak University, Thailand
- 7. Jantawee S, Leelatanon S, Diawanich P, Matan N (2016) A new assessment of internal stress within kiln-dried lumber using a restoring force technique on a half-split specimen. Wood Sci Technol 50: 1277-1292
- 8. Kretschmann DE, Mechanical properties of wood, in: R.J. Ross (Ed) Wood handbook (wood as an engineering material), Forest Products Laboratory, United States Department of Agriculture Forest Service, Madison, 2010, pp 5/1-5/46.
- 9. McMillen JM (1958) Stresses in wood during drying (Report 1652). Department of Agriculture, Forest Service, Forest Products Laboratory, Madison
- 10. Matan N, Kyokong B (2003) Effect of moisture content on some physical and mechanical properties of juvenile rubberwood. Songklanakarin J Sci Technol 25(3):327–340
- 11. Pang S, Simpson IG, Haslett AN (2001) Cooling and steam conditioning after high-temperature drying of Pinus Radiata board: Experimental investigation mathematical modeling. Wood Sci Technol 35: 487-502
- 12. Perré P, Passard J (2007) Stress development. In: Perré P (ed) Fundamentals of wood drying, European COST A.R.BO.LOR., Nancy, pp 243-271
- 13. Simpson WT (1991) Dry kiln operator's manual. In: Agriculture Handbook AH-188. Department of Agriculture, Forest Service, Forest Products Laboratory, Madison

- 14. Simpson WT (1999) Chapter 12: drying and control of moisture content and dimensional changes. In: Wood handbook (Wood as an Engineering Material). Department of Agriculture, Forest Service, Forest Products Laboratory, Madison
- 15. Sonderegger W, Martienssen A, Nitsche C, Ozyhar T, Kaliske M, Niemz P (2013) Investigations on the physical and mechanical behavior of sycamore maple (*Acer pseudoplatanus* L.), Eur. J. Wood Wood Prod. 71: 91–99
- 16. Welling J (Ed) (1994) EDG-Recommendation on assessment of drying quality of timber, European drying group (EDG), Hamburg
- 17. Wengert E (1992) Techniques for equalizing and conditioning lumber. Cooperative extension programs No. 65. Department of Forest and Wildlife Ecology, University of Wisconsin, Madison

# Chapter 6

# Interpretation of the restoring force of lumber at various thicknesses

### 6.1 Introduction

One of limitations in the calculation of the internal stress from the restoring force profile is that the model based on simple elastic cantilever beam theory described in Chapter 4 is only capable of describing the restoring force profile within a flexural response range at relatively long half-split length. Outside this range especially at relatively short half-split length in the narrow piece of lumber, the model is fail. The geometrical shape factor derived by means of the elastic cantilever beam theory is not valid outside the flexural response range. The main objective of this chapter is to find a general solution of the geometrical shape factor and to employ a numerical model of finite element analysis to validate and derive the shape factor for an entire rage of half-split length.

### 6.2 Materials and methods

6.2.1 Measurements of restoring force, released strain and modulus of elasticity

The flat-sawn industrial kiln-dried rubberwood lumbers were collected from a local sawmill in Nakhon Si Thammarat, Thailand. They were the produce of 25- to 30- year-old rubber trees. The defect-free pieces of lumber were cut to one-meter long in the longitudinal direction to the wood grain. Two sizes of lumber thickness (*d*) in the radial direction were selected in this study including 30 mm and 55 mm. They all had the same width of 130 mm (W) in the tangential direction. Before making the samples, then, the end of each lumber was cut out approximately 50 mm to get rid of the stress relaxation. Three adjacent pieces of 50-mm-long (*b*) specimens were prepared to measure the restoring force to measure the released strain obtained by the McMillen slice test (McMillen 1958) and the moisture content, and to measure the modulus of elasticity in the tangential direction to the grain of wood (Figure 6.1a). Three replicates of each test were examined.

The first assessment was performed right after the dried lumbers was brought out the kiln and was cooled down in the ambient temperature for one hour. The specimens in the first assessment could be denoted as "HS" which stands for the high stress level. The rest pieces of lumbers were coated with aluminum foil at both ends and were kept in a conditioning room at 20°C and 65% RH for a month. After that they were tested again as the second assessment and could be denoted as "LS" because the internal stress was partially relaxed to the low level.

The restoring force measurement was performed according to Jantawee et al. (2016). The specimen was clamped onto the steel frame by the screws at a distance (g) of 10 mm from the top surface as shown in Figure 6.1b-c. The specimen clamped to the steel frame

was cut at half thickness in a wide direction along a half-split length (l). The restoring force was then recorded at 5 mm intervals until the specimen was divided into two pieces or the crack was observed. For the McMillen slice test, the specimen surfaces in the thickness direction were first slightly planned to remove irregularities to obtain a relatively smooth surface before being marked by divided lines so it could be cut into six or eleven equal slices for 30- or 55-mm-thick specimens respectively. The initial width of each pre-cut slice  $(W_b)$  was measured by calipers having a precision of 0.01 mm. Measurement positions and numbers on each slice were marked so that the following width measurements after slicing could be performed at the same positions. The specimens were then cut along the premarked lines (Figure 6.1d). Each slice was subsequently pressed flat before its width,  $W_0$ , was measured. Care was also taken to ensure that about the same force was applied on the caliper for every measurement. The released strain of each slice was calculated according to  $\varepsilon = \frac{W_a - W_b}{W}$ . All slices were tested to determine the Young's modulus in the tangential direction  $(E_T)$  using a universal testing machine (Lloyd 150kN, UK) equipped with a strain gauge (Epsilon Technology, USA). A section of each slice was also weighted before and after oven-drying at 103±2°C for 24 hours to determine its moisture content.

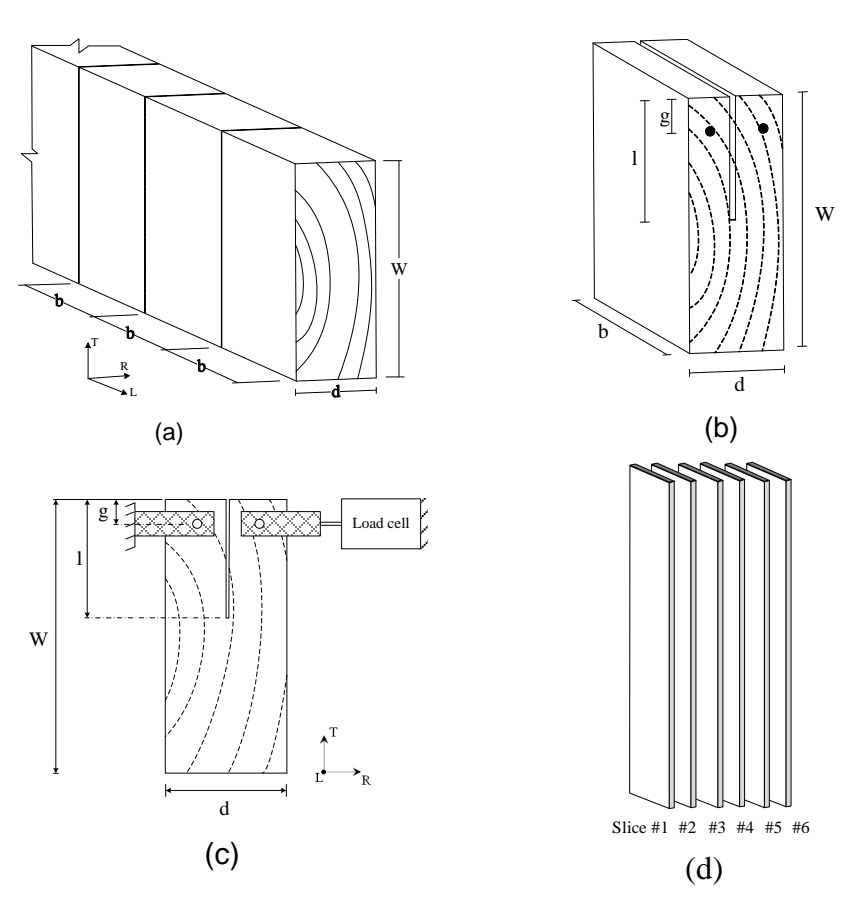


**Figure 6.1** (a) The test specimen cut from the lumber board, (b) the half-split specimen for the restoring force measurement, (c) diagram of the restoring force measuring apparatus and (d) the McMillen slice test

## 6.2.2 Finite element model of the restrained half-split specimen

To determine the geometrical shape factor of the restrained half-split specimen, the three-dimensional finite element (FE) model was generated using SOLID186 elements in ANSYS v12. The constitutive model of linearly elastic three mutually orthogonal materials was given into the computational process. The modulus of elasticity in the T-direction of all elements was set to a constant of 500 MPa., and all other moduli were determined as ratios of the modulus of elasticity in the T-direction ( $E_L:E_R:E_T=20:1.6:1$ ,  $G_{LR}:G_{LT}:G_{RT}=10:9.4:1$  and  $E_L:G_{LR}=14:1$ ) according to Bodig and Janye, (1982). Three Poisson's ratios were estimated to be  $\mu_{RL}=0.02$ ,  $\mu_{LT}=0.02$  and  $\mu_{RT}=0.35$  (Bodig and Jayne 1982; Kretschmann 2010). Since the specimen had two planes of symmetry, only a quarter of specimen was generated (Figure 6.2) to reduce computational time in the solving process. Two planes of symmetry (LT and RT) were fixed in the R- and L-directions, respectively. All nodes in the clamping (screw) area were restrained in the L-, R-, and T-direction to deduce the calculated restoring force,  $P_{FE}$ . The linear profile of internal stress was assigned to the model by using the shrinkage coefficient due to temperature change to reach the maximum internal stress of 1 MPa at the outer surface and the inner core as presented in Figure 2b.

The same model was employed to verify the restoring force obtained by the experiment. However, in this study, the released strain and the measured Young's modulus in the T-direction of the specimen were applied to the layers corresponded to the tests. All other moduli were calculated as ratios of the measured modulus of elasticity in the tangential direction as described previously.

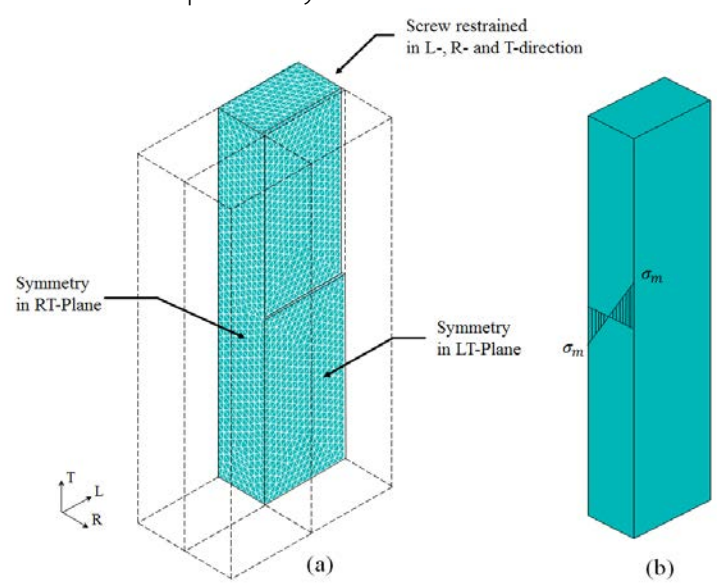


**Figure 6.2** The 3D mesh of a quarter of the specimen and boundary conditions used in finite element simulation and (b) linear distribution of the internal stress for obtaining the geometrical shape factor.

### 6.3 Results and discussion

6.3.1 Analytical model of the restoring force and the geometrical shape factor by the beam theory

The restoring force technique is basically developed from the beam theory by assuming a linear distribution of internal stress across half thickness of lumber as depicted in Figure 6.3a. Without restraint, the specimen could be deformed (Figure 6.3b) after cutting due to the existing internal stress developed during drying process. However, it could not independently bend because it is clamped on the restoring force device. This behaves the same as a cantilever beam subjected to point load at the free end (Figure 6.3c) and the force required to keep the specimen in place is so-called the restoring force.

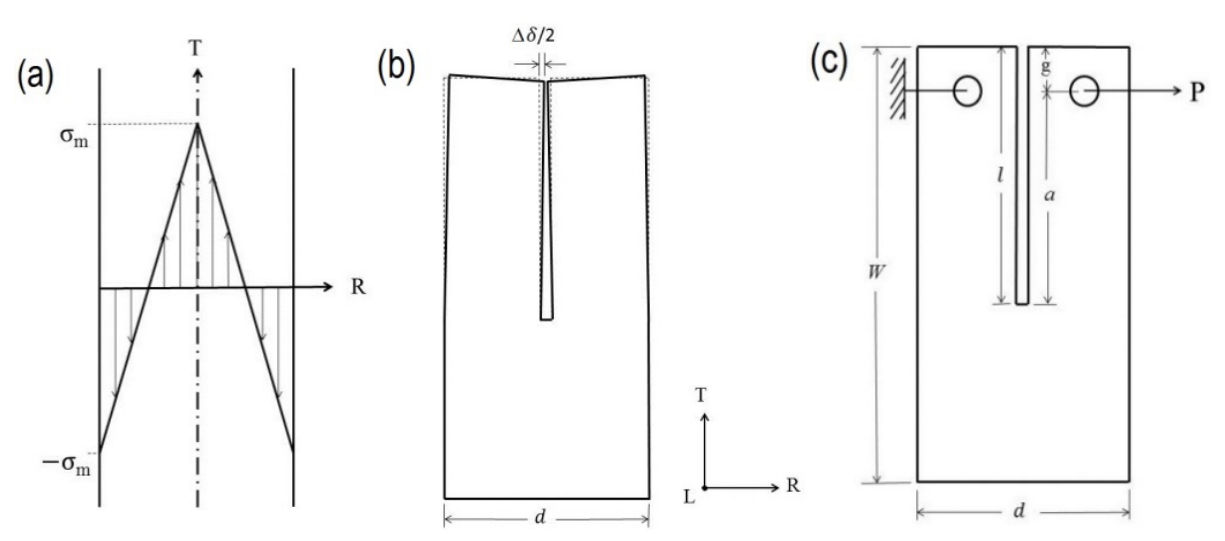


**Figure 6.3** (a) Linear distribution of through thickness internal stress within lumber, (b) deflection of half-split specimen caused by internal stress after sawing and (c) application of restoring force to restrain half-split specimen in original configuration prior to sawing.

The magnitude of maximum stress, assumed to be equal at the outer surface and the inner core, can be calculated by a deflection of the half-split specimen as express by

$$\sigma_m = \frac{E \cdot \Delta \delta \cdot d}{4I^2} \tag{6.1}$$

where E,  $\delta$ , d and l are Young's modulus in the tangential direction, mouth opening, thickness and half-split length of the specimen, respectively (Walton, 2002). The restoring force, P, required to keep the half-split specimen in the original configuration can be computed using

$$P = \frac{E \cdot \Delta \delta \cdot b}{S} \tag{6.2}$$

where b is sample length and S is a geometrical shape factor (Lados and Apelian, 2006). By combining equation (6.1) and (6.2), the maximum stress at the surface and the core layers can be expressed as (Diawanich et al., 2012; Jantawee et al., 2016)

$$\sigma_m = S \frac{d}{4bl^2} P \tag{6.3}$$

The equation (6.3) presents that the internal stress can be determined by the measured force and the geometric shape factor. Most importantly, it does not need the modulus of elasticity in the calculation.

In this study, the geometric shape factor is focused and determined by three models including long beam theory, short beam theory and the finite element method. The equation (6.3) can be re-written as

$$S = \frac{4bl^2}{Pd} \sigma_{\rm m} \tag{6.4}$$

The calculated restoring force ( $P_{cal}$ ) by those three models will lead to the calculation of the geometric shape factor by fixing the same stress level and the same dimensions.

For the long beam theory (also known as Euluer-Bernoulli beam theory), according to Hibbeler (2012), the deflection at the free end of a cantilever beam subjected point load can be calculated by

$$\frac{\Delta \delta}{2} = \frac{P(l-g)^2}{6EI} \left( 3l - (l-g) \right) \tag{6.5}$$

By substituting the moment of inertia  $I = \frac{bd^3}{96}$  into the equation (6.5)

$$\frac{\Delta \delta}{2} = \frac{16P(l-g)^2(2l+g)}{Ebd^3}$$
 (6.6)

By combining the equation (6.2) and (6.6), the geometrical shape factor derived from the long beam theory can be expressed as

$$S_{long} = \frac{32(l-g)^{2}(2l+g)}{d^{3}}$$
 (6.7)

For the short beam theory (also known as Timoshenko beam theory), the effect of shear deformation is included into equation of the deflection at the free end of a cantilever beam subjected point load and can be expressed as

$$\frac{\Delta \delta}{2} = \frac{P(l-g)^2}{6EI} (3l - (l-g)) + \frac{P(l-g)}{A_V G}$$
 (6.8)

where  $A_V = \kappa A$  and  $\kappa$  is the Timoshenko shear coefficient which depends on beam geometry. Normally,  $\kappa$  equals to 5/6 for a rectangular cross section. A is the cross section area of the beam and G is the shear modulus. In this case E is the modulus of elasticity in the tangential direction (T-direction) and G is the shear modulus in the RT-plane. Normally, the ratio of  $\frac{E_T}{G_{RT}}$  equals to 7 for wood (Bodig and Janye, 1982). In this study, the ratio of

$$\frac{E_T}{G_{RT}}$$
 can be denoted as  $\gamma = \frac{E_T}{G_{RT}}$ 

By substituting the moment of inertia  $I = \frac{bd^3}{96}$  into the equation (6.8) and combining with the equation (6.2), the geometrical shape factor derived from the short beam theory can be expressed as

$$S_{short} = \frac{4(l-g)}{d} \left( \frac{8(l-g)(2l+g)}{d^2} + \frac{\gamma}{\kappa} \right)$$
 (6.9)

According to the equation (6.9), the result of shear deformation effects on the shallow saw kerf because the specimen behaves like a short beam. It highly depends on the factor  $\gamma$  which is the ratio of  $\frac{E_T}{G_{RT}}$ . The effect of  $\gamma$  becomes less when the half-split length (1) of

the specimen reaches the infinity and the geometrical shape factor obtained from the equations (6.7) and (6.9) will become almost the same value.

# 6.3.2 Finite element model of the restoring force and the geometrical shape factor

The FE model was employed to deduce the restoring force for the 30 mm thick half-split specimen. By assuming a linear distribution of internal stress of 1 MPa from the outer surface through the core with a uniform value of Young's modulus of 500 MPa in the tangential direction of across the specimen thickness. The calculated restoring force of the 30-mm-thick lumber,  $P_{FE}$ , was obtained as shown in Figure 6.4a. Then, the value of geometrical shape factor S was obtained from the simulated restoring force. The derived geometrical shape factor plotted against half-split length for various widths of 30-mm-thick lumber is shown in Figure 6.4b. It is interesting to note that all geometrical data fall into a single master curve. The minimum value occurs at the sawn depth of 15mm corresponding to a half of the specimen thickness. The geometrical factor starts to deviate and increase sharply away from the master curve at the sawn depth of about 30 mm from the end of the specimen width. The geometrical factor becomes infinite as the sawn depth approaches the width of the specimen.

At the sawn depth of less than a half of specimen thickness ( $l < 15 \mathrm{mm}$ ), higher internal stress relaxation occurs at a deeper saw kerf. Higher resultant restoring force at the clamping points leads to a reduction of the geometrical factor in this regime. However, at the sawn depth greater than a half of the specimen thickness ( $l > 15 \mathrm{mm}$ ), flexural response of the half-split specimen became more influential. The specimen with a deeper saw depth (behaving similar to a longer beam with one end attached to a support) caused a reduction of the restoring force at the clamping points and therefore an increase in the value of the geometrical shape factor.

For a relatively wide specimen with respect to the sawn depth, the stress field altered by the presence of the saw kerf is not influenced by the end of the specimen width. Each leg of the half-split specimen behaves like a beam with one end rigidly attached to a fixed support (relatively large section of the uncut specimen). In this situation, the

geometrical factor is that according to the master curve. The stress field altered by the presence of the saw kerf is affected by the end of the specimen width in a relatively deep sawn specimen. Relaxation of stress in the form of strain takes place at the end of the specimen width. The leg of the half-split specimen cannot be thought as if one end is attached to a fixed support anymore. Therefore, lesser magnitude of the restoring force is required to restrain the legs at the clamping points. The reduction in the restoring force causes the increase of the geometrical shape factor and the deviation from the master curve. The geometrical factor derived can be directly used in the estimation of the level of the internal stress within lumber from the measured restoring force. Moreover, the FE derived geometrical shape factor could be described by both long beam theory and short beam theory at the relatively long half-split length.

Since the geometrical factor S is a function of the half-split length l, equation 6.4 can be rewritten as

$$S' = \frac{S}{l^2} = \frac{4b}{d} \frac{\sigma_{\text{max}}}{P_{FE}} \tag{6.10}$$

where S having a unit of (mm<sup>-2</sup>) is a geometrical factor per a square of half-split length. The value of S is plotted against the half-split length in Figure 6.5. The minimum value of S occurs at the sawn depth of 25mm which is further away from the clamping point at 10mm by a half of the specimen thickness (15mm). This coincides with the half-split length where the maximum restoring force observed experimentally. In the similar manner as S, the value of S fall into a single master curve and starts to deviate and increase sharply away from the master curve at the sawn depth of about 30 mm from the end of the specimen width. Further work in this area should be directed at elucidating the effect of clamping position and clamping configuration on the value of the geometrical factor S and the geometrical factor per a square of sawn depth S.

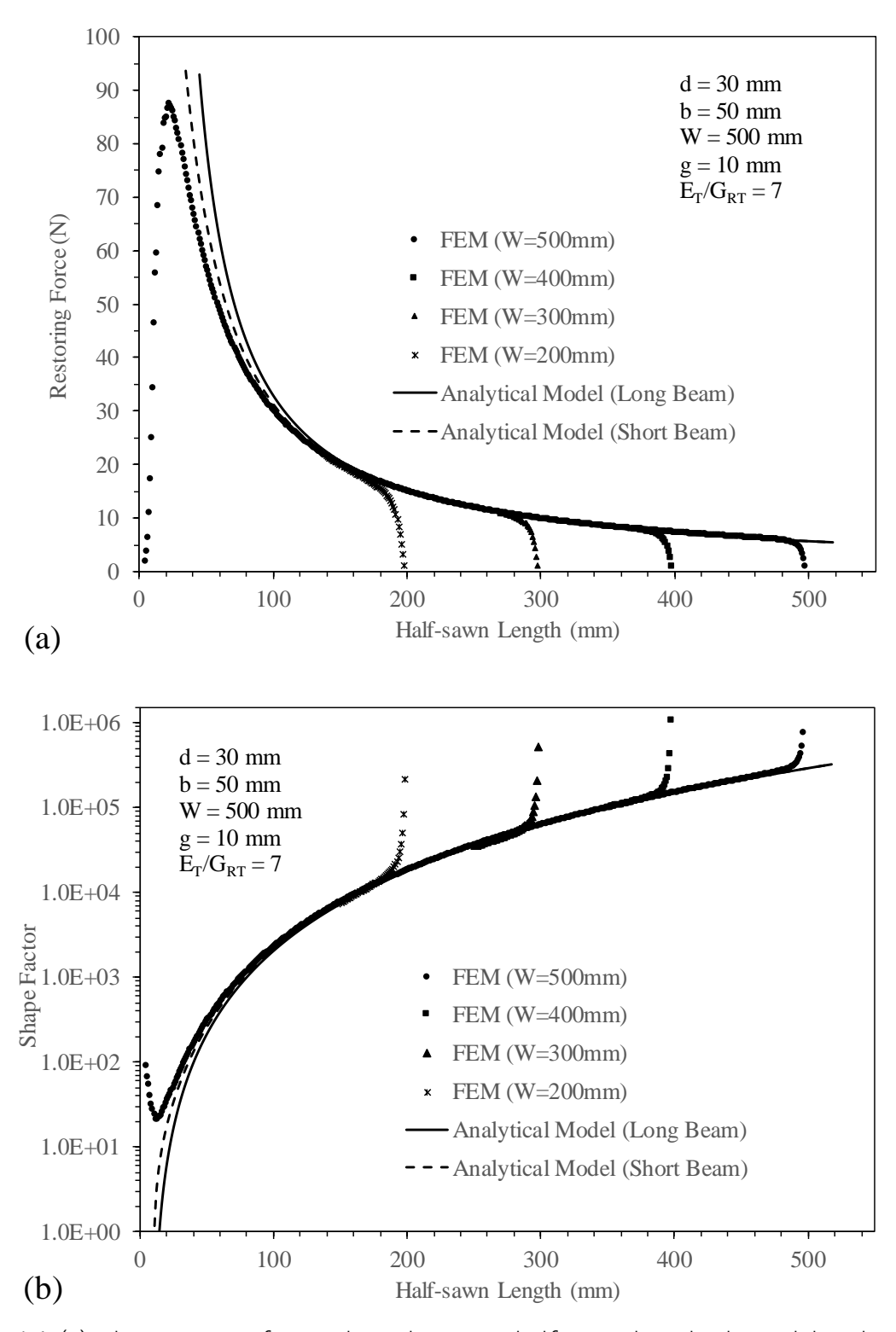


**Figure 6.4** (a) The restoring force plotted against half-sawn length derived by the finite element model of 30-mm-thick lumber and compared with the beam theories (b) The geometrical shape factor for various widths of lumber

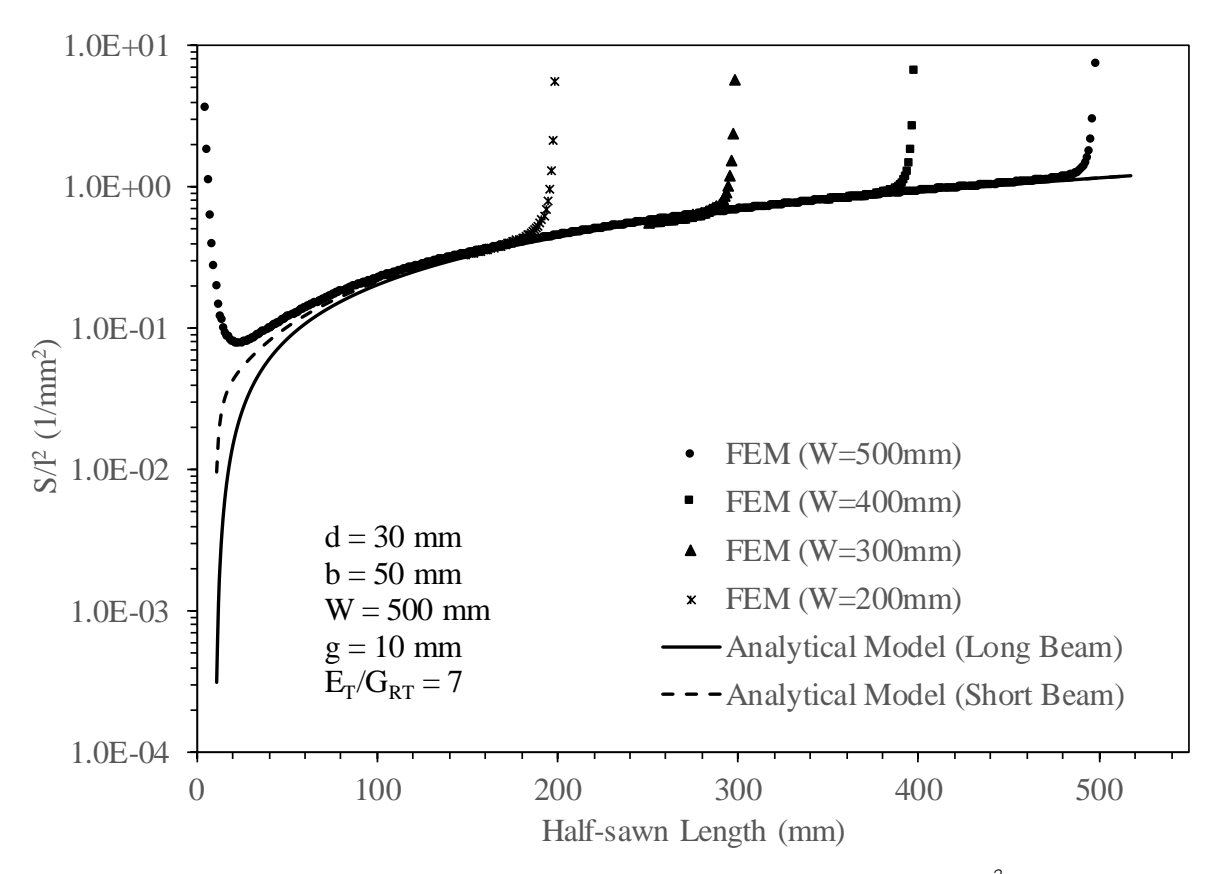


**Figure 6.5** The geometrical shape factor per a square of sawn-depth,  $S/l^2$ , as a function of sawn-depth, l, for the 30mm thick lumber with various widths of lumber

The FE model was also employed to deduce the geometrical shape factor S for the 50 mm thick half-split specimen. The linearly distributed internal stress profile with the maximum magnitude of 1 MPa at the surface and the core layers with a uniform value of Young's modulus in the tangential direction of 500 MPa were assumed. The restoring force and the geometrical shape factor calculated by FE model and the beam theory are shown in Figure 6.6a and 6.6b. The restoring force of the 50-mm-thick specimen computed by the FE model showed more curving outward than the 30-mm-thick specimen, and the beam theories fit to the FE result at the farther half-split length. The restoring force calculated by the beam theory converged to the FE result at about the half-sawn length of 130 mm and 220 mm for the 30- and 50-mm-thick specimen respectively. However, it has to be noted that they were used same length (b) of 50 mm, so they had the different aspect ratio which might affect to the comparison. Additionally, a geometrical shape factor per a square of sawn depth (S) can be plotted against the sawn depth I as presented in Figure 6.7.

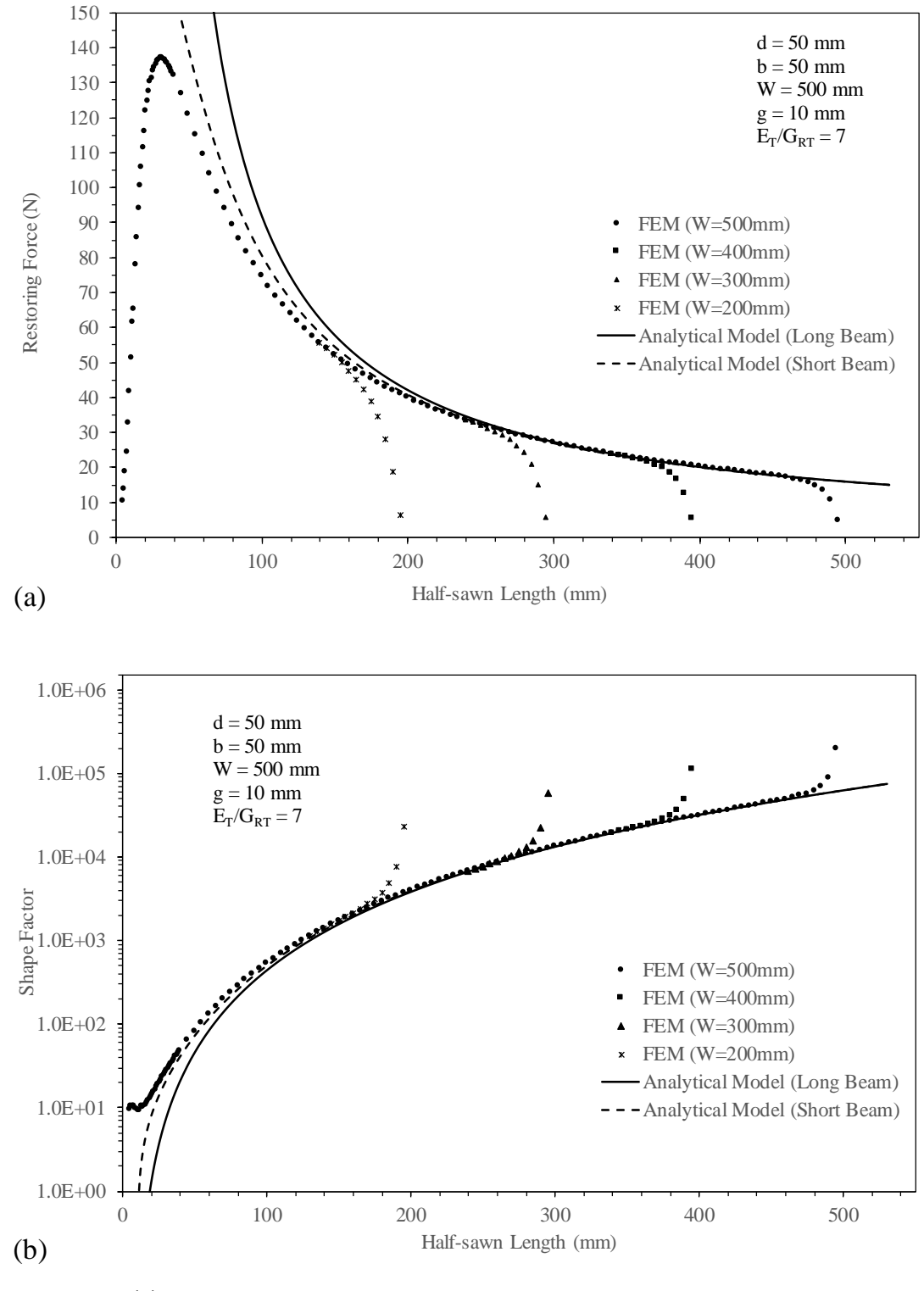


**Figure 6.6** (a) The restoring force plotted against half-sawn length derived by the finite element model of 50-mm-thick lumber and compared with the beam theories (b) The geometrical shape factor for various widths of lumber

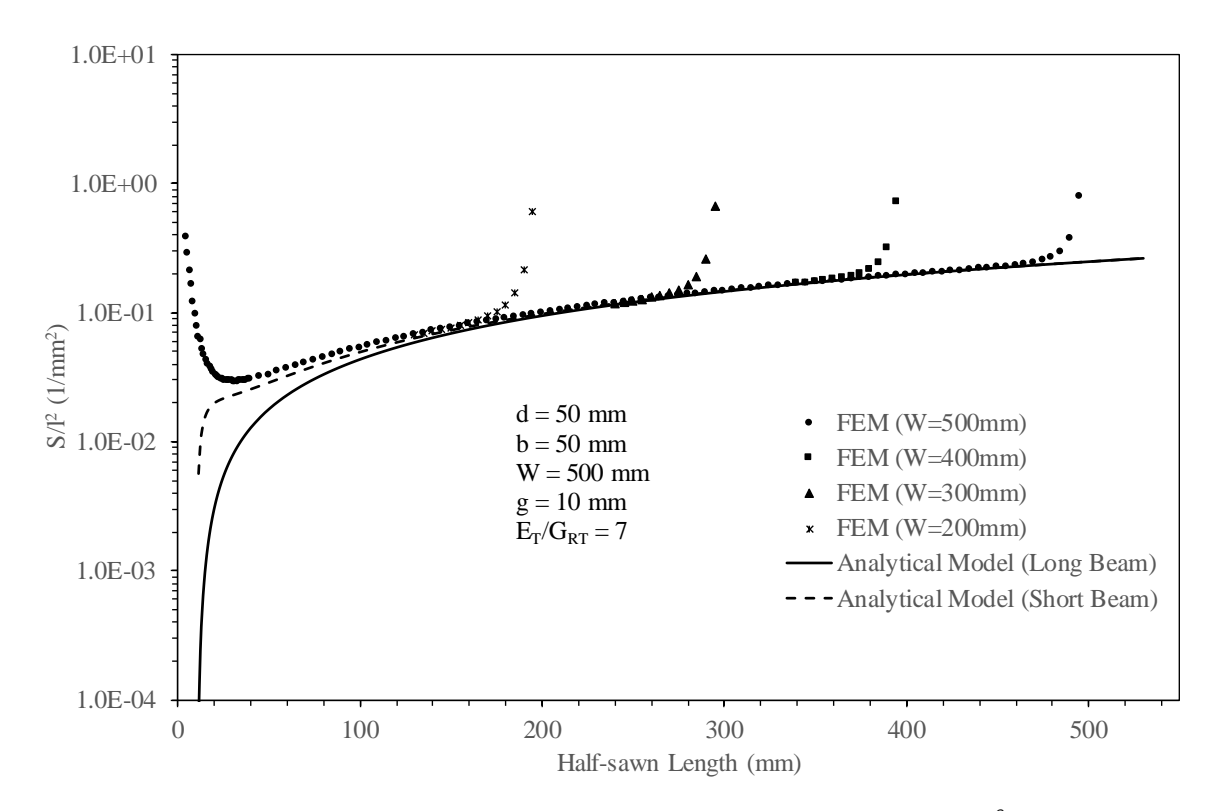


**Figure 6.7** The geometrical shape factor per a square of sawn-depth,  $S/l^2$ , as a function of sawn-depth, l, for the 50mm thick lumber with various widths of lumber

6.3.3 The evaluation of the internal stress within kiln-dried lumber using beam theory According to the research work done by Jantawee et al. in 2016, the internal stress within the kiln-dried wood could be measured using the restoring force technique without testing of modulus of elasticity. This research project has been continuing the same procedure testing of the 30-mm-thick specimens to determine the relation between the restoring force and the residual stress.

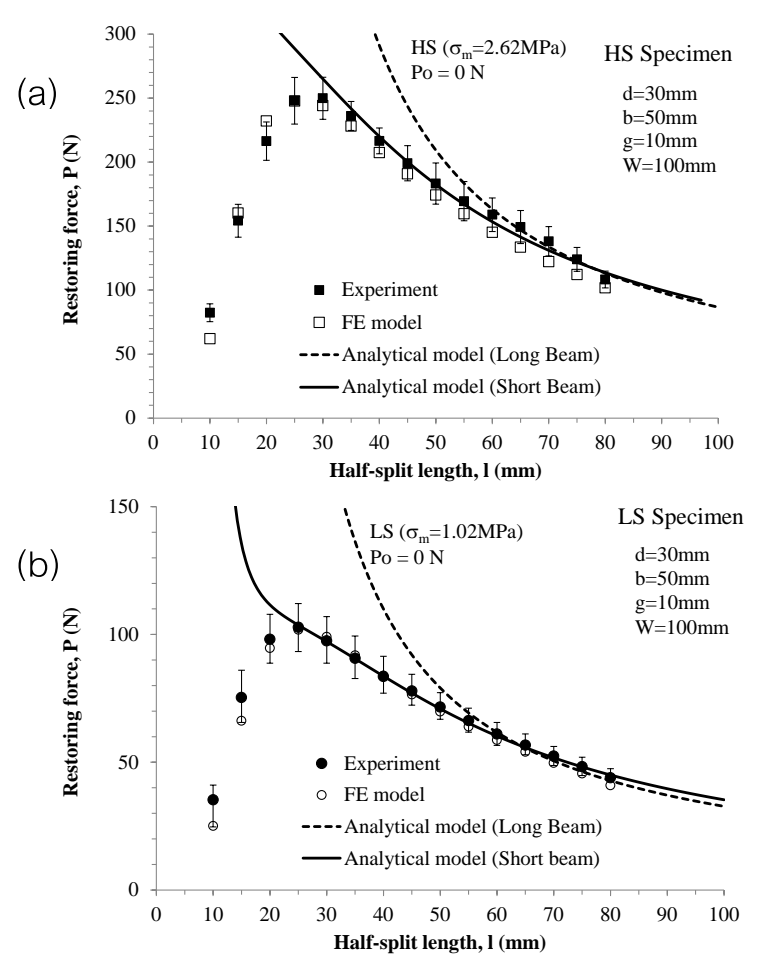
By considering the beam theory with only flexural deformation, the internal stress in the 30-mm-thick specimens were 2.62 MPa and 1.02 MPa for the high stress level (HS) and the low stress level (LS) respectively as shown in the dash line in Figure 6.8. Moreover the experiment, the filled symbol, was validated by the FE method depicted as the open symbol. The good correspondence between the FE result and the experimental result were observed with some acceptable error. However, the long beam theory was able to predict the internal stress only in the flexural regime located at about 60% to 80% of the sample's width. Therefore, some adjustment factor is needed to improve the prediction of stress. This requirement is also needed for thicker specimens.

The geometrical factor was modified by taking the shear deformation into bending equation, also known as short beam theory. Previously the geometrical factor can be obtained using the equation (6.7). The geometrical factor is derived from the long beam theory which is appropriate for only a narrow lumber such as  $30 \, \mathrm{mm} \times 130 \, \mathrm{mm}$  (Jantawee et

al., 2016). Flexure dominates the deformation of the narrow half-split specimen, so the restoring force measured at the half-sawn length of about 70% of lumber's width (Jantawee et al., 2016). For deformation in a thicker lumber, however, shear becomes more dominant than flexure, so the geometrical factor is modified to take the ratio between Young's modulus and shear modulus into account as presented in the equation (6.9).

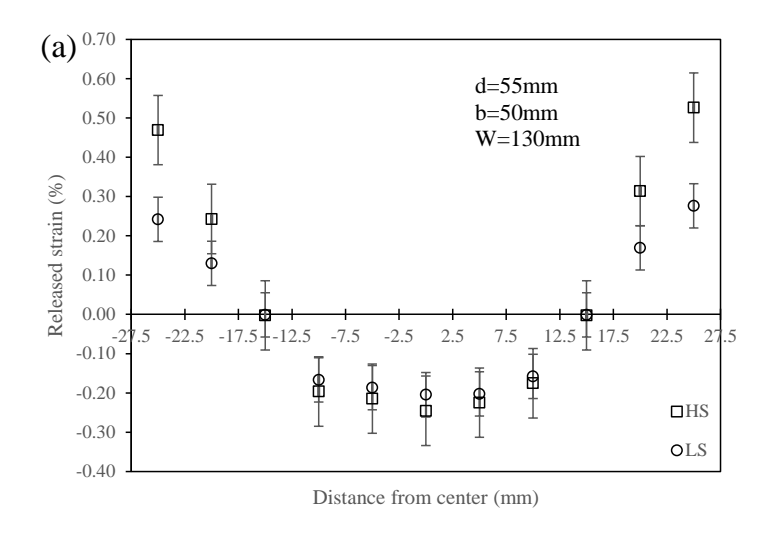
The analytical result using the short beam theory, a solid line, showed the better relation between the prediction and the experiment compared the one using the long beam theory. A crucial parameter in the analytical model for the short beam theory, however, was needed to figure it out which is the ratio of Young's modulus in tangential direction and shear modulus in RT-plane ( $\frac{E_T}{G_{RT}}$ ). It could be varied in a wide range from 3 to 27 for

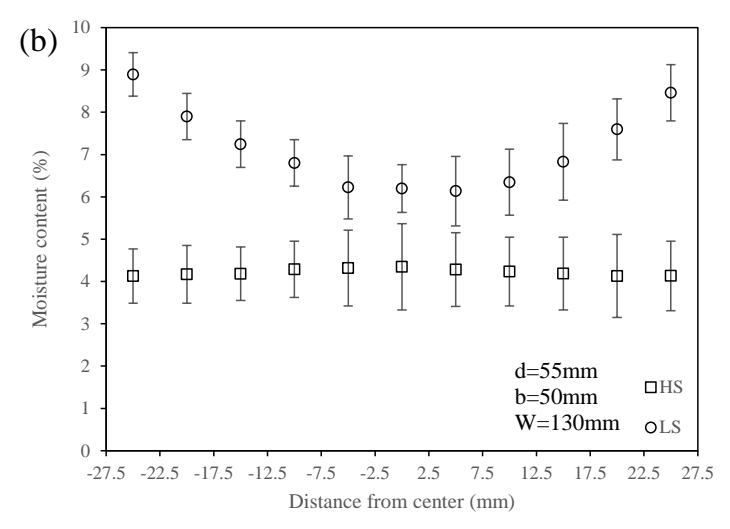
hardwood species (Kretschmann, 2010). In the case of 30-mm-thick as shown in Figure 6.8 the appropriate E/G is 14.0 and 16.5 for HS and LS respectively.



**Figure 6.8** Comparison of experimental (filled symbols) and FE simulated restoring force (open symbols) profiles of the 30mm thick Po~0 half-split (a) HS and (b) LS rubberwood specimens as a function of the half-split length. Profiles of the calculated restoring forces based on an elastic cantilever beam theory (solid lines) with Po=0 are also plotted for comparison.

In addition to the investigation of the 30-mm-thick lumber, the 55-mm thick specimens were prepared for measuring the restoring force, released strain, moisture content and modulus of elasticity. The released strain, moisture content and Young's modulus in the tangential direction along the thickness of the 50-mm thick and 125-mm wide HS and LS specimens are shown in Figure 6.9a-6.9c. The elastic strains due to the release of internal stresses were not uniform. Moisture content of the HS specimen was quite uniform along the lumber thickness with the average values of 4.22±0.8 %. After a month of moisture absorption, the moisture content of the LS specimen was not uniform. Since the specimen was quite thick, the outer layers which were exposed to the surrounded air had more moisture than the inner ones. The Young's modulus in HS specimens (563±24 MPa) was higher than that in the LS specimens (479±33 MPa) because the moisture content in the HS specimen was lower than in the LS specimens.





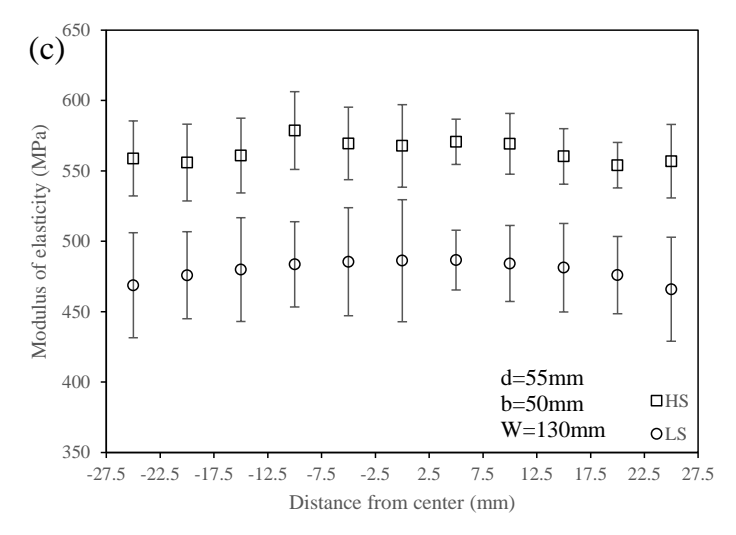


**Figure 6.9** Profile of (a) released strain (b) moisture content and (c) modulus of elasticity within the 55-mm thick HS and LS kiln-dried lumber

The relation of the restoring force of the 55-mm thick specimen presented in Figure 6.4 had the similar shape compared to that of the 30-mm thick specimen. The restoring force increased at the beginning of the test and then reached the maximum force at the half-sawn length of about 35 mm to 40 mm. For the 30-mm thick specimen, the maximum force could be observed at the half-sawn length between 25mm and 30mm as previously shown in Figure 6.2. Both thicknesses of specimen had the same screw distance (g) of 10mm. Interestingly, the maximum restoring force of both thickness could be located on the half-sawn length as a function of  $g + \frac{d}{2}$ .

Since the evaluation of the internal stress in a thick lumber using the short beam theory requires the ratio of the modulus of elasticity and the shear modulus (E/G) and the test of shear modulus is hard to set it up. To avoid the difficulty of obtaining the E/G ratio, the approximation of the internal stress within the 55-mm thick specimen would be initially calculated by using the long beam theory. The assumption of the analysis is that the internal stress and the restoring force calculated by both short and long beam theory must be equal at the far half-sawn length (l). By using this assumption, the prediction of the restoring force derived by the short beam theory can reveal the appropriate E/G ratio by fitting the curve from the experiment. The appropriated E/G ratio must be in the possible range of 3 to 27 for hardwood (Kretschmann, 2010).

The analysis of the long beam theory using the far half-sawn length (l) showed that the HS specimen had the internal stress in tangential direction of 1.31 MPa with the presence of the other stress component (Po = 227.2 N), while the LS specimen showed that the internal stress in tangential direction relaxed to 0.53 MPa (Po = 91.3 N). By substituting the same numbers of internal stress and  $P_o$  obtained by the long beam theory into the

restoring force equation based on the short beam theory, the E/G ratio could be discovered. As a result of doing this procedure, the E/G ratio of the HS and LS specimen was 4.5 and 5.0 respectively. These ratios are relatively low compared to the possible range of 3 to 27 according to the FPL Handbook (Kretschmann, 2010). However, the restoring force calculated by the long and short beam theory showed good agreement to the experiment. But the restoring force predicted by the short beam theory was able to capture the behavior of the 55-mm thick lumber better than that predicted by the long beam theory.

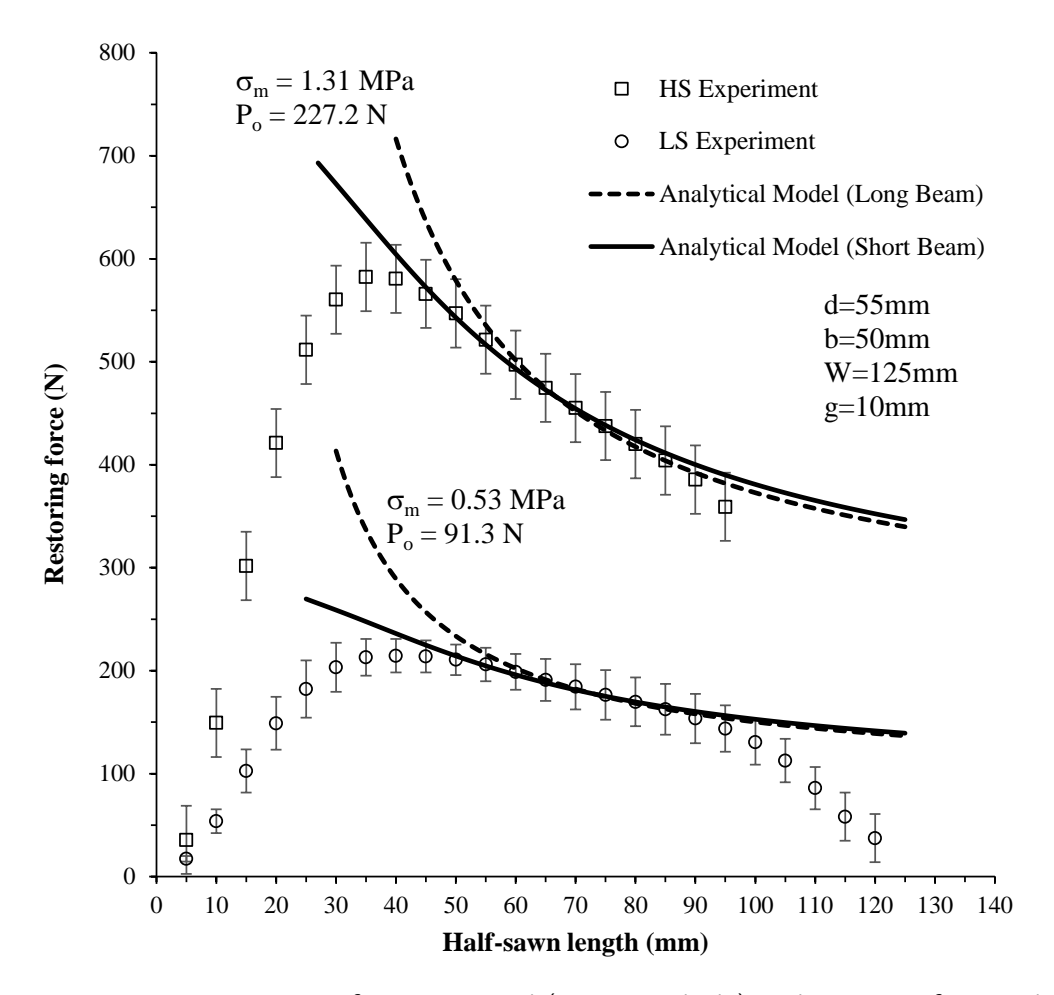


Figure 6.10 Comparison of experimental (open symbols) and restoring force calculated by the long beam theory (dash lines) and by the short beam theory (solid line) of the 55-mm thick  $P_o \neq 0$  half-split

### 6.4 Conclusions

The following conclusions can be drawn from this work:

1) A general solution of the analytical model based on both long beam theory and short beam theory have been successfully developed to directly quantify the main internal stress within kiln-dried lumbers without other stress components. The general form of the geometrical shape factor derived by the beam theories

- are coincident with the solution obtained by FE model at the long half-split length.
- 2) The finite element analysis shows good agreement between the predicted and measured restoring forces in the case that the other stress component do not exist. Not only the flexural zone where the half-split length is too long which corresponds to the beam theory, but the numerical results is also satisfactorily predicted to the measured ones in a short range of the half-split length and the peak.

## References

- 1. Cai L, Oliveira LC (2004) Equalizing and conditioning spruce-pine-subalpine fir lumber. Forest Prod J 54: 126-131
- 2. European Committee for Standardization (2010) Sawn timber-method for assessment of case-hardening. CEN standard ENV 14464
- 3. Hibbeler RC (2012) Structural analysis. *Prentice Hall*, New Jersey
- 4. Jantawee S, Leelatanon S, Diawanich P, Matan N (2016) A new assessment of internal stress within kiln-dried lumber using a restoring force technique on a half-split specimen. Wood Sci Technol 50: 1277-1292
- 5. Kretschmann DE (2010) Mechanical properties of wood, in: R.J. Ross (Ed) Wood handbook (wood as an engineering material), Forest Products Laboratory, United States Department of Agriculture Forest Service, Madison.
- 6. McMillen JM (1958) Stresses in wood during drying (Report 1652). Department of Agriculture, Forest Service, Forest Products Laboratory, Madison
- 7. Simpson WT (1991) Dry kiln operator's manual. In: Agriculture Handbook AH-188. Department of Agriculture, Forest Service, Forest Products Laboratory, Madison
- 8. Simpson WT (1999) Chapter 12: drying and control of moisture content and dimensional changes. In: Wood handbook (Wood as an Engineering Material). Department of Agriculture, Forest Service, Forest Products Laboratory, Madison
- 9. Welling J (Ed) (1994) EDG-Recommendation on assessment of drying quality of timber, European drying group (EDG), Hamburg
- 10. Wengert E (1992) Techniques for equalizing and conditioning lumber. Cooperative extension programs No. 65. Department of Forest and Wildlife Ecology, University of Wisconsin, Madison

# Chapter 7

# Comparison of the restoring force against the standard techniques

### 7.1 Introduction

Assessment of residual internal drying stress is an important procedure for quality control of kiln-dried lumber (Welling 1994). After drying, a piece of lumber is usually under compressive and tensile stresses at the outer layer and the inner core, respectively (McMillen 1958; Simpson 1999). Without an effective stress relief, remanufacturing of the stress-containing lumber often increases losses due to distortion (Wengert 1992). Various stress-relaxing techniques such as hole-drilling, contour method and slitting method are widely used to determine residual stresses in alloys and ceramics (Schajer and Ruud 2013). Conventionally, an assessment of internal stress within industrial kiln-dried lumber has been carried out by using the stress relaxing of the McMillen slice test (McMillen 1958), the standard CEN case-hardening test (European Committee for Standardization 2010) and the prong test (Simpson 1991). Strain or deflection accompanying the elastic relaxation of internal stress caused by sectioning or splitting is measured. Information on the elastic modulus of wood is required for an interpretation of strain or deflection into stress (Schajer and Ruud 2013; Walton 2002). However, the modulus of elasticity of lumber, depending on several factors such as moisture content, specific gravity and grain orientation (Bodig and Jayne 1982; Matan and Kyokong 2003; Sonderegger et al. 2013), is not conveniently measured by kiln operator in sawmills. Usually only measured strain profile or deflection is reported. This variation or change in the modulus of lumber could affect the quantitative interpretation of the internal stress in terms of deflection or strain profile. In addition, the prong test was reported to potentially provide an ambiguous reading on the level of the internal stress depending on the amount of the wood removed (Fuller and Hart 1994).

The aims of this chapter are to compare the results obtained from the proposed restoring force technique against those according to the existing techniques and to quantify the magnitude of the internal stress using the measured restoring force data. A numerical model of finite element (FE) analysis is first employed to simulate the measured restoring force and then to deduce the geometrical shape factor used in the internal stress calculation. Emphasis is placed on investigation of internal stress behavior of the 30mm thick kiln-dried rubberwood lumber with various widths.

## 7.2 Background

At the beginning of the drying period, internal stress is generated as soon as the moisture content in the outer layer of lumber is below the fiber saturation point. Elastic response to the incompatible shrinkage strains to preserve dimensional continuity within a

piece of lumber induces tensile and compressive stresses in the outer layer and inner core, respectively. As the drying process continues, the internal stresses reverse as a result of viscoelastic and machano-sorptive creep. Then up until the end of drying, a lumber outer layer is under compressive stress while an inner core layer is under tensile stress (Perré and Passard 2007).

By assuming a linear distribution of internal stress across half thickness of lumber (Figure 7.1a), magnitude of maximum stress,  $\sigma_{\rm m}$ , assumed to be equal at the outer surface and the inner core, can be calculated by a deflection of the half-split specimen (Figure 7.1b) as expressed by

$$\sigma_{\rm m} = \frac{E \cdot \Delta \delta \cdot d}{4l^2} \tag{7.1}$$

where E,  $\Delta\delta$ , d and l are Young's modulus in the tangential direction, mouth opening, thickness and sawed depth of the specimen, respectively (Walton, 2002). The restoring force, P, required to keep the half-split specimen in the original configuration (Figure 7.1c) can be computed using

$$P = \frac{E \cdot \Delta \delta \cdot b}{S} \tag{7.2}$$

where b is sample length and S is a geometrical shape factor (Lados and Apelian 2006).. By combining equations (7.1) and (7.2), the maximum stress at the surface and the core layers can be expressed as (Diawanich et al. 2012)

$$\sigma_{\rm m} = S \frac{d}{4bl^2} P \tag{7.3}$$

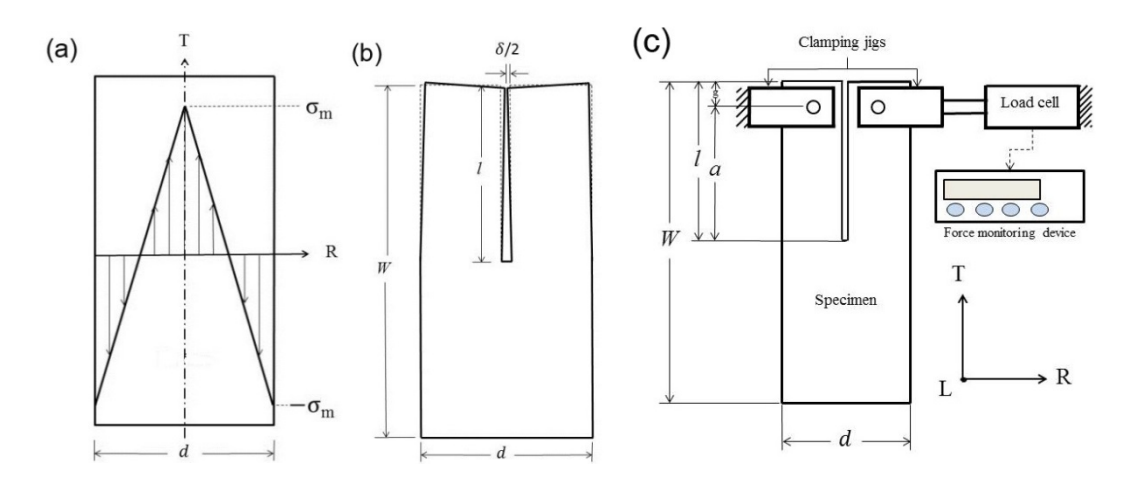


Figure 7.1 (a) Linear distribution of through thickness internal stress within lumber, (b) deflection of half-split specimen caused by internal stress after sawing and (c) application of restoring force to restrain half-split specimen in original configuration prior to sawing.

It should be noted that by this means the magnitude of internal stress can be calculated directly from the measured restoring force P without any knowledge of the Young's modulus, E, of the wood. However, the value of the geometrical shape factor S is dependent on half-split specimen configuration such as specimens' size, half-split length and configuration of the applied force. Within this work, the values of S for the test specimens are deduced by the FE technique.

### 7.3 Materials and method

# 7.3.1 The restoring force measuring device

The restoring force measuring device (Figure 1c) was designed based on the concept proposed by Diawanich et al. (2012). The equipment (Figure 7.2) consists mainly of a relatively rigid steel frame, two clamping jigs of 56 mm wide and a load cell (Cooper Instrument, USA). One jig was fixed to the frame and another one was attached to a steel rod connected to the load cell. A rubberwood specimen of 50 mm long, b, was first fixed to the device by being clamped onto the jigs at a distance, g, of 10 mm away from the top end. Care was taken to ensure that optimum torque of 2-3 N·m was applied with a contact area of 24 mm<sup>2</sup> to hold the specimen to the jigs without damaging the specimen. While being clamped to the frame, the specimen was cut at half the thickness in a wide direction of lumber for half length (l/W=0.5). The device was designed such that the specimen clamped to the frame can be sawed in the wide direction using a band saw. Since the specimen is restrained to the frame and to a steel rod connected to the load cell, a net force generated by relaxation of internal stress within the half-split specimen was transferred to the load cell. The sign and magnitude of the force were then displayed on the force reading device (Figure 7.2).

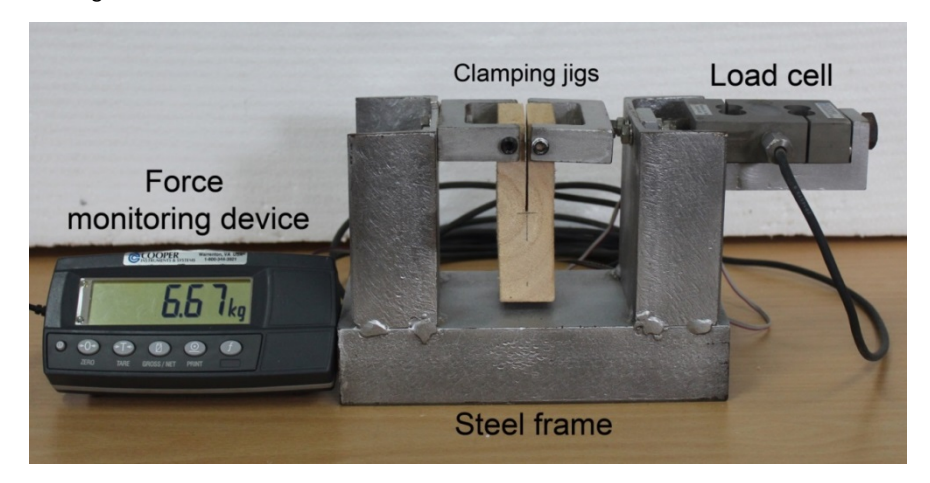


**Figure 7.2** Photograph of the wood specimen installed in the restoring force measuring device

### 7.3.2 Assessment of internal stress in industrial rubberwood kiln dried lumber

Kiln dried rubberwood lumber (30mm thick and 1300mm long) with three different widths (56 mm, 78 mm and 100 mm) was taken immediately after drying from a local sawmill in Nakhon Si Thammarat, Thailand. Ten pieces of lumber were used for each group. The ring orientation was controlled to neglect the effect of the grain orientation by selecting normal to the growth ring aligned parallel to the thickness of lumber. For each lumber, two adjacent specimens were cut at approximately 50 mm from the end of lumber (Figure 7.3a). The first specimen with the length of 50 mm was used to determine the restoring force and the released strain according to the McMillen slice test (McMillen, 1958). The specimen was first marked by divided lines so it could be cut into six equal slices. The initial width of each pre-marked slice ( $W_b$ ) was measured by calipers to an accuracy of 0.01 mm (Figure 7.3c). The specimen was assembled into the restoring force measuring apparatus and were cut through the pre-marked half thickness line for a half width (l/W=0.5). The restoring force was then recorded. The specimens were then cut into slices along the pre-marked lines and the width,  $W_o$ , of each slice was immediately measured. The released strain of each slice,  $\boldsymbol{\varepsilon}$ , was calculated according to  $\boldsymbol{\varepsilon} = \frac{W_a - W_b}{W_b}$ .

For the FE model verification, Young's modulus in the tangential direction of each slice of the two sets of 100 mm wide specimens with relatively high levels of internal stress (HS) and low levels of internal stress (LS) were assessed using a universal testing machine (Lloyd 150kN, UK) equipped with a strain gauge (Epsilon Technology, USA). A section of each slice was also weighted before and after oven-drying at 104 °C for 24 hours to determine its moisture content.

The second specimen cut at the length of 15 mm was sawed into two halves by its thickness according to the case-hardening test method (European Committee for Standardization, 2010) (Figure 7.3d). The two test pieces were then placed flat on a test jig with 75 mm pin distance and the maximum gap distance between the two test pieces at midpoint was measured with an accuracy of 0.1 mm. The measured value, subtracted with the diameter of the test jig pins, was multiplied by a factor of 1.78 to obtain the equivalent maximum gap distance measured at the 100 mm pin separation,  $G_{100}$ , according to EN (European Committee for Standardization, 2010).

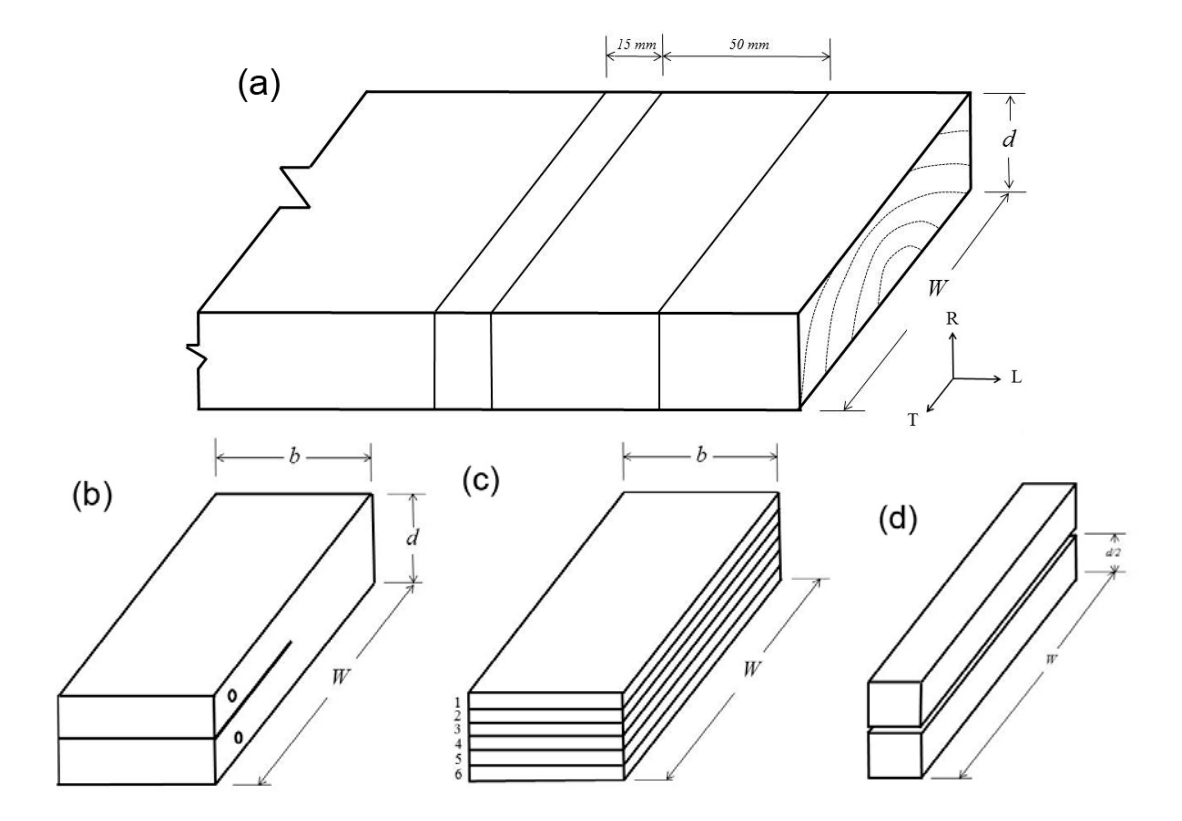


Figure 3 Sample layouts of (a) the test specimen cut from the lumber, (b) the half-split specimen for the restoring force measurement and the McMillen slice test and (c) the case-hardening test.

The remaining pieces of lumber were coated with aluminum paint at both ends and stored in ambient condition (28±2°C and 75±6% RH). Assessment of internal stress was then performed at a week interval for up to three weeks to examine the lower levels internal stress. For the case-hardening test using a test jig with 75 mm pin distance (European Committee for Standardization, 2010), only pieces of lumber with 78 mm and 100 mm wide were examined. In addition, some pieces of rubberwood lumber stored in ambient condition for a longer time for up to 4 months were also tested for a very low level of internal stress.

## 7.3.3 Finite Element (FE) analysis of the restrained half-split specimen

The FE method was employed to verify the mechanical response of the restrained half-split specimen and to determine the geometrical shape factor for the three different widths of lumber. The 3D model was created using the commercial FE software, ANSYS v12. The constitutive model of linearly elastic orthotropic materials was assigned into the computational procedure. Young's moduli and shear moduli used in the FE analysis were calculated as ratios of the measured Young's modulus in the tangential direction  $(E_L: E_R: E_T = 20: 1.6: 1, G_{LR}: G_{LT}: G_{RT} = 10: 9.4: 1$  and  $E_L: G_{LR} = 14: 1$ ). Three Poisson's ratios were estimated to be  $\mu_{RL} = 0.02$ ,  $\mu_{LT} = 0.02$  and  $\mu_{RT} = 0.35$  (Bodig and Jayne 1982, Kretschmann 2010). To reduce computational time in the solving process, only a quarter of

specimen was modeled as presented in Figure 7.4. The plane of symmetry was fixed in the L-direction. All nodes in the clamping area were restrained in the R-direction to deduce the calculated restoring force,  $P_{col}$ .

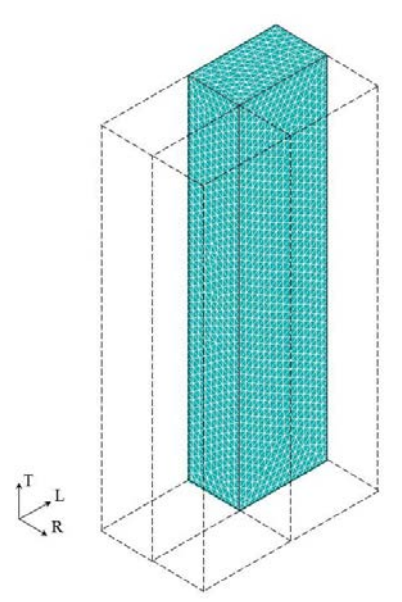


Figure 7.4 The 3D mesh for a quarter of the specimen used in finite element simulation

To validate the FE model, the released strain and Young's modulus data determined by the McMillan slice test were applied to the layers corresponded to the tests. For the determination of the geometrical shape factor, S, the linearly distributed internal stress profile with the maximum magnitude of  $\pm 1$  MPa at the surface and the core layers with a uniform value of Young's modulus in the tangential direction of 500 MPa were employed.

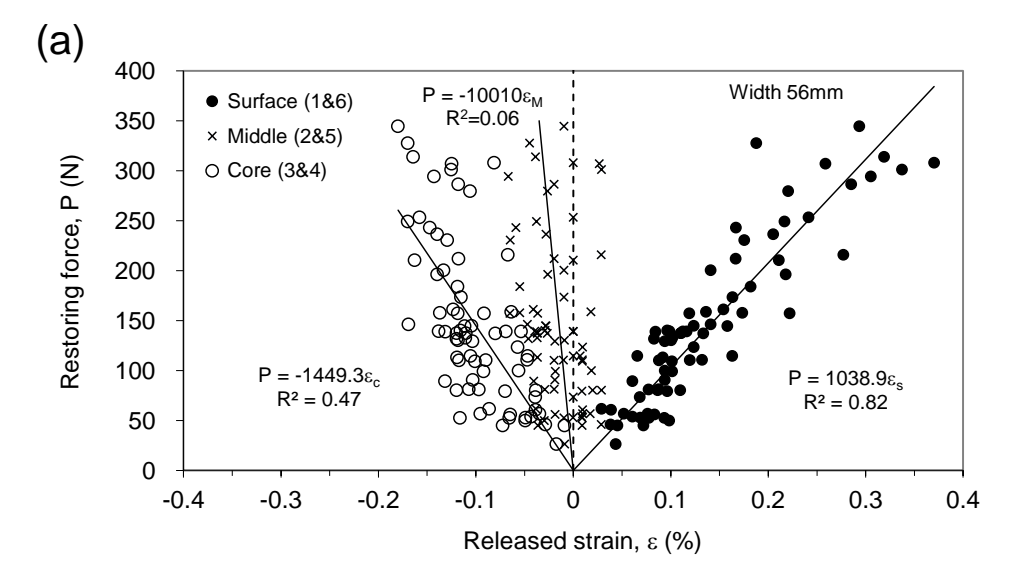
### 7.4 Results and discussion

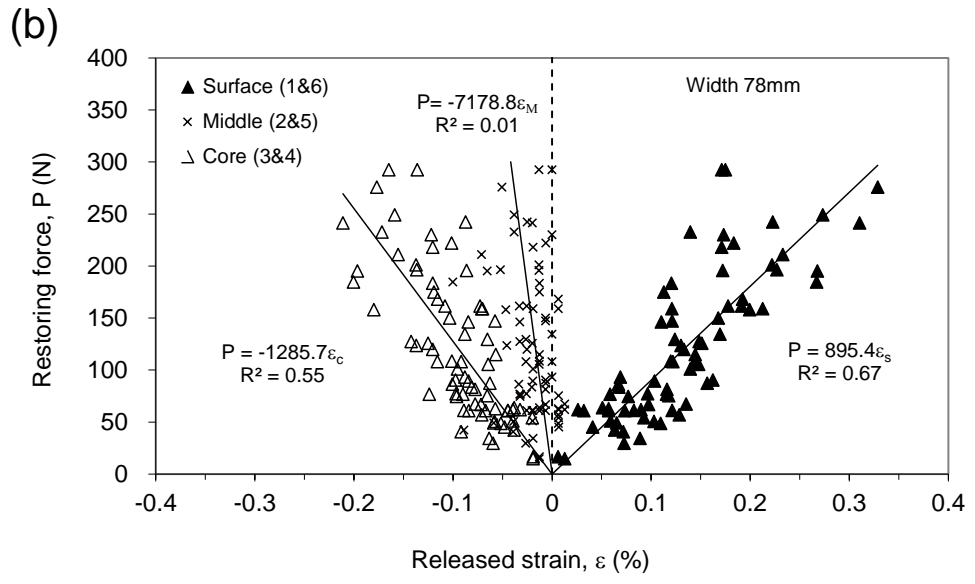
### 7.4.1 Measurement of internal stress

The measured values of restoring force are plotted against the measured released strain data for each layer of the kiln-dried lumber with various widths in Figure 7.5a-c. After kiln drying, the outer and the inner layers of the lumber are often under compressive and tensile stresses, respectively. A resultant force generated across the core through the surface layers of the half-split specimen therefore bent the two legs inward. The device was designed to restrain the specimen to the initial position at the clamping points. As a result, a tensile (positive) restoring force was detected on the load cell. After slicing of the surface layer, lengthening with a positive value of released strain indicates that the wood in this layer was under compressive internal stress before being sliced. On the other hand, a negative released strain observed at the core layer indicates a tensile internal stress. This

behavior has been reported for casehardening of kiln-dried lumber by various authors (McMillen 1958, Perre' and Passard 2007).

The magnitude of the restoring force at the surface and the core layers appears to be proportional to the level of the released strain. Linear coefficients, which are dependent on lumber width, are lower at the surface layer with respect to those at the core layer by 30%. The values of the linear coefficients of the 58 mm to 100 mm wide lumber decrease from 1,039 N/% to 676 N/% at the surface layer and from -1,449 N/% to -978 N/% at the core layer. At a particular level of the restoring force, the magnitude of the positive released strain at the surface layer is slightly greater than that of the negative one at the core layer while the released strain of the middle layer is slightly less than zero. Therefore, the released strain profile across the specimen thickness could be assumed to be linearly distributed across lumber thickness although the actual profile is not perfectly linear.





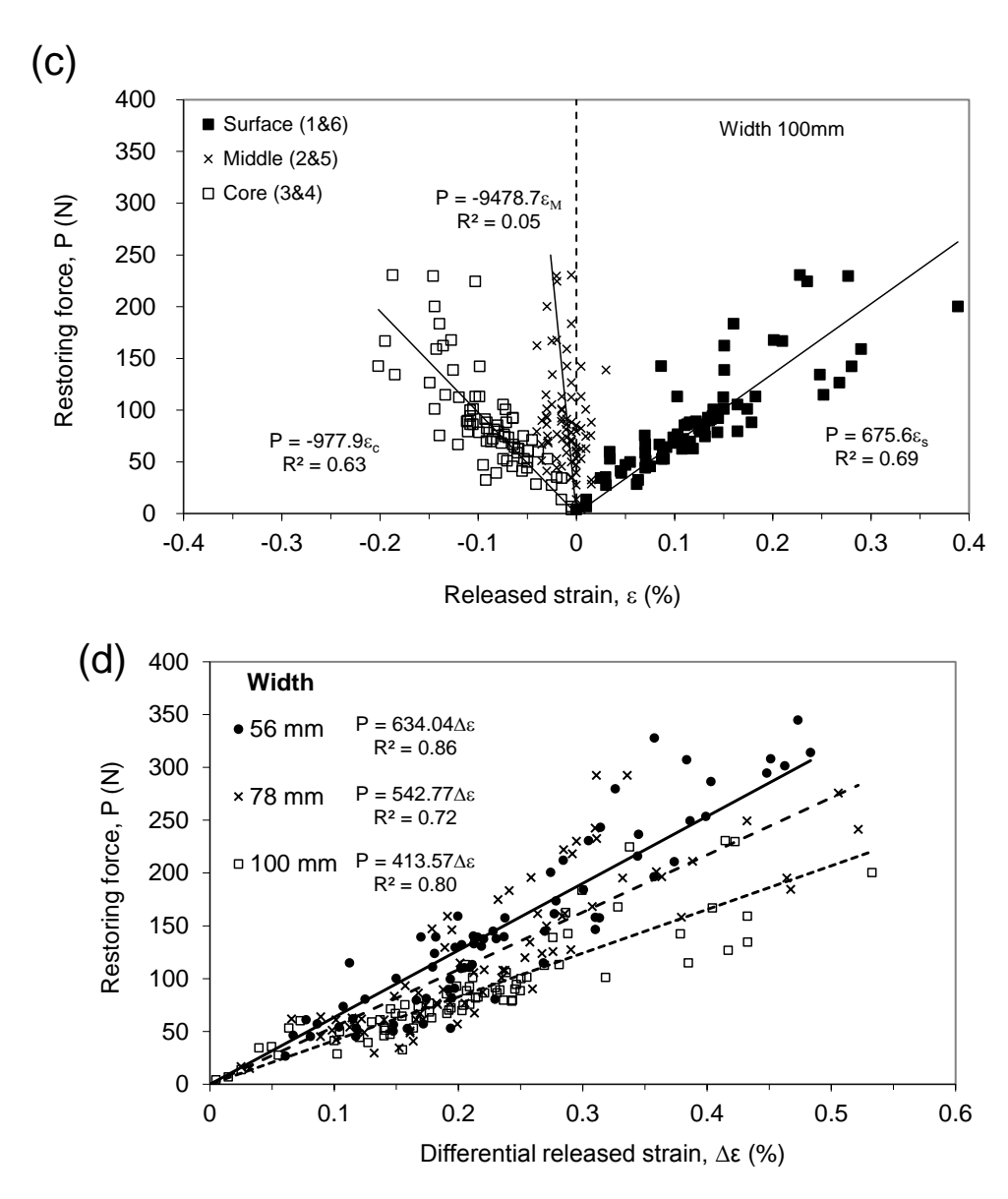


Figure 7.5 Comparison of the restoring force and the released strain at the surface, middle and core layers of the 30mm thick and (a) 56mm, (b) 78mm and (c) 100mm wide kiln-dried rubberwood lumber and (d) plot of resorting force against differential released strain between the surface and the core layer at various lumber widths.

Similar linear correlation is also observed when comparing the maximum gap distance according to the case-hardening test method against the magnitude of the released strain. The linear coefficients are independent of the timber width (Figure 7.6a-b). For the case-hardening test, equation (7.1) can be rearranged as  $\Delta \delta = \frac{4W^2}{d} E \sigma_{\rm m}$  given that the half-split length is equal to width of timber (l=W). Therefore, the value of  $\Delta \delta$ , bending of the half slice and therefore the maximum gap measured in the case-hardening test, varies with square of the timber width (Welling 1994).

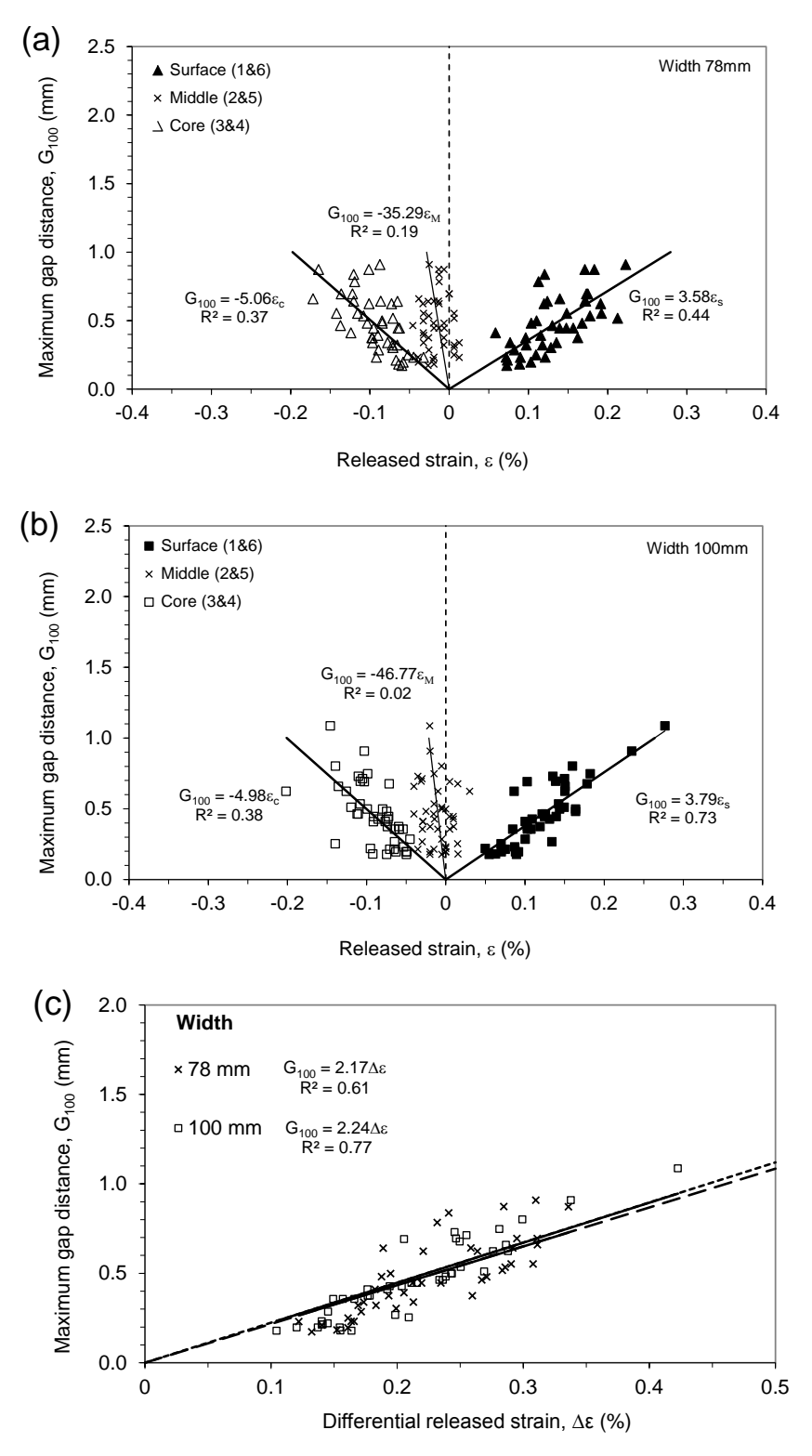
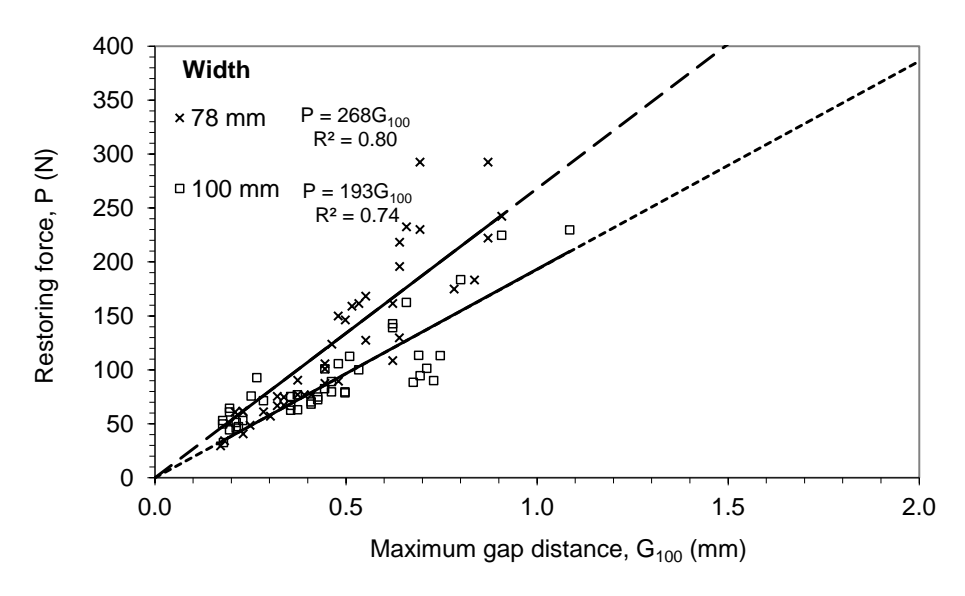


Figure 7.6 Comparison of the measured maximum gap distance and the released strain at the surface, middle and core layers of the 30mm thick and (a) 78mm and (b) 100mm wide kiln-dried rubberwood lumber and (c) plot of maximum gap distance against differential released strain between the surface and the core layer at various lumber widths.

Comparison of the restoring force and the maximum gap distance with the released strain data (Figures 7.5d and 7.6c, respectively) is best facilitated by plotting those against the differential released strain,  $\Delta \varepsilon$ , calculated according to the equation  $\Delta \varepsilon = \varepsilon_s - \varepsilon_c$  where  $\varepsilon_s$  is the average released strain of the surface layer (slices 1 and 6) and  $\varepsilon_c$  is the average released strain of the core layer (slices 3 and 4). It is clear that sensitivities, the slopes of the plots, of the restoring force technique (Figure 7.5d) decrease with the timber width while those of the case-hardening test (Figure 7.6c) are unaffected. At the same level of the differential released strain, the wider timber produces the lesser restoring force but yields constant level of  $G_{100}$ . Finally, linear relationship between the restoring force and the maximum gap distance is obtained (Figure 7.7).



**Figure 7.7** Comparison of the measured restoring force and the measured maximum gap distance at various widths of the 30mm thick kiln-dried rubberwood lumber.

It is obvious that the results obtained by the restoring force technique are consistent with those of the traditional McMillen slice test (McMillen 1958) and the standard test method of the case-hardening test (European Committee for Standardization 2010). Furthermore, the magnitude of the restoring force possesses a linear relationship with the released strain obtained from the McMillen slice test and the maximum gap distance according to the case-hardening test, therefore the restoring force measurement technique could be used as an alternative means for an assessment of the internal stress within industrial kiln-dried lumber. An attempt is made in the following sections to relate the size dependent restoring force to the internal stress level within the lumber.

7.4.2 Validation of FE model and determination of the geometrical shape factor

The released elastic strain and Young's modulus in the tangential direction and
moisture content distributions within the 30 mm thick and 100 mm wide HS and LS

specimens obtained from the McMillen's slice test are shown in Figure 7.8a-c. The elastic strains due to the release of internal stresses were not uniform (Figure 7.8a). Moisture content was approximately uniform across the lumber thickness with the average values of  $5.8\pm0.5~\%$  and  $11.0\pm0.4~\%$  in the HS and LS specimens, respectively (Figure 8b). Since moisture content was lower in the HS specimens therefore Young's modulus in these specimens ( $562\pm57~\text{MPa}$ ) was higher than that in the LS specimens ( $461\pm55~\text{MPa}$ ) (Figure 8c). The experimental restoring forces measured at the cutting depth ratio  $l/W=0.5~\text{are}~183\pm16~\text{N}$  and  $72\pm6~\text{N}$  for the HS and LS specimens, respectively.

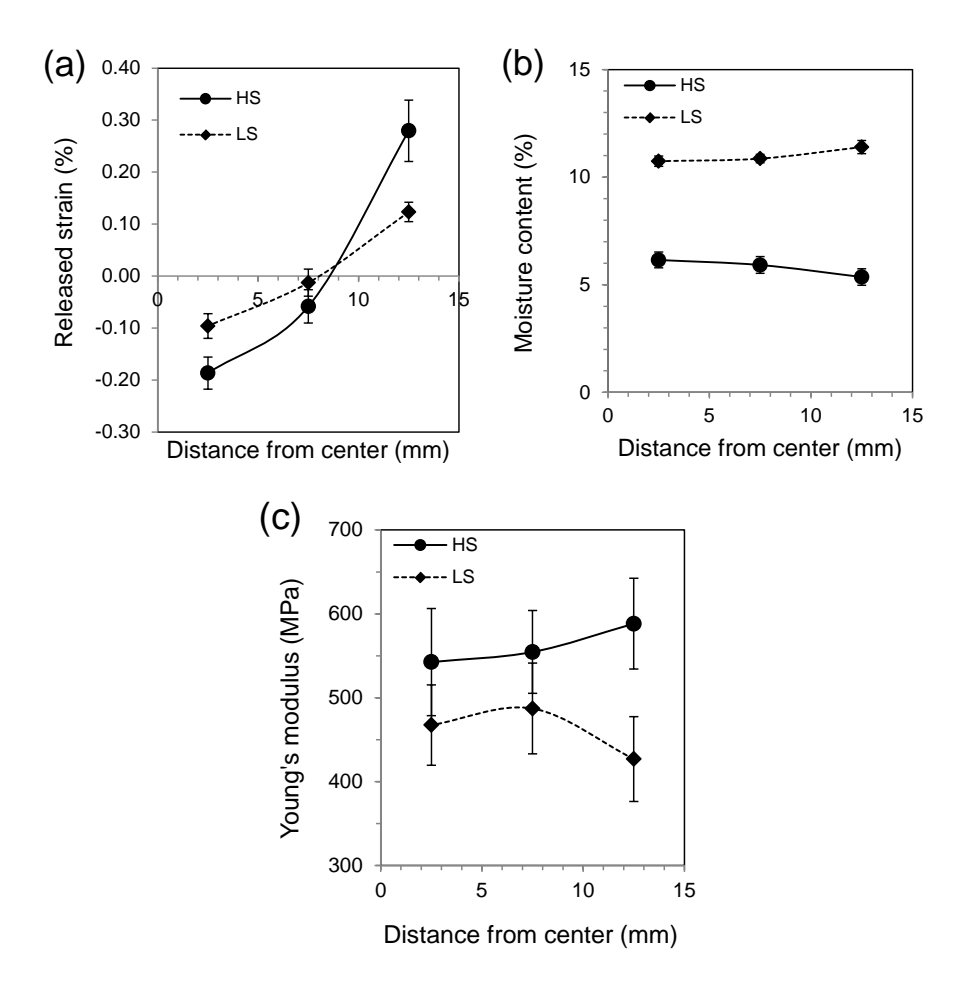


**Figure 7.8** Distributions of (a) released elastic strain, (b) moisture content (c) Young's modulus within the 30 mm thick HS and LS rubberwood kiln-dried lumber.

Using the released strain (Figure 7.8a) and the average Young's modulus profiles in the tangential direction, the mechanical state of the HS specimen before and after half-splitting and restraining as predicted by the FE model are shown in Figure 7.9. By fixing all nodes within the clamping area on both legs of the half-split specimen, the restoring force  $P_{col}$  of 174 N was obtained from the FE model. The distribution of transverse internal stress in the restrained half-split HS specimen (Figure 7.9b) is approximately similar to that within the initial specimen prior to sawing (Figure 7.9a).

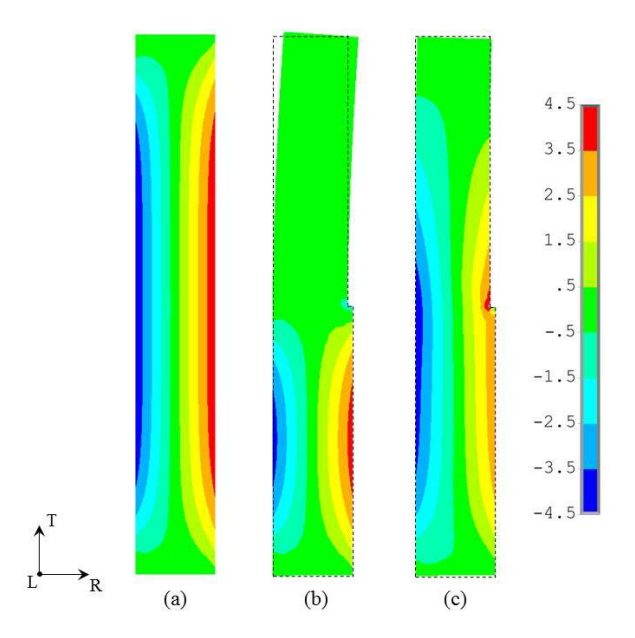


Figure 7.9 Contour plots of transverse internal stress predicted across the thickness of (a) the initial HS specimen and (b) the half-split HS specimen (l/W=0.5) with the restoring force (Pcal= 174 N) applied at 10mm away from the top that keep the specimen in its initial configuration prior to sawing.

Actually for an ideal restraining, the distribution of the internal stress within the restrained half-split specimen should be as similar as possible to that within the initial specimen prior to sawing. However, this is very difficult to achieve and it is not practically possible to fully restrain the specimen for all stress/strain components. Within this work, only transverse stress/strain components were of the interest. It should be emphasized that an improvement on restraining of the half-split specimen could still be made and is worthy of further study. The predicted restoring force obtained from the FE model (174 N and 70 N of the HS and LS specimens, respectively) are in good agreement with the experimental restoring forces (183±16 N and 72±6 N for the HS and LS specimens, respectively) within experimental errors.

After being validated, the FE model was employed to deduce the geometrical shape factor S for the 30 mm thick half-split specimen. By assuming a linear distribution of internal stress from the outer surface through the core and a constant Young's modulus in the tangential direction across the specimen thickness, the value of geometrical factor S was obtained from the simulated restoring force  $P_{cal}$  as

$$S = \frac{4bl^2}{d} \frac{\sigma_{\rm m}}{P_{cal}} \tag{7.4}$$

where b, l and d are length in the longitudinal direction, half-split length and thickness of the specimen, respectively. The derived geometrical shape factor plotted against width of lumber at various cutting depth ratios (l/W) is shown in Figure 10. The geometrical factor

increases with the lumber width and the cutting depth ratio. The factor at each cutting depth ratio is best described by the second-degree polynomial equations. The fitted constants and the corresponding correlation coefficients are also shown in Figure 7.10. Together with equation 7.3, the geometrical factor derived can be directly used in an estimation of the internal stress level within lumber from the measured restoring force. Determination of the geometrical shape factor for various lumber sizes and restraining configurations should be pursued as a future work.

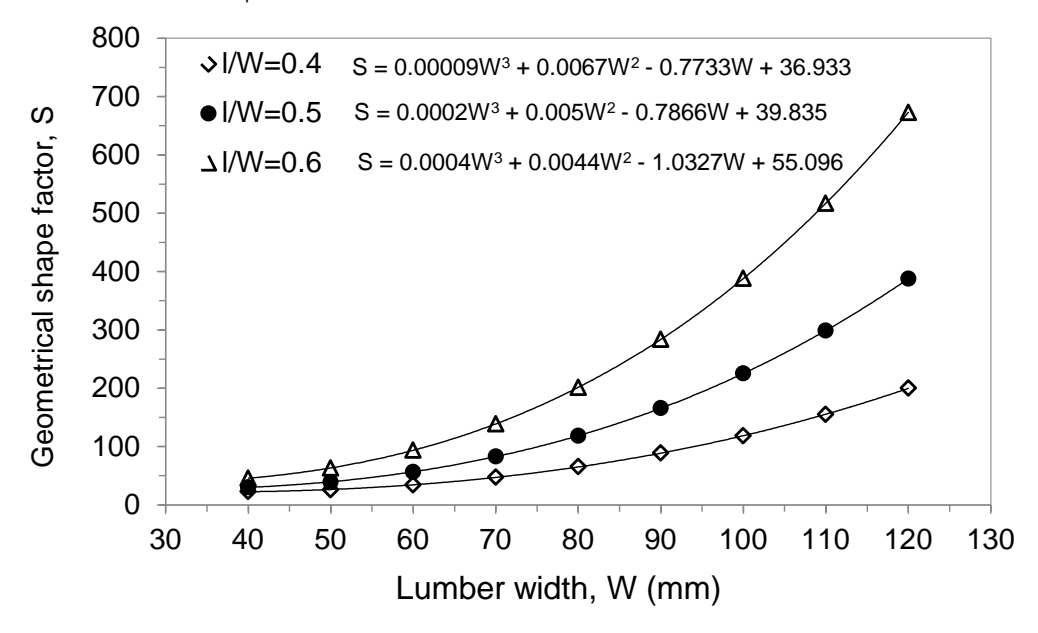
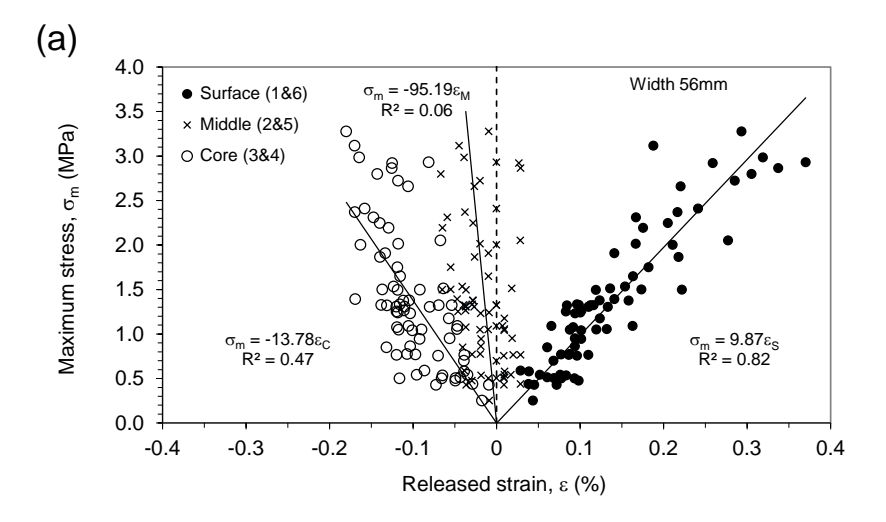


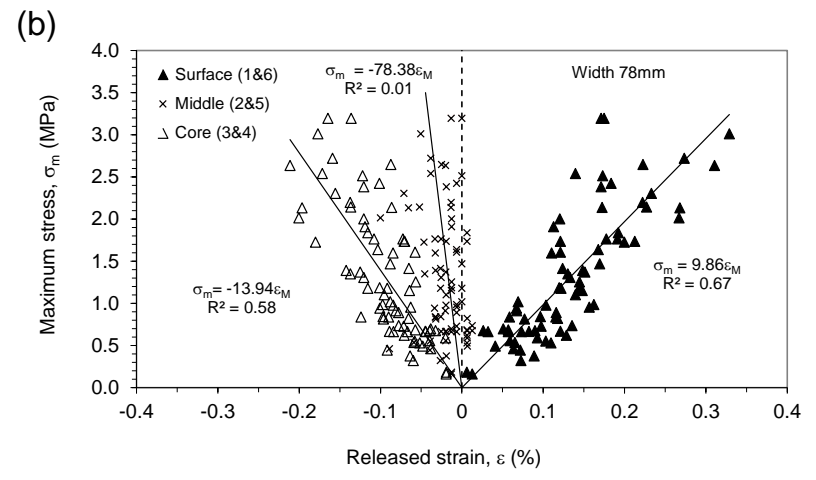
Figure 7.10 The geometrical shape factor S derived by the FE model plotted against width of the half-split 30mm thick lumber at various cutting depth ratios (l/W). Solid lines, the best third-degree polynomial fits to the data, together with the fitted constants are also displayed.

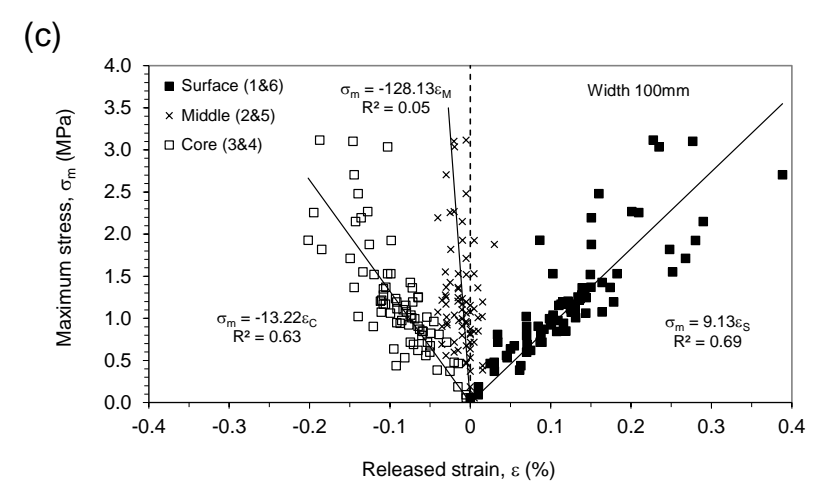
### 7.4.3 Evaluation of internal stress within kiln-dried lumber

To assess the level of the internal stress within the lumber, the maximum internal stresses  $\sigma_m$  were calculated from the restoring force data by means of the equation 7.3 with the use of the geometrical factor calculated from the third-degree polynomial equations and the constants in Figure 7.10. The calculated maximum internal stresses are plotted against the released strain data measured for each layer of the kiln-dried lumber with various widths in Figures 7.11a-c. The magnitude of the maximum internal stress both at the surface and the core layers is proportional to the level of the released strain with linear coefficients of 8.48 $\pm$ 0.26 MPa/% and -12.10 $\pm$ 0.43 MPa/%, respectively, independent of the lumber width. By plotting the calculated maximum stress against the differential released strain (Figure 7.11d), a linear relationship is obtained and data from different widths of lumber seem to fall into a single curve. The linear constant of the best fit line deduced from the graph is 514 $\pm$ 136 MPa. The scatter of the data points around the best-fit line is due

to variation in the Young's modulus of the kiln dried rubberwood lumber which depends on several factors such as specific gravity and moisture content of the lumber.







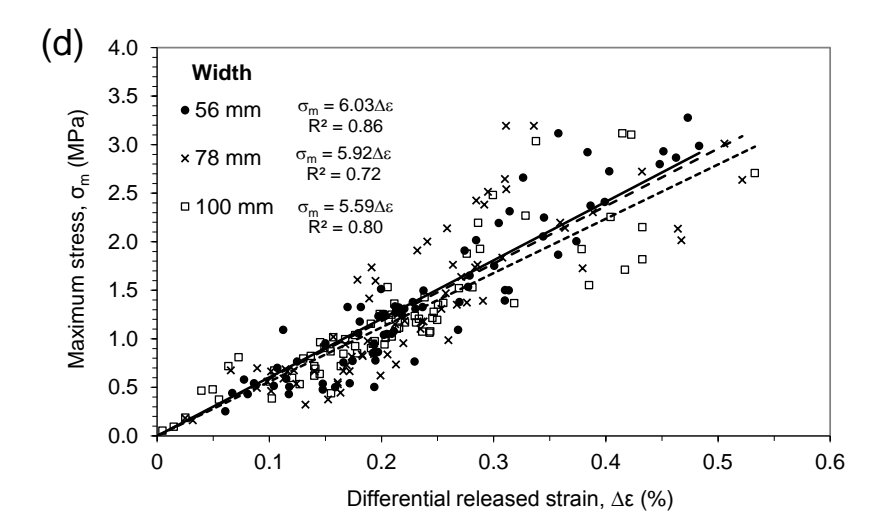
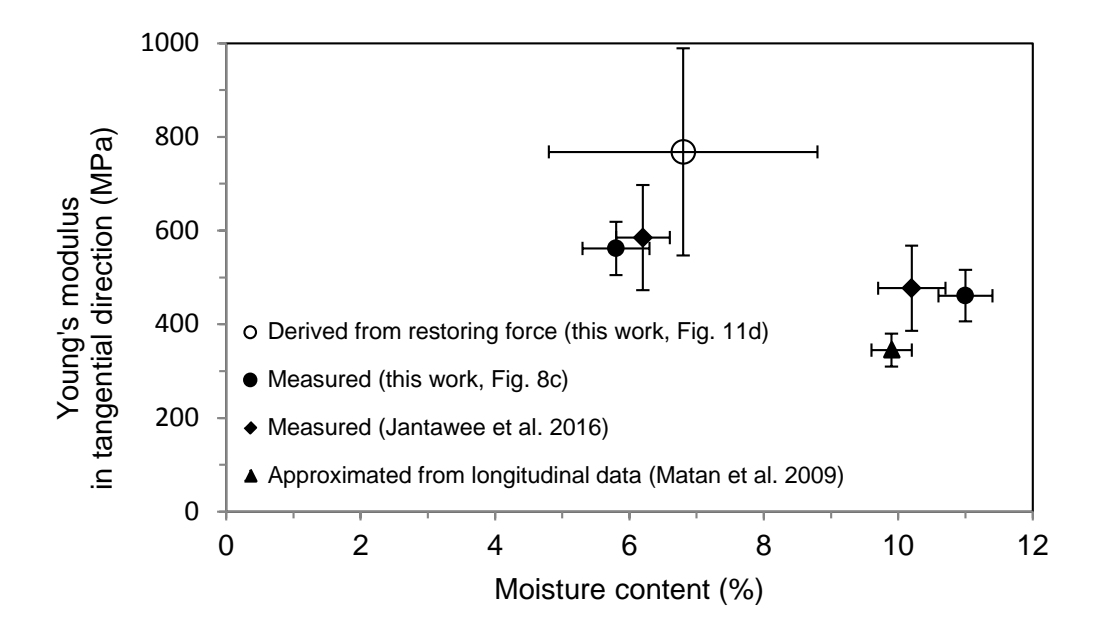


Figure 7.11 Comparison of calculated maximum internal stress  $\sigma_m$  and the released strain at the surface, middle and core layers of the 30mm thick and (a) 56mm, (b) 78mm and (c) 100mm wide kiln-dried rubberwood lumber and (d) plot of maximum internal stress against differential released strain between the surface and the core layer at various lumber widths.

If it is assumed that Young's modulus of each lumber in the transverse (tangential) direction is somewhat constant, stress at the surface layer  $(\sigma_s)$  and stress at the core layer  $(\sigma_c)$  can be expressed as  $\sigma_s = E\varepsilon_s$  and  $\sigma_c = E\varepsilon_c$ , respectively. It can be estimated that  $\sigma_s - \sigma_c \sim \frac{4}{3}\sigma_m = E(\varepsilon_s - \varepsilon_c) = E\Delta\varepsilon$ . Therefore, the maximum internal stress is proportional to differential released strain between the surface and the core layers via the equation  $\sigma_m = \frac{3}{4}E\Delta\varepsilon$ . As a result, the average value of Young's modulus in the tangential direction of 685±181MPa could be deduced from the linear constants obtained in Figure 7.11d.

The average moisture content of the tested specimens is 6.8±2.0%. Given that the information concerning modulus in the tangential direction of rubberwood is very sparse, a general agreement between the calculated and the experimental (Figure 7.8c) and other sources (Jantawee, et al. 2016; Matan et al. 2009) data of Young's modulus as a function of moisture content can be observed in Figure 7.12. In addition, the coefficient of variation (CV) of 26% in the value of Young's modulus, is in the reasonable range according to the nature of wood (Bodig and Jayne 1982, Matan and Kyokong 2003), provided that the test samples were randomly selected from a pile of industrial kiln-dried rubberwood lumber.



**Figure 7.12** Plot of Young's modulus in the tangential direction against moisture content of rubberwood; calculated value and experimental data from this work and other sources.

Figure 7.13 shows the calculated maximum internal stress plotted against the maximum gap distance values obtained from the case-hardening test. Both values follow a linear relationship and the maximum gap distance value is independent of the width of the timber meaning that different sizes of timber yield similar gap distance values if they possess a similar level of the internal stress. This behavior is also confirmed by a plot of the maximum gap distance against the differential released strain (Figure 7.6c) in which linear constants obtained are independent of the width of the timber.

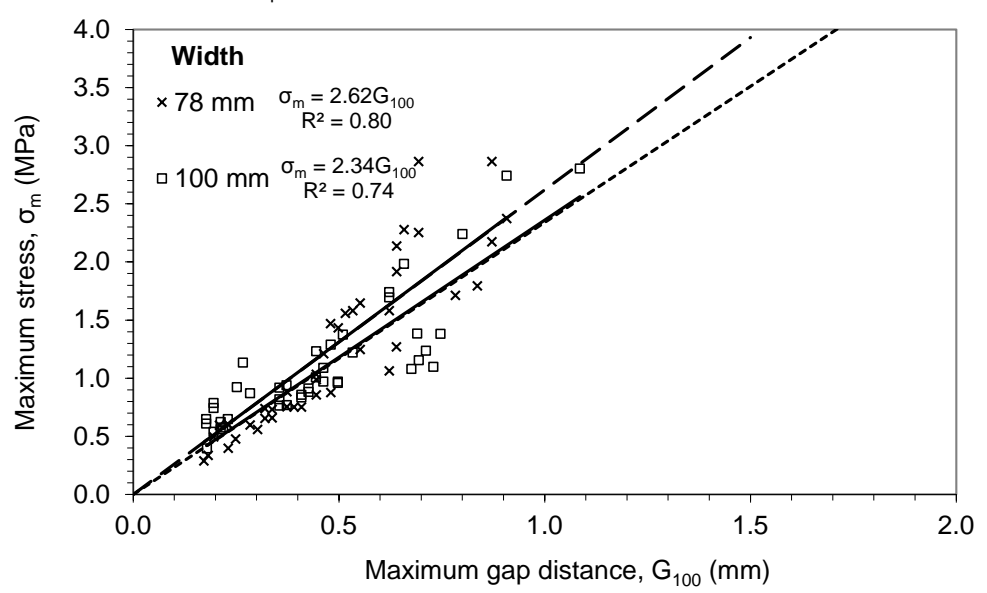


**Figure 7.13** Plot of maximum internal stress against maximum gap distance at various widths of the 30mm thick kiln-dried rubberwood lumber.

Although the information obtained from the conventional McMillen slice test and the standard test of the case-hardening test is consistent with that obtained from the restoring force measurement, but the restoring force technique is relatively easy to perform and the level of the internal stress can be directly calculated without the use of the modulus data of the wood. The released strain and the deflection occurring according to the McMillen slicing and the case-hardening techniques are usually small and are difficult to measure. For the case-hardening test, the deflection obtained appeared to be lumber size dependence which could give an ambiguous indication on the level of the internal stress. The proposed restoring force technique circumvents many difficulties mentioned above. It also gives a reliable and meaningful measurement of the extent of the internal stress within the kiln-dried lumber. In addition, this technique has been adapted to monitor in real-time the evolution of the internal stress during drying, conditioning and storage of the kiln-dried lumber (Diawanich et al. 2010, Tomad et al. 2012).

#### 7.5 Conclusions

The following conclusions can be drawn from this work:

- 1. The measured restoring force of the half-split specimen, mechanically corresponding to the relaxation of the internal stress caused by the half-split cutting, is linearly related to the released strain measured by the McMillan slice test and the case-hardening test values according to the CEN standard test method. The results obtained by the new technique are consistent with those of the two conventional ones.
- 2. A numerical model based on finite element analysis for the restoring force technique is presented. Experimental validation of the model is performed by restoring force and released strain measurements. The predicted and measured restoring forces are shown to be in agreement. The model is then employed to deduce the geometrical shape factor for an evaluation of the internal stress level within the 30 mm thick lumber as functions of lumber's width and cutting depth ratio.
- 3. With the use of the derived geometrical shape factor, the magnitude of the maximum internal stress can be directly estimated from the measured restoring force. The calculated stresses, regardless of lumber size, linearly vary in a similar manner with the released strain data according to the McMillen slice test. The derived Young's modulus is in general agreement with the experimental data in the literatures.
- 4. The restoring force measurement on a half-split specimen has potential to be an alternative method to the conventional techniques for a reliable and meaningful assessment of drying stress within industrial kiln-dried lumber. The technique allows the internal stress level within the lumber to be estimated without prior knowledge of the modulus of wood.

#### References

- 1. Bodig J, Jayne BA (1982) Mechanics of wood and wood composites. Van Nostrand Reinhold Company, New York
- 2. Diawanich P, Matan N, Kyokong B (2010) Evolution of internal stress during drying, cooling and conditioning of rubberwood lumber. Eur J Wood Prod 68(1):1–12
- 3. Diawanich P,Tomad S, Matan N, Kyokong B (2012) Novel assessment of casehardening in kiln-dried lumber. Wood Sci Technol 46: 101-114
- 4. European Committee for Standardization (2010) Sawn timber-method for assessment of case-hardening. CEN standard ENV 14464
- 5. Fuller J, Hart CA (1994) Factors that influence the prong test. In: Proceedings of the 4th IUFRO international wood drying conference. Rotorua, pp 313–320
- 6. Jantawee S, Leelatanon S, Diawanich P, Matan N (2016) A new assessment of internal stress within kiln-dried lumber using a restoring force technique on a half-split specimen, Wood Sci Technol DOI 10.1007/s00226-016-0852-y
- 7. Kretschmann DE, Mechanical properties of wood, in: R.J. Ross (Ed) Wood handbook (wood as an engineering material), Forest Products Laboratory, United States Department of Agriculture Forest Service, Madison, 2010, pp 5/1-5/46.
- 8. Lados DA, Apelian D (2006) The effect of residual stress on the fatigue crack growth behavior of Al-Si-Mg cast alloys-mechanisms and corrective mathematical models.

  Metall Mater Trans A 37: 133–145
- 9. Matan N, Kyokong B (2003) Effect of moisture content on some physical and mechanical properties of juvenile rubberwood. Songklanakarin J Sci Technol 25(3): 327–340
- 10. Matan N, Kyokong B, Preechatiwong W, Wongprot T, Tomad T (2009) Heat treatment of rubberwood in hot compressed water. Final report, Wood Science and Engineering Research Unit, Walailak University, Nakhon Si Thammarat, Thailand (in Thai)
- 11. McMillen JM (1958) Stresses in wood during drying (Report 1652). Department of Agriculture, Forest Service, Forest Products Laboratory, Madison
- 12. Perré P, Passard J (2007) Stress development. In: Perré P (ed) Fundamentals of wood drying, European COST A.R.BO.LOR., Nancy, pp 243-271
- 13. Schajer GS, Ruud CO (2013) Overview of residual stresses and their measurement. In: Schajer GS (ed) Practical Residual Stress Measurement Methods, John Wiley & Sons, West Sussex, pp1-27
- 14. Simpson WT (1991) Dry kiln operator's manual. In: Agriculture Handbook AH-188. Department of Agriculture, Forest Service, Forest Products Laboratory, Madison
- 15. Simpson WT (1999) Drying and control of moisture content and dimensional changes. In: Wood handbook (Wood as an Engineering Material). Department of Agriculture, Forest Service, Forest Products Laboratory, Madison

- 16. Sonderegger W, Martienssen A, Nitsche C, Ozyhar T, Kaliske M, Niemz P (2013) Investigations on the physical and mechanical behavior of sycamore maple (*Acer pseudoplatanus* L.), Eur. J. Wood Wood Prod. 71: 91–99
- 17. Tomad S, Matan N, Diawanich P, Kyokong B (2012) Internal stress measurement during drying of rubberwood lumber: effects of wet-bulb temperature in various drying strategies. Holzforschung 66: 645-654
- 18. Walton HW (2002) Deflection methods to estimate residual stress. In: Totten G, Howes M, Inoue T (eds) Handbook of residual stress and deformation of steel. ASM International, Ohio, pp 89–98
- 19. Welling J (Ed) (1994) EDG-Recommendation on assessment of drying quality of timber, European drying group (EDG), Hamburg
- 20. Wengert E (1992) Techniques for equalizing and conditioning lumber. Cooperative extension programs No. 65. Department of Forest and Wildlife Ecology, University of Wisconsin, Madison

## Chapter 8

# Within-tree variability of internal stress generated during drying of rubberwood lumber

#### 8.1 Introduction

Since several pieces of lumber are commonly dried together inside a batch kiln, natural variability in wood properties must therefore be accounted for in the design of drying procedures (Langrish and Walker 2006). Variation in the properties among pieces and even within each piece of lumber causes variability in drying rate and sensitivity to drying defects (Perré and Martin 1994). While the former has been extensively investigated both theoretically and experimentally (Perré and Turner 1999; Tremblay et al. 2000; Perré and Turner 2007), the latter has been largely examined through a variety of mathematical models in which a number of parameters required have been determined by experiments (Pang 2000; Perré and Passard 2004; Moutee et al. 2007; Moutee et al. 2010). At the beginning of drying, the internal stress is initially generated within a piece of wood as a result of differential shrinkage between the surface and the core sections. The tensile and compressive stresses are developed at the outer and inner layers, respectively. As drying continues, the internal stress then reverses as a result of viscoelastic and mechano-sorptive creep (Perré and Passard 2007; Moutee et al. 2007). Defects such as surface and internal checks and splits could take place if the internal tensile stress exceeds the wood's strength at any moment during drying. Generation of drying stress and its potential for causing defects have been extensively studied both in lumber (Ormarsson et al. 1998; Ormarsson et al. 1999; Ormarsson et al. 2000) and wood discs (Kang and Lee 2002; Larsen and Ormarsson 2013).

Rubber trees, widely grown in Southeast Asia for the production of latex, are used in this study. The trees are usually cut down after 25 to 30 years for replanting when their production of latex is uneconomical (Balsiger et al. 2000). Rubberwood logs, the byproduct of felled rubber trees, are usually transferred to local sawmills around the area. The production of rubberwood lumber consists mainly of log sawing, chemical impregnation and kiln drying of the sawn lumber (Hong 1995; Teoh et al. 2011). Attempts to accelerate drying of rubberwood lumber by increasing temperature and lower humidity inside the drying kiln have been studied (Theppaya and Prasertsan 2004; Srivaro et al. 2008). Lumber quality is normally examined at the end of drying (Ratnasingam et al. 2010). To cope with variability in wood properties, kiln operators tend to employ conservative drying schedules which could unnecessarily prolong the drying time. Since trees have orthogonal symmetry as a result, wood properties (such as specific gravity plus physical and mechanical ones) vary with the radius from the pith as well as height (Haygreen and Bowyer 1989; Ferreira et al. 2011).

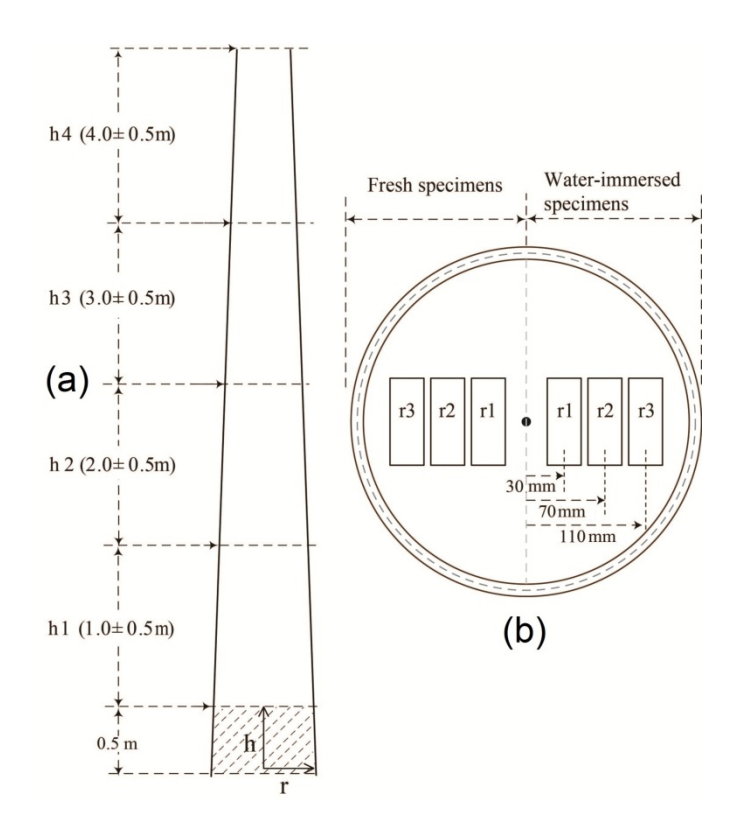
The objective of this chapter is to examine the evolution of internal stress within the lumber prepared from different locations of the rubber tree trunks during drying. A real-time assessment of the internal stress is performed by using a restoring force technique on a half-split specimen (Diawanich et al. 2010; Tomad et al. 2012). An attempt is also made to understand the underlying mechanisms responsible for variability in the stress profiles observed.

#### 8.2 Materials and method

#### 8.2.1 Rubber trees and preparation of test specimens

Two adjacent rubber trees roughly 25 years old from a plantation in the Thasala district of the Nakhon Si Thammarat province in Thailand were used in this work. The trees were sawn into 150 - 170 mm thick discs. Each disc was cut in half into two sections. One section was put in a plastic bag and kept in ambient air and the other was immersed in water for up to 6 months. Prior to testing, the half discs were impregnated with water in a pressure vessel at 12 bar for 60 minutes to attain the saturated moisture content with the full-cell process. A vacuum of -0.8 bar was performed for 15 minutes both before and after the pressurization.

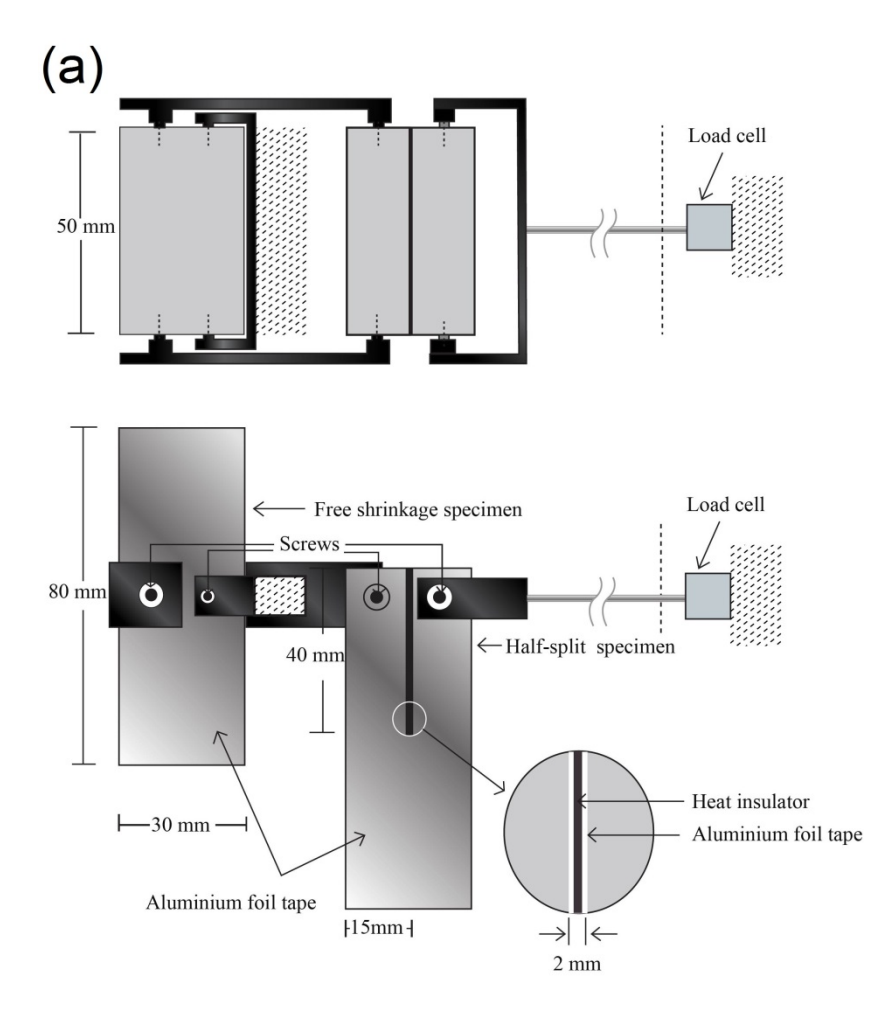
Specimens for internal stress measurement were prepared from the half discs at different locations within the trunk. Orthogonal coordinates (i.e. distance from pith, r, and height from ground level, h) were employed to specify each specimen's location within the tree trunk. Specimens were divided into four coordinate groups along the height i.e.  $h_1$  at  $1.0\pm0.5$  m,  $h_2$  at  $2.0\pm0.5$  m,  $h_3$  at  $3.0\pm0.5$  m and  $h_4$  at  $4.0\pm0.5$  m (Figure 8.1a) and into three coordinate groups along the radial direction (i.e.  $r_1$  at  $30\pm15$  mm,  $r_2$  at  $70\pm15$  mm and  $r_3$  at  $110\pm15$ mm) from the pith (Figure 8.1b).



**Figure 8.1** Schematic diagram illustrating locations of specimens within the rubber tree trunk divided into (a) four coordinate groups along the height ( $h_1$ ,  $h_2$ ,  $h_3$  and  $h_4$ ) and (b) three coordinate groups along the radial direction ( $r_1$ ,  $r_2$  and  $r_3$ ).

#### 8.2.2 Internal stress measurement

Evolution of the internal stress within the rubberwood specimens during drying was monitored using the force measurement technique proposed and verified with the McMillen slice test by Diawanich et al. (2010) and Tomad et al. (2012). The restoring force required to restrain a so-called "half-split" specimen (Figure 8.2a) during drying was measured via a load cell (Cooper instruments, USA). The specimen of dimensions 30mm (thickness in radial direction) × 80mm (width in tangential direction) × 50mm (length in longitudinal direction) was sawed in the tangential direction by a half width (40mm) in order to divide the thickness in half (15mm). The saw line was 2 mm wide. Longitudinal surfaces and the half-sawn faces were sealed with thin aluminium tape to prevent moisture loss before inserting a thin piece of heat insulation into the saw line to prevent direct heat transfer into the core of the specimen. Force generated as a result of the half-split specimen's shrinkage was compensated for by adding a "free shrinkage" specimen of the same dimensions (Diawanich et al. 2010). The restoring force measuring device equipped on both the half-split and the free shrinkage specimens is shown in Figure 8.2b.



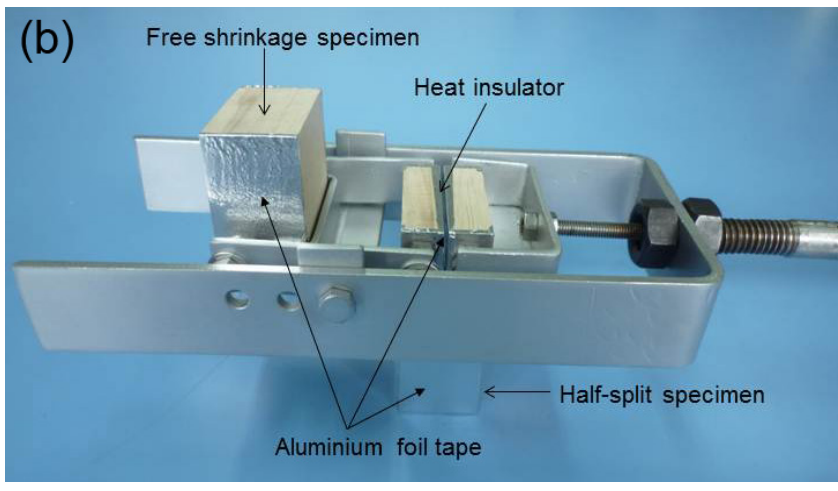


**Figure 8.2** (a) Schematic diagram illustrating details of the restoring force measuring device equipped with the half-split and the free shrinkage specimens and (b) photograph of the device.

#### 8.2.3 Drying procedure

Drying was carried out in a  $15m^3$  drying kiln (Eurasia, Singapore). A stack of lumber, separated by two 30mm fillets, was placed inside the kiln. For each run, a restoring force

measuring device was placed within the lumber stack. Only airflow through the lumber stack was allowed. Fan speed was adjusted to achieve an air velocity through the lumber stack of 4 m/s. The drying schedule was executed via the control system (LabView, National Instruments, USA). A single step drying schedule at the dry-bulb temperature of 90° C and the wet-bulb temperature of 60° C (Haslett 1998; Srivaro et al. 2008) for 70 hours was performed for all drying tests. Steam used to provide heat and humid air within the kiln was generated by an electric boiler (Sahathai Factory, Thailand). Steam pressure at the boiler was maintained at 5 bar. For determination of the drying curves in some specific treatments, two pieces of lumber (30 mm in the radial direction × 80 mm in the tangential direction × 120 mm in the longitudinal direction) were placed inside the lumber stack and periodically weighed for the calculation of moisture content.

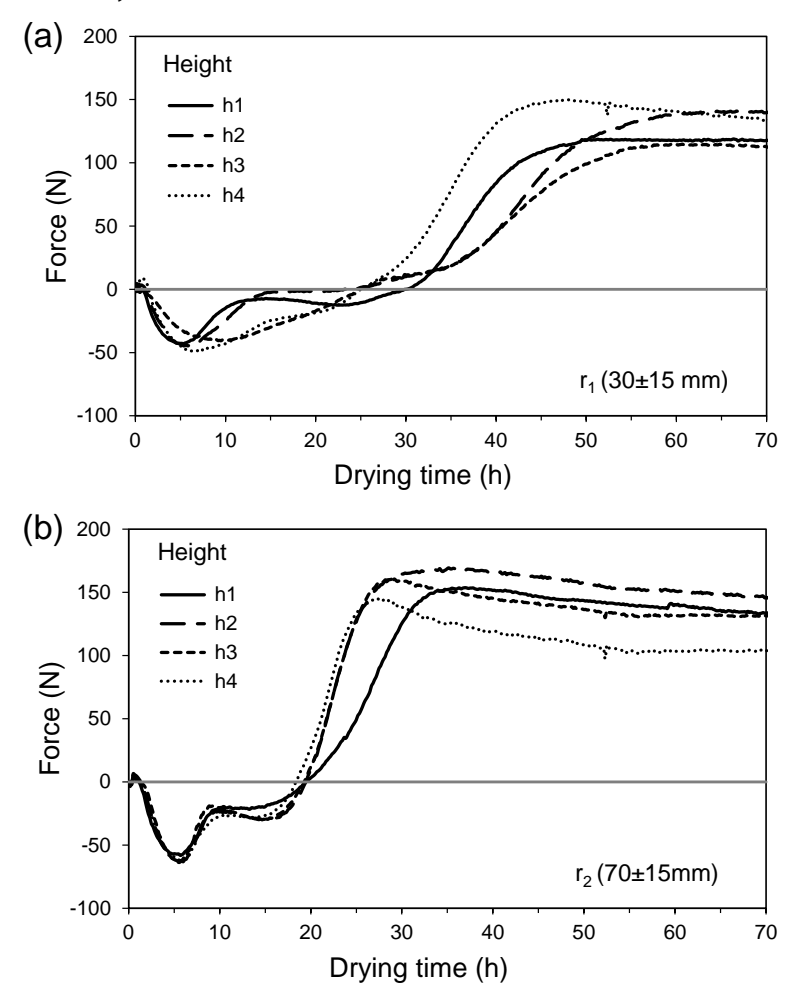
#### 8.3 Results and discussion

8.3.1 Drying of the fresh specimens

In general, the behavior of all measured restoring force profiles (Figure 8.3a-c) is consistent with the mechanisms underlying drying stress generation previously described by various authors (McMillen 1958; Simpson 1991; Perré and Passard 2007). At the beginning of drying, the measured restoring force remains at zero for a very short period of time of about 1 hour. At this stage, only free water evaporates out of wood and the moisture content of the whole lumber is still higher than the fiber saturation point (FSP) and therefore no internal stress is generated. As drying continues, the outer layer dries to below the FSP, while the inner layer is still above the FSP. Both the tensile and compressive stresses are induced at the outer and inner layers, respectively. The internal stresses are generated as a result of an elastic response to the incompatible shrinkage strains. Since the specimen is split at a half thickness, a net resulting stress across the inner through the outer layers produces a force trying to bend the half-split specimen outward. A device is designed to keep the specimen at its original configuration. As a result, a negative force is observed at the load cell. While drying continues, the surface and core layers are dried under tensile and compressive stresses, respectively. The internal stress at the surface and in the core layers is reversed from tensile to compressive and then from compressive to tensile, respectively, as a result of viscoelastic and mechano-sorptive creep (Perré and Passard 2007; Moutee et al. 2007). During this stage, the negative force measured at the load cell decreases and changes its sign to a positive one. After reaching a maximum positive value, the force slightly continues to decline until the end of drying. The relatively higher level of stress in the second part of drying in the inner part of the wood is probably due to the fact that the high temperature and moisture content at the start of drying produced a high level of mechanosorptive and viscoelatic creep at the surface, which in turn tends to produce a higher level of stress in tension in the inner part at the end of the drying process. Future research to

bring further the measurement of stress evolution by adding a conditioning step at the end of the drying schedule (Pang et al. 2001; Diawanich et al. 2010) should be performed.

The restoring forces appear to be largely unrelated to the height of the rubber trees. At the same distance from the pith, the restoring force profiles of the specimens prepared from different heights approximately evolve with time in a similar manner (Figure 8.3a-c). On the other hand, the force profiles clearly change with a radial distance from the pith as longer drying time was required for the completion of stress reversal in the  $r_1$  specimens near the pith with respect to those of the  $r_2$  and  $r_3$  specimens further away. Although the reversal of stress for all specimens started after 5 hours of drying, its completion was from 40 to 50 hours for the  $r_1$  specimens (Figure 8.3a) but was only from 25 to 30 hours for the  $r_2$  and  $r_3$  specimens (Figure 8.3b-c). According to Ferreira et al (2011), a separation of the juvenile and mature wood zones in the rubber tree was determined by changes of the fiber length of about 40 - 55 mm from the pith. Therefore, the  $r_1$  specimens are in the juvenile wood zone while the  $r_2$  and  $r_3$  specimens are in the mature wood zone. Because several properties of the mature wood are roughly constant with the radial distance from the pith (Haygreen and Bowyer 1989), the internal stress profiles of the  $r_2$  and  $r_3$  specimens (Figure 8.3b-c) are approximately similar.



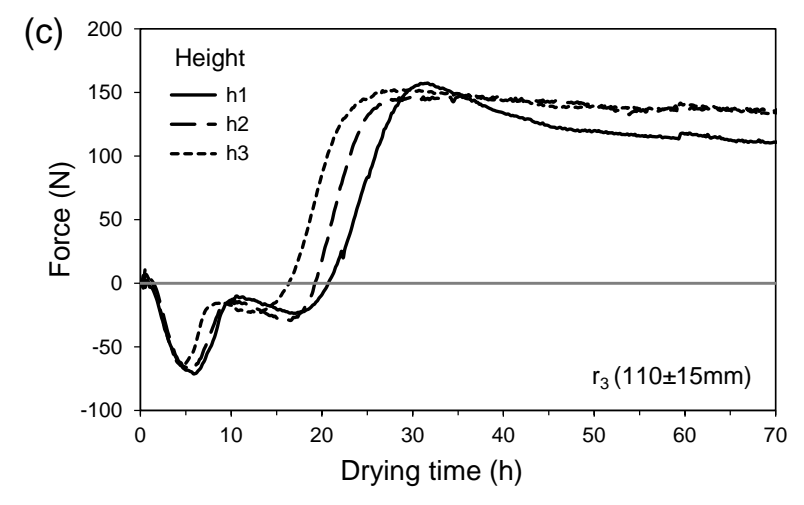


**Figure 8.3** The restoring force profiles of the specimens prepared from rubber tree trunks at distances of (a)  $r_1$  (30±15 mm), (b)  $r_2$  (70±15 mm) and (c)  $r_3$  (110±15 mm) from the pith at various heights  $h_1$  (1.0±0.5 m),  $h_2$  (2.0±0.5 m),  $h_3$  (3.0±0.5m) and  $h_4$  (4.0±0.5 m) during the drying at dry-bulb and wet-bulb temperatures of 90°C and 60°C, respectively.

Figure 8.4a-b show the average drying curves of the  $r_1$  and  $r_3$  specimens at two different heights,  $h_1$  and  $h_3$ . All specimens were impregnated with water to attain saturation prior to testing. It is evident that the saturated moisture contents of the  $r_1$  and  $r_3$  specimens at a particular height are equal. But lower saturated moisture content was observed at higher heights. An examination of the specimens' specific gravity revealed higher values of specific gravity at greater heights which varied from  $0.62\pm0.05$  at  $h_1$  to  $0.69\pm0.02$  at  $h_3$  above ground. It is well known that the saturated moisture content in wood has an inverse relation to specific gravity (Skaar 1972; Glass and Zelinka 2010). Therefore, the increase in specific gravity should be responsible for the lower saturated moisture content observed in the  $h_3$  specimens with respect to  $h_1$ .

The drying curves, reflecting the rate of water evaporation out of the lumber, also reveal some underlying mechanisms of the observed restoring force profiles. For up to 5 hours at the beginning of drying, the  $r_1$  and  $r_3$  specimens at the same heights possess similar linear drying rates (equal slopes in Figure 8.4a-b). Variation within trees should have little influence on the movement of moisture, in both free and bound water, on lumber at this early stage of drying. As a result the restoring force profiles for all tests within this period (Figure 8.3a-c) are rather similar. Internal stress generated during this drying period, with the drying of the outer layer below the FSP and the inner layer above the FSP, is thereupon largely unaffected by the variation within tree. The  $r_3$  specimens then started to dry faster than the  $r_1$  specimens and reached the equilibrium moisture content (EMC) at 3.5±0.1% after about 30 - 40 hours of drying. In comparison, it took up to about 50 hours for the  $r_1$  specimens to reach that level of EMC. At this later stage of drying, variation within the trees appears to play a significant role on the drying of lumber especially on the movement of

bound water within the wood cell wall (Perré and Turner 2007). Thus, the slower drying rate in the  $r_1$  specimens with respect to that of the  $r_3$  specimens (Figure 8.4a-b) must be responsible for the longer stress reversal period observed in these specimens (Figure 8.3a-c). The internal stress profiles of the  $r_1$  and  $r_3$  specimens hardly changed after the specimens reached the EMC.

It should be noted that the restoring force profiles always contain two negative force maxima during the stress reversal. The first global maximum of negative force in all specimens was observed at drying times of 5 to 6 hours. There was a slight increase of the magnitude of the maximum negative force from  $-45\pm4$  N of the juvenile  $r_1$  specimens near the pith to  $-62\pm4$  N of the mature  $r_2$  and  $r_3$  specimens further from the pith (Figure 8.3a-c). The second local maximum of the negative force at  $-26\pm4$  N took place during 15 $\pm2$  hours of drying in the  $r_2$  and  $r_3$  specimens; this force was less obvious and occurred at a longer drying time of about 20 to 30 hours in the  $r_1$  specimens. After attaining the second local maximum, the force magnitude decreases and changes to a positive sign. The restoring force of all specimens increases and reaches the maximum positive force of 148 $\pm15$  N before slightly declining until the end of drying. Because the maximum negative force (indicating the risk of surface checking) and the maximum positive force (indicating the risk of internal checking) are roughly insensitive to wood locations within the trunk, it is therefore suggested that there is no need for a rubberwood lumber classification for drying in the lumber industry.

It is well known that viscoelastic and mechano-sorptive creep causes stress reversal in lumber during drying (Perré and Passard 2007; Moutee et al. 2007). The maxima of two negative forces during stress reversal indicate that at least two distinct sources of creep should be operative. Main cell wall amorphous constituents such as hemicelluloses, lignin and non-crystalline cellulose (Haygreen and Bowyer 1989) exhibit viscoelastic and mechanosorptive creep behaviors when exposed to high temperature under the constant and cyclic conditions of humidity, respectively (Glasser et al. 1998). In contrast, extractive substances within the cell wall have been reported to retard creep deformation (Ajuong and Breese 1997). An attempt is made in the following section to deconvolute the influences of main amorphous constituents and extractives within cell walls on the generation of internal stress.

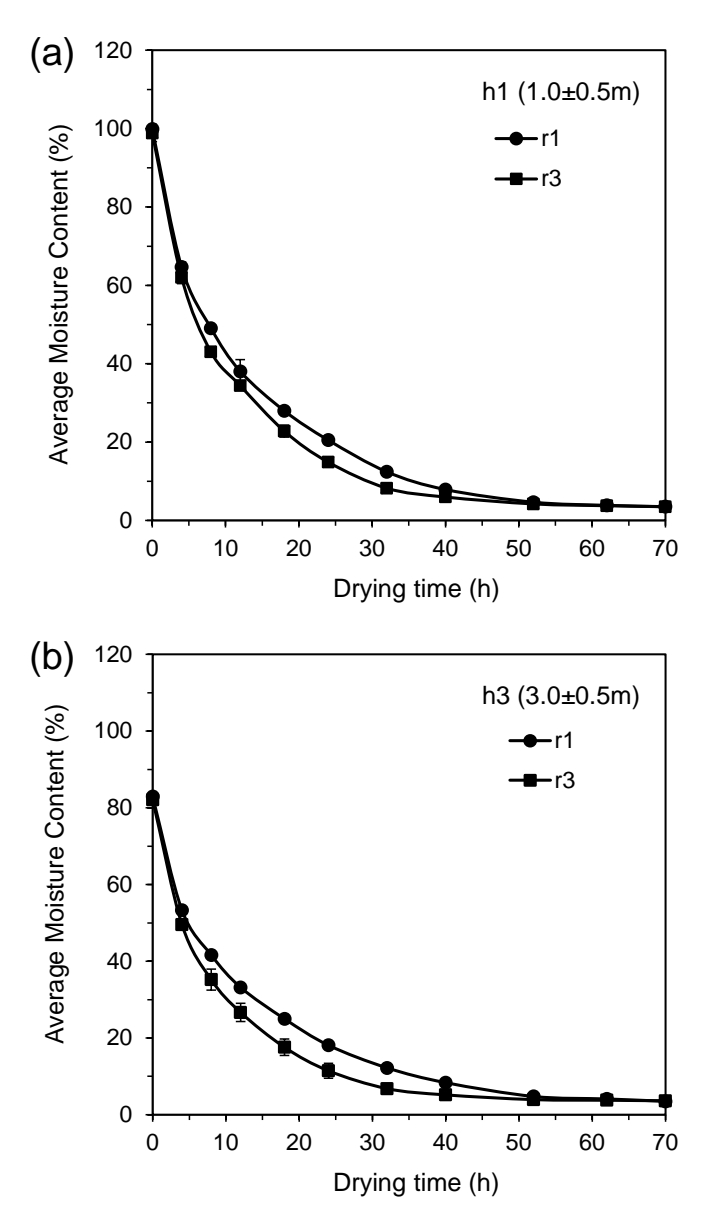
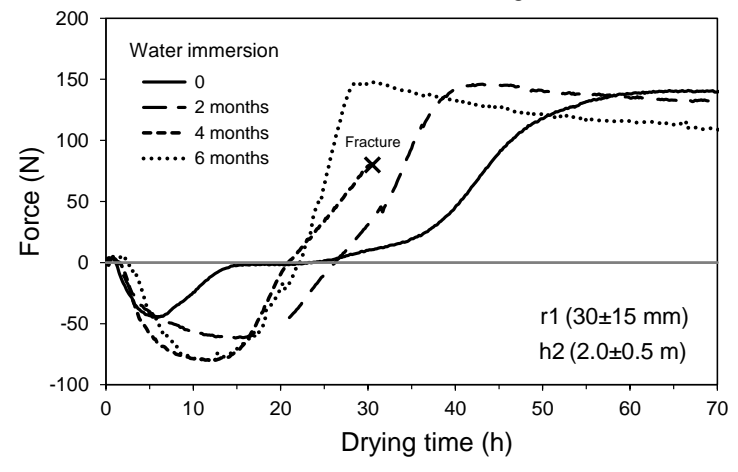


**Figure 8.4** The drying curves of the specimens prepared from rubber tree trunks at distances of  $r_1$  (30±15 mm) and  $r_3$  (110±15 mm) from the pith at heights of (a)  $h_1$  (1.0±0.5 m) and (b)  $h_3$  (3.0±0.5 m) above ground.

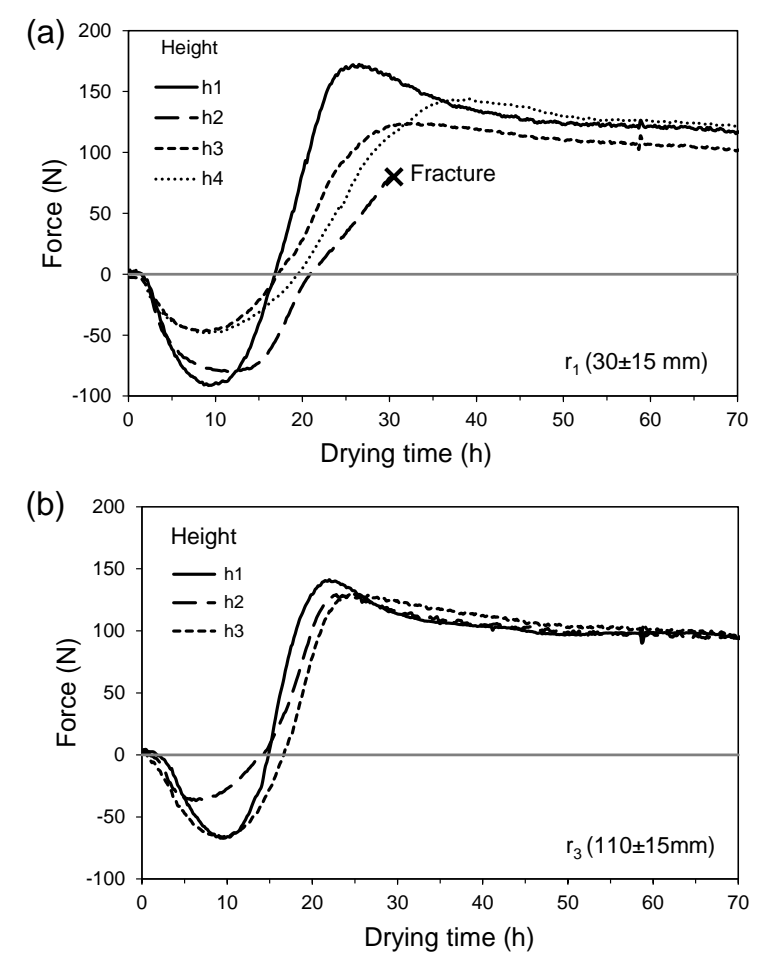
#### 8.3.2 Drying of the water-immersed specimens

Figure 8.5 shows the restoring force profiles of the  $r_1$  specimens that were immersed in water for up to 6 months. It is obvious that the longer the immersion time, the quicker the stress reversal and the gradual disappearance of the second maximum negative force. After 4 months of water immersion, the second maximum negative force completely disappeared and water immersion hardly affects the internal stress profile. The internal stress profiles of the specimens immersed in water for 4 and 6 months are rather similar. Higher magnitudes of the maximum negative force took place at longer drying times of around 10 to 15 hours. In addition, specimens prepared from all locations within the tree

trunk also exhibited comparable restoring force profiles with only a single negative maximum force after immersion in water for 4 months (Figure 8.6a-b).

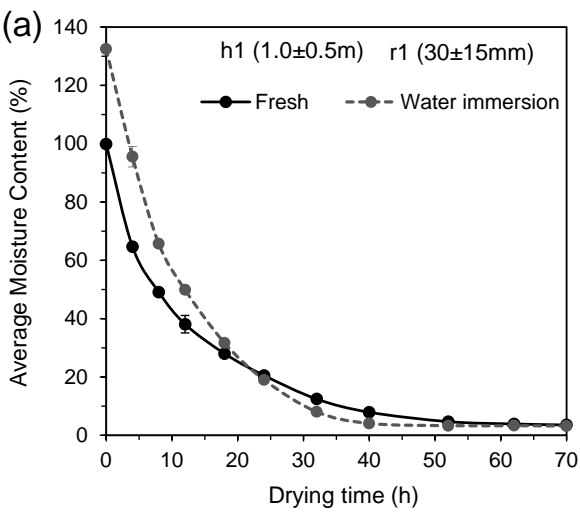


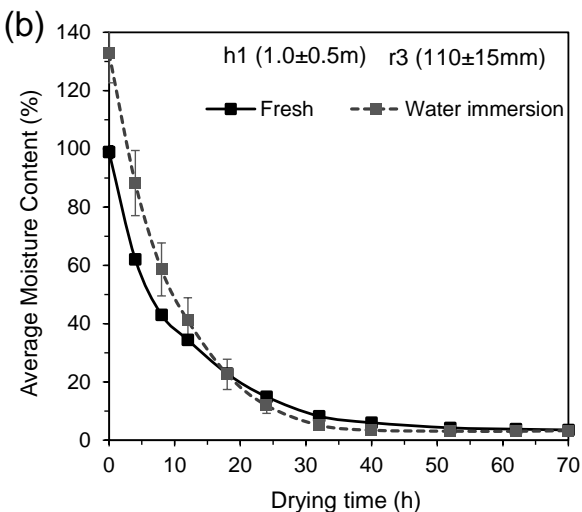
**Figure 8.5** The restoring force profiles of the specimens immersed in water for up to 6 months prepared from rubber tree trunks at distance of  $r_1$  (30±15 mm) from the pith and at height of  $h_2$  (2.0±0.5 m) above ground.



**Figure 8.6** The restoring force profiles of the water immersed specimens prepared from rubber tree trunks at distances of (a)  $r_1$  (30±15 mm) and (b)  $r_3$  (110±15 mm) from the pith at various heights above ground.

The drying curves of the specimens before and after 4 months of water immersion are shown in Figure 8.7a-d. All specimens were impregnated with water to attain saturation prior to testing. Higher initial saturation of moisture content, observed in the water-immersed specimens, should be responsible for the longer drying time (10 to 15 hours) required for the maximum negative force to take place. While the initial linear drying rates in the fresh and the water-immersed specimens (initial slopes in Figure 8.7a-d) are similar, the drying rates of the water-immersed specimens in the second stage of drying are clearly higher than those of the fresh specimens. The equilibrium moisture contents of both fresh and water-immersed specimens are approximately equal at 3.4±0.2%. Provided that the water-immersed specimens possessed higher initial moisture content, they reached the EMC prior to the fresh specimens (Figure 8.7a-d). Thus, the movement of bound water within the cell walls of the water-immersed specimens must be easier. The quicker drying rate in the second stage of drying in the water-immersed specimens corresponds well to the faster stress reversal observed in these specimens with respect to the fresh ones.





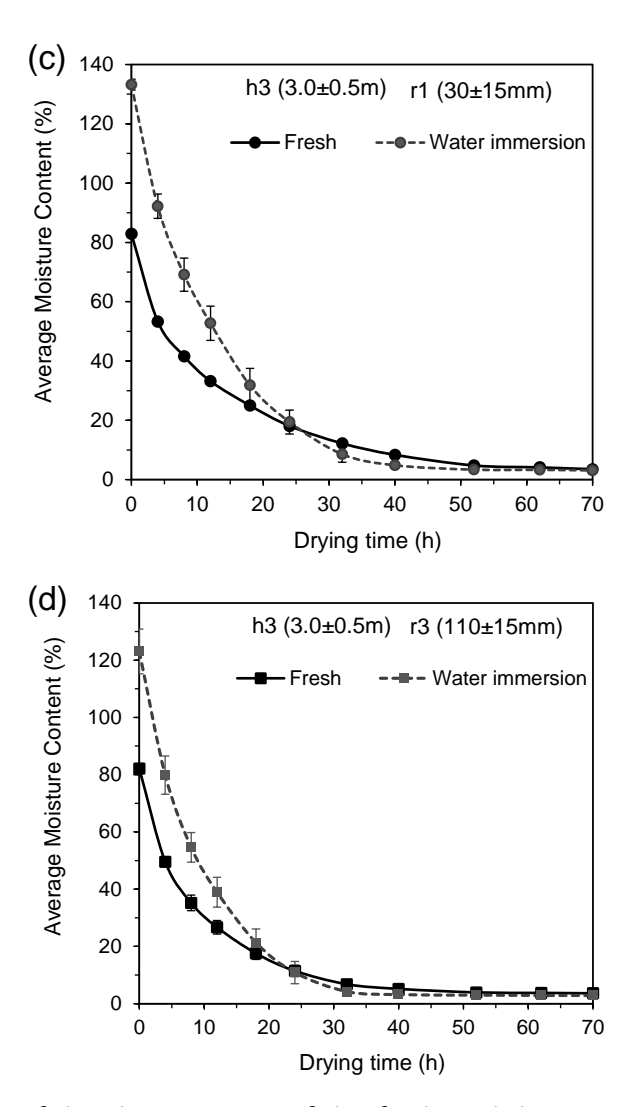


**Figure 8.7** Comparison of the drying curves of the fresh and the water immersed specimens prepared from rubber tree trunks at heights of  $h_1$  (1.0±0.5m) above ground at distances of (a)  $r_1$  (30±15 mm) and (b)  $r_3$  (110±15 mm) from the pith and of  $h_3$  (3.0±0.5 m) above ground at distances of (c)  $r_1$  (30±15 mm) and (d)  $r_3$  (110±15 mm) from the pith.

#### 8.3.3 Discussion on underlying mechanisms

The results from the experimentation raise various points which warrant further discussion and rationalization. The issues are taken in turn.

#### - Role of cell wall extractives

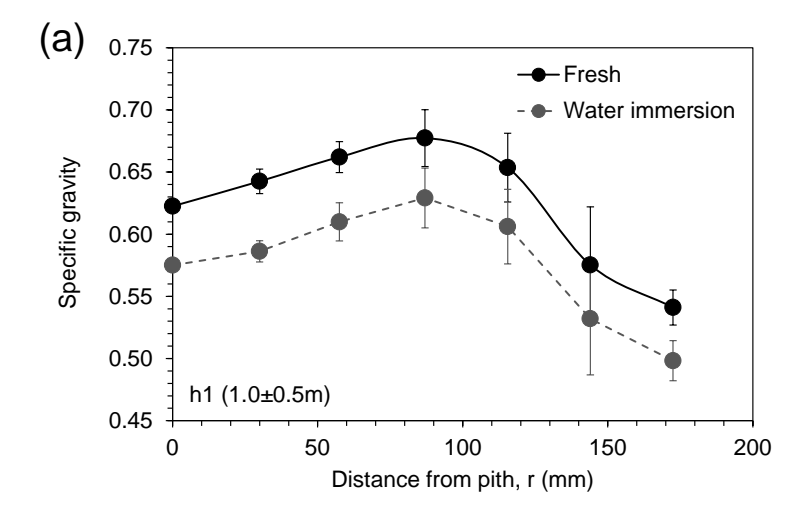
During water immersion, water-soluble extractives both within cell cavities and cell walls should be gradually depleted over time. The extractives of rubberwood are mainly hydrophilic compounds of free sugar, starch and amino acids (Simatupang et al. 1994). However, Ajuong and Breese (1997) reported that the lumen-located extractive fractions have no significant effect on short-term creep. In addition, a similar initial linear drying rate in the fresh and water-immersed specimens (Figure 8.7a-d) also indicates the insignificant role of extractives in the cell cavities on the movement of free water out of the lumber. As a

consequence, the shorter stress reversal time (Figure 8.5 and Figure 8.6a-b) plus the increase in the drying rate during the second stage (Figure 8.7a-d) should be related to the depletion of water-soluble extractive substances from the cell wall during water immersion. Without the presence of the extractives, the movement of bound water within the cell wall should be easier. In addition, bacterial attack during the water immersion could have contributed to the higher drying rate as compared to the fresh specimens (Kobayashi et al. 1998). This warrants further investigation and is a subject of future work.

The cell wall extractives have been reported to retard creep deformation. Acceleration of creep has been observed with the gradual depletion of extractive substances from the cell wall and with the removal of water-soluble extractives, resulting in great creep deformation (Ajuong and Breese 1997). It was suggested that the water-soluble extractives, which are frequently contained in the side chain sugar residue, are chemically bonded through the side chain to lignin, hemicellulose and/or cellulose (Ajuong and Breese 1997). The cell wall extractives have also been reported to enhance modulus (Golpayegani et al. 2012), hardness (Tze et al. 2007), dimensional stability (Kuo and Arganbright 1980) and softening temperature (Song et al. 2014) of the wood cell wall.

Higher saturation of moisture content was also observed in the water-immersed specimens (Figure 8.7a-d). Grigsby et al. (2013) reported that the majority of bound water was distributed in pore networks having pore sizes of less than 50 nm within the wood cell wall. Extractives have been suggested to deposit in the matrix and pore of the wood cell wall (Song et al. 2014; Yin et al. 2015). It is expected that during water immersion, water-soluble extractives are dissolved away and are replaced by water molecules. In addition, Mantanis et al. (1994) found an increase in maximum swelling of wood in water after the removal of extractives.

The values of specific gravity in the water saturated moisture content of rubberwood specimens, both fresh and water-immersed, are shown in Figure 8.8a-b. Specific gravity slightly increases with height. At the bottom section of  $h_1$ , specific gravity first increases in the radial direction up to ~100 mm from the pith before decreasing to the outside bark. The values of specific gravity are roughly constant at the top of section  $h_4$ . Since the restoring force profiles are relatively insensitive to height (Figure 3a-c), variation in specific gravity within tree trunk  $(0.62\pm0.05\ to\ 0.69\pm0.03)$  should therefore have little influence on the internal stress generated during drying. Furthermore, an approximately equal reduction of  $8.4\pm0.9\%$  in specific gravity after water immersion is observed at all examined locations within the tree trunk. An apparent reduction in specific gravity observed in the water-immersed specimens should roughly reflect the total loss of water-soluble extractives both within cell cavities and cell walls during water immersion. Severo et al. (2013) also reported an equal content of total extractives at 7.7% found in both the juvenile and the mature sections of rubber tree trunks.



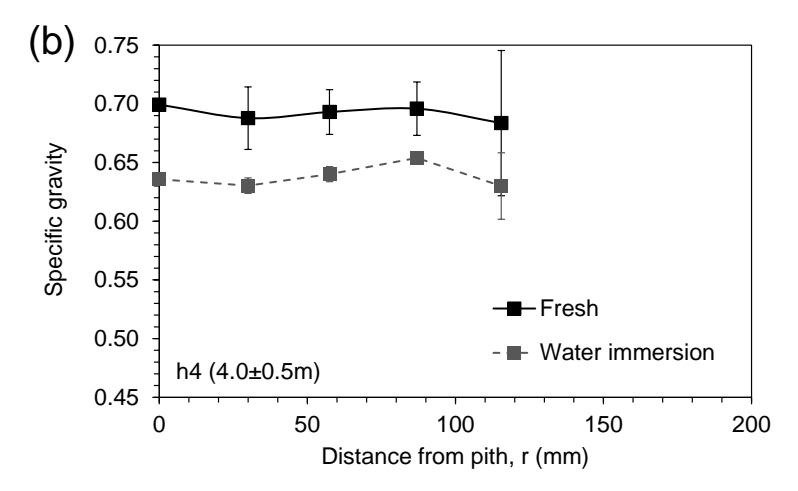


**Figure 8.8** Radial variation of specific gravity measured at dried condition of the fresh and the water immersed specimens prepared from rubber tree trunks at heights of (a)  $h_1$  (1.0±0.5 m) and (b)  $h_4$  (4.0±0.5 m) above ground.

The fact that stress reversal took place for a longer time in the  $r_1$  specimens near the pith compared to those of the  $r_2$  and  $r_3$  specimens further away suggests that the water-soluble extractives within the cell walls should be higher in the inner juvenile  $r_1$  specimens. During the sapwood–heartwood transition, more extractives are deposited in the wood cell walls while the composition of the main components of cell walls remains almost unaltered (Song et al. 2014). The extractives have been suggested to be deposited in the mesopores of heartwood cell walls (Yin et al. 2015). An examination of the types and amounts of extractives within cell walls is a subject for future work.

#### - Role of main amorphous cell wall constituents

The first negative maximum, which was still observed after immersion of the specimens in water, should be associated with the creep behavior of the main call wall amorphous constituents. Apart from being adsorbed in the amorphous hemicellulose, a large fraction of water molecules has been suggested to be adsorbed at the interface

between the crystalline cellulose and amorphous hemicellulose within the cell wall. Water molecules adsorbed on the interface push away polymer chains, forcing the two phases to separate and cause breaking of hydrogen bonds. At high moisture content, water is adsorbed preferentially at the interface; this leads to additional swelling and porosity increase at the interface (Kulasinski et al. 2015). During water immersion, more water molecules could be adsorbed into the cell walls which should additionally contribute to an increase in the values of saturated moisture content observed in the water-immersed specimens. It is emphasized that detailed studies on the roles of cell wall extractives and call wall amorphous constituents on the movement of bound water and creep properties which are underlying mechanisms of the generation of internal stress during drying should be explored in the future.

#### 8.4 Conclusions

The following conclusions can be drawn from this work:

- 1) The measured restoring force profiles, representing the internal drying stress within the lumber during drying, change along the radial direction of rubber tree trunk. A longer time of stress reversal has been observed in the inner juvenile wood zone with respect to the outer mature wood zone. While having a similar drying rate at the early stage of drying, the juvenile wood specimens dried at a slower rate than the mature wood specimens in the second drying stage during the time of stress reversal.
- 2) During stress reversal, there appears to be two negative force maxima which attribute to the creep responses during drying of the main amorphous constituents and the extractives within the cell walls, respectively. The second negative maximum gradually disappeared upon water immersion of the specimens. In these specimens, faster stress reversal and higher drying rate in the second drying stage have been observed with respect to the fresh specimens. The force profiles of the water-immersed specimens seem to be insensitive to locations within the tree trunk.
- 3) The results from this work suggest that variability of the internal stress within the rubber tree trunk originates from the roles of cell wall extractives and cell wall amorphous constituents on the movement of bound water out of lumber and on the creep properties during drying which needs to be further explored in the future.

#### References

- 1. Ajuong EMA, Breese MC (1997) The role of extractives on short-term creep in compression parallel to the grain of Pai wood (*Afzelia Africana* Smith) Wood Fiber Sci 29(2): 161-170
- 2. Balsiger J, Bahdon J, Whiteman A (2000) The Utilization, Processing and Demand for Rubberwood as a Source of Wood Supply. Forestry Policy and Planning Division, Rome
- 3. Diawanich P, Matan N, Kyokong B (2010) Evolution of internal stress during drying, cooling and conditioning of rubberwood lumber. Eur J Wood Prod 68(1):1–12
- 4. Diawanich P,Tomad S, Matan N, Kyokong B (2012) Novel assessment of casehardening in kiln-dried lumber. Wood Sci Technol 46: 101-114
- 5. European Committee for Standardization (2002) Sawn timber-method for assessment of case-hardening. CEN standard ENV 14464
- 6. Ferreira AL, Severo ETD, Calonego FW (2011) Determination of fiber length and juvenile and mature wood zones from *Hevea* brasiliensis trees grown in Brazil. Eur J Wood Prod 69:659–662
- 7. Grigsby WJ, Kroese H, Dunningham EA (2013) Characterisation of pore size distributions in variously dried Pinus radiata: analysis by thermoporosimetry. Wood Sci Technol 47: 737-747
- 8. Glass SV, Zelinka SL (2010) Moisture relations and physical properties of wood. In: Wood handbook—wood as an engineering material, General Technical Report, FPL-GTR-190. USDA Forest Service, Forest Products Laboratory, Madison, Wisconsin, pp 4-1-4-19
- 9. Glasser WG, Rials TG, Kelley SS, Dave V (1998) Studies of the molecular interaction between cellulose and lignin as a model for the hierarchical structure of wood. In: Heinze TJ, Glasser WG (eds) Cellulose derivatives modification, characterization, and nanostructures. American Chemical Society, Washington, pp 265–282
- 10. Golpayegani AS, Brémaud I, Gril J, Thevenon MF, Arnould O, Pourtahmasi K (2012) Effect of extractions on dynamic mechanical properties of white mulberry (*Morus alba*) J Wood Sci 58:153–162
- 11. Haslett, AN (1998) Drying Radiata Pine in New Zealand, New Zealand Forest Research Institute Limited, Rotorua, New Zealand
- 12. Haygreen JG, Bowyer JL (1989) Forest Products and Wood Science. Iowa State University Press, Ames.
- 13. Hong LT (1995) Rubberwood utilization: a success story. Paper presented at the XX International Union of Forestry Research Organizations (IUFRO) World Congress, Tampere, Finland

- 14. Kang W, Lee N-H (2002) Mathematical modeling to predict drying deformation and stress due to differential shrinkage within a tree disk. Wood Sci Technol 36:463–476
- 15. Kobayashi Y, Iida I, Imamura Y, Watanabe U (1998) Drying and anatomical characteristics of sugi wood attacked by bacteria during pond storage. J Wood Sci 44:432-437
- 16. Kulasinski K, Guyer R, Derome D, Carmeliet J (2015) Water adsorption in wood microfibril-hemicellulose system: role of the crystalline–amorphous Interface. Biomacromolecules 16: 2972–2978
- 17. Kuo ML, Arganbright DC (1980) Cellular distribution of extractives in redwood and incense cedar: Part 1, radial variation in cell wall extractive content. Holzforschung, 34(1):17-22
- 18. Langrish T, Walker, J (2006) Drying of timber. In: Walker J (ed) Primary wood processing: principles and practice. Springer, Berlin, pp 251-295
- 19. Larsen F, Ormarsson S (2013) Numerical and experimental study of moisture-induced stress and strain field developments in timber logs. Wood Sci Technol 47:837–852
- 20. Mantanis GI, Young RA, Rowell RM (1994) Swelling of wood Part 1: Swelling in water. Wood Sci Technol 28: 119-134
- 21. McMillen JM (1958) Stresses in wood during drying (Report 1652). Department of Agriculture, Forest Service, Forest Products Laboratory, Madison
- 22. Moutee M, Fortin Y, Fafard M (2007) A global rheological model of wood cantilever as applied to wood drying. Wood Sci Technol 41(3):209–234
- 23. Moutee M, Fortin Y, Laghdir A, Fafard M (2010) Cantilever experimental setup for rheological parameter identification in relation to wood drying. Wood Sci Technol 44:31–49
- 24. Ormarsson S, Dahlblom O, Petersson H (1998) A numerical study of the shape stability of sawn timber subjected to moisture variation part 1: theory. Wood Sci Technol 32: 325–334
- 25. Ormarsson S, Dahlblom O, Petersson H (1999) A numerical study of the shape stability of sawn timber subjected to moisture variation part 2: simulation of drying board. Wood Sci Technol 33: 407–423
- 26. Ormarsson S, Dahlblom O, Petersson H (2000) A numerical study of the shape stability of sawn timber subjected to moisture Part 3: Influence of annual ring orientation. Wood Sci Technol 34(3): 207-219
- 27. Pang S (2000) Modelling of stress development during drying and relief during steaming in *Pinus radiata* lumber. Dry Technol 18(8): 1677–1696
- 28. Pang S, Simpson IG, Haslett AN (2001) Cooling and steam conditioning after high-temperature drying of Pinus Radiata board: experimental investigation mathematical modeling. Wood Sci Technol 35:487-502

- 29. Perré P, Martin M (1994) Drying at high temperature of heartwood and sapwood: theory, experiment and practical consequence on kiln control. Dry Technol 12: 1915–1941
- 30. Perré P, Passard J (2004) A physical and mechanical model able to predict the stress field in wood over a wide range of drying conditions. Dry Technol 22: 27–44
- 31. Perré P, Passard J (2007) Stress development. In: Perré P (ed) Fundamentals of wood drying, European COST A.R.BO.LOR., Nancy, pp 243-271
- 32. Perré P, Turner IW (1999) A 3-D version of TransPore: a comprehensive heat and mass transfer computational model for simulating the drying of porous media. Int J Heat Mass Tran 42: 4501-4521
- 33. Perré P, Turner IW (2007) Coupled heat and mass transfer In: Perré P (ed) Fundamentals of wood drying, European COST A.R.BO.LOR., Nancy, pp 203-241
- 34. Ratnasingam J, Grohmann R, Scholz F (2010) Drying quality of rubberwood: an industrial perspective. Eur J Wood Prod 68: 115–116
- 35. Severo ETD, Oliveira Jr EF, Sansı golo CA, Rocha CD, Calonego FW (2013) Properties of juvenile and mature woods of *Hevea brasiliensis* untapped and with tapping panels. Eur J Wood Prod 71: 815-818
- 36. Simatupang MH, Schmitt U, Kasim A (1994) Wood extractives of rubberwood (*Hevea Brasiliensis*) and their influences on the setting of the inorganic binder in gypsumbonded particleboards. J Trop For Sci 6(3): 269 285
- 37. Simpson WT (1991) Dry kiln operator's manual. Agric. Handbook AH-188. U.S. Department of Agriculture, Forest Service, Forest Products Laboratory. Madison, WI
- 38. Skaar C (1972) Water in wood. Syracuse University Press, New York
- 39. Song K, Yin Y, Salmén L, Xiao F, Jiang X (2014) Changes in the properties of wood cell walls during the transformation from sapwood to heartwood. J Mater Sci 49: 1734–1742
- 40. Srivaro S, Wongprot T, Matan N, Kyokong B (2008) Accelerated conventional temperature drying of 30mm thick rubberwood lumber. Songklanakarin J Sci Technol 30(4): 475-483
- 41. Teoh YP, Don MM, Ujang S (2011) Assessment of the properties, utilization, and preservation of rubberwood (*Hevea brasiliensis*): a case study in Malaysia. J Wood Sci 57: 255–266
- 42. Theppaya T, Prasertsan S (2004) Optimization of rubber wood drying by response surface method and multiple contour plots. Dry Technol 7(7): 1637-1660
- 43. Tomad S, Matan N, Diawanich P, Kyokong B (2012) Internal stress measurement during drying of rubberwood lumber: effects of wet-bulb temperature in various drying strategies. Holzforschung 66: 645-654

- 44. Tremblay C, Cloutier A, Fortin Y (2000) Experimental determination of the convective heat and mass transfer coefficients for wood drying. Wood Sci Technol 34: 253-276
- 45. Tze WTY, Wang S, Rials TG, Pharr GM, Kelley SS (2007) Nanoindentation of wood cell walls: continuous stiffness and hardness measurements. Composites Part A 38: 945–953
- 46. Yin J, Song K, Lu Y, Zhao G, Yin Y (2015) Comparison of changes in micropores and mesopores in the wood cell walls of sapwood and heartwood. Wood Sci Technol 49: 987–1001

## Chapter 9

### Outputs from this project

#### 9.1 Research articles

- Published
- 1. Sataporn Jantawee, Satjapan Leelatanon, Prawate Diawanich and Nirundorn Matan (2016) "A new assessment of internal stress within kiln-dried lumber using a restoring force technique on a half-split specimen" Wood Science and Technology 50(6): 1277-1292. (IF=1.509, Q1: Forestry, Q1: Materials science) (Details are in Chapters 3 & 4 and Appendix A1)
- 2. Sataporn Jantawee, Satjapan Leelatanon, Prawate Diawanich, Sornthep Vannarat and Nirundorn Matan (2018) "Comparison of techniques for quantification of internal stress within industrial kiln-dried timber" European Journal of Wood and Wood Products, 76(2): 617-627. (IF=1.082, Q1: Forestry, Q2: Materials science) (Details are in Chapter 7 and Appendix A2)
- 3. Jaipet Tomad, Sataporn Jantawee, Wanchart Preechatiwong and Nirundorn Matan (2018) "Within-tree variability of internal stress generated during drying of rubberwood lumber" European Journal of Wood and Wood Products, 76(1): 113-122. (IF=1.082, Q1: Forestry, Q2: Materials science) (Details are in Chapter 8 and Appendix A3)
- Manuscript in preparation
- 1. Satjapan Leelatanon, Sataporn Jantawee, Sornthep Vannarat and Nirundorn Matan (2018) "Interpretation of internal stress within lumber containing several stress components using a restoring force technique" European Journal of Wood and Wood Products (to be submitted)
  - (IF=1.082, Q1: Forestry, Q2: Materials science) (Details are in Chapter 5)
- 2. Satjapan Leelatanon, Sataporn Jantawee, Sornthep Vannarat and Nirundorn Matan (2018) "Derivation and validation of geometrical shape factor for an interpretation of internal stress within various sizes of lumber using a restoring force technique" Mechanics of Materials (to be submitted)

(IF=1.082, Q1: Materials science, Q1: Instrumentation, Q1: Mechanics of materials) (Details are in Chapter 6)

#### 9.2 Research utilizations

- Academic

There are 2 PhD and 1 MSc students in Materials Science and Engineering, School of Engineering and Resources, Walailak University enrolled in this project:

- 1. Jaipet Tomad completed his MSc study with a thesis on "Within-tree variability of internal stress generated during drying of rubberwood lumber" in 2016.
- 2. Sataporn Jantawee completed his PhD study with a thesis on "Assessment of internal stress within kiln-dried lumber using a restoring force technique on a half-split specimen" in 2016.
- 3. Satjapan Leelatanon is currently in his final year (2018) to complete his PhD study with a thesis on "Simulation of internal stress developed within kiln-dried lumber".

#### 9.3 Miscellaneous

- International conferences (Appendix A4)
  - Sataporn Jantaweea, Satjapan Leelatanon, Prawate Diawanich, Nirundorn Matan (2016) "Design and construction of a restoring force measuring apparatus for assessment of internal stress within kiln-dried lumber" The 9th International conference on materials science and technology. 14<sup>th</sup>-15<sup>th</sup> December 2016, Swissotel Le Concorde, Bangkok, Thailand (Oral).
  - 2. Jaipet Tomad, Sataporn Jantawee, Wanchart Preechatiwong, Nirundorn Matan (2016) Effect of cell wall constituents on internal stress generation during drying of lumber prepared from rubber tree trunks" The 9th International conference on materials science and technology. 14<sup>th</sup>-15<sup>th</sup> December 2016, Swissotel Le Concorde, Bangkok, Thailand (Oral).
  - 3. Sataporn Jantawee, Jaipet Tomad, Nirundorn Matan (2017) "Effect of pre-drying on development of internal stress within rubberwood lumber during drying" The IUFRO 2017 Division 5 Conference & SWST 60<sup>th</sup> International convention. 12<sup>th</sup>-16<sup>th</sup> June 2017, Vancouver Canada (Oral).
  - 4. Nirundorn Matan, Choosak Rittiphet, Jaipet Tomad, Sataporn Jantawee (2017) "A real-time internal stress controlled drying of lumber" The IUFRO 2017 Division 5 Conference & SWST 60<sup>th</sup> International convention. 12<sup>th</sup>-16<sup>th</sup> June 2017, Vancouver Canada (Oral).

#### - Invited speakers

- Nirundorn Matan (2016) Quality Drying of Lumber: From Laboratory to Industry.
   The 9th International conference on materials science and technology (arranged by MTEC). 14<sup>th</sup>-15<sup>th</sup> December 2016, Swissotel Le Concorde, Bangkok, Thailand.
   <a href="https://www.mtec.or.th/MSAT-9/index.php/speakers.html">https://www.mtec.or.th/MSAT-9/index.php/speakers.html</a>
- Nirundorn Matan (2018) Smart (Fast-Cheap-Quality) Wood Drying: From Basic Science to Industrial Applications. Conference on Natural Rubber and Rubber Wood 2018 (arranged by Prince of Songkla University, Surat Thani Campus). 3<sup>rd</sup> 4<sup>th</sup> May 2018, Siam Thani, Surat Thani, Thailand. <a href="http://nri2018.surat.psu.ac.th/activity.html">http://nri2018.surat.psu.ac.th/activity.html</a>

## Appendix 1

Sataporn Jantawee, Satjapan Leelatanon, Prawate Diawanich and Nirundorn Matan (2016) "A new assessment of internal stress within kilndried lumber using a restoring force technique on a half-split specimen" Wood Science and Technology 50(6): 1277-1292.

(IF=1.509, Q1: Forestry, Q1: Materials science)

## CrossMark

#### ORIGINAL

## A new assessment of internal stress within kiln-dried lumber using a restoring force technique on a half-split specimen

Sataporn Jantawee<sup>1</sup> · Satjapan Leelatanon<sup>1</sup> · Prawate Diawanich<sup>2</sup> · Nirundorn Matan<sup>1</sup>

Received: 3 March 2016/Published online: 23 August 2016

© Springer-Verlag Berlin Heidelberg 2016

Abstract Due to difficulties in determining modulus of elasticity of wood, only strain or deflection profiles caused by relaxation of internal stress are normally evaluated for industrial kiln-dried lumber. To directly assess the level of internal stress within the lumber, a new technique of measuring the restoring force on a halfsplit specimen has been presented and the corresponding device has been designed and constructed. Kiln-dried rubberwood specimens with dimensions of 30 or 50 mm (thickness), 130 mm (width) and 50 mm (length) were used in the study. The measured restoring force appears to vary with half-split length and specimen thickness. A mathematical model based on an elastic cantilever beam theory has been successfully developed to describe the restoring force behavior in a flexural response regime. The magnitude of the maximum linearly averaged internal stress  $\sigma_{\rm m}$  can be derived without prior knowledge of the modulus of elasticity of wood. For the 30-mm-thick lumber, the derived values of  $\sigma_{\rm m}$  are in general agreement with the ones obtained from the conventional McMillen slice test. Very close agreement is observed when the internal stress is at a relatively low level and its profile is approximately linear. But for the 50-mm-thick lumber, the determination of  $\sigma_{\rm m}$  is less appropriate because of its relatively short flexural range. A restoring forceinternal stress chart has been proposed for practical use in the lumber industry. This assessment was performed to investigate the evolution of internal stress during the conditioning and storage stages of kiln-dried rubberwood lumber.



Materials Science and Engineering, School of Engineering and Resources, Walailak University, Thasala District, Nakhon Si Thammarat 80160, Thailand

Nakhon Si Thammarat Seaboard Industrial College, Pakpanang District, Nakhon Si Thammarat 80140, Thailand

#### Introduction

The drying process always creates internal stress within lumber that continues to exist, even after the lumber is dried (Perré and Passard 2007). The outer layer of kiln-dried lumber is generally under compressive stress, while its inner core layer is under tensile stress (McMillen 1958; Simpson 1999). In practice, these internal stresses are generally relieved by steaming done at the end of the drying process (Wengert 1992). A reliable technique for the assessment of internal stress is therefore essential for effective stress relief and quality control of kiln-dried lumber.

The stress-relaxing techniques of the McMillen slice test (McMillen 1958), the case-hardening test (European Committee for Standardization 2010) and the prong test (Simpson 1991) have been traditionally used to estimate the internal stress magnitude within kiln-dried lumber. These techniques analyze structural deformations in terms of strain or deflection that accompany the stress redistribution which occurs when internal stresses are elastically released by sectioning or splitting. Internal stress can then be determined by analyzing the measured strains or deflections, provided that the elasticity values of the materials are known (Schajer and Ruud 2013; Walton 2002; Rossini et al. 2012). The elastic modulus of wood depends on several factors including moisture content and specific gravity (Bodig and Jayne 1982; Matan and Kyokong 2003; Sonderegger et al. 2013), and it is not practical in the industry to measure every piece of lumber. It is quite common that only strain profiles or deflections obtained from the test methods mentioned above are reported (McMillen 1958; European Committee for Standardization 2010; Fuller 1995).

A novel approach of a restoring force measurement on "half-split" specimens has been proposed by Diawanich et al. (2012). This idea has also been extended to monitor in real time the internal stress during drying, conditioning and storage of lumber (Diawanich et al. 2010; Tomad et al. 2012). In their work, the width of lumber was sawn at half thickness by a half length before being transferred to a device attached to the universal testing machine to measure the force required to restore the specimen back to its initial configuration. However, just a small error in the thickness measurement during restraining of the half-split specimen to its original configuration could lead to a large variation in the measured force. Therefore, further improvement to this technique is required.

The purpose of this research is to design and construct a restoring force measuring apparatus suitable to be used in the lumber industry. An interpretation of the measured restoring force in terms of the internal stress is developed. The derived internal stress is compared with one of the traditional slicing techniques. Finally, a chart for converting the restoring force to the internal stress is proposed for convenience in the industry. Emphasis is placed on estimating the internal stress level within kiln-dried rubberwood lumber.



#### Materials and methods

#### Design of restoring force measuring apparatus

The principle of restoring force measurement on half-split specimen was based on the concept proposed by Diawanich et al. (2012). The equipment (Fig. 1a, b) consists mainly of a relatively stiff steel frame, two 56-mm-wide clamping jigs and a load cell (Cooper Instrument, USA). One jig was fixed to the steel frame, and another was attached to a steel rod connected to the load cell. A wood specimen cut to a length (b) of 50 mm was clamped onto the jigs at a distance (g) of 10 mm away from the top end. Care was taken to ensure that optimum torque of 2-3 N m was applied with a contact area of 24 mm<sup>2</sup> to hold the specimen to the jigs without damaging it. While being clamped to the frame, the specimen was half-split at half the thickness for a required length (l). The apparatus was designed so that the width of the specimen clamped to the frame can be sawn with a band saw (Fig. 1c). The kerf from the saw was 2 mm wide. Without restraining the specimen, the relaxation of internal stress would cause the two legs of the half-split specimen to be deformed inward or outward. Since the specimen is restrained to the frame and to a steel rod connected to the load cell, the net force generated as a result of internal stress relaxation within the half-split specimen was transferred to the load cell. The sign and magnitude of the force, displayed on the force reading device (Fig. 1d), was recorded and transferred to the computer in real-time mode during and after cutting.

#### Restoring force and slice test measurements

Six pieces of industrial kiln-dried rubberwood obtained from a local sawmill in Nakhon Si Thammarat, Thailand, were used in this study. The restoring force was measured as a function of the half-split length (1) for thicknesses (d) of 30 and 50 mm (three replicates for each size) in the radial (R) direction. The flat-sawn lumber was 130 mm wide (W) in the tangential (T) direction and approximately 1 m long in the longitudinal (L) direction. For each piece of lumber, two sets of specimens with relatively high levels of internal stress (HS) and low levels of internal stress (LS) were prepared. All specimens were free of defects such as knots and spiral grain. The HS specimens were tested immediately after kiln drying, while the LS specimens were left in ambient air  $(28 \pm 2 \, ^{\circ}\text{C})$  and  $75 \pm 6 \, ^{\circ}$  RH) for 3 weeks prior to testing. The specimens were cut to a length (b) of 50 mm (Fig. 2a) and marked into a half thickness line at 5-mm intervals (Fig. 2b). For the 30-mmthick specimens, they were also marked by divided lines so they could be cut into six equal slices according to the McMillen slice test (McMillen 1958) (Fig. 2c). The initial width of each pre-marked slice  $(W_b)$  was measured by calipers to an accuracy of 0.01 mm. Specimens were then assembled into the restoring force measuring apparatus and cut through the pre-marked half thickness line. The restoring force was monitored at 5-mm intervals up to 125 mm. They were then cut into slices along the pre-marked lines, and the width  $(W_a)$  of each slice was immediately measured. The released strain of each slice ( $\varepsilon$ ) was calculated according to



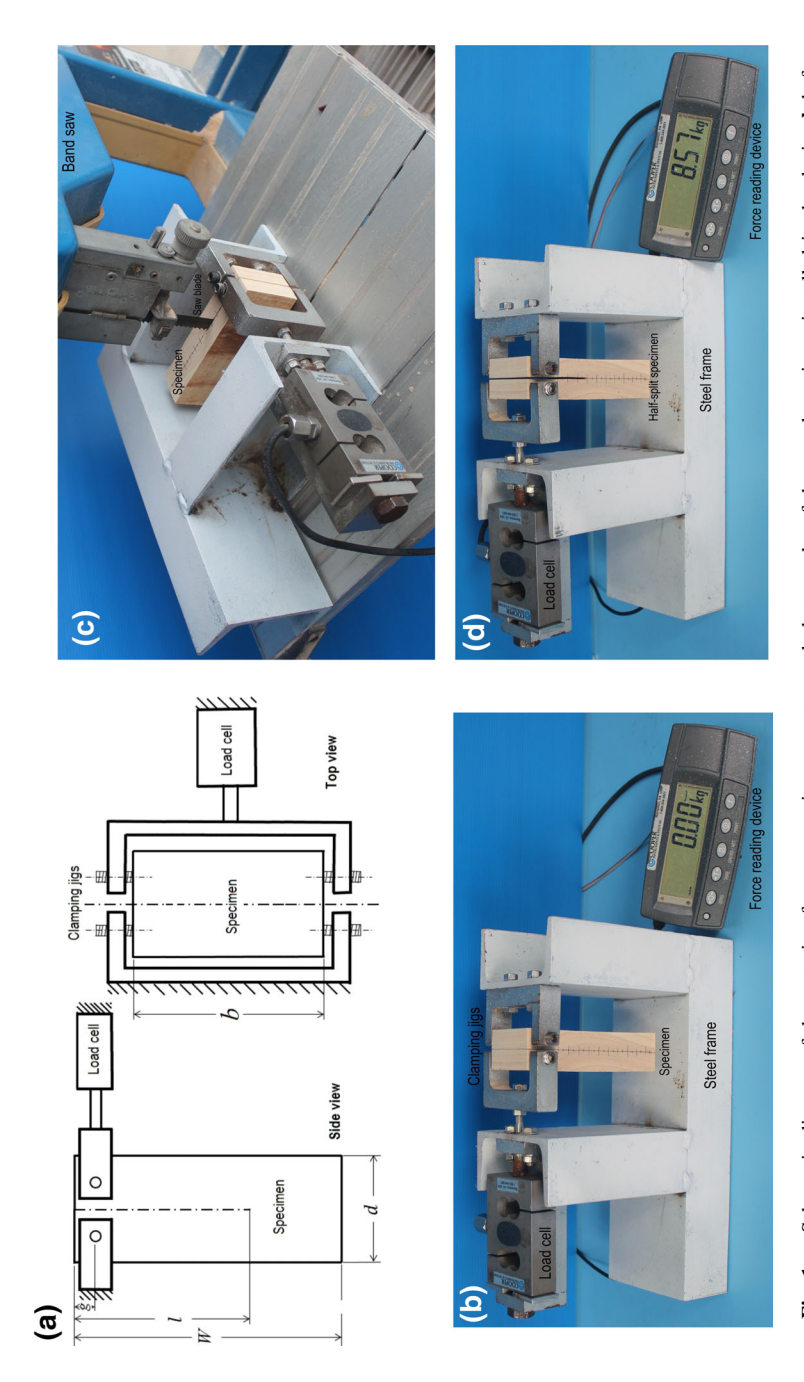


Fig. 1 a Schematic diagram of the restoring force measuring apparatus and photographs of the wood specimen installed in the device b before, c during and d after half-split sawing using a band saw



 $\varepsilon = \frac{W_a - W_b}{W_b}$ . Each slice was then subjected to a tensile test using a universal testing machine (Lloyd 150kN, UK) equipped with a strain gauge (Epsilon Technology, USA) to determine the value of Young's modulus in the tangential direction. After testing, a section of each slice was weighted both before and after oven-drying at 104 °C for 24 h to determine its moisture content.

#### Internal stress relaxation of kiln-dried rubberwood lumber

Six pieces of kiln-dried rubberwood lumber (30 mm thick, 130 mm wide and approximately 1 m long) were taken from a local sawmill in Nakhon Si Thammarat, Thailand. The growth ring orientation was selected such that the lumber thickness aligned in the radial direction (Fig. 2a). Defect-free specimens measuring 50 mm long were cut at least 50 mm from the end of each lumber. Restoring force measurement was then carried out on the half-split specimens at cutting lengths

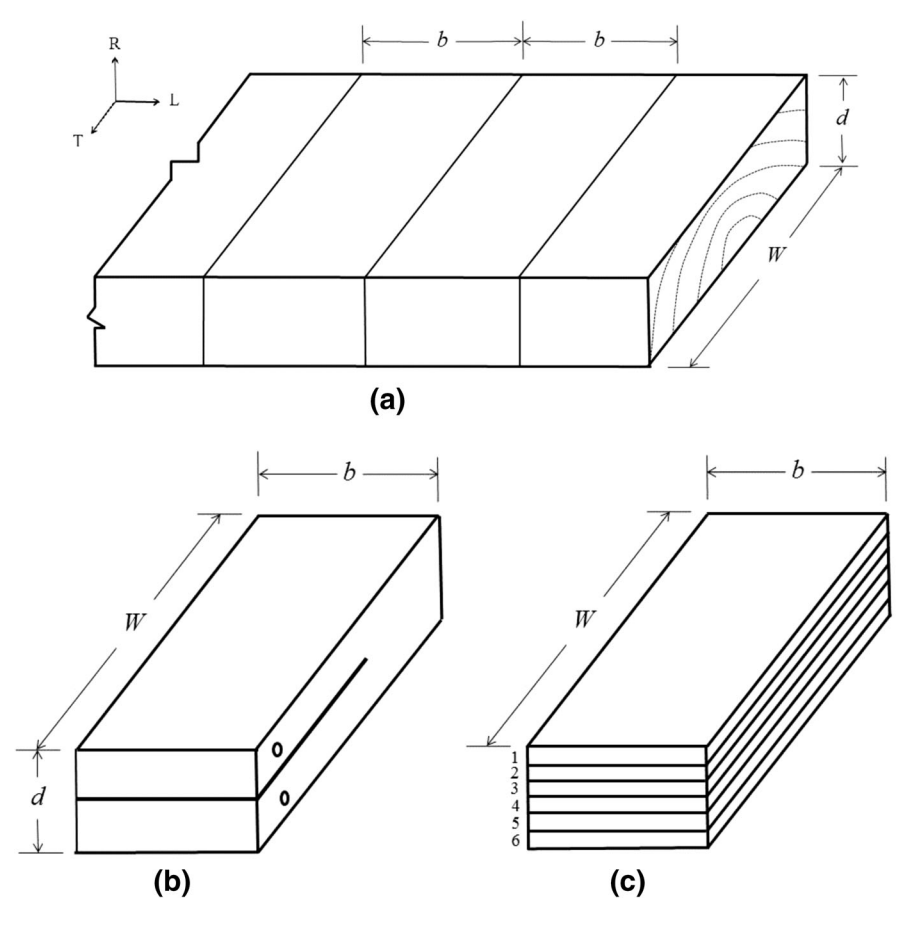


Fig. 2 Sample layouts of  $\mathbf{a}$  the test specimens cut from the lumber,  $\mathbf{b}$  the half-split specimen for the restoring force measurement and  $\mathbf{c}$  the specimen for the McMillen slice test



from 60 to 100 mm. The remaining pieces of lumber were coated with aluminum paint at both ends. Three pieces of lumber were placed in a conditioning chamber (Binder, Germany) at 85 °C and 80 % RH. Another three pieces were left in ambient air at  $28 \pm 2$  °C and  $75 \pm 6$  % RH. Assessments of internal stress were later performed after 30 and 90 min of conditioning and at 10 and 20 days of storage, respectively.

#### Results and discussion

#### Restoring force measurement on half-split specimens

Internal compressive and tensile stresses often remain in both an outer layer and an inner core of lumber after kiln drying (McMillen 1958; Simpson 1999). A resultant force generated due to relaxation of these internal stresses tends to bend the two legs of the half-split specimen inward. This behavior is similar to the prong response of kiln-dried lumber which is commonly observed in sawmill industry; however, the deflection degree of half-split specimens is relatively small. According to the prong test, the central portion accounting for about one-third of the thickness is generally removed (Simpson 1991) so that the deflection of the two legs could be easily measured. However, removing a bigger central portion of lumber would lead to a larger error in quantifying the internal stress level because the degree of prong deflection is only caused by redistribution of the internal stresses within the remaining portion of lumber. Fuller and Hart (1994) also reported an ambiguous reading on the internal stress level of the prong test as a result of the amount of the wood removed.

Within this work, the apparatus was designed to hold the half-split specimen to the initial position at the clamping points. As a result, a tensile (positive) restoring force was detected on the load cell. Figure 3a shows typical evolution of the force value reading on the load cell before, during and after half-split sawing. Before cutting, the force was set to zero. The force increased during the sawing to a required length. A slight fluctuation in the force value as a result of saw blade vibration can be observed. An instantaneous elastic response of the restoring force was recorded immediately after half-splitting the specimen to the required length and removing the specimen from the saw blade. Thereafter, the force value slightly increased with time as a result of viscoelastic creep. Mechano-sorptive creep should also play a role over time as moisture could easily diffuse into or out of the inner section of the specimen via the saw kerf. Creep response of the specimen could affect the measured values of the restoring force when multiple sawing at various half-split lengths was performed (Fig. 3b). To minimize such an effect from creep to <3 %, the multiple sawing on each specimen was completed in a short time of <3 min. Detailed analysis of the creep response is beyond the scope of the present paper and should be explored in the future.

The curves of the restoring force as a function of half-split length obtained from the 30- and 50-mm-thick specimens are shown in Fig. 4a, b, respectively. For the 50-mm-thick HS specimens, measurements could be taken up to the half-split length



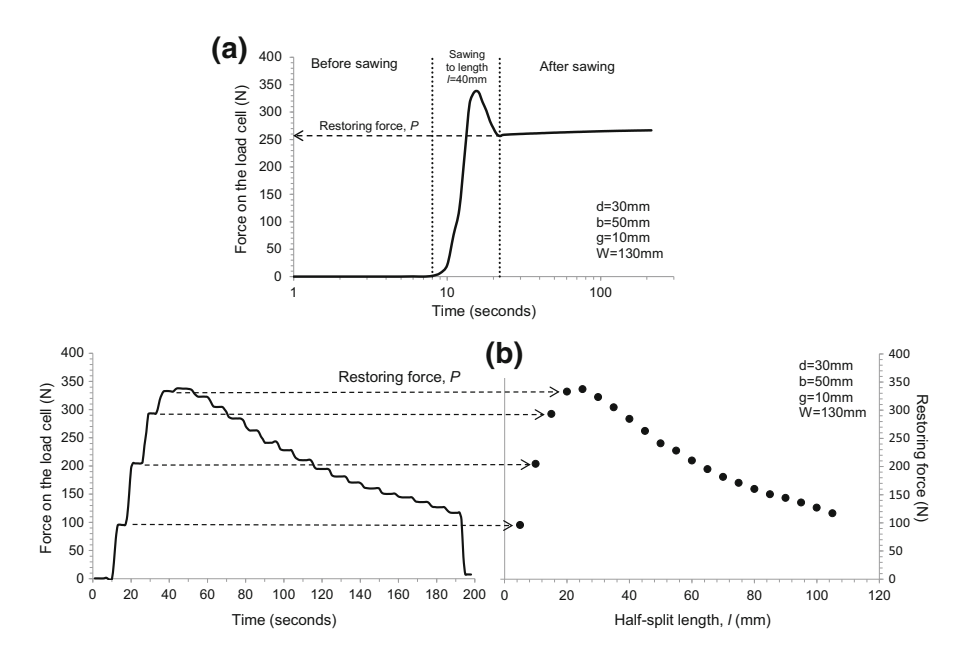


**Fig. 3** Typical evolution of the detected force on the load cell before, during and after half-split sawing of the specimen fixed to the restoring force measuring device using **a** a single sawing at 40-mm and **b** multiple sawing at 5-mm intervals. Some values of the derived restoring force are also indicated in the *graphs* 

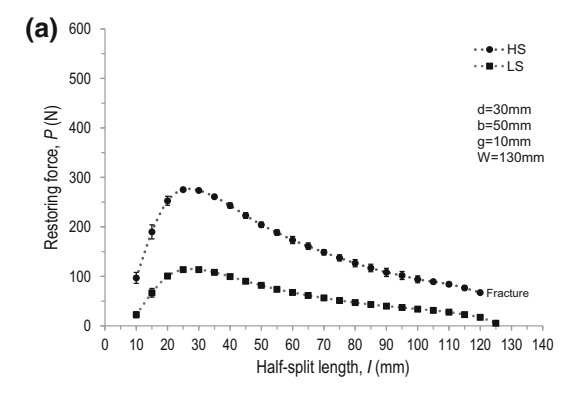
of 100 mm (Fig. 4b) because of the presence of cracks at the tip of the kerf. For both lumber thickness sizes, the magnitude of the restoring force varied with the half-split length. The restoring force first abruptly increased and reached the maximum values at the half-split lengths of around 25 mm for the 30-mm-thick specimens and around 35–45 mm for the 50-mm-thick specimens. After exceeding the maximum value, the restoring force gradually decreased with the increase in the half-split length. The magnitude of the restoring force appears to reflect the internal stress level within the specimen. The restoring forces of the HS specimens are clearly higher than those of the LS specimens. However, the observed force values should also be influenced by the specimen's geometry. As shown in Fig. 4, higher restoring force levels were detected in the thicker specimens. In the following section, an attempt was made to relate the magnitudes of the restoring force to the level of the internal stress within the lumber.

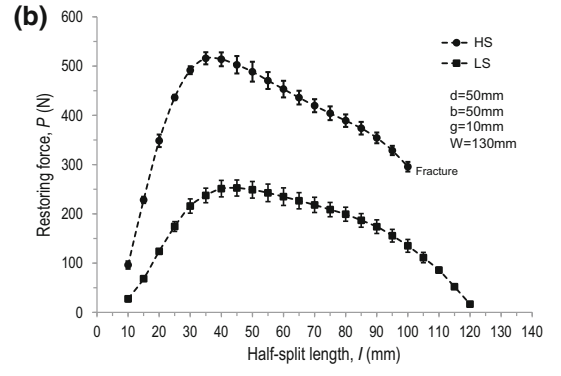
#### Estimation of the internal stress

By assuming a linear distribution of internal stress across half thickness of lumber (Fig. 5a), the maximum linearly averaged internal stress  $\sigma_{\rm m}$  was assumed to be equal at the outer surface and at the inner core. This can be calculated by a deflection of the half-split specimen (Fig. 5b) as expressed by



Fig. 4 Experimental restoring force profiles as a function of half-split length of a the 30-mm and b the 50-mm-thick kiln-dried rubberwood specimens with widths of 130 mm and lengths of 50 mm containing high levels (HS) and low levels (LS) of internal stress





$$\sigma_{\rm m} = \frac{E \cdot \Delta \delta \cdot d}{4l^2} \tag{1}$$

where E,  $\Delta\delta$ , d and l are Young's modulus in the tangential (T) direction, mouth opening, thickness and sawed depth of the specimen, respectively (Walton 2002). A restoring force (P) is applied at distance a away from the end of the kerf (or at distance a away from the specimen end) to keep the half-split specimen in the original configuration prior to sawing (Fig. 5c). According to Lados and Apelian (2006), the restoring force (P) can then be expressed as

$$P = \frac{E \cdot \Delta \delta \cdot b}{S} \tag{2}$$

where b is the sample length and S is the geometrical shape factor.

It can be considered that each leg of the half-split specimen acts as a cantilever beam that is rigidly fixed at one end and free at the other end. In addition, it is assumed that the internal stress is fully relaxed across the thickness of the specimen and the effects of other stress components (including stresses in the thickness and the length directions, shear stresses and stress concentration around the end of the kerf) are negligible. The restoring force (*P*) is calculated using the cantilever beam equation (Hibbeler 2012) according to



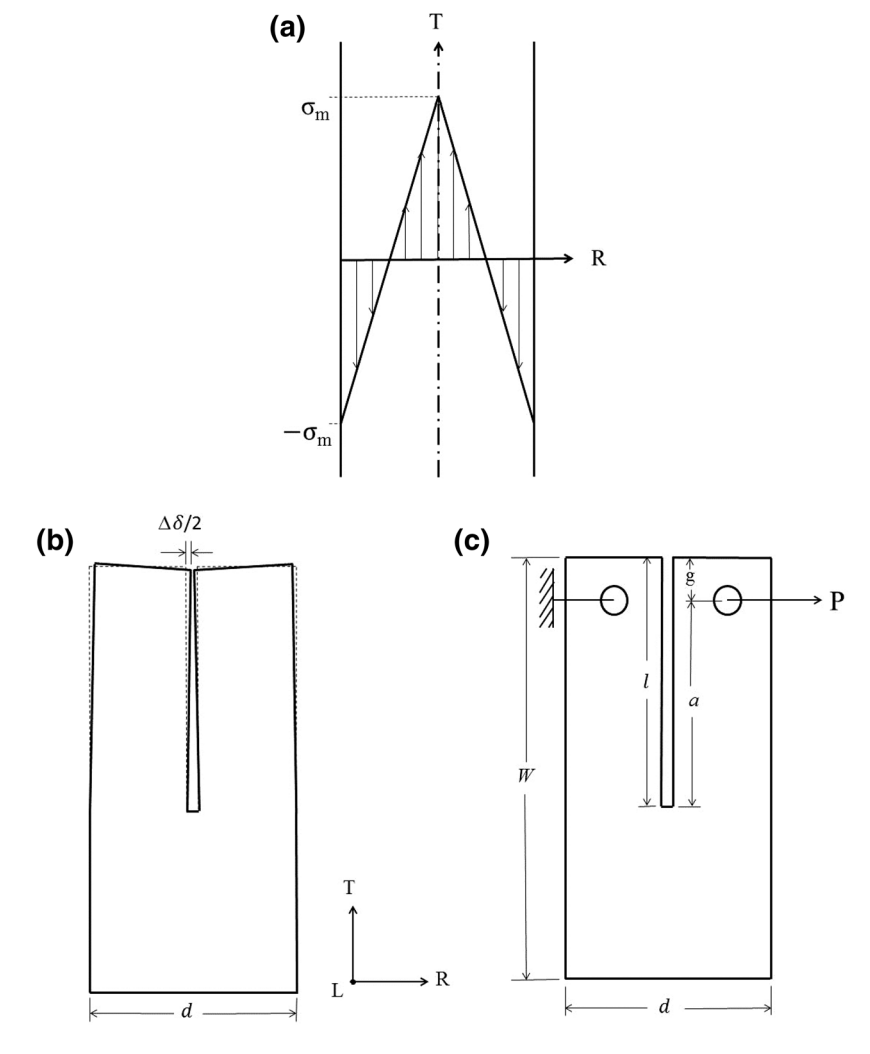


Fig. 5 a Linear distribution of through thickness internal stress within lumber, b deflection of half-split specimen caused by internal stress after sawing and c application of restoring force to restrain the half-split specimen in original configuration prior to sawing

$$P = \frac{6EI}{a^2(3l - a)} \frac{\Delta \delta}{2} = \frac{6EI}{(l - g)^2(2l + g)} \frac{\Delta \delta}{2}$$
 (3)

where *I* is the second moment of area which is equal to  $\frac{bd^3}{96}$ . By combining Eqs. (1), (2) and (3), the restoring force *P* can be expressed as

$$P = \frac{4bl^2}{Sd} \sigma_{\rm m} \tag{4}$$

where the geometrical factor is  $S = \frac{32(l-g)^2(2l+g)}{d^3}$ . It should be emphasized that according to Eq. (4), the magnitude  $\sigma_{\rm m}$  can be straightforwardly calculated from the measured restoring force without prior knowledge of the Young's modulus E of the wood.

By plotting the restoring force (P) against the term  $\frac{4bl^2}{Sd}$ , the value of  $\sigma_{\rm m}$  can then be deduced from the slope of the graph. It appears that the model well describes the experimental restoring data at relatively small values of  $\frac{4bl^2}{Sd}$ . In this flexural response regime, the restoring force is proportional to the term  $\frac{4bl^2}{Sd}$  (Fig. 6a, b). Alternatively, one could plot the term  $\frac{PSd}{4bl^2}$  against the half-split length (l) and the maximum, and constant value of the term  $\frac{PSd}{4bl^2}$  is the value of  $\sigma_{\rm m}$  (Fig. 6c, d). The magnitudes of  $\sigma_{\rm m}$  derived from the graphs are 2.90 and 1.08 MPa for the 30-mm-thick HS and LS specimens, respectively (Fig. 6a, c), and are 3.37 and 1.67 MPa for the 50-mm-thick HS and LS specimens, respectively (Fig. 6, d). It should be noted that the presence of other stress components especially in the thickness direction could also affect the measured restoring force value. For the purpose of this study, all pieces of flat-sawn lumber were selected such that stresses in thickness direction were relatively small compared to those in the direction of width. In the future, the effects of other stress components could be included in the calculations.

According to Eq. (4), the calculated restoring forces at those magnitudes of  $\sigma_{\rm m}$ derived are compared with the experimental values in Fig. 7a, b. As expected, a good agreement between the calculated and the measured restoring force values is obtained in the flexural response regime between the half-split lengths from 60 to 100 mm in the 30 mm-thick and 130-mm-wide specimens (Fig. 7a). Outside this range, the calculated restoring forces overestimate the experimental values. At halfsplit lengths <60 mm, it is expected that the internal stress was not fully relaxed across the whole specimen thickness, and the presence of stress field around the tip of the kerf had not yet been taken into account in the calculation. At the half-split lengths more than 100 mm, stress field generated by the deep kerf should have covered across the end of specimen with a width of 130 mm. Therefore, one end of a half-split specimen leg cannot be considered to be fixed to a rigid support. A modification of Eq. (4) to cope with such behaviors outside the flexural response regime warrants further investigation and is a subject of future work. This is crucial for thicker lumber such as the 50-mm-thick specimens where the flexural response range was rather small of 80–95 mm (Fig. 7b). Estimation of the internal stress within thicker lumber using the purely flexural model proposed is still possible but is no longer appropriate. Analysis in the following section is therefore restricted to the 30-mm-thick and 130-mm-wide rubberwood lumber.

#### Validation of $\sigma_{\rm m}$ derived from the restoring force technique

The released strain and Young's modulus in the tangential direction plus moisture content distributions within the 30-mm-thick HS and LS specimens obtained from the McMillen slice test are shown in Fig. 8a-c. The elastic strains due to the release of internal stresses were not uniform (Fig. 8a). After slicing of the surface layer,



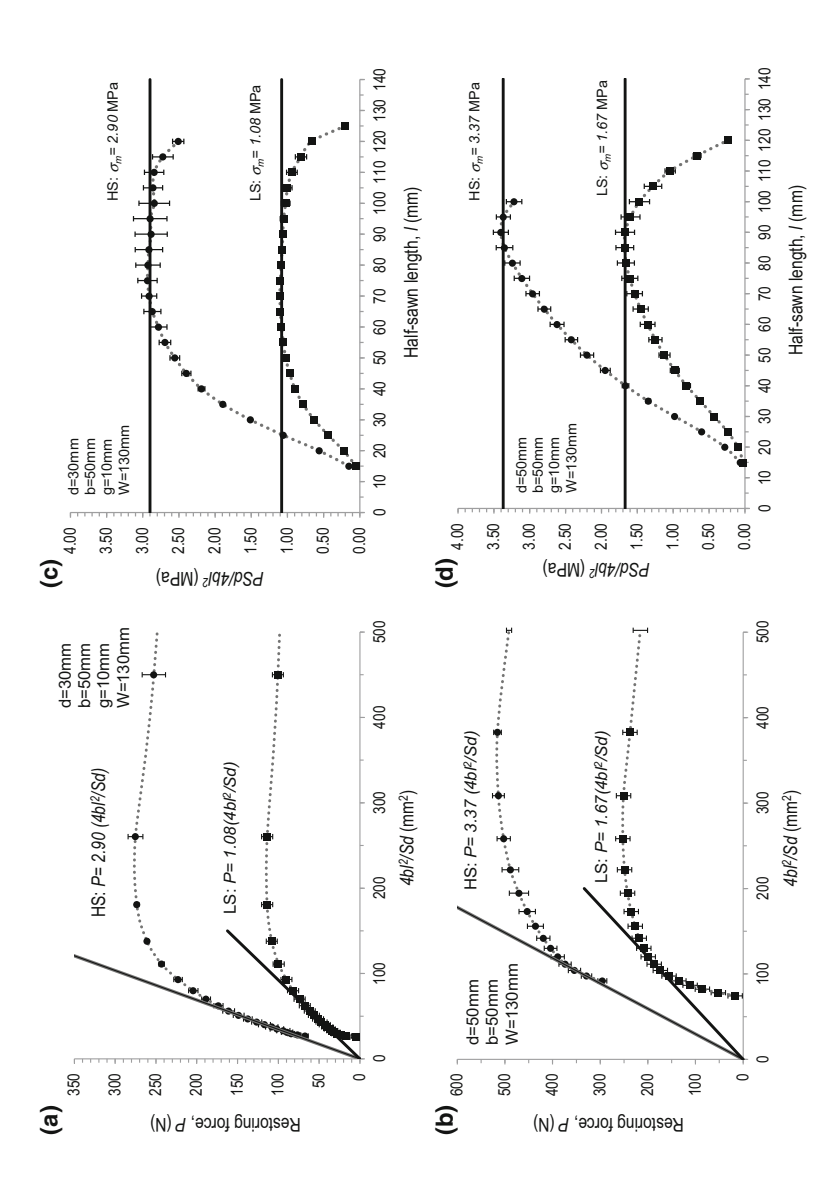
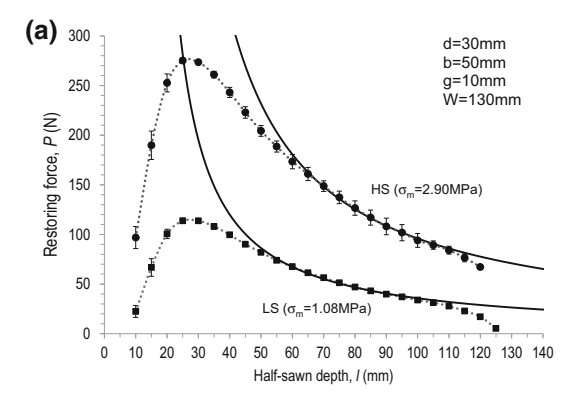
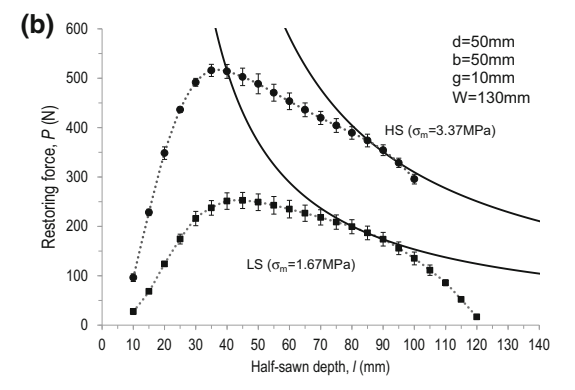


Fig. 6 Plots of the restoring force versus  $\frac{4h^2}{5d}$  for a the 30-mm and b the 50-mm-thick half-split rubberwood specimens and plots of  $\frac{PSd}{4h^2}$  versus the half-split length for the c 30-mm and d the 50-mm-thick half-split rubberwood specimens containing relatively high (HS) and low (LS) levels of internal stress. Solid lines represent the best fits to the experimental data in the flexural response regime



Fig. 7 Comparison of experimental (symbols) and calculated restoring force (solid lines) profiles of the a 30-mm and b 50-mm-thick half-split rubberwood specimens containing relatively high (HS) and low (LS) levels of internal stress at various half-split lengths





lengthening with a positive value of released strain indicates that the wood in this layer was under compressive internal stress before being sliced. On the other hand, a negative released strain observed at the core layer indicates a tensile internal stress. This behavior has been reported for casehardening of kiln-dried lumber by various authors (McMillen 1958; Simpson 1999). Moisture content was approximately uniform across the lumber thickness with the average values of  $6.2 \pm 0.4$  % and  $10.2 \pm 0.5$  % in the HS and LS specimens, respectively (Fig. 8b). Since moisture content was lower in the HS specimens, Young's modulus in these specimens (585  $\pm$  112 MPa) was higher than that in the LS specimens (477  $\pm$  91 MPa) (Fig. 8c).

Corresponding internal stress profiles, product of the released strain and the Young's modulus for each slice, are shown in Fig. 8d, e. The Poisson's ratio effect is assumed to be negligible. A linear average to the stress data was performed across the thickness. Corresponding maximum stresses  $\sigma_{\rm m}$  obtained were 2.10 and 0.97 MPa for the HS and LS specimens, respectively. These values are in general agreement with those derived from the restoring force technique of 2.90 and 1.08 MPa for the HS and LS specimens, respectively. A very close agreement is observed in the LS specimens where the internal stress profile is relatively low and roughly linear (Fig. 8e). At higher levels of internal stress, the stress profile deviates from the linear distribution. The maximum stresses at the surface and the core layer



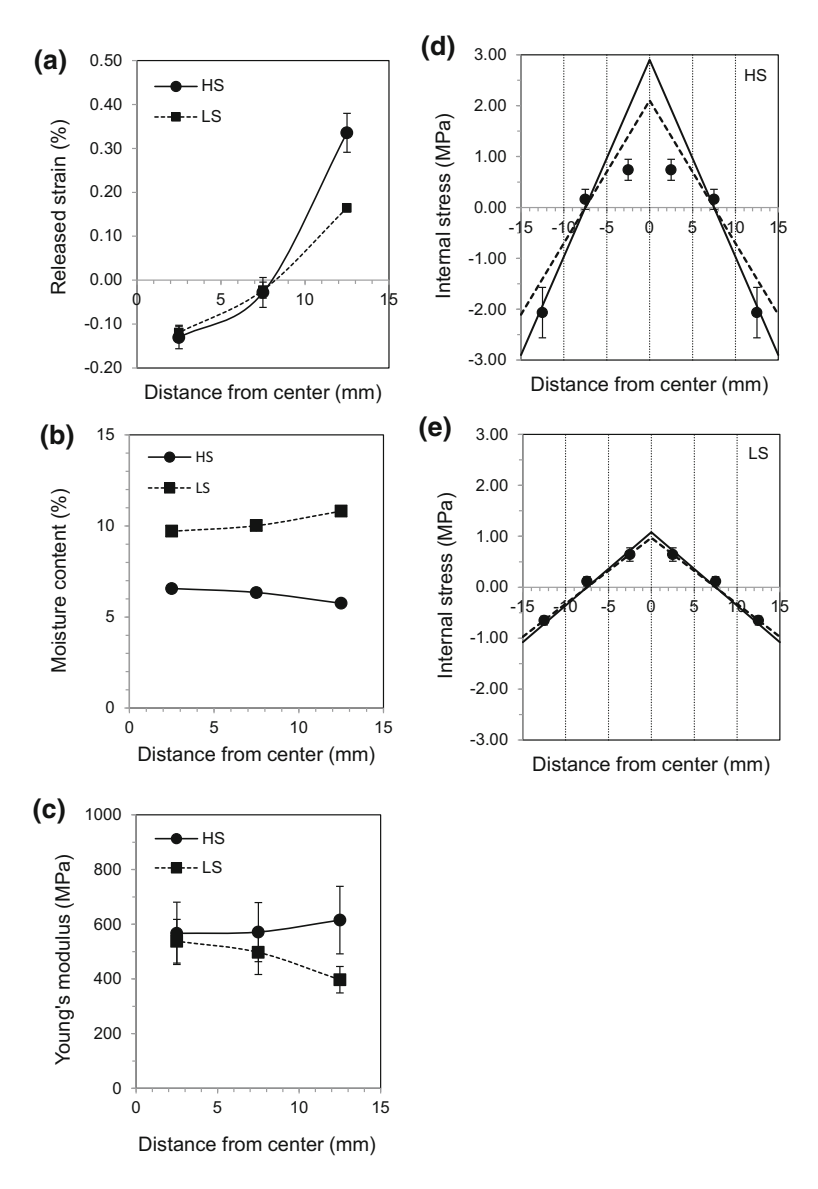


Fig. 8 Distributions of  $\mathbf{a}$  released elastic strain,  $\mathbf{b}$  moisture content,  $\mathbf{c}$  Young's modulus within the HS and LS specimens and distributions of the calculated internal stresses within  $\mathbf{d}$  the HS and  $\mathbf{e}$  the LS specimens. Linearly averaged internal stress profiles obtained from the slice test (*dashed lines*) and the proposed restoring force technique (*solid lines*) are also displayed for comparison

are different. Values of  $\sigma_m$  both underestimate and overestimate the maximum compressive stress at the surface layer and the maximum tensile stress at the core layers, respectively (Fig. 8d). Nevertheless, a single value of  $\sigma_m$ , representing the average maximum magnitude of the internal stress within the kiln-dried lumber, should be a simple and convenient stress indicator to be used in lumber industry.

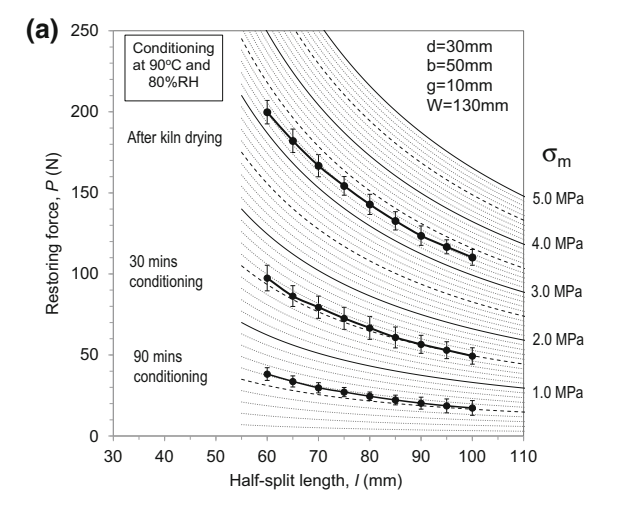


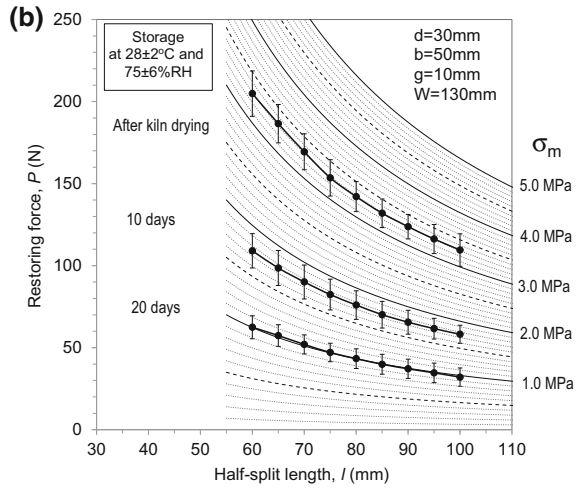
Validation of  $\sigma_m$  obtained from the restoring force technique should be performed against other well-developed internal stress measurement techniques (Schajer and Ruud 2013) in the future.

#### The restoring force-internal stress chart

Intended for practical use in the lumber industry, the chart of restoring force versus half-split length plotted at different levels of internal stress is created in Fig. 9a, b. The demonstration was made in this work for 30-mm-thick lumber with length in the longitudinal direction of 50 mm and the restraining point at 10 mm from the top end. Two sets of three 30-mm-thick industrial kiln-dried rubberwood lumber were used. Stress relaxation of the kiln-dried lumber during conditioning at 85 °C and 80 % RH inside the conditioning chamber and during storage in ambient air at

Fig. 9 Determination of  $\sigma_m$  using the restoring force—internal stress chart by plotting the measured values of the restoring force as a function of the half-split length of the 30-mm-thick and 130-mm-wide kiln-dried lumber during a conditioning at 85 °C and 80 % RH and  ${\bf b}$  storage in ambient air at 28  $\pm$  2 °C and 75  $\pm$  6 % RH







 $28 \pm 2$  °C and  $75 \pm 6$  % RH was investigated using the chart. The half-split length employed was from 60 mm to 100 mm, a suitable range as mentioned in "Estimation of the internal stress" section.

The measured restoring forces obtained from each group of lumber roughly follow a particular stress level line. The magnitude of  $\sigma_{\rm m}$  can be directly assessed through the chart. Figure 9a shows that after kiln drying,  $\sigma_{\rm m}$  was 3.3 MPa and after conditioning for 30 and 90 min, it was reduced to 1.5 and 0.6 MPa, respectively. For the second set of kiln-dried lumber, storage in ambient air for 10 and 20 days reduced  $\sigma_{\rm m}$  to 1.8 to 1.0 MPa, respectively (Fig. 9b).

The restoring force measurement on the half-split specimens together with the use of the proposed restoring force–internal stress chart should be a useful tool in estimating the magnitude of internal stress within industrial kiln-dried lumber. This technique, still a destructive method similar to the traditional prong one, should give a reliable and meaningful stress measurement and is easy to perform. Ongoing research focuses on determining  $\sigma_{\rm m}$  outside the flexural response regime, which is not covered by this model especially with relatively narrow (W < 90 mm) or thick (d > 30 mm) lumber. Finite element analysis will be employed to study the complex stress behavior outside the flexural response regime.

#### Conclusion

The following conclusions can be drawn from this work.

- A procedure and an apparatus for the assessment of internal stress within kilndried lumber have been presented. The restoring force measured on the halfsplit specimens appears to be a reliable quantitative measure of the magnitude of the internal stress.
- 2. The magnitude of the restoring force is dependent on the half-split length and thickness of the specimens. With increased half-split length, the restoring force sharply increases, reaches the maximum value and then gradually decreases. Higher restoring force is obtained in the thicker lumber.
- 3. The model based on an elastic cantilever beam theory has been successfully developed to directly deduce the maximum linearly averaged internal stress from the measured restoring force data within the flexural response regime. No information on the modulus of wood is required in the calculation. In the 30-mm-thick lumber, the flexural range is between the half-split lengths from 60 to 100 mm. This flexural range becomes smaller in the thicker lumber.
- 4. General agreement is found between the magnitudes of the maximum linearly averaged internal stress derived from the restoring force technique and the conventional McMillen slice technique, especially in the specimens having a relatively low and roughly linear stress profile.
- The restoring force-internal stress chart has been proposed for a practical use in the lumber industry. A demonstration was carried out to follow stress relaxation during conditioning and during storage of industrial kiln-dried rubberwood lumber.



Acknowledgments One of the authors (SJ) wishes to thank the Commission on Higher Education and Rajabhat Nakhon Si Thammarat University, Thailand, for a scholarship to study PhD at Walailak University. The authors gratefully acknowledge the Thailand Research Fund and Walailak University for their financial support (Grant No. RSA5880025). Special thanks are reserved for Nakornsri Parawood Co., Ltd. of Nakhon Si Thammarat for providing the kiln-dried rubberwood lumber used within this work.

#### Compliance with ethical standards

Conflict of interest The authors declare that they have no conflict of interest.

#### References

- Bodig J, Jayne BA (1982) Mechanics of wood and wood composites. Van Nostrand Reinhold Company, New York
- Diawanich P, Matan N, Kyokong B (2010) Evolution of internal stress during drying, cooling and conditioning of rubberwood lumber. Eur J Wood Prod 68(1):1–12
- Diawanich P, Tomad S, Matan N, Kyokong B (2012) Novel assessment of casehardening in kiln-dried lumber. Wood Sci Technol 46:101–114
- European Committee for Standardization (2010) Sawn timber-method for assessment of case-hardening. CEN standard ENV 14464
- Fuller J (1995) Conditioning stress development and factors that influence the prong test. Res. Pap. FPL–RP–537. Department of Agriculture, Forest Service, Forest Products Laboratory, Madison
- Fuller J, Hart CA (1994) Factors that influence the prong test. In: Proceedings of the 4th IUFRO international wood drying conference, Rotorua, pp 313–320
- Hibbeler RC (2012) Structural analysis. Prentice Hall, New Jersey
- Lados DA, Apelian D (2006) The effect of residual stress on the fatigue crack growth behavior of Al-Si-Mg cast alloys—mechanisms and corrective mathematical models. Metall Mater Trans A 37:133-145
- Matan N, Kyokong B (2003) Effect of moisture content on some physical and mechanical properties of juvenile rubberwood. Songklanakarin J Sci Technol 25(3):327–340
- McMillen JM (1958) Stresses in wood during drying (Report 1652). Department of Agriculture, Forest Service, Forest Products Laboratory, Madison
- Perré P, Passard J (2007) Stress development. In: Perré P (ed) Fundamentals of wood drying. European COST A.R.B.O.LOR, Nancy, pp 243–271
- Rossini NS, Dassisti M, Benyounis KY, Olabi AG (2012) Methods of measuring residual stresses in components. Mater Des 35:572-588
- Schajer GS, Ruud CO (2013) Overview of residual stresses and their measurement. In: Schajer GS (ed) Practical residual stress measurement methods. Wiley, West Sussex, pp 1–27
- Simpson WT (1991) Dry kiln operator's manual. In: Agriculture Handbook AH-188. Department of Agriculture, Forest Service, Forest Products Laboratory, Madison
- Simpson WT (1999) Drying and control of moisture content and dimensional changes. In: Wood handbook (Wood as an Engineering Material). Department of Agriculture, Forest Service, Forest Products Laboratory, Madison
- Sonderegger W, Martienssen A, Nitsche C, Ozyhar T, Kaliske M, Niemz P (2013) Investigations on the physical and mechanical behavior of sycamore maple (*Acer pseudoplatanus* L.). Eur J Wood Prod 71:91–99
- Tomad S, Matan N, Diawanich P, Kyokong B (2012) Internal stress measurement during drying of rubberwood lumber: effects of wet-bulb temperature in various drying strategies. Holzforschung 66:645–654
- Walton HW (2002) Deflection methods to estimate residual stress. In: Totten G, Howes M, Inoue T (eds) Handbook of residual stress and deformation of steel. ASM International, Ohio, pp 89–98
- Wengert E (1992) Techniques for equalizing and conditioning lumber. Cooperative extension programs No. 65. Department of Forest and Wildlife Ecology, University of Wisconsin, Madison



## Appendix 2

Sataporn Jantawee, Satjapan Leelatanon, Prawate Diawanich, Sornthep Vannarat and Nirundorn Matan (2018) "Comparison of techniques for quantification of internal stress within industrial kiln-dried timber" European Journal of Wood and Wood Products, *76(2): 617-627*. (IF=1.082, Q1: Forestry, Q2: Materials science)

Eur. J. Wood Prod. DOI 10.1007/s00107-017-1243-2

## CrossMark

#### **ORIGINAL**

## Comparison of techniques for quantification of internal stress within industrial kiln-dried timber

Sataporn Jantawee $^1$  · Satjapan Leelatanon $^1$  · Prawate Diawanich $^2$  · Sornthep Vannarat $^3$  · Nirundorn Matan $^1$ 

Received: 15 September 2016

© Springer-Verlag GmbH Germany 2017

**Abstract** For a quantification of internal stress within industrial kiln-dried timber, a comparison of a new restoring force (RF) technique is made against the McMillen slice test and the standard case-hardening test. Simulation of the RF has been performed by using a numerical model of finite element (FE) analysis. 30 mm thick industrial kilndried rubberwood timber with 58, 78 and 100 mm widths was used in the study. The measured RFs for each timber size are proportional to the released strain data measured by the McMillan slice test and the gap openings measured according to the case-hardening test. The FE simulated and measured RFs are in good agreement. The geometrical shape factor as functions of timber width and cutting depth ratio is derived so that the internal stress can then be calculated without accounting for the modulus of elasticity. The calculated maximum internal stresses of all the examined timber sizes fall into a single curve and linearly relate to the released strain data. The RF measurement has the potential to be an alternative method to the existing techniques for a reliable and meaningful assessment of drying stress within industrial kiln-dried timber.

Nirundorn Matan mnirundo@wu.ac.th

Published online: 25 October 2017

- Materials Science and Engineering, School of Engineering and Resources, Walailak University, Thasala district, Nakhon Si Thammarat 80160, Thailand
- Nakhon Si Thammarat Seaboard Industrial College, Pakpanang district, Nakhon Si Thammarat 80140, Thailand
- Internet Innovation Laboratory, National Electronics and Computer Technology Center, Pathumthani 12120, Thailand

#### 1 Introduction

Assessment of residual internal drying stress is an important procedure for quality control of kiln-dried timber (Welling 1994). After drying, a piece of timber is usually under compressive and tensile stresses at the outer layer and the inner core, respectively (McMillen 1958; Simpson 1999). Without an effective stress relief, remanufacturing of the stress-containing timber often increases losses due to distortion (Wengert 1992). Various stress-relaxing techniques such as hole-drilling, contour method and slitting method are widely used to determine residual stresses in alloys and ceramics (Schajer and Ruud 2013). Conventionally, an assessment of internal stress within industrial kiln-dried timber has been carried out by using the stress relaxing of the McMillen slice test (McMillen 1958), the standard CEN case-hardening test (CEN/TS 2010) and the prong test (Simpson 1991). Strain or deflection accompanying the elastic relaxation of internal stress caused by sectioning or splitting is measured. Distributions of released strain and moisture content across the thickness of timber are commonly reported in the McMillen slice test. For the casehardening test, maximum gap between two half slices after conditioning is successfully used to classify different drying quality of kiln dried timber. The prong test, however, was reported to potentially provide an ambiguous reading on the level of the internal stress depending on the amount of the wood removed (Welling 1994; Fuller and Hart 1994). Strain related measurement is useful to describe and quantify wood warping such as cupping when the cut piece of timber is free. However, information related to stress would be appropriate if the cut piece of timber is in a restrained configuration. This includes, for example, the force acting on a saw blade during splitting of the casehardened lumber and the internal stress built up within composite member such as glulam where many pieces of timber are glued together. Information on the elastic



modulus of wood is required for an interpretation of strain or deflection into stress (Schajer and Ruud 2013; Walton 2002). However, the modulus of elasticity of timber, depending on several factors such as moisture content, specific gravity and grain orientation (Bodig and Jayne 1982; Matan and Kyokong 2003; Sonderegger et al. 2013), is not conveniently measured by kiln operator in sawmills. A new concept to measuring a restoring force on a so-called "half-split" specimen has been proposed and the corresponding device suitable for industrial uses has been designed and constructed (Diawanich et al. 2012; Jantawee et al. 2016).

The aims of this research are to compare the results obtained from the proposed restoring force technique against those according to the existing techniques (McMillen 1958; CEN/TS 2010) and to quantify the magnitude of the internal stress using the measured restoring force data. A numerical model of finite element (FE) analysis is first employed to simulate the measured restoring force and then to deduce the geometrical shape factor used in the internal stress calculation. Emphasis is placed on investigation of internal stress behavior of the 30 mm thick kiln-dried rubberwood timber with various widths.

#### 2 Background

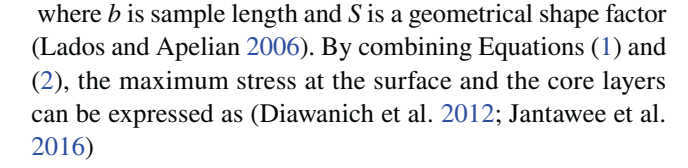
At the beginning of the drying period, internal stress is generated as soon as the moisture content in the outer layer of timber is below the fiber saturation point. Elastic response to the incompatible shrinkage strains to preserve dimensional continuity within a piece of timber induces tensile and compressive stresses in the outer layer and inner core, respectively. As the drying process continues, the internal stresses reverse as a result of viscoelastic and mechano-sorptive creep. Then up until the end of drying, a timber outer layer is under compressive stress while an inner core layer is under tensile stress (Perré and Passard 2007).

By assuming a linear distribution of internal stress across half thickness of timber, magnitude of maximum stress,  $\sigma_m$ , assumed to be equal at the outer surface and the inner core, can be calculated by a deflection of the half-split specimen as expressed by

$$\sigma_{\rm m} = \frac{E \cdot \Delta \delta \cdot d}{4l^2} \tag{1}$$

where E,  $\Delta\delta$ , d and l are Young's modulus in the tangential direction, mouth opening, thickness and sawed depth of the specimen, respectively (Walton 2002). The restoring force, P, required to keep the half-split specimen in the original configuration can be computed using

$$P = \frac{E \cdot \Delta \delta \cdot b}{S} \tag{2}$$



$$\sigma_m = S \frac{d}{4bl^2} P \tag{3}$$

It should be noted that by this means the magnitude of internal stress can be calculated directly from the measured restoring force P without any knowledge of the Young's modulus, E, of the wood. It should be noted that the restoring force technique applies a shear force load to the half-split specimen. The resultant internal stresses induced by the applied force are accounted for in the geometrical shape factor S, which is dependent on half-split specimen configuration such as specimens' size, half-split length and configuration of the applied force. Within this work, the values of S for the test specimens are deduced by the FE technique.

#### 3 Materials and methods

#### 3.1 The restoring force measuring device

The restoring force measuring device proposed by Jantawee et al. (2016) was used in this study. The equipment (Fig. 1) consists mainly of a relatively rigid steel frame, two clamping jigs of 56 mm wide and a load cell (Cooper Instrument, USA). One jig was fixed to the frame and another one was attached to a steel rod connected to the load cell. A rubberwood specimen of 50 mm long, b, was first fixed to the device by being clamped onto the jigs at a distance, g, of 10 mm away from the top end. Care was taken to ensure that optimum torque of 2–3 N m was applied with a contact area of 24 mm<sup>2</sup> to hold the specimen to the jigs without damaging the specimen. While being clamped to the frame, the specimen was cut at half the thickness in the tangential direction by half the width (l/W=0.5). The device was designed such

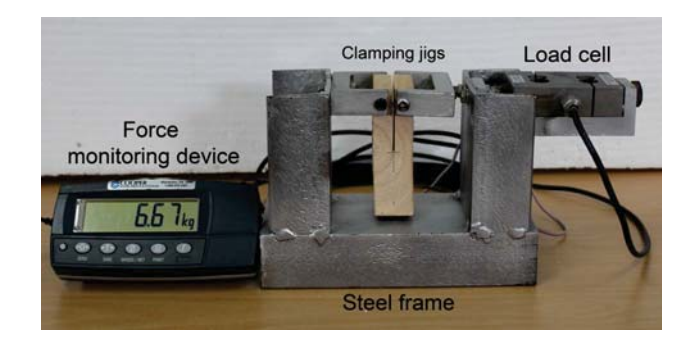


Fig. 1 Photograph of the wood specimen installed in the restoring force measuring device



that the specimen clamped to the frame can be sawed in the direction of the width using a band saw. Since the specimen is restrained to the frame and to a steel rod connected to the load cell, a net force generated by relaxation of internal stress within the half-split specimen was transferred to the load cell. The sign and magnitude of the force were then displayed on the force reading device (Fig. 1).

## 3.2 Assessment of internal stress in industrial kiln dried rubberwood timber

Kiln dried rubberwood timber (30 mm thick and 1300 mm long) with three different widths (56, 78 and 100 mm) was taken immediately after drying from a local sawmill in Nakhon Si Thammarat, Thailand. Ten boards from the same drying cycle were used for each group. The ring orientation was controlled by selecting flat sawn boards. An average moisture content of the kiln-dried boards was  $3.6 \pm 1.0\%$  with moisture content gradient between the surface and the core layers of  $0.7 \pm 0.2\%$ . For each timber, two adjacent specimens were cut at approximately 50 mm from the end of timber (Fig. 2a). The first specimen with the length of 50 mm was used to determine the restoring force and the released strain according to the McMillen slice test (McMillen 1958). The timber surfaces in the thickness direction were first slightly planed to remove irregularities to obtain a relatively smooth surface. The specimen was marked by divided lines so it could be cut into six equal slices. The initial width of each pre-marked slice  $(W_b)$  was measured by calipers having a precision of 0.01 mm. Measurement positions on each slice were marked so that the following width measurements after slicing could be performed at the same positions. The specimen was then assembled into the restoring force measuring apparatus and cut through the premarked half thickness line for a half width (l/W = 0.5). The restoring force was recorded. The specimens were then cut into slices along the pre-marked lines. Each slice was subsequently pressed flat before its width,  $W_a$ , was measured. Care was also taken to ensure that about the same force was applied to the caliper for every measurement. The released strain of each slice,  $\varepsilon$ , was calculated according to  $\varepsilon = \frac{W_a - W_b}{W_c}$ .

A section of each slice was weighted before and after ovendrying at 104 °C for 24 h to determine its moisture content. The second specimen cut at the length of 15 mm was sawed into two halves by its thickness according to the case-hardening test method (CEN/TS 2010). The two test pieces were then placed flat on a test jig with 75 mm pin distance and the maximum gap distance between the two test pieces at midpoint was immediately measured with an accuracy of 0.1 mm. The measured value, subtracted with the diameter of the test jig pins, was multiplied by a factor of 1.78 to obtain the equivalent maximum gap distance measured at

the 100 mm pin separation,  $G_{100}$ , according to the case-hardening test method (CEN/TS 2010).

The remaining pieces of timber were coated with aluminum paint at both ends and stored in ambient condition  $(28\pm2~^{\circ}\text{C}\text{ and }75\pm6\%\text{ RH})$ . Assessment of internal stress was then performed at a week interval for up to three weeks to examine the lower levels internal stress. For the case-hardening test using a test jig with 75 mm pin distance (CEN/TS 2010), only pieces of timber 78 and 100 mm wide were examined. The pin distance is shorter than the width of the 56 mm wide timber. In addition, some pieces of rubberwood timber stored in ambient condition for a longer time for up to 4 months were also tested for a very low level of internal stress.

For the FE model verification, a single 30 mm thick and 100 mm wide rubberwood board dried to a moisture content of  $5.8 \pm 0.5\%$  was used. Two sets of specimens (five replicates for each set) with relatively high level of internal stress (HS) and low level of internal stress (LS) were prepared for the restoring force test and the McMillen slice test mentioned above. The HS specimens were tested immediately after kiln drying while the LS specimens were left in ambient air  $(28 \pm 2$  °C and  $75 \pm 6\%$  RH) for 7 weeks prior to testing. In addition, Young's modulus in the tangential direction of each slice of the HS and LS specimens were assessed using a universal testing machine (Lloyd 150kN, UK) equipped with a strain gauge (Epsilon Technology, USA).

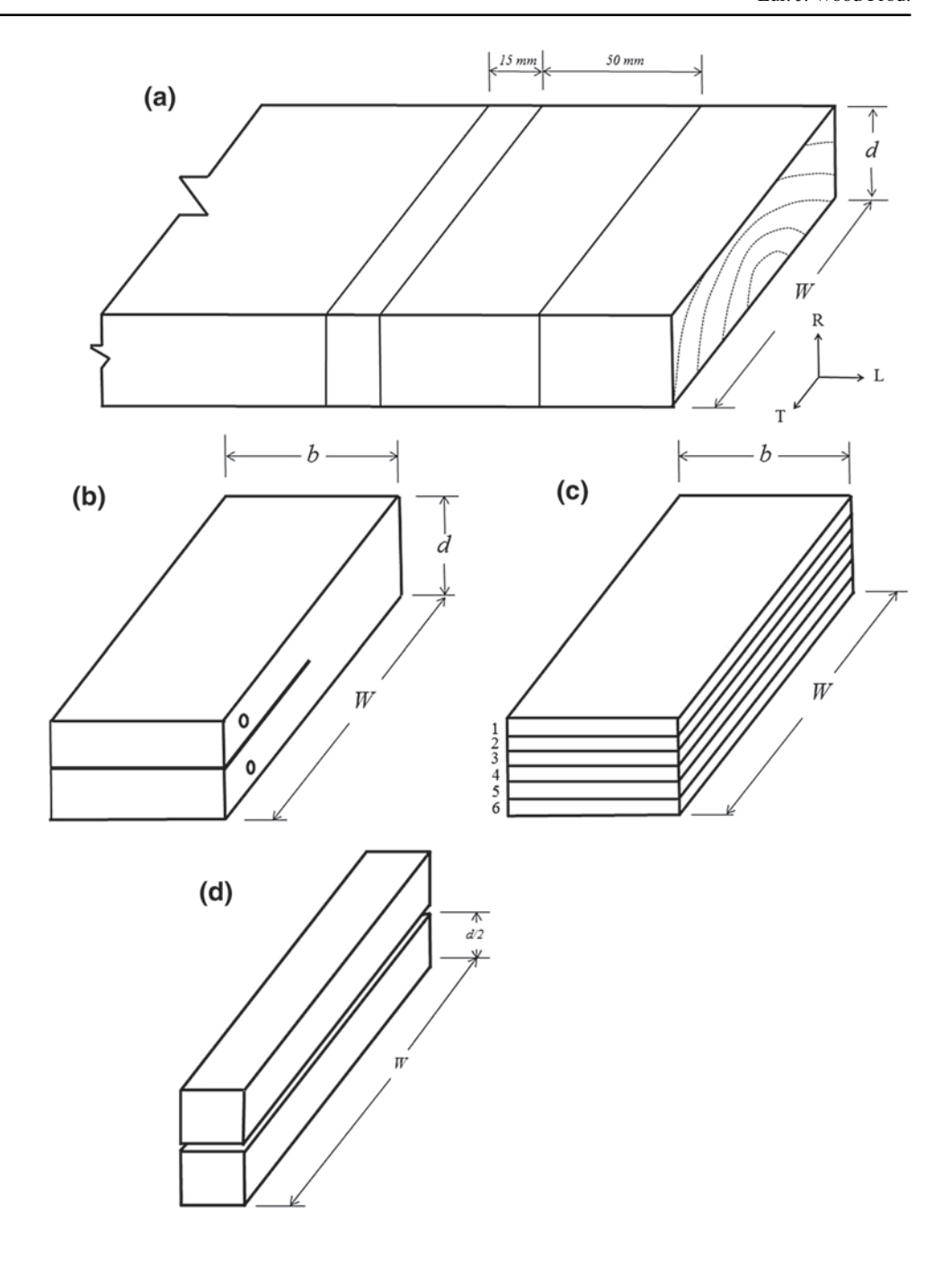
## 3.3 Finite element (FE) analysis of the restrained half-split specimen

The FE method was employed to verify the mechanical response of the restrained half-split specimen and to determine the geometrical shape factor for the three different widths of timber. The 3D model was created using the commercial FE software, ANSYS v12. The constitutive model of linearly elastic orthotropic materials was assigned to the computational procedure. Young's moduli and shear moduli used in the FE analysis were calculated as ratios of the measured Young's modulus in the tangential direction  $(E_L: E_R: E_T = 20: 1.6: 1,$  $G_{LR}$ :  $G_{LT}$ :  $G_{RT}$  = 10 : 9.4 : 1 and  $E_L$ :  $G_{LR}$  = 14 : 1). Three Poisson's ratios were estimated to be  $\mu_{RL} = 0.02$ ,  $\mu_{LT} = 0.02$  and  $\mu_{RT} = 0.35$  (Bodig and Jayne 1982; Kretschmann 2010). To reduce computational time in the solving process, only a quarter of specimen was modeled as presented in Fig. 3. The plane of symmetry was fixed in the L-direction. All nodes in the clamping area were restrained in the R-direction to deduce the calculated restoring force,

To validate the FE model, the released strain and Young's modulus data determined by the McMillan slice test were



Fig. 2 Sample layouts of a the test specimen cut from the timber, b the half-split specimen for the restoring force measurement, c the McMillen slice test and d the case-hardening test



applied to the layers corresponding to the tests. For the determination of the geometrical shape factor, S, the linearly distributed internal stress profile with the maximum magnitude of  $\pm 1$  MPa at the surface and the core layers with a uniform value of Young's modulus in the tangential direction of 500 MPa was employed.

#### 4 Results and discussion

#### 4.1 Measurement of internal stress

The measured values of restoring force are plotted against the measured released strain data for each layer of the



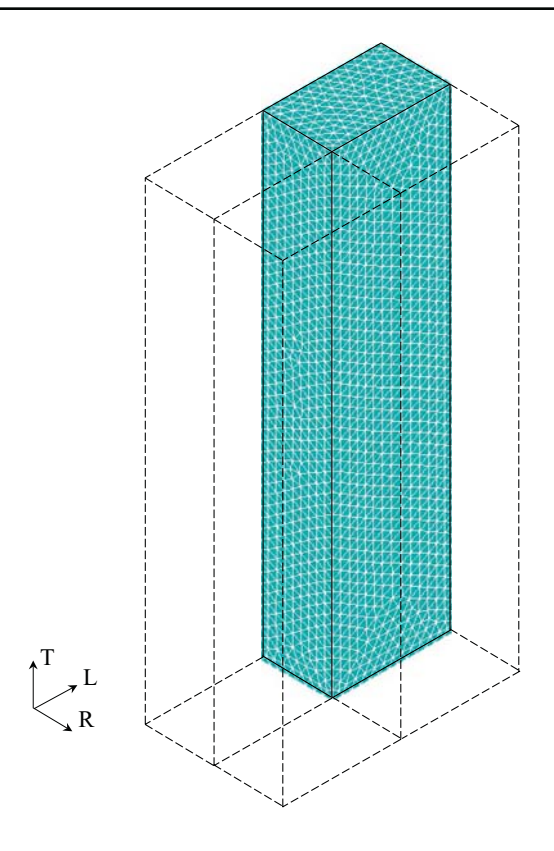
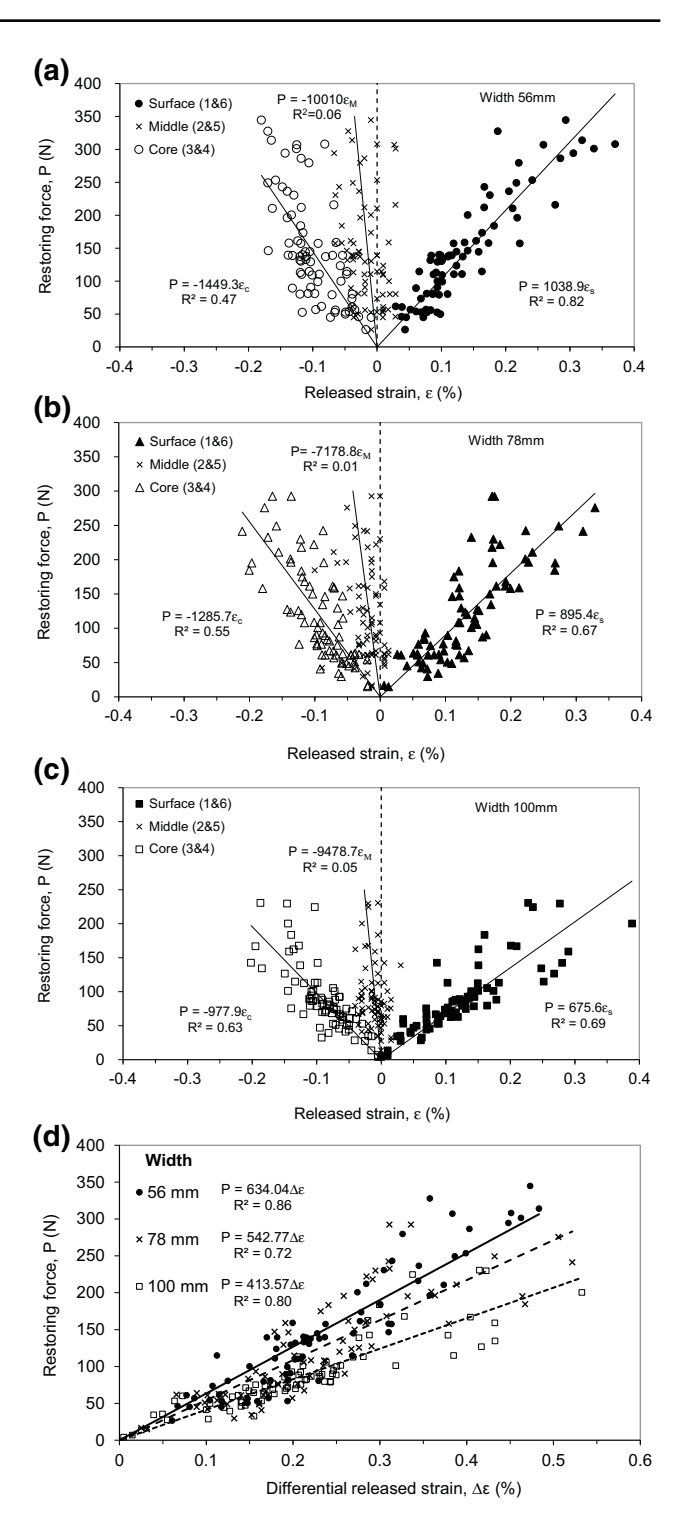


Fig. 3 3D mesh for a quarter of the specimen used in finite element simulation

kiln-dried timber with various widths in Fig. 4a–c. After kiln drying, the outer and the inner layers of the timber are often under compressive and tensile stresses, respectively. A resultant force generated across the core through the surface layers of the half-split specimen therefore bent the two legs inward. The device was designed to restrain the specimen to the initial position at the clamping points. As a result, a tensile (positive) restoring force was detected on the load cell. After slicing of the surface layer, lengthening with a positive value of released strain indicates that the wood in this layer was under compressive internal stress before being sliced. On the other hand, a negative released strain observed at the core layer indicates a tensile internal stress. This behavior has been reported for casehardening of kiln-dried timber by various authors (McMillen 1958; Perré and Passard 2007).

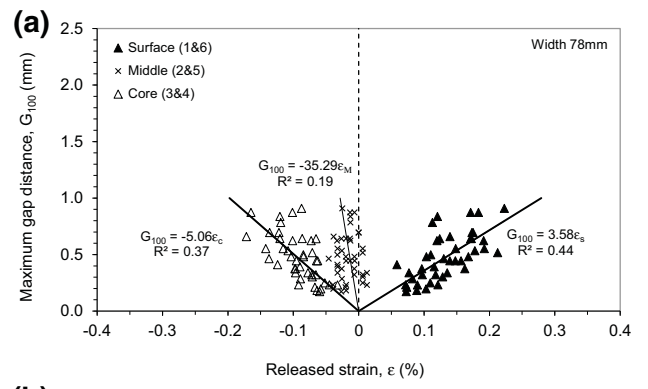
The magnitude of the restoring force at the surface and the core layers appears to be proportional to the level of the released strain. Linear coefficients, which are dependent on timber width, are lower at the surface layer with respect to those at the core layer by 30%. The values of the linear coefficients of the 58–100 mm wide timber decrease from 1039 to 676 N/% at the surface layer and from – 1449 to – 978 N/% at the core layer. For the restoring force test, Eq. (3) can be rearranged as  $P = \frac{bW^2}{Sd} \sigma_m$  given that the half-split length is equal to half of the width of timber (l = W/2).

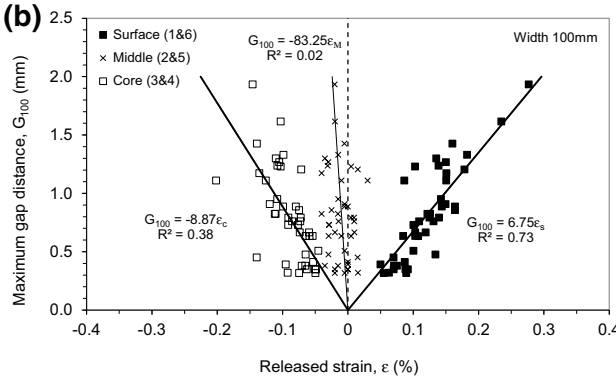


**Fig. 4** Comparison of the restoring force and the released strain at the surface, middle and core layers of the 30 mm thick and **a** 56 mm, **b** 78 mm and **c** 100 mm wide kiln-dried rubberwood timber and **d** plot of restoring force against differential released strain between the surface and the core layer at various timber widths



Since the geometrical shape factor S also varies with W with the third-degree polynomial equation (see Sect. 4.2) so that the term  $\frac{bW^2}{Sd}$  decreases with increasing W. As a consequence, wider specimen yields lower P value. At a particular level of the restoring force, the magnitude of the positive released strain at the surface layer is slightly greater than that of the negative one at the core layer, while the released strain of the middle layer is slightly less than zero. Therefore, the released strain profile across the specimen thickness could be assumed to be linearly distributed across timber thickness, although the actual profile is not perfectly linear. Similar linear correlation is also observed when comparing the





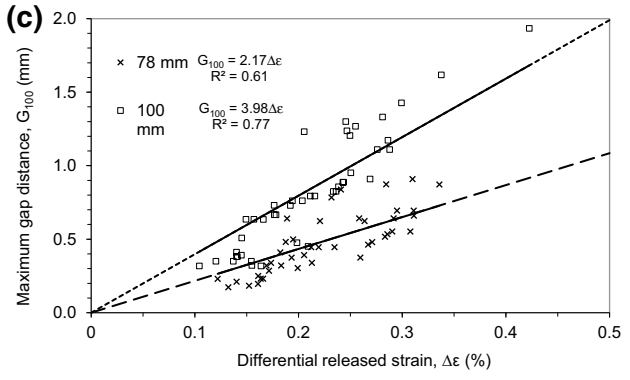
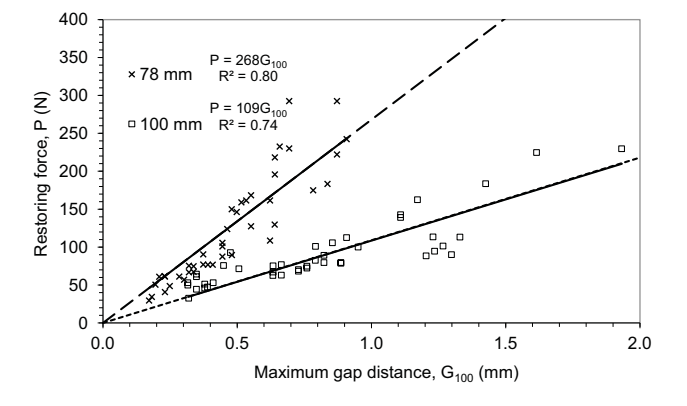


Fig. 5 Comparison of the measured maximum gap distance and the released strain at the surface, middle and core layers of the 30 mm thick and a 78 mm and b 100 mm wide kiln-dried rubberwood timber and c plot of maximum gap distance against differential released strain between the surface and the core layer at various timber widths

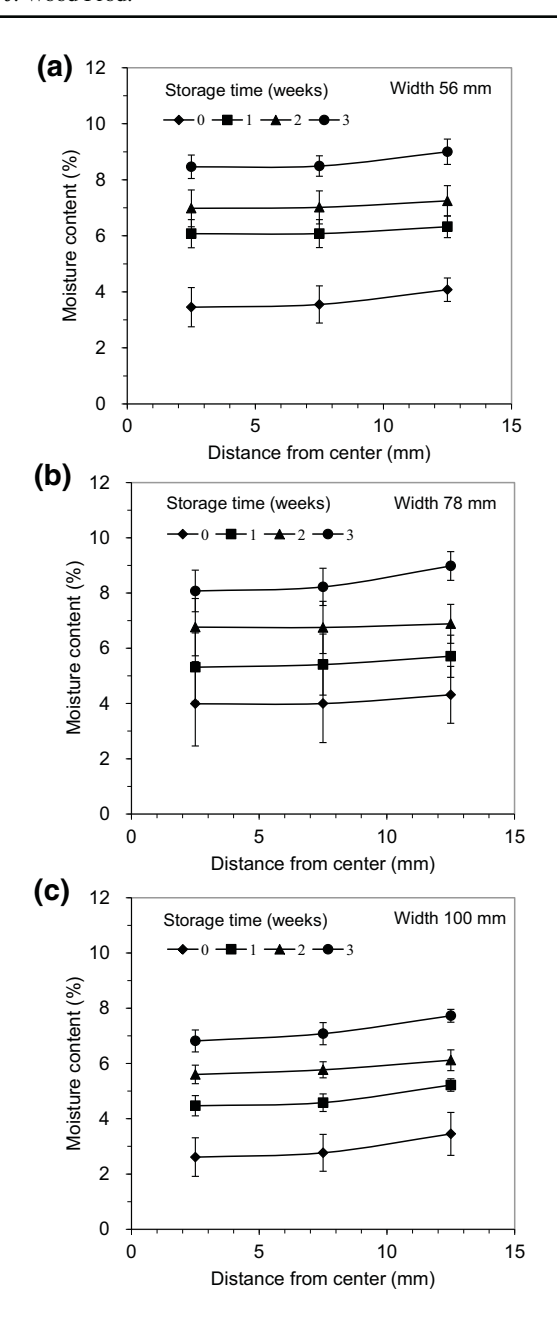
maximum gap distance according to the case-hardening test method against the magnitude of the released strain except that higher values of linear coefficients are observed in the wider timber (Fig. 5a, b). For the case-hardening test, Eq. (1) can be rearranged as  $\Delta \delta = \frac{4W^2}{d} E \sigma_m$  given that the half-split length is equal to width of timber (l=W). Therefore, wider specimen gives higher value of  $\Delta \delta$ , bending of the half slice and therefore the maximum gap measured in the case-hardening test. Comparison of the restoring force and the maximum gap distance with the released strain data (Figs. 4d, 5c, respectively) is best facilitated by plotting those against the differential released strain,  $\Delta \varepsilon$ , calculated according to the equation  $\Delta \varepsilon = \varepsilon_s - \varepsilon_c$  where  $\varepsilon_s$  is the average released strain of the surface layer (slices 1 and 6) and  $\varepsilon_c$ is the average released strain of the core layer (slices 3 and 4). It is clear that sensitivities, the slopes of the plots, of the restoring force technique (Fig. 4d) and the case-hardening test (Fig. 5c) decrease and increase with the timber width, respectively. At the same level of the differential released strain, the wider timber produces the lesser restoring force and the higher maximum gap distance. Finally, linear relationship between the restoring force and the maximum gap distance is obtained (Fig. 6).

It is reasonable that the results obtained by the restoring force technique are consistent with those of the traditional McMillen slice test (McMillen 1958) and the standard test method of the case-hardening test (CEN/TS 2010). Furthermore, the magnitude of the restoring force possesses a linear relationship with the released strain obtained from the McMillen slice test and the maximum gap distance according to the case-hardening test, therefore the restoring force measurement technique could be used as an alternative means for the assessment of the internal stress within industrial kiln-dried timber. Figure 7a–c show that average moisture content of timber continuously increased from  $3.6 \pm 1.0$  to  $8.1 \pm 0.9\%$  after 3 weeks of storage in

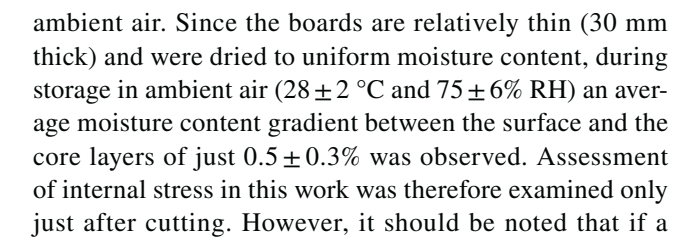


**Fig. 6** Comparison of the measured restoring force and the measured maximum gap distance at various widths of the 30 mm thick kilndried rubberwood timber





**Fig. 7** Distribution of moisture content across thickness of the 30 mm thick and **a** 56 mm, **b** 78 mm and **c** 100 mm wide kiln-dried rubberwood timber stored in ambient air  $(28\pm2~^{\circ}\text{C}\text{ and }75\pm6\%\text{ RH})$  for up to 3 weeks



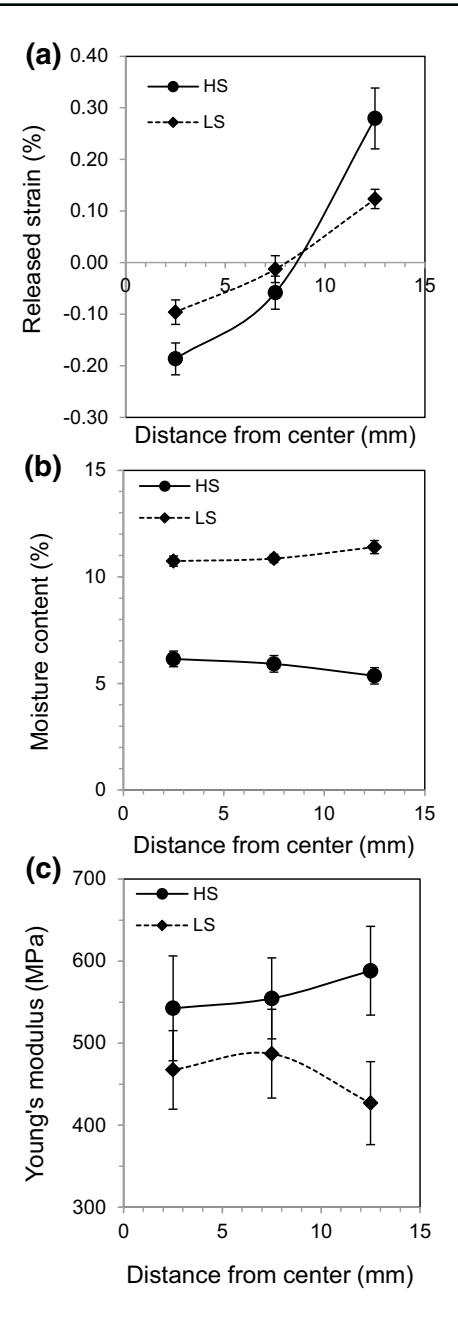


**Fig. 8** Distributions of **a** released elastic strain, **b** moisture content **c** Young's modulus within the 30 mm thick HS and LS rubberwood kiln-dried timber

significant moisture gradient exists such as in a relatively thick board, then assessment of internal stress should be performed both just after cutting and after equalization of moisture content (Welling 1994; Sandland 2001; Milić and Kolin 2008). This is beyond the scope of this work and is a subject of future work. An attempt is made in the following sections to relate the size dependent restoring force to the internal stress level within the timber.



## **4.2** Validation of FE model and determination of the geometrical shape factor

The released elastic strain and Young's modulus in the tangential direction and moisture content distributions within the 30 mm thick and 100 mm wide HS and LS specimens obtained from the McMillen's slice test are shown in Fig. 8a–c. The elastic strains due to the release of internal stresses were not uniform (Fig. 8a). Moisture content was approximately uniform across the timber thickness with the average values of  $5.8 \pm 0.5$  and  $11.0 \pm 0.4\%$  in the HS and LS specimens, respectively (Fig. 8b). Since moisture content was lower in the HS specimens, Young's modulus in these specimens ( $562 \pm 57$  MPa) was higher than that in the LS specimens ( $461 \pm 55$  MPa) (Fig. 8c). The experimental restoring forces measured at the cutting depth ratio l/W = 0.5 are  $183 \pm 16$  N and  $72 \pm 6$  N for the HS and LS specimens, respectively.

Using the released strain (Fig. 8a) and the average Young's modulus profiles in the tangential direction (Fig. 8c), the mechanical state of the HS specimen before and after half-splitting and restraining as predicted by the FE model are shown in Fig. 9. Without restraining, the internal stress within the half-split section is fully relaxed and elastic deformation of the leg of the half-split specimen is observed (Fig. 9b). By fixing all nodes within the clamping area on both legs of the half-split specimen, the restoring force  $P_{cal}$ 

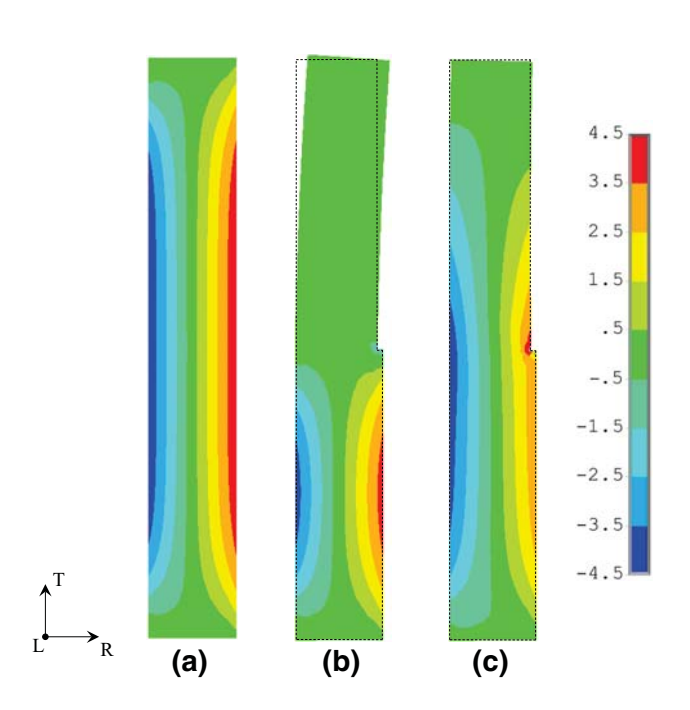


**Fig. 9** Contour plots of transverse internal stress predicted across the thickness of one quarter of  $\bf a$  the initial HS specimen and the half-split HS specimen (l/W=0.5)  $\bf b$  without restraining and  $\bf c$  with the restoring force ( $P_{cal}=174$  N) applied at 10 mm away from the top that keep the specimen in its initial configuration prior to sawing

of 174 N was obtained from the FE model. The distribution of transverse internal stress in the restrained half-split HS specimen (Fig. 9c) is approximately similar to that within the initial specimen prior to sawing (Fig. 9a). Actually for an ideal restraining, the distribution of the internal stress within the restrained half-split specimen should be as similar as possible to that within the initial specimen prior to sawing. However, this is very difficult to achieve and it is not practically possible to fully restrain the specimen for all stress/ strain components. Within this work, only transverse stress/ strain components were of interest. It should be emphasized that an improvement on restraining of the half-split specimen could still be made and is worth further study. The predicted restoring force obtained from the FE model (174 and 70 N of the HS and LS specimens, respectively) is in good agreement with the experimental restoring forces (183  $\pm$  16 and  $72 \pm 6$  N for the HS and LS specimens, respectively) within experimental errors.

After being validated, the FE model was employed to deduce the geometrical shape factor S for the 30 mm thick half-split specimen. By assuming a linear distribution of internal stress from the outer surface through the core and a constant Young's modulus in the tangential direction across the specimen thickness, the value of geometrical shape factor S was obtained from the simulated restoring force  $P_{cal}$  as

$$S = \frac{4bl^2}{d} \frac{\sigma_m}{P_{cal}} \tag{4}$$

where b, l and d are length in the longitudinal direction, half-split length and thickness of the specimen, respectively. The derived geometrical shape factor plotted against width of timber at various cutting depth ratios (l/W) is shown in Fig. 10. The geometrical shape factor increases with the timber width and the cutting depth ratio. The factor at each

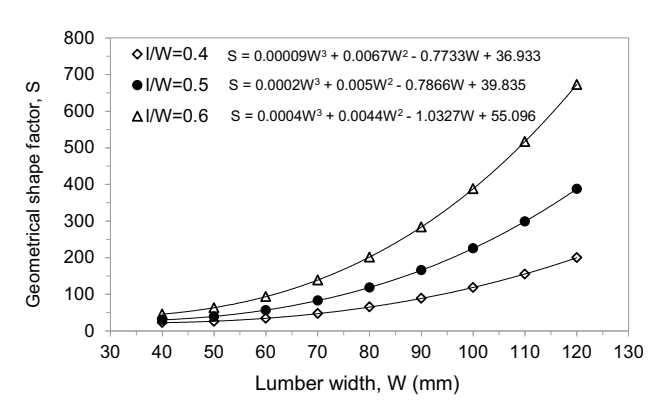


Fig. 10 Geometrical shape factor S derived by the FE model plotted against width of the half-split 30 mm thick timber at various cutting depth ratios (l/W). Solid lines, the best third-degree polynomial fits to the data, together with the fitted constants are also displayed



cutting depth ratio is best described by the third-degree polynomial equations. The fitted constants and the corresponding correlation coefficients are also shown in Fig. 10. Together with the Eq. 3, the geometrical shape factor derived can be directly used in an estimation of the internal stress level within timber from the measured restoring force. Determination of the geometrical shape factor for various timber sizes and restraining configurations should be pursued in a future work.

## 4.3 Evaluation of internal stress within kiln-dried timber

To assess the level of the internal stress within the timber, the maximum internal stresses  $\sigma_m$  were calculated from the restoring force data by means of Eq. 3 with the use of the geometrical shape factor calculated from the third-degree polynomial equations and the constants in Fig. 10. The calculated maximum internal stresses are plotted against the released strain data measured for each layer of the kiln-dried timber with various widths in Fig. 11a-c. The magnitude of the maximum internal stress both at the surface and the core layers is proportional to the level of the released strain with linear coefficients of  $9.62 \pm 0.42$  and  $-13.65 \pm 0.38$  MPa/%, respectively, independent of the timber width. By plotting the calculated maximum stress against the differential released strain (Fig. 11d), a linear relationship is obtained and data from different widths of timber seem to fall into a single curve. The linear constant of the best fit line deduced from the graph is  $514 \pm 136$  MPa. The scatter of the data points around the best-fit line is due to variation in the Young's modulus of the kiln dried rubberwood timber which depends on several factors such as specific gravity and moisture content of the timber. If it is assumed that Young's modulus of each timber in the transverse (tangential) direction is somewhat constant, stress at the surface layer  $(\sigma_s)$  and stress at the core layer  $(\sigma_s)$  can be expressed as  $\sigma_s = E \varepsilon_s$  and  $\sigma_c = E \varepsilon_c$ , respectively. It can be estimated that  $\sigma_s - \sigma_c \sim \frac{4}{3}\sigma_m = E(\varepsilon_s - \varepsilon_c) = E\Delta\varepsilon$ . Therefore, the maximum internal stress is proportional to differential released strain between the surface and the core layers via the equation  $\sigma_m = \frac{3}{4}E\Delta\varepsilon$ . As a result, the average value of Young's modulus in the tangential direction of  $685 \pm 181$  MPa could be deduced from the linear constants obtained in Fig. 11d. The average moisture content of all tested specimens in Fig. 11d is  $6.8 \pm 2.0\%$ . Given that the information concerning modulus in the tangential direction of rubberwood is very sparse, a general agreement between the calculated and the experimental (Fig. 7c) and other sources (Jantawee et al. 2016; Matan et al. 2009) data of Young's modulus as a function of moisture content can be observed in Fig. 12. In addition, the coefficient of variation (CV) of 26% in the value of Young's modulus, is in the reasonable range according to the

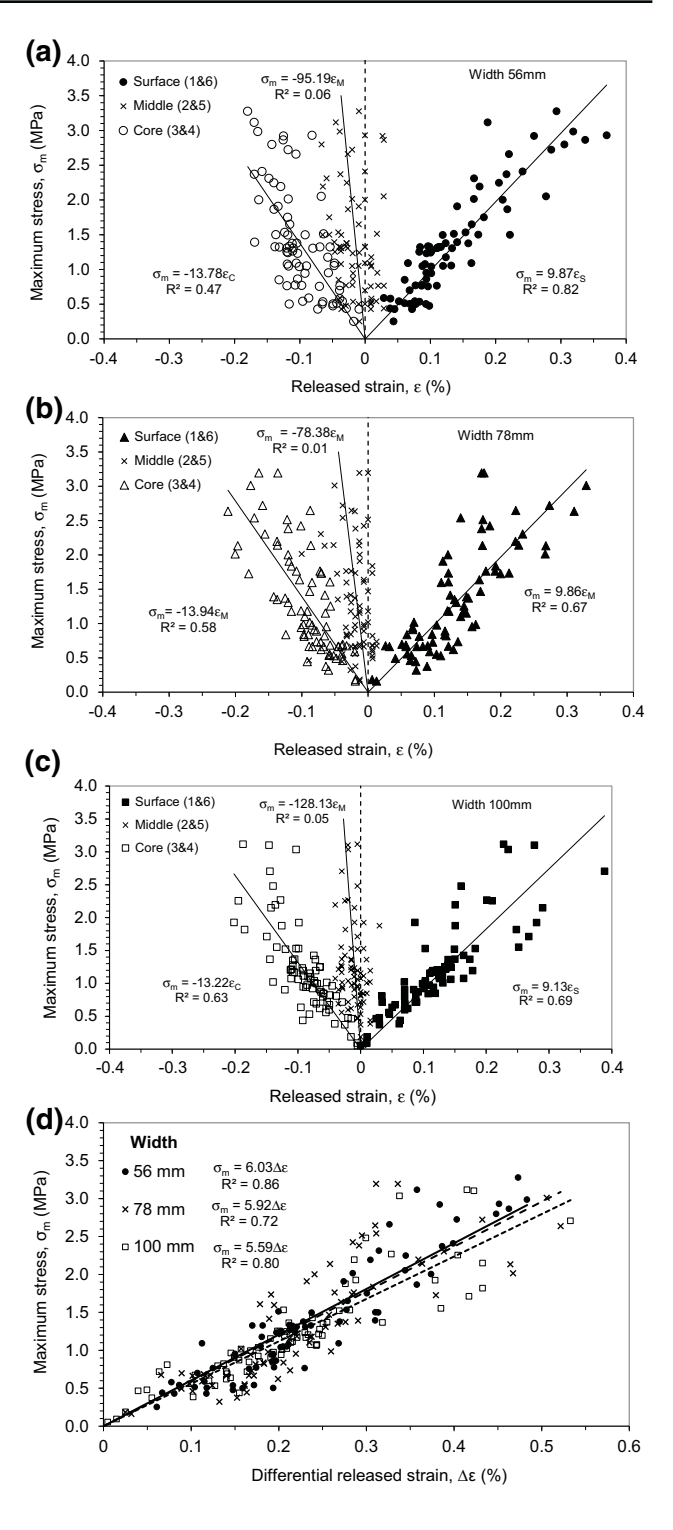


**Fig. 11** Comparison of calculated maximum internal stress  $\sigma_m$  and the released strain at the surface, middle and core layers of the 30 mm thick and **a** 56 mm, **b** 78 mm and **c** 100 mm wide kiln-dried rubberwood timber and **d** plot of maximum internal stress against differential released strain between the surface and the core layer at various timber widths



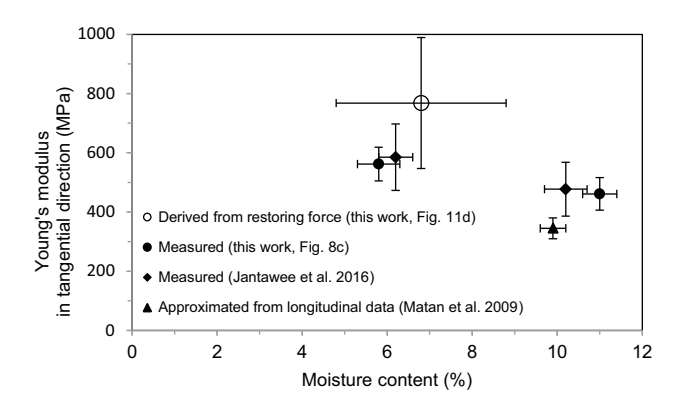


Fig. 12 Plot of Young's modulus in the tangential direction against moisture content of rubberwood; calculated value and experimental data from this work and other sources

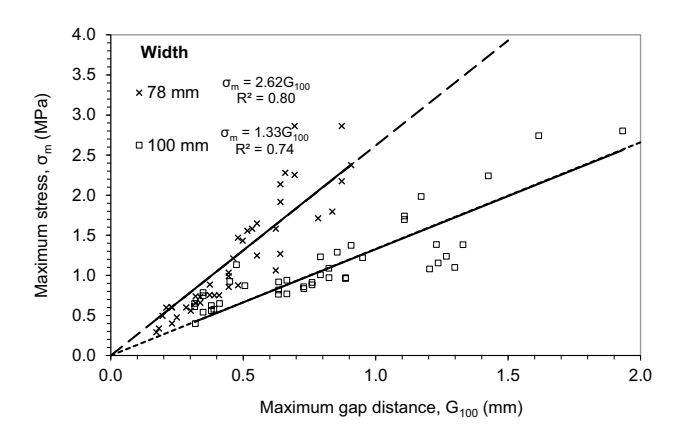


Fig. 13 Plot of maximum internal stress against maximum gap distance at various widths of the 30 mm thick kiln-dried rubberwood timber

nature of wood (Bodig and Jayne 1982; Matan and Kyokong 2003), provided that the test samples were randomly selected from a pile of industrial kiln-dried rubberwood timber.

Figure 13 shows the calculated maximum internal stress plotted against the maximum gap distance values obtained from the case-hardening test. Although both values follow a linear relationship, the maximum gap distance value is dependent on the width of the timber meaning that different sizes of timber could yield different gap distance values even though they possess a similar level of internal stress. This behavior is also confirmed by a plot of the maximum gap distance against the differential released strain (Fig. 5c) in which linear constants obtained are dependent on the width of the timber.

The information obtained from the restoring force measurement is consistent with that obtained from the conventional McMillen slice test and the standard test of the case-hardening test. In addition, the restoring force technique is relatively easy to perform and the level of the internal stress

can be directly calculated without the use of the modulus data of the wood. The released strain and the deflection occurring according to the McMillen slicing and the case-hardening techniques are usually small and difficult to measure. The proposed restoring force technique gives a reliable and meaningful measurement of the extent of the internal stress within the kiln-dried timber. Recently, this technique has been adapted to monitor in real-time the evolution of the internal stress during drying, conditioning and storage of the kiln-dried timber (Diawanich et al. 2010; Tomad et al. 2012).

#### 5 Conclusion

The following conclusions can be drawn from this work:

- 1. The measured restoring force of the half-split specimen, mechanically corresponding to the relaxation of the internal stress caused by the half-split cutting, is linearly related to the released strain measured by the McMillan slice test and the case-hardening test values according to the CEN standard test method. The results obtained by the new technique are consistent with those of the two conventional ones.
- 2. A numerical model based on finite element analysis for the restoring force technique is presented. Experimental validation of the model is performed by restoring force and released strain measurements. The predicted and measured restoring forces are shown to be in agreement. The model is then employed to deduce the geometrical shape factor for an evaluation of the internal stress level within the 30 mm thick timber as functions of timber width and cutting depth ratio.
- 3. With the use of the derived geometrical shape factor, the magnitude of the maximum internal stress can be directly estimated from the measured restoring force. The calculated stresses, regardless of timber size, linearly vary in a similar manner with the released strain data according to the McMillen slice test. The derived Young's modulus is in general agreement with the experimental data in the literature.
- 4. The restoring force measurement on a half-split specimen has potential to be an alternative method to the conventional techniques for a reliable and meaningful assessment of drying stress within industrial kiln-dried timber. The technique allows the internal stress level within the timber to be estimated without prior knowledge of the modulus of wood.

**Acknowledgements** One of the authors (SJ) wishes to thank the Commission on Higher Education and Rajabhat Nakhon Si Thammarat University, Thailand for a scholarship to study PhD at Walailak



University. The authors gratefully acknowledge the Thailand Research Fund and Walailak University for their financial support (Grant No. RSA5880025) and the National e-Science Infrastructure Consortium (http://www.e-science.in.th) for providing computing resources that have partly contributed to the research results reported in this paper. Special thanks are reserved for Khao Mahachai Parawood Co., Ltd. and Nakornsri Parawood Co., Ltd. of Nakhon Si Thammarat for providing the kiln-dried rubberwood timber used within this work.

#### Compliance with ethical standards

**Conflict of interest** The authors declare that they have no conflict of interest.

#### References

- Bodig J, Jayne BA (1982) Mechanics of wood and wood composites. Van Nostrand Reinhold Company, New York
- CEN/TS (2010) Sawn timber-method for assessment of case-hardening. CEN standard ENV 14464
- Diawanich P, Matan N, Kyokong B (2010) Evolution of internal stress during drying, cooling and conditioning of rubberwood lumber. Eur J Wood Prod 68(1):1–12
- Diawanich P, Tomad S, Matan N, Kyokong B (2012) Novel assessment of casehardening in kiln-dried lumber. Wood Sci Technol 46:101–114
- Fuller J, Hart CA (1994) Factors that influence the prong test. In: Proceedings of the 4th IUFRO international wood drying conference. Rotorua, pp 313–320
- Jantawee S, Leelatanon S, Diawanich P, Matan N (2016) A new assessment of internal stress within kiln-dried lumber using a restoring force technique on a half-split specimen. Wood Sci Technol 50(6):1277–1292
- Kretschmann DE (2010) Mechanical properties of wood. In: Ross RJ (ed) Wood handbook (wood as an engineering material). Forest Products Laboratory, United States Department of Agriculture Forest Service, Madison, pp 5/1–5/46
- Lados DA, Apelian D (2006) The effect of residual stress on the fatigue crack growth behavior of Al–Si–Mg cast alloys-mechanisms and corrective mathematical models. Metall Mater Trans A 37:133–145
- Matan N, Kyokong B (2003) Effect of moisture content on some physical and mechanical properties of juvenile rubberwood. Songklanakarin J Sci Technol 25(3):327–340

- Matan N, Kyokong B, Preechatiwong W, Wongprot T, Tomad T (2009)

  Heat treatment of rubberwood in hot compressed water. Final report. Wood Science and Engineering Research Unit, Walailak University, Nakhon Si Thammarat
- McMillen JM (1958) Stresses in wood during drying (Report 1652).

  Department of Agriculture, Forest Service, Forest Products Laboratory, Madison
- Milić G, Kolin B (2008) Moisture content distribution across thickness of kiln dried oak and beech lumber during conditioning phase. Holz Roh-Werkst 66(2):83–87
- Perré P, Passard J (2007) Stress development. In: Perré P (ed) Fundamentals of wood drying. European COST A.R.BO.LOR., Nancy, pp 243–271
- Sandland KM (2001) Prediction of required duration of the conditioning process to reduce the casehardening level in LT-dried sawn timber—initial experiments. Holz Roh Werkst 59(3):183–189
- Schajer GS, Ruud CO (2013) Overview of residual stresses and their measurement. In: Schajer GS (ed) Practical residual stress measurement methods. Wiley, New York, pp 1–27
- Simpson WT (1991) Dry kiln operator's manual. In: Agriculture handbook AH-188. Department of Agriculture, Forest Service, Forest Products Laboratory, Madison
- Simpson WT (1999) Drying and control of moisture content and dimensional changes. In: Wood handbook (Wood as an Engineering Material). Department of Agriculture, Forest Service, Forest Products Laboratory, Madison
- Sonderegger W, Martienssen A, Nitsche C, Ozyhar T, Kaliske M, Niemz P (2013) Investigations on the physical and mechanical behavior of sycamore maple (*Acer pseudoplatanus* L.). Eur J Wood Prod 71:91–99
- Tomad S, Matan N, Diawanich P, Kyokong B (2012) Internal stress measurement during drying of rubberwood lumber: effects of wet-bulb temperature in various drying strategies. Holzforschung 66:645–654
- Walton HW (2002) Deflection methods to estimate residual stress. In: Totten G, Howes M, Inoue T (eds) Handbook of residual stress and deformation of steel. ASM International, Ohio, pp 89–98
- Welling J (ed) (1994) EDG-Recommendation on assessment of drying quality of timber. European drying group (EDG), Hamburg
- Wengert E (1992) Techniques for equalizing and conditioning lumber. Cooperative extension programs No. 65. Department of Forest and Wildlife Ecology, University of Wisconsin, Madison



#### CORRECTION



## Correction to: Comparison of techniques for quantification of internal stress within industrial kiln-dried timber

Sataporn Jantawee<sup>1</sup> · Satjapan Leelatanon<sup>1</sup> · Prawate Diawanich<sup>2</sup> · Sornthep Vannarat<sup>3</sup> · Nirundorn Matan<sup>1</sup>

Published online: 11 January 2018 © Springer-Verlag GmbH Germany, part of Springer Nature 2018

#### Correction to: Eur. J. Wood Prod. https://doi.org/10.1007/s00107-017-1243-2

Unfortunately, an unintentional mistake has been made during calculation of maximum gap distance  $G_{100}$  for the 100 mm wide timber in the presented article.

The G100 values of the 100 mm wide timber displayed in Fig. 5b, Fig. 5c, Fig. 6 and Fig. 13 were calculated using an incorrect equation  $G_{100} = G_{75} \times 1.78 \times 1.78$  where  $G_{75}$  is the maximum gap distance measured at 75 mm pin separation. Referring to the standard case-hardening test, the value of  $G_{100}$  is calculated according to  $G_{100} = G_{75} \times 1.78$ . The mistake has led to an inaccurate discussion that the  $G_{100}$  value is dependent on the width of the timber when being compared to the results obtained from the restoring force technique and the McMillen slice test.

The corrected results reveal that the  $G_{100}$  value is independent of the timber width and the proposed restoring force technique, the McMillen slice test and the standard case-hardening test are quantitatively consistent among each other. The changes do not affect final conclusions in the published article. However, some discussions related to the standard case-hardening test do contain errors that require corrections.

The original article can be found online at https://doi.org/10.1007/s00107-017-1243-2.

- Materials Science and Engineering, School of Engineering and Resources, Walailak University, Thasala district, Nakhon Si Thammarat 80160, Thailand
- Nakhon Si Thammarat Seaboard Industrial College, Pakpanang district, Nakhon Si Thammarat 80140, Thailand
- Internet Innovation Laboratory, National Electronics and Computer Technology Center, Pathumthani 12120, Thailand

#### Error 1: Fig. 5b and related discussions in Sect. 4.1

Errors in the published article:

Similar linear correlation is also observed when comparing the maximum gap distance according to the case-hardening test method against the magnitude of the released strain except that higher values of linear coefficients are observed in the wider timber (Fig. 5a, b). For the case-hardening test, Eq. (1) can be rearranged as  $\Delta \delta = \frac{4W^2}{d} E \sigma_{\rm m}$  given that the half-split length is equal to width of timber (l=W). Therefore, wider specimen gives higher value of  $\Delta \delta$ , bending of the half slice and therefore the maximum gap measured in the case-hardening test.

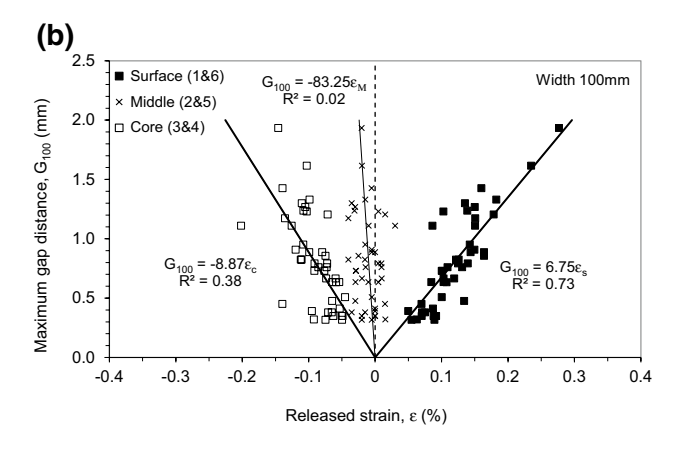


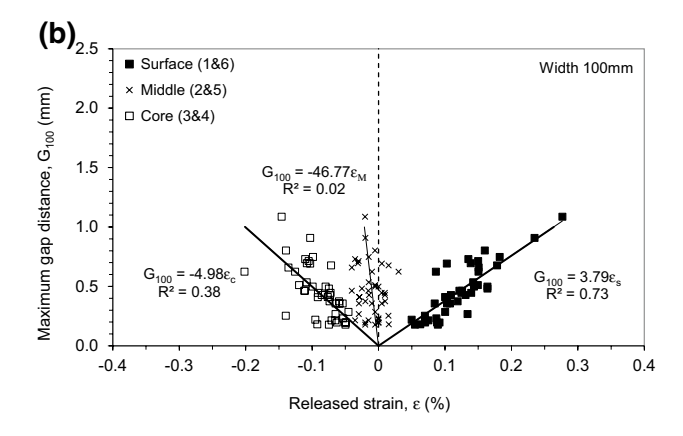
Figure 5b in the published article contains errors. The  $G_{100}$  values plotted in the vertical axis of all data were calculated using an incorrect equation  $G_{100} = G_{75} \times 1.78 \times 1.78$ .

#### Corrections:

Similar linear correlation is also observed when comparing the maximum gap distance according to the case-hardening test method against the magnitude of the released strain. The linear coefficients are independent of the timber width (Figs. 5a-b). For the case-hardening test, Eq. (1) can be rearranged as  $\Delta \delta = \frac{4W^2}{d} E \sigma_{\rm m}$  given that the



half-split length is equal to width of timber (l = W). Therefore, the value of  $\Delta \delta$ , bending of the half slice and therefore the maximum gap measured in the case-hardening test, varies with square of the timber width (Welling 1994).



The  $G_{100}$  values are corrected according to  $G_{100} = G_{75} \times 1.78$ .

#### Error 2: Fig. 5c and related discussions in Sect. 4.1

Errors in the published article:

It is clear that sensitivities, the slopes of the plots, of the restoring force technique (Fig. 4d) and the case-hardening test (Fig. 5c) decrease and increase with the timber width, respectively. At the same level of the differential released strain, the wider timber produces the lesser restoring force and the higher maximum gap distance.

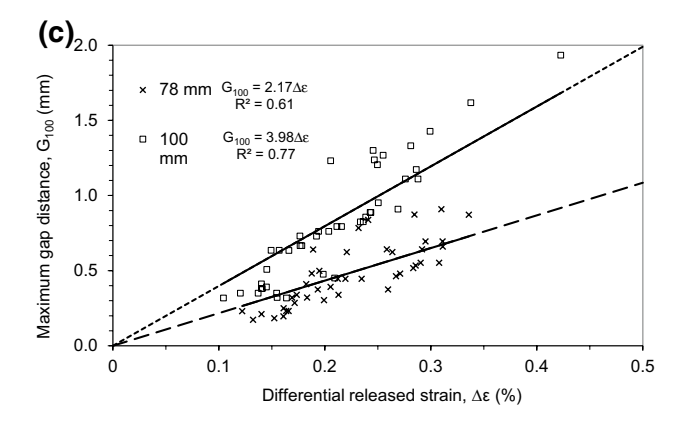
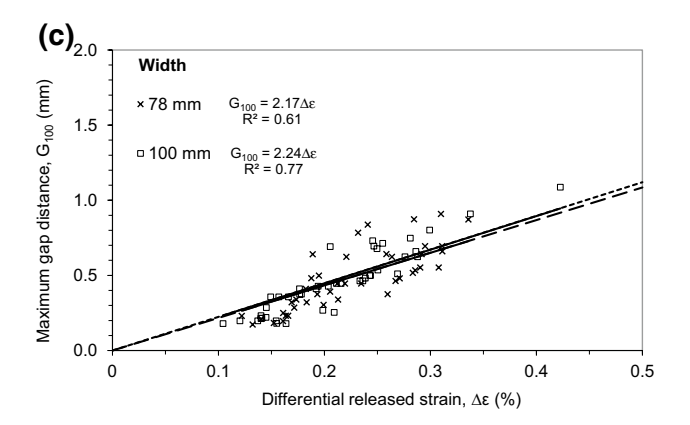


Figure 5c in the published article contains errors. The  $G_{100}$  values of the 100 mm wide timber (open square symbols) plotted in the vertical axis were calculated using an incorrect equation  $G_{100} = G_{75} \times 1.78 \times 1.78$ .

#### Corrections:

It is clear that sensitivities, the slopes of the plots, of the restoring force technique (Fig. 4d) decrease with the timber width while those of the case-hardening test (Fig. 5c) are unaffected. At the same level of the differential released strain, the wider timber produces the lesser restoring force but yields constant level of  $G_{100}$ .



The  $G_{100}$  values of the 100 mm wide timber (open square symbols) are corrected according to  $G_{100} = G_{75} \times 1.78$ .

Error 3: Fig. 6

Errors in the published article:

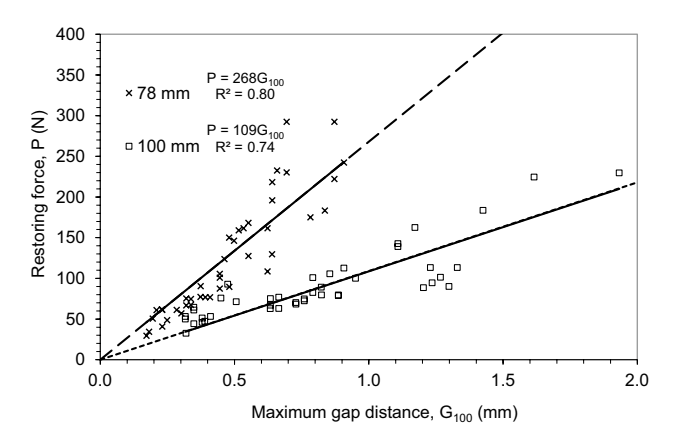
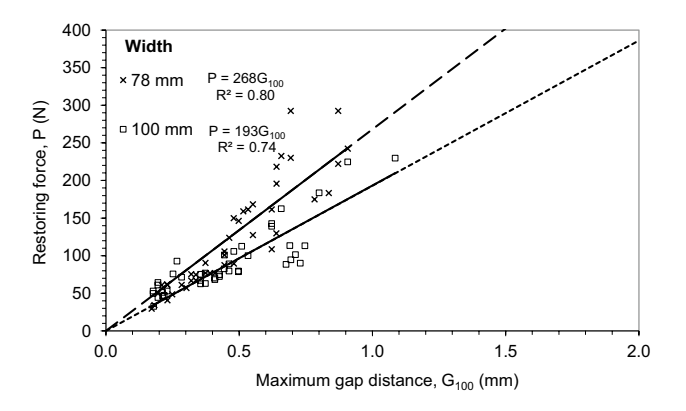


Figure 6 in the published article contains errors. The  $G_{100}$  values of the 100 mm wide timber (open square symbols) plotted in the horizontal axis were calculated using an incorrect equation  $G_{100} = G_{75} \times 1.78 \times 1.78$ .



#### Corrections:



The  $G_{100}$  values of the 100 mm wide timber (open square symbols) are corrected according to  $G_{100} = G_{75} \times 1.78$ .

#### Error 4: Fig. 13 and related discussion in Sect. 4.3

*Errors in the published article:* 

Figure 13 shows the calculated maximum internal stress plotted against the maximum gap distance values obtained from the case-hardening test. Although both values follow a linear relationship, the maximum gap distance value is dependent on the width of the timber meaning that different sizes of timber could yield different gap distance values even though they possess a similar level of internal stress. This behavior is also confirmed by a plot of the maximum gap distance against the differential released strain (Fig. 5c) in which linear constants obtained are dependent on the width of the timber.

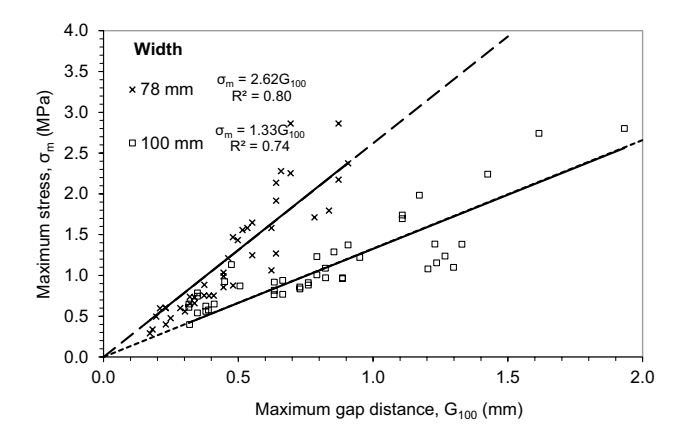
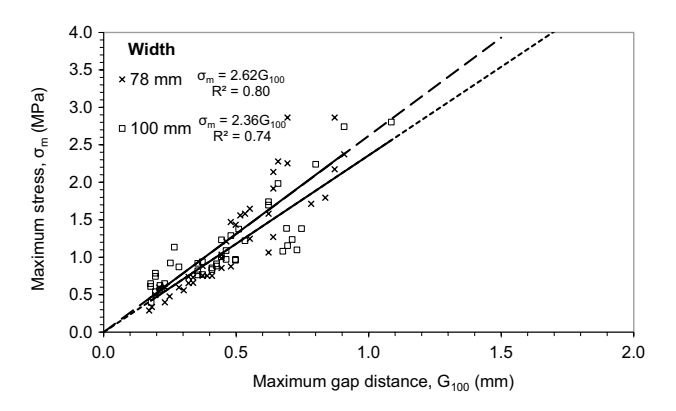


Figure 13 in the published article contains errors. The  $G_{100}$  values of the 100 mm wide timber (open square symbols) plotted in the horizontal axis were calculated using an incorrect equation  $G_{100} = G_{75} \times 1.78 \times 1.78$ .

#### Corrections:

Figure 13 shows the calculated maximum internal stress plotted against the maximum gap distance values obtained from the case-hardening test. Both values follow a linear relationship and the maximum gap distance value is independent of the width of the timber meaning that different sizes of timber yield similar gap distance values if they possess a similar level of the internal stress. This behavior is also confirmed by a plot of the maximum gap distance against the differential released strain (Fig. 5c) in which linear constants obtained are independent of the width of the timber.



The  $G_{100}$  values (open square symbols) of the 100 mm wide timber are corrected according to  $G_{100} = G_{75} \times 1.78$ .



## Appendix 3

Jaipet Tomad, Sataporn Jantawee, Wanchart Preechatiwong and
Nirundorn Matan (2018) "Within-tree variability of internal stress generated
during drying of rubberwood lumber"

European Journal of Wood and Wood Products, 76(1): 113-122.

(IF=1.082, Q1: Forestry, Q2: Materials science)

Eur. J. Wood Prod. DOI 10.1007/s00107-017-1204-9

**ORIGINAL** 



#### Within-tree variability of internal stress generated during drying of rubberwood lumber

Jaipet Tomad<sup>1</sup> · Sataporn Jantawee<sup>1</sup> · Wanchart Preechatiwong<sup>1</sup> · Nirundorn Matan<sup>1</sup>

Received: 28 June 2016

© Springer-Verlag Berlin Heidelberg 2017

**Abstract** The generation of drying stress within the lumber from the trunk of a rubber tree prepared from different locations (radial distance up to 110 mm and height up to 4 m) has been investigated in real-time by using a restoring force measurement on half-split specimens. Drying was performed at constant dry-bulb and wet-bulb temperatures of 90 and 60 °C, respectively. The entire restoring force profiles do not vary significantly with height. In addition, before and after the reversal of stress, the force profiles are largely similar and the maximum negative and positive forces are approximately equal regardless of wood locations within the tree trunk. However in the radial direction, the process of stress reversal consisting of two negative force maxima appears to proceed slower in the inner juvenile wood than in the outer mature wood. Upon water immersion of the specimens for 4 months, the second negative force maximum gradually disappears and the force profiles with a shorter stress reversal period become less sensitive to the wood locations. An examination of the drying curves in the second stage of drying during stress reversal also indicates a slower migration of bound water out of the lumber in the juvenile wood compared to that in the mature wood. The drying is also faster in the water-immersed specimens. It is concluded that variability of the internal stress within the trunk of a rubber tree originated from the role of cell wall amorphous constituents and cell wall extractives on creep property and the movement of bound water within the wood cell wall during drying.

Published online: 23 May 2017

#### 1 Introduction

Since several pieces of lumber are commonly dried together inside a batch kiln, natural variability in wood properties must therefore be accounted for in the design of drying procedures (Langrish and Walker 2006). Variation in the properties among pieces and even within each piece of lumber causes variability in drying rate and sensitivity to drying defects (Perré and Martin 1994). While the former has been extensively investigated both theoretically and experimentally (Perré and Turner 1999, 2007; Tremblay et al. 2000), the latter has been largely examined through a variety of mathematical models in which a number of parameters required were determined by experiments (Pang 2000; Perré and Passard 2004; Moutee et al. 2007, 2010). At the beginning of drying, the internal stress is initially generated within a piece of wood as a result of differential shrinkage between the surface and the core sections. The tensile and compressive stresses are developed at the outer and inner layers, respectively. As drying continues, the internal stress then reverses as a result of viscoelastic and mechano-sorptive creep (Perré and Passard 2007; Moutee et al. 2007). Defects such as surface and internal checks and splits could take place when the internal tensile stress exceeds the wood's strength at any moment during drying. Generation of drying stress and its potential for causing defects have been extensively studied both in lumber (Ormarsson et al. 1998, 1999, 2000) and wood discs (Kang and Lee 2002; Larsen and Ormarsson 2013).

Although an interrupted assessment of internal stress is possible by using standard techniques such as the McMillen slice test (McMillen 1958) and the case-hardening test (CEN/TS 2010), note that information, especially during any rapid changes in the magnitude of stress, could be lost. Diawanich et al. (2010) introduced a real-time internal



Mirundorn Matan mnirundo@wu.ac.th

Materials Science and Engineering, School of Engineering and Resources, Walailak University, 222, Thaiburi, Thasala District, Nakhon Si Thammarat 80160, Thailand

stress assessment by measuring the restoring force required to restrain a half-split specimen. This force was proven to be proportional to the differential of the released strain between the lumber's surface and core layers according to the McMillen slice test (Diawanich et al. 2012; Tomad et al. 2012). This technique has been used to study the effects of wet-bulb temperature patterns on the evolution of internal stress within lumber during drying (Tomad et al. 2012). By using a real-time assessment of internal stress, it is possible to pinpoint the moment when internal stress is the highest and when the defects are likely to occur during drying.

Rubber trees, widely grown in Southeast Asia for the production of latex, are used in this study. The trees are usually cut down after 25-30 years for replanting when their production of latex is uneconomical (Balsiger et al. 2000). Rubberwood logs, the byproduct of felled rubber trees, are usually transferred to local sawmills around the area. The production of rubberwood lumber consists mainly of log sawing, chemical impregnation and kiln drying of the sawn lumber (Hong 1995; Teoh et al. 2011). Attempts to accelerate drying of rubberwood lumber by increasing temperature and lower humidity inside the drying kiln have been studied (Theppaya and Prasertsan 2004; Srivaro et al. 2008). Lumber quality is normally examined at the end of drying (Ratnasingam et al. 2010). To cope with variability in wood properties, kiln operators tend to employ conservative drying schedules which could unnecessarily prolong the drying time. Since trees have orthogonal symmetry as a result, wood properties (such as specific gravity plus physical and mechanical ones) vary with the radius from the pith as well as height (Haygreen and Bowyer 1989; Ferreira et al. 2011).

The objective of this research is to examine the evolution of internal stress within the lumber prepared from different locations of the rubber tree trunks during drying. A real-time assessment of the internal stress is performed by using a restoring force technique on a half-split specimen (Diawanich et al. 2010; Tomad et al. 2012). An attempt is also made to understand the underlying mechanisms responsible for variability in the stress profiles observed.

#### 2 Materials and methods

#### 2.1 Rubber trees and preparation of test specimens

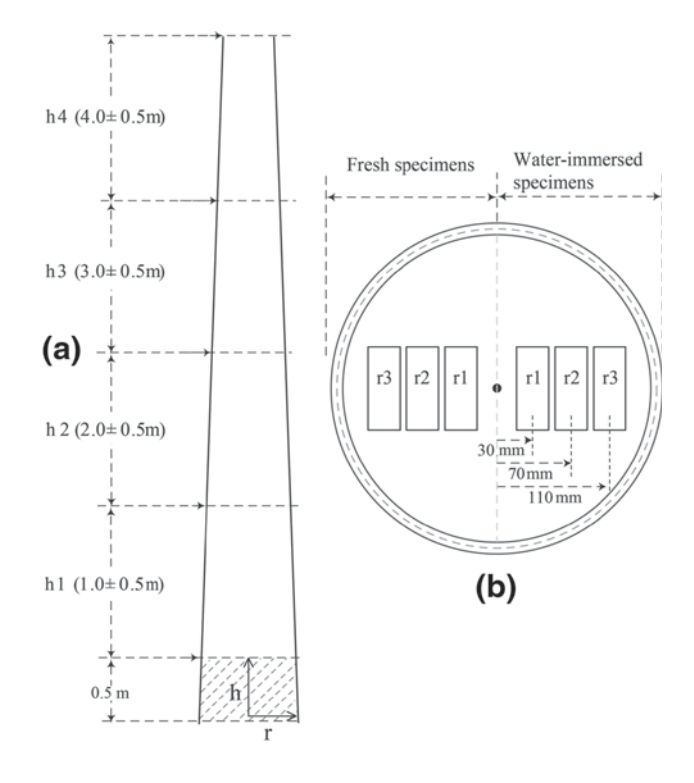
Two adjacent rubber trees roughly 25 years old from a plantation in the Thasala district of the Nakhon Si Thammarat province in Thailand were used in this work. The trees were sawn into 150–170 mm thick discs. Each disc was cut in half into two sections. One section was put in a plastic bag and kept in ambient air and the other was immersed in water for up to 6 months. Prior to testing, the half discs

were impregnated with water in a pressure vessel at 12 bar for 60 min to attain the saturated moisture content with the full-cell process. A vacuum of -0.8 bar was performed for 15 min both before and after the pressurization.

Specimens for internal stress measurement were prepared from the half discs at different locations within the trunk. Orthogonal coordinates (i.e. distance from pith, r, and height from ground level, h) were employed to specify each specimen's location within the tree trunk. Specimens were divided into four coordinate groups along the height, i.e.  $h_1$  at  $1.0\pm0.5$  m,  $h_2$  at  $2.0\pm0.5$  m,  $h_3$  at  $3.0\pm0.5$  m and  $h_4$  at  $4.0\pm0.5$  m (Fig. 1a) and into three coordinate groups along the radial direction (i.e.  $r_1$  at  $30\pm15$  mm,  $r_2$  at  $70\pm15$  mm and  $r_3$  at  $110\pm15$  mm) from the pith (Fig. 1b).

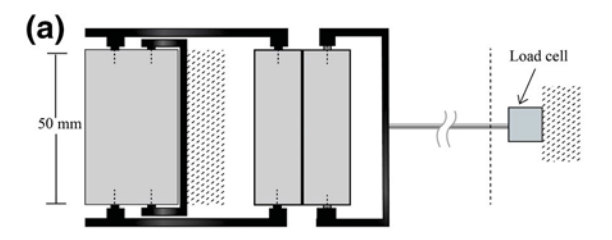
#### 2.2 Internal stress measurement

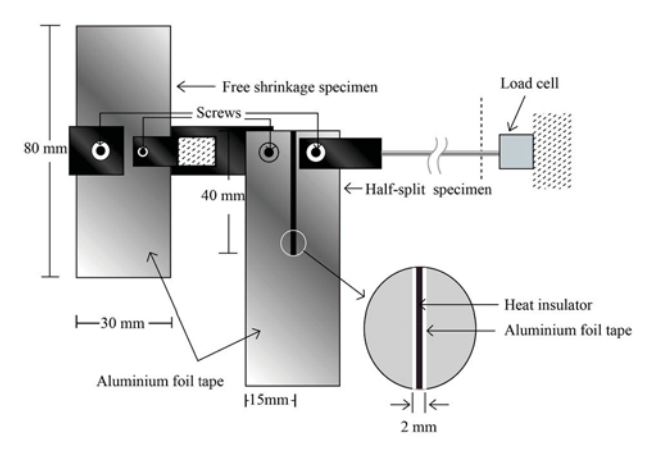
Evolution of the internal stress within the rubberwood specimens during drying was monitored using the force measurement technique proposed and verified with the McMillen slice test by Diawanich et al. (2010) and Tomad et al. (2012). The restoring force required to restrain a so-called "half-split" specimen (Fig. 2a) during drying was measured via a load cell (Cooper instruments, USA). The specimen of dimensions 30 mm (thickness



**Fig. 1** Schematic diagram illustrating locations of specimens within the rubber tree trunk divided into **a** four coordinate groups along the height  $(h_1, h_2, h_3 \text{ and } h_4)$  and **b** three coordinate groups along the radial direction  $(r_1, r_2 \text{ and } r_3)$ 







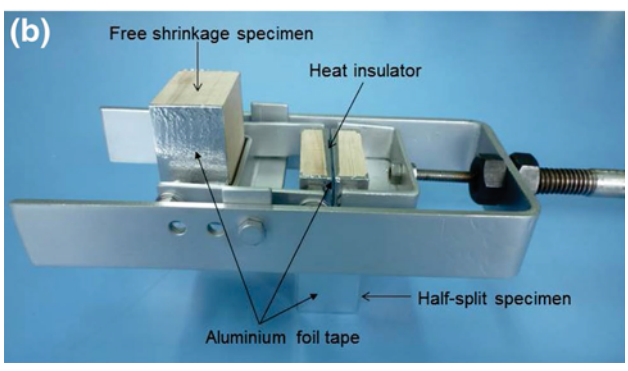


**Fig. 2** a Schematic diagram illustrating details of the restoring force measuring device equipped with the half-split and the free shrinkage specimens and **b** photograph of the device

in radial direction)×80 mm (width in tangential direction)×50 mm (length in longitudinal direction) was sawn in the tangential direction by a half width (40 mm) to divide the thickness in half (15 mm). The saw line was 2 mm wide. Longitudinal surfaces and the half-sawn faces were sealed with thin aluminium tape to prevent moisture loss before inserting a thin piece of heat insulation into the saw line to prevent direct heat transfer into the core of the specimen. Force generated as a result of the half-split specimen's shrinkage was compensated for by adding a "free shrinkage" specimen of the same dimensions (Diawanich et al. 2010). The restoring force measuring device equipped on both the half-split and the free shrinkage specimens is shown in Fig. 2b.

#### 2.3 Drying procedure

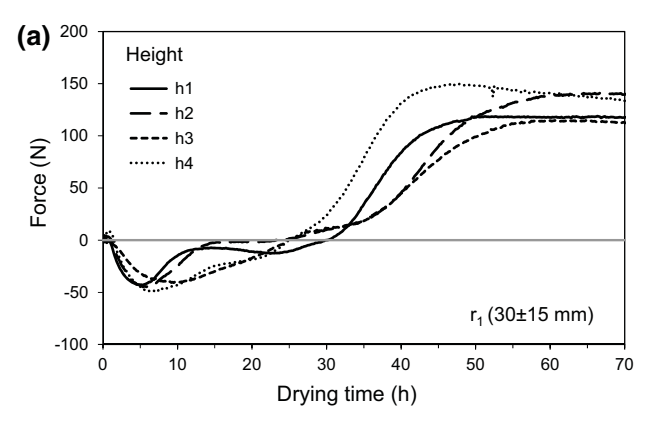
Drying was carried out in a 15 m<sup>3</sup> drying kiln (Eurasia, Singapore). A stack of lumber, separated by two 30 mm fillets, was placed inside the kiln. For each run, a restoring force measuring device was placed within the lumber stack. Only airflow through the lumber stack was allowed. Fan speed was adjusted to achieve an air velocity through the lumber stack of 4 m/s. The drying schedule was executed via the control system (LabView, National Instruments, USA). A single step drying schedule at the dry-bulb temperature of 90 °C and the wet-bulb temperature of 60 °C (Haslett 1998; Srivaro et al. 2008) for 70 h was performed for all drying tests. Steam used to provide heat and humid air within the kiln was generated by an electric boiler (Sahathai Factory, Thailand). Steam pressure at the boiler was maintained at 5 bar. For determination of the drying curves in some specific treatments, two pieces of lumber (30 mm in the radial direction × 80 mm in the tangential direction × 120 mm in the longitudinal direction) were placed inside the lumber stack and periodically weighed for the calculation of moisture content.

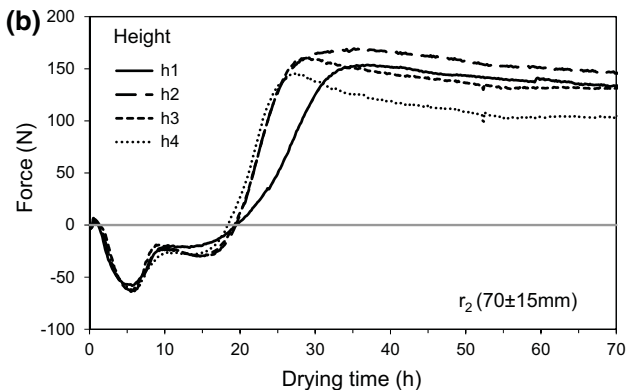
#### 3 Results and discussion

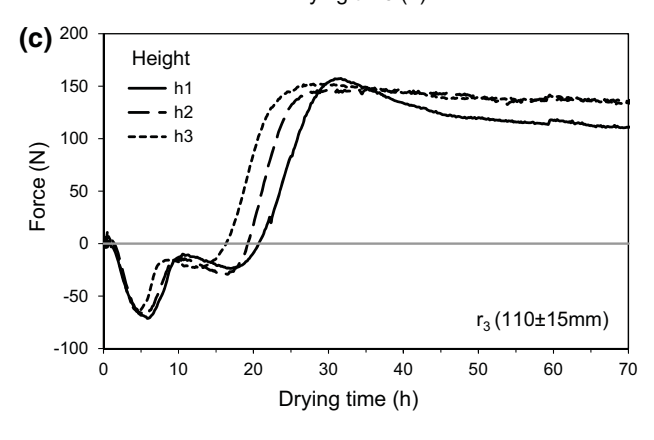
#### 3.1 Drying of the fresh specimens

In general, the behavior of all measured restoring force profiles (Fig. 3a-c) is consistent with the mechanisms underlying drying stress generation previously described by various authors (McMillen 1958; Simpson 1991; Perré and Passard 2007). At the beginning of drying, the measured restoring force remains at zero for a very short period of time of about 1 h. At this stage, only free water evaporates out of wood and the moisture content of the whole lumber is still higher than the fiber saturation point (FSP) and therefore no internal stress is generated. As drying continues, the outer layer dries to below the FSP, while the inner layer is still above the FSP. Both the tensile and compressive stresses are induced at the outer and inner layers, respectively. The internal stresses are generated as a result of an elastic response to the incompatible shrinkage strains. Since the specimen is split at a half thickness, a net resulting stress across the inner through the outer layers produces a force trying to bend the half-split specimen outward. A device is designed to keep the specimen at its original configuration. As a result, a negative force is observed at the load cell. While drying continues, the surface and core layers are dried under tensile and compressive stresses, respectively. The internal stress at the surface and in the core layers is reversed from tensile to compressive and then from compressive to tensile, respectively, as



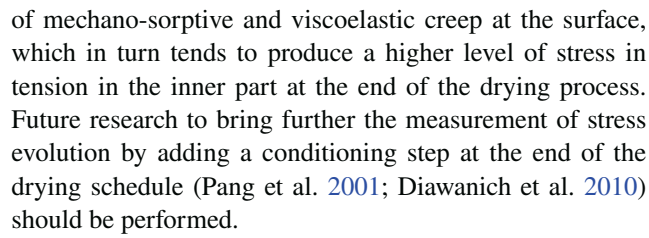






**Fig. 3** The restoring force profiles of the specimens prepared from rubber tree trunks at distances of **a**  $r_1$  (30±15 mm), **b**  $r_2$  (70±15 mm) and **c**  $r_3$  (110±15 mm) from the pith at various heights  $h_1$  (1.0±0.5 m),  $h_2$  (2.0±0.5 m),  $h_3$  (3.0±0.5 m) and  $h_4$  (4.0±0.5 m) during the drying at dry-bulb and wet-bulb temperatures of 90 and 60 °C, respectively

a result of viscoelastic and mechano-sorptive creep (Perré and Passard 2007; Moutee et al. 2007). During this stage, the negative force measured at the load cell decreases and changes its sign to a positive one. After reaching a maximum positive value, the force slightly continues to decline until the end of drying. The relatively higher level of stress in the second part of drying in the inner part of the wood is probably due to the fact that the high temperature and moisture content at the start of drying produced a high level

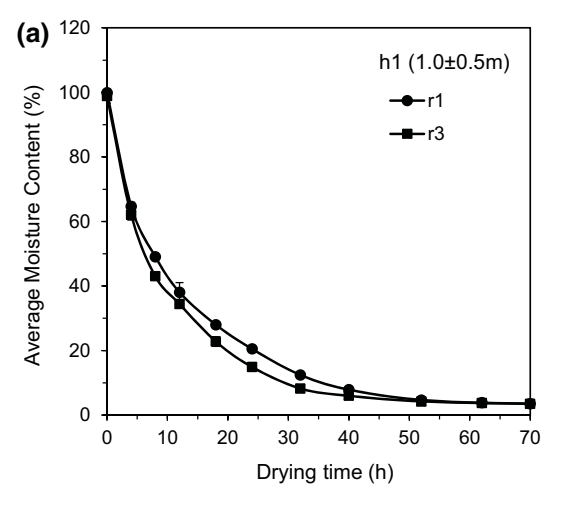


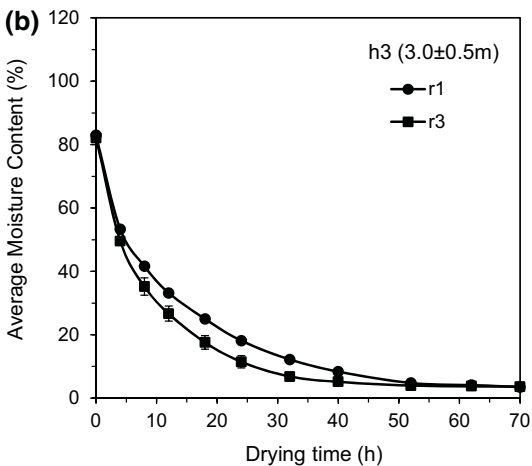
The restoring forces appear to be largely unrelated to the height of the rubber trees. At the same distance from the pith, the restoring force profiles of the specimens prepared from different heights approximately evolve with time in a similar manner (Fig. 3a-c). On the other hand, the force profiles clearly change with a radial distance from the pith as longer drying time was required for the completion of stress reversal in the r<sub>1</sub> specimens near the pith compared to those of the r<sub>2</sub> and r<sub>3</sub> specimens further away. Although the reversal of stress for all specimens started after 5 h of drying, its completion was from 40 to 50 h for the r<sub>1</sub> specimens (Fig. 3a) but was only from 25 to 30 h for the r<sub>2</sub> and r<sub>3</sub> specimens (Fig. 3b, c). According to Ferreira et al. (2011), a separation of the juvenile and mature wood zones in the rubber tree was determined by changes of the fiber length of about 40–55 mm from the pith. Therefore, the  $r_1$ specimens are in the juvenile wood zone while the r<sub>2</sub> and r<sub>3</sub> specimens are in the mature wood zone. Because several properties of the mature wood are roughly constant with the radial distance from the pith (Haygreen and Bowyer 1989), the internal stress profiles of the  $r_2$  and  $r_3$  specimens (Fig. 3b, c) are approximately similar.

Figure 4a, b show the average drying curves of the  $r_1$  and  $r_3$  specimens at two different heights,  $h_1$  and  $h_3$ . All specimens were impregnated with water to attain saturation prior to testing. It is evident that the saturated moisture contents of the  $r_1$  and  $r_3$  specimens at a particular height are equal. But lower saturated moisture content was observed at higher heights. An examination of the specimens' specific gravity revealed higher values of specific gravity at greater heights which varied from  $0.62\pm0.05$  at  $h_1$  to  $0.69\pm0.02$  at  $h_3$  above ground. It is well known that the saturated moisture content in wood has an inverse relation to specific gravity (Skaar 1972; Glass and Zelinka 2010). Therefore, the increase in specific gravity should be responsible for the lower saturated moisture content observed in the  $h_3$  specimens compared to  $h_1$ .

The drying curves, reflecting the rate of water evaporation out of the lumber, also reveal some underlying mechanisms of the observed restoring force profiles. For up to 5 h at the beginning of drying, the  $r_1$  and  $r_3$  specimens at the same heights possess similar linear drying rates (equal slopes in Fig. 4a, b). Variation within trees should have little influence on the movement of moisture, in both free and bound water, on lumber at this early stage of drying. As a result the restoring force profiles for all tests within







**Fig. 4** Drying curves of the specimens prepared from rubber tree trunks at distances of  $r_1$  (30±15 mm) and  $r_3$  (110±15 mm) from the pith at heights of **a**  $h_1$  (1.0±0.5 m) and **b**  $h_3$  (3.0±0.5 m) above ground

this period (Fig. 3a-c) are rather similar. Internal stress generated during this drying period, with the drying of the outer layer below the FSP and the inner layer above the FSP, is thereupon largely unaffected by the variation within tree. The r<sub>3</sub> specimens then started to dry faster than the r<sub>1</sub> specimens and reached the equilibrium moisture content (EMC) at  $3.5 \pm 0.1\%$  after about 30–40 h of drying. In comparison, it took up to about 50 h for the r<sub>1</sub> specimens to reach that level of EMC. At this later stage of drying, variation within the trees appears to play a significant role in the drying of lumber especially the movement of bound water within the wood cell wall (Perré and Turner 2007). Thus, the slower drying rate in the  $r_1$  specimens compared to that of the r<sub>3</sub> specimens (Fig. 4a, b) must be responsible for the longer stress reversal period observed in these specimens (Fig. 3a-c). The internal stress profiles of the  $r_1$  and r<sub>3</sub> specimens hardly changed after the specimens reached the EMC.

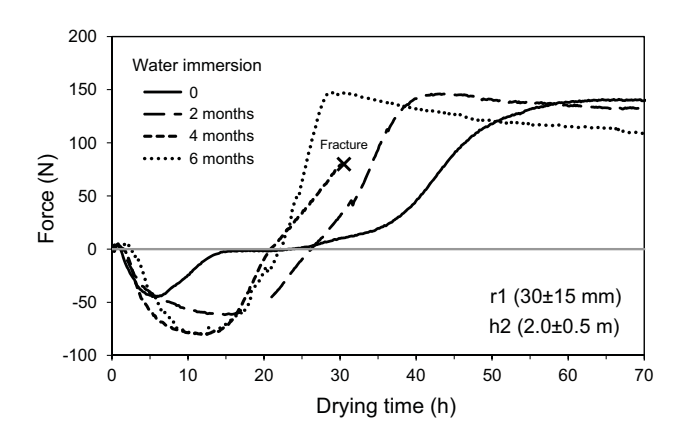
It should be noted that the restoring force profiles always contain two negative force maxima during the stress reversal. The first global maximum of negative force in all specimens was observed at drying times of 5-6 h. There was a slight increase of the magnitude of the maximum negative force from  $-45 \pm 4$  N of the juvenile  $r_1$  specimens near the pith to  $-62 \pm 4$  N of the mature  $r_2$  and  $r_3$  specimens further from the pith (Fig. 3a-c). The second local maximum of the negative force at  $-26 \pm 4$  N took place during  $15 \pm 2$  h of drying in the r<sub>2</sub> and r<sub>3</sub> specimens; this force was less obvious and occurred at a longer drying time of about 20-30 h in the r<sub>1</sub> specimens. After attaining the second local maximum, the force magnitude decreases and changes to a positive sign. The restoring force of all specimens increases and reaches the maximum positive force of  $148 \pm 15$  N before slightly declining until the end of drying. Because the maximum negative force (indicating the risk of surface checking) and the maximum positive force (indicating the risk of internal checking) are roughly insensitive to wood locations within the trunk, it is therefore suggested that there is no need for a rubberwood lumber classification for drying in the lumber industry.

It is well known that viscoelastic and mechano-sorptive creep causes stress reversal in lumber during drying (Perré and Passard 2007; Moutee et al. 2007). The maxima of two negative forces during stress reversal indicate that at least two distinct sources of creep should be operative. Main cell wall amorphous constituents such as hemicelluloses, lignin and non-crystalline cellulose (Haygreen and Bowyer 1989) exhibit viscoelastic and mechano-sorptive creep behaviors when exposed to high temperature under the constant and cyclic conditions of humidity, respectively (Glasser et al. 1998). In contrast, extractive substances within the cell wall have been reported to retard creep deformation (Ajuong and Breese 1997). An attempt is made in the following section to deconvolute the influences of main amorphous constituents and extractives within cell walls on the generation of internal stress.

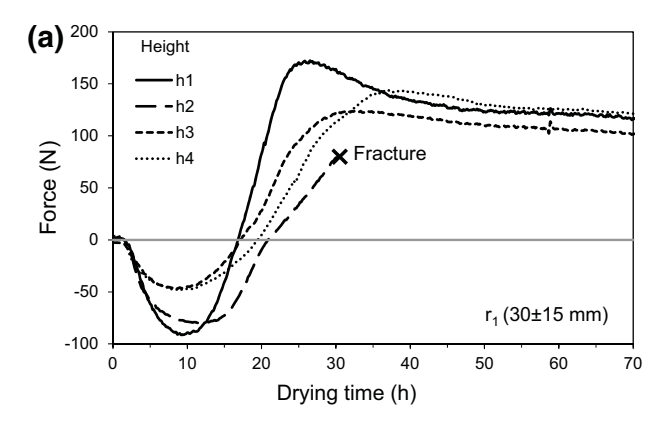
#### 3.2 Drying of the water-immersed specimens

Figure 5 shows the restoring force profiles of the r<sub>1</sub> specimens that were immersed in water for up to 6 months. It is obvious that the longer the immersion time, the quicker the stress reversal and the gradual disappearance of the second maximum negative force. After 4 months of water immersion, the second maximum negative force completely disappeared and water immersion hardly affects the internal stress profile. The internal stress profiles of the specimens immersed in water for 4 and 6 months are rather similar. Higher magnitudes of the maximum negative force took place at longer drying times of around 10–15 h. In addition, specimens prepared from all locations within the tree trunk





**Fig. 5** Restoring force profiles of the specimens immersed in water for up to 6 months prepared from rubber tree trunks at distance of  $r_1$  (30±15 mm) from the pith and at height of  $h_2$  (2.0±0.5 m) above ground



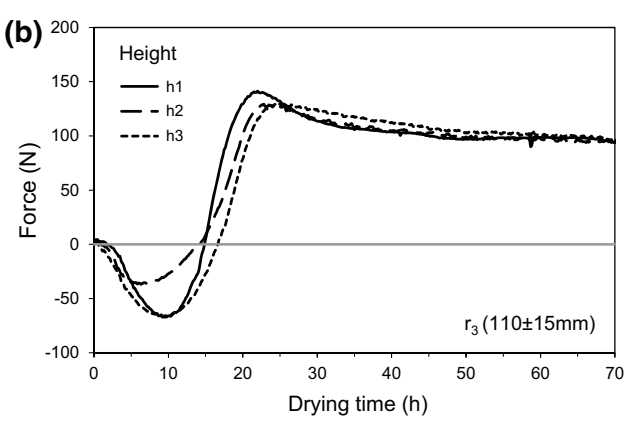
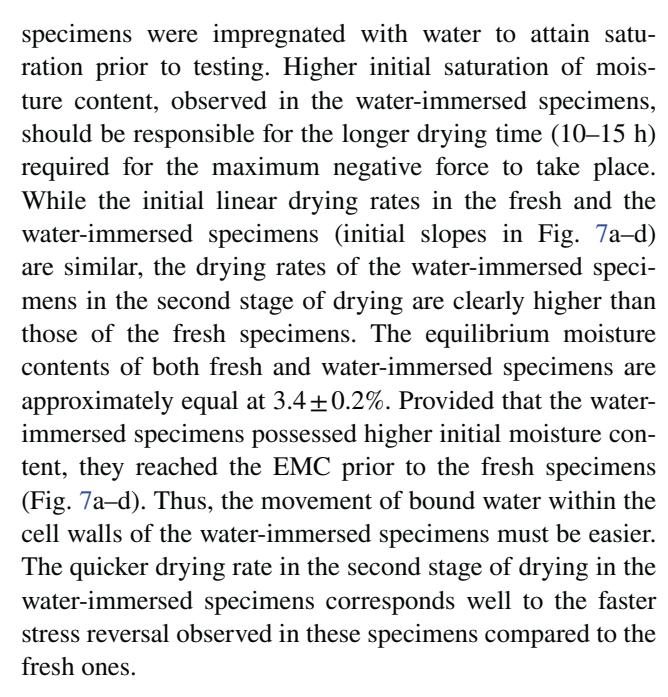


**Fig. 6** Restoring force profiles of the water immersed specimens prepared from rubber tree trunks at distances of **a**  $r_1$  (30±15 mm) and **b**  $r_3$  (110±15 mm) from the pith at various heights above ground

also exhibited comparable restoring force profiles with only a single negative maximum force after immersion in water for 4 months (Fig. 6a, b).

The drying curves of the specimens before and after 4 months of water immersion are shown in Fig. 7a-d. All



#### 3.3 Discussion on underlying mechanisms

The results from the experimentation raise various points which warrant further discussion and rationalization. The issues are taken in turn.

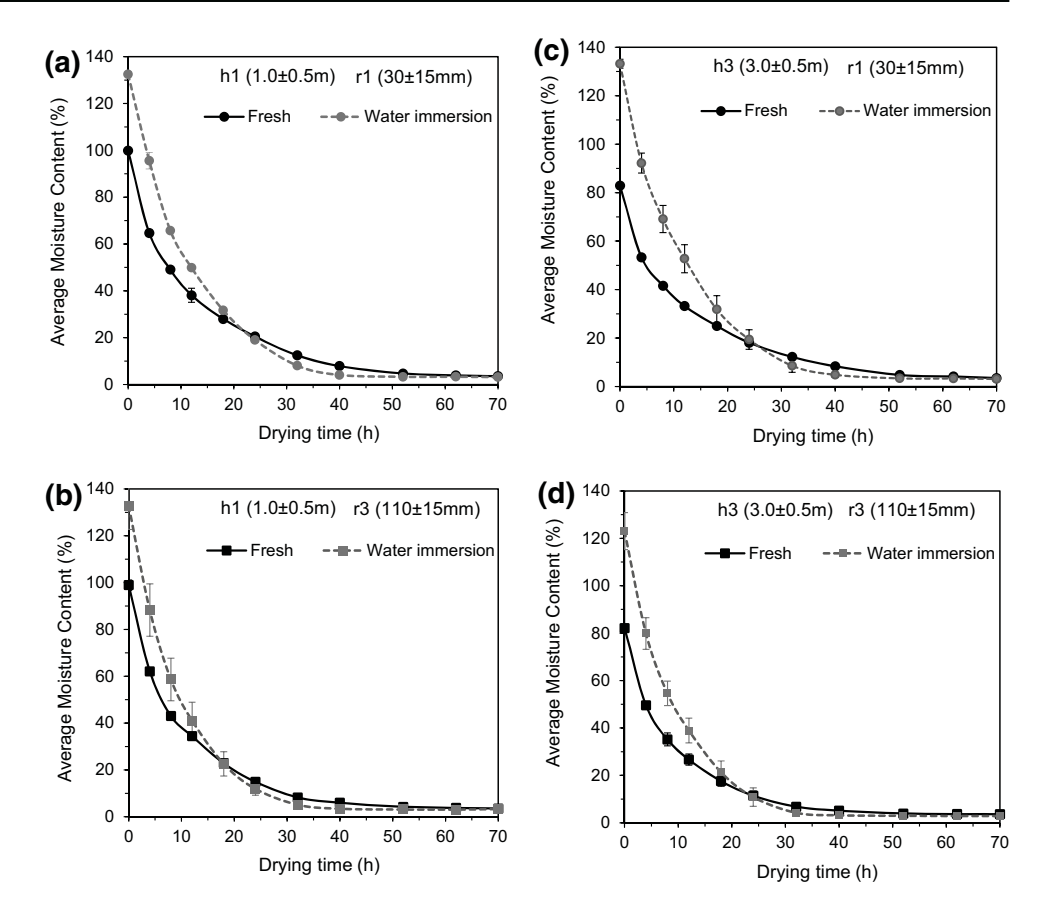
#### 3.3.1 Role of cell wall extractives

During water immersion, water-soluble extractives both within cell cavities and cell walls should be gradually depleted over time. The extractives of rubberwood are mainly hydrophilic compounds of free sugar, starch and amino acids (Simatupang et al. 1994). However, Ajuong and Breese (1997) reported that the lumen-located extractive fractions have no significant effect on short-term creep. In addition, a similar initial linear drying rate in the fresh and water-immersed specimens (Fig. 7a-d) also indicates the insignificant role of extractives in the cell cavities on the movement of free water out of the lumber. As a consequence, the shorter stress reversal time (Figs. 5, 6a, b) plus the increase in the drying rate during the second stage (Fig. 7a-d) should be related to the depletion of water-soluble extractive substances from the cell wall during water immersion. Without the presence of the extractives, the movement of bound water within the cell wall should be easier. In addition, bacterial attack during the water immersion could have contributed to the higher drying rate as compared to the fresh specimens (Kobayashi et al. 1998). This warrants further investigation and is a subject for future work.

The cell wall extractives have been reported to retard creep deformation. Acceleration of creep has been observed



Fig. 7 Comparison of the drying curves of the fresh and the water immersed specimens prepared from rubber tree trunks at heights of  $h_1$   $(1.0\pm0.5 \text{ m})$  above ground at distances of a  $r_1$   $(30\pm15 \text{ mm})$  and b  $r_3$   $(110\pm15 \text{ mm})$  from the pith and of  $h_3$   $(3.0\pm0.5 \text{ m})$  above ground at distances of c  $r_1$   $(30\pm15 \text{ mm})$  and d  $r_3$   $(110\pm15 \text{ mm})$  from the pith



with the gradual depletion of extractive substances from the cell wall and with the removal of water-soluble extractives, resulting in great creep deformation (Ajuong and Breese 1997). It was suggested that the water-soluble extractives, which are frequently contained in the side chain sugar residue, are chemically bonded through the side chain to lignin, hemicellulose and/or cellulose (Ajuong and Breese 1997). The cell wall extractives have also been reported to enhance modulus (Golpayegani et al. 2012), hardness (Tze et al. 2007), dimensional stability (Kuo and Arganbright 1980) and softening temperature (Song et al. 2014) of the wood cell wall.

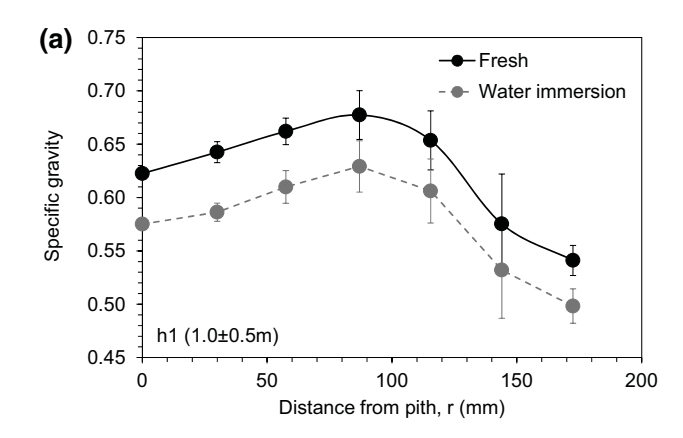
Higher saturation of moisture content was also observed in the water-immersed specimens (Fig. 7a–d). Grigsby et al. (2013) reported that the majority of bound water was distributed in pore networks having pore sizes of less than 50 nm within the wood cell wall. Extractives have been suggested to deposit in the matrix and pore of the wood cell wall (Song et al. 2014; Yin et al. 2015). It is expected that during water immersion, water-soluble extractives are dissolved away and are replaced by water molecules. In addition, Mantanis et al. (1994) found an increase in maximum swelling of wood in water after the removal of extractives.

The values of specific gravity in the water saturated moisture content of rubberwood specimens, both fresh and

water-immersed, are shown in Fig. 8a, b. Specific gravity slightly increases with height. At the bottom section of h<sub>1</sub>, specific gravity first increases in the radial direction up to ~100 mm from the pith before decreasing to the outside bark. The values of specific gravity are roughly constant at the top of section h<sub>4</sub>. Since the restoring force profiles are relatively insensitive to height (Fig. 3a-c), variation in specific gravity within tree trunk  $(0.62 \pm 0.05 - 0.69 \pm 0.03)$ should therefore have little influence on the internal stress generated during drying. Furthermore, an approximately equal reduction of  $8.4 \pm 0.9\%$  in specific gravity after water immersion is observed at all examined locations within the tree trunk. An apparent reduction in specific gravity observed in the water-immersed specimens should roughly reflect the total loss of water-soluble extractives both within cell cavities and cell walls during water immersion. Severo et al. (2013) also reported an equal content of total extractives at 7.7% found in both the juvenile and the mature sections of rubber tree trunks.

The fact that stress reversal took place for a longer time in the  $r_1$  specimens near the pith compared to those of the  $r_2$  and  $r_3$  specimens further away suggests that the water-soluble extractives within the cell walls should be higher in the inner juvenile  $r_1$  specimens. During the sapwood–heart-wood transition, more extractives are deposited in the wood





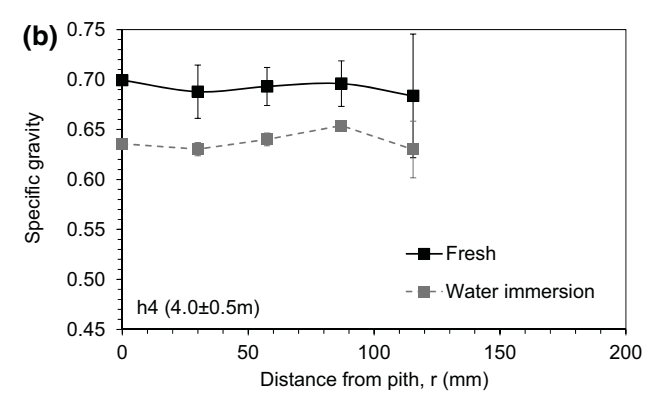
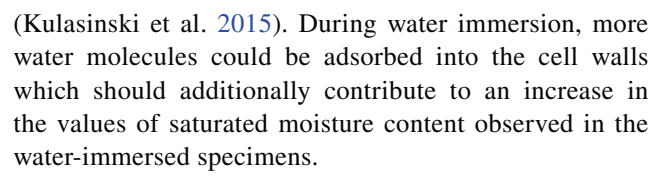


**Fig. 8** Radial variation of specific gravity measured at dried condition of the fresh and the water immersed specimens prepared from rubber tree trunks at heights of **a**  $h_1$  (1.0±0.5 m) and **b**  $h_4$  (4.0±0.5 m) above ground

cell walls while the composition of the main components of cell walls remains almost unaltered (Song et al. 2014). The extractives have been suggested to be deposited in the mesopores of heartwood cell walls (Yin et al. 2015). An examination of the types and amounts of extractives within cell walls is a subject for future work.

#### 3.3.2 Role of main amorphous cell wall constituents

The first negative maximum, which was still observed after immersion of the specimens in water, should be associated with the creep behavior of the main cell wall amorphous constituents. Apart from being adsorbed in the amorphous hemicellulose, a large fraction of water molecules has been suggested to be adsorbed at the interface between the crystalline cellulose and amorphous hemicellulose within the cell wall. Water molecules adsorbed on the interface push away polymer chains, forcing the two phases to separate and cause breaking of hydrogen bonds. At high moisture content, water is adsorbed preferentially at the interface; this leads to additional swelling and porosity increase at the interface



It is emphasized that detailed studies on the roles of cell wall extractives and cell wall amorphous constituents on the movement of bound water and creep properties which are underlying mechanisms of the generation of internal stress during drying should be explored in the future.

#### 4 Conclusion

The following conclusions can be drawn from this work:

- 1. The measured restoring force profiles, representing the internal drying stress within the lumber during drying, change along the radial direction of rubber tree trunk. A longer time of stress reversal has been observed in the inner juvenile wood zone compared to the outer mature wood zone. While having a similar drying rate at the early stage of drying, the juvenile wood specimens dried at a slower rate than the mature wood specimens in the second drying stage during the time of stress reversal.
- 2. During stress reversal, there appear to be two negative force maxima which attribute to the creep responses during drying of the main amorphous constituents and the extractives within the cell walls, respectively. The second negative maximum gradually disappeared upon water immersion of the specimens. In these specimens, faster stress reversal and higher drying rate in the second drying stage have been observed compared to the fresh specimens. The force profiles of the waterimmersed specimens seem to be insensitive to locations within the tree trunk.
- 3. The results from this work suggest that variability of the internal stress within the rubber tree trunk originates from the roles of cell wall extractives and cell wall amorphous constituents on the movement of bound water out of lumber and on the creep properties during drying which needs to be further explored in the future.

**Acknowledgements** One of the authors (JT) wishes to thank the Institute of Research and Development at Walailak University for a scholarship to study for an MSc degree. The authors gratefully acknowledge the financial support from the Commission on Higher Education (Grant No. NRPM 2557A30562006) as well as the Thailand Research Fund and Walailak University (Grant No. RSA5880025).



#### Compliance with ethical standards

**Conflict of interest** The authors declare that they have no conflict of interest.

#### References

- Ajuong EMA, Breese MC (1997) The role of extractives on short-term creep in compression parallel to the grain of Pai wood (*Afzelia Africana* Smith). Wood Fiber Sci 29(2):161–170
- Balsiger J, Bahdon J, Whiteman A (2000) The utilization, processing and demand for rubberwood as a source of wood supply. Forestry Policy and Planning Division, Rome
- CEN/TS (2010) Sawn timber-method for assessment of case-hardening. CEN standard ENV 14464. BSI Standards Publication, London
- Diawanich P, Matan N, Kyokong B (2010) Evolution of internal stress during drying, cooling and conditioning of rubberwood lumber. Eur J Wood Prod 68(1):1–12
- Diawanich P, Tomad S, Matan N, Kyokong B (2012) Novel assessment of casehardening in kiln-dried lumber. Wood Sci Technol 46:101–114
- Ferreira AL, Severo ETD, Calonego FW (2011) Determination of fiber length and juvenile and mature wood zones from *Hevea brasiliensis* trees grown in Brazil. Eur J Wood Prod 69:659–662
- Glass SV, Zelinka SL (2010) Moisture relations and physical properties of wood. In: Wood handbook—wood as an engineering material, general technical report, FPL-GTR-190. USDA Forest Service, Forest Products Laboratory, Madison, pp 4-1–4-19
- Glasser WG, Rials TG, Kelley SS, Dave V (1998) Studies of the molecular interaction between cellulose and lignin as a model for the hierarchical structure of wood. In: Heinze TJ, Glasser WG (eds) Cellulose derivatives modification, characterization, and nanostructures. American Chemical Society, Washington, pp 265–282
- Golpayegani AS, Brémaud I, Gril J, Thevenon MF, Arnould O, Pourtahmasi K (2012) Effect of extractions on dynamic mechanical properties of white mulberry (*Morus alba*). J Wood Sci 58:153–162
- Grigsby WJ, Kroese H, Dunningham EA (2013) Characterisation of pore size distributions in variously dried *Pinus radiata*: analysis by thermoporosimetry. Wood Sci Technol 47:737–747
- Haslett, AN (1998) Drying radiata pine in New Zealand. New Zealand Forest Research Institute Limited, Rotorua
- Haygreen JG, Bowyer JL (1989) Forest products and wood science. Iowa State University Press, Ames
- Hong LT (1995) Rubberwood utilization: a success story. In: Paper presented at the XX International Union of Forestry Research Organizations (IUFRO) World Congress, Tampere
- Kang W, Lee N-H (2002) Mathematical modeling to predict drying deformation and stress due to differential shrinkage within a tree disk. Wood Sci Technol 36:463–476
- Kobayashi Y, Iida I, Imamura Y, Watanabe U (1998) Drying and anatomical characteristics of sugi wood attacked by bacteria during pond storage. J Wood Sci 44:432–437
- Kulasinski K, Guyer R, Derome D, Carmeliet J (2015) Water adsorption in wood microfibril-hemicellulose system: role of the crystalline–amorphous interface. Biomacromolecules 16:2972–2978
- Kuo ML, Arganbright DC (1980) Cellular distribution of extractives in redwood and incense cedar: Part 1. Radial variation in cell wall extractive content. Holzforschung 34(1):17–22

- Langrish T, Walker J (2006) Drying of timber. In: Walker J (ed) Primary wood processing: principles and practice. Springer, Berlin, pp 251–295
- Larsen F, Ormarsson S (2013) Numerical and experimental study of moisture-induced stress and strain field developments in timber logs. Wood Sci Technol 47:837–852
- Mantanis GI, Young RA, Rowell RM (1994) Swelling of wood Part 1. Swelling in water. Wood Sci Technol 28:119–134
- McMillen JM (1958) Stresses in wood during drying (report 1652).

  Department of Agriculture, Forest Service, Forest Products Laboratory, Madison
- Moutee M, Fortin Y, Fafard M (2007) A global rheological model of wood cantilever as applied to wood drying. Wood Sci Technol 41(3):209–234
- Moutee M, Fortin Y, Laghdir A, Fafard M (2010) Cantilever experimental setup for rheological parameter identification in relation to wood drying. Wood Sci Technol 44:31–49
- Ormarsson S, Dahlblom O, Petersson H (1998) A numerical study of the shape stability of sawn timber subjected to moisture variation Part 1: theory. Wood Sci Technol 32:325–334
- Ormarsson S, Dahlblom O, Petersson H (1999) A numerical study of the shape stability of sawn timber subjected to moisture variation Part 2: Simulation of drying board. Wood Sci Technol 33:407–423
- Ormarsson S, Dahlblom O, Petersson H (2000) A numerical study of the shape stability of sawn timber subjected to moisture Part 3: Influence of annual ring orientation. Wood Sci Technol 34(3):207–219
- Pang S (2000) Modelling of stress development during drying and relief during steaming in *Pinus radiata* lumber. Dry Technol 18(8):1677–1696
- Pang S, Simpson IG, Haslett AN (2001) Cooling and steam conditioning after high-temperature drying of *Pinus Radiata* board: experimental investigation mathematical modeling. Wood Sci Technol 35:487–502
- Perré P, Martin M (1994) Drying at high temperature of heartwood and sapwood: theory, experiment and practical consequence on kiln control. Dry Technol 12:1915–1941
- Perré P, Passard J (2004) A physical and mechanical model able to predict the stress field in wood over a wide range of drying conditions. Dry Technol 22:27–44
- Perré P, Passard J (2007) Stress development. In: Perré P (ed) Fundamentals of wood drying. European COST A.R.BO.LOR., Nancy, pp 243–271
- Perré P, Turner IW (1999) A 3-D version of TransPore: a comprehensive heat and mass transfer computational model for simulating the drying of porous media. Int J Heat Mass Tran 42:4501–4521
- Perré P, Turner IW (2007) Coupled heat and mass transfer. In: Perré P (ed) Fundamentals of wood drying. European COST A.R.BO.LOR., Nancy, pp 203–241
- Ratnasingam J, Grohmann R, Scholz F (2010) Drying quality of rubberwood: an industrial perspective. Eur J Wood Prod 68:115-116
- Severo ETD, Oliveira EF Jr, Sansı´golo CA, Rocha CD, Calonego FW (2013) Properties of juvenile and mature woods of *Hevea brasiliensis* untapped and with tapping panels. Eur J Wood Prod 71:815–818
- Simatupang MH, Schmitt U, Kasim A (1994) Wood extractives of rubberwood (*Hevea Brasiliensis*) and their influences on the setting of the inorganic binder in gypsum-bonded particleboards. J Trop For Sci 6(3):269–285
- Simpson WT (1991) Dry kiln operator's manual. Agric. handbook AH-188. US Department of Agriculture, Forest Service, Forest Products Laboratory, Madison
- Skaar C (1972) Water in wood. Syracuse University Press, New York



- Song K, Yin Y, Salmén L, Xiao F, Jiang X (2014) Changes in the properties of wood cell walls during the transformation from sapwood to heartwood. J Mater Sci 49:1734–1742
- Srivaro S, Wongprot T, Matan N, Kyokong B (2008) Accelerated conventional temperature drying of 30 mm thick rubberwood lumber. Songklanakarin J Sci Technol 30(4): 475–483
- Teoh YP, Don MM, Ujang S (2011) Assessment of the properties, utilization, and preservation of rubberwood (*Hevea brasiliensis*): a case study in Malaysia. J Wood Sci 57:255–266
- Theppaya T, Prasertsan S (2004) Optimization of rubber wood drying by response surface method and multiple contour plots. Dry Technol 7(7): 1637–1660
- Tomad S, Matan N, Diawanich P, Kyokong B (2012) Internal stress measurement during drying of rubberwood lumber: effects of

- wet-bulb temperature in various drying strategies. Holzforschung 66:645–654
- Tremblay C, Cloutier A, Fortin Y (2000) Experimental determination of the convective heat and mass transfer coefficients for wood drying. Wood Sci Technol 34:253–276
- Tze WTY, Wang S, Rials TG, Pharr GM, Kelley SS (2007) Nanoindentation of wood cell walls: continuous stiffness and hardness measurements. Compos Part A 38:945–953
- Yin J, Song K, Lu Y, Zhao G, Yin Y (2015) Comparison of changes in micropores and mesopores in the wood cell walls of sapwood and heartwood. Wood Sci Technol 49:987–1001



## Appendix 4

International conferences



### **Abstract Book**



# The 9th International Conference on Materials Science and Technology

December 14th\_15th, 2016

Swissôtel Le Concorde, Bangkok, Thailand

Organizers















Supporter

**Platinum Sponsor** 

**Gold Sponsor** 

**Bronze Sponsor** 









**Exhibitiors** 







www.mtec.or.th/msat-9











#### **ENV-O-12**

#### Effect of Cell Wall Constituents On Internal Stress Generation During Drying of Lumber Prepared From Rubber Tree Trunks

#### <u>Jaipet Tomad</u><sup>a,\*</sup>, Sataporn Jantawee<sup>a</sup>, Wanchart Preechatiwong<sup>a</sup>, Nirundorn Matan<sup>a</sup>

<sup>a</sup> Materials Science and Engineering, School of Engineering and Resources, Walailak University, Thasala district, Nakhon Si Thammarat 80160, Thailand \*E-mail: TJaipet@hotmail.com

Keywords: Internal Stress, Drying, Cell Wall Constituents, Rubberwood

The objective of this research is to study effect of extractives and amorphous cell wall constituents on the internal stress profile of lumber prepared from different locations (radius from pith and height from ground) of rubber tree trunks. All specimens prepared from two rubber trees were impregnated with water to attain saturated moisture content prior to testing. Assessment of the internal stress development within the lumber during the drying was monitored in real-time using a restoring force measurement on half-split specimens. The corresponding drying curve was at the same time monitored by periodically weighting two pieces of lumber placed inside the lumber stack in the drying kiln. Drying condition at dry-bulb and wet-bulb temperatures of 90°C and 60°C was used throughout this work. It was shown that the generated internal stress appear to be largely unrelated to the height of the rubber trees. Time required for stress reversal to take place was found to be shorter for the lumber prepared from outer with respect to inner sections of the trunk. However, minimum and maximum forces detected were relatively insensitive to locations of lumber within the trunk. There are two negative force maxima which could attribute to the creep responses during drying of the main amorphous constituents and the extractives within the cell walls, respectively. The second negative maximum gradually disappeared upon water immersion of the specimens. In these specimens, faster stress reversal and higher drying rate in the second drying stage have been observed with respect to the fresh specimens. The force profiles of the water-immersed specimens seem to be insensitive to locations within the tree trunk. The results suggest that the presence of cell wall extractives should retard creep deformation and slow down diffusion of bound water within the cell walls. On the other hand, a large fraction of water molecules suggested to be adsorbed at the interface between the crystalline cellulose and amorphous hemicellulose within the cell wall should accelerate creep deformation and speed up diffusion of the bound water. For a practical point of view, it is suggested that there is no need for rubberwood lumber classification for drying because the minimum force (indicating the risk of surface checking) and the maximum force (indicating the risk of internal checking) were observed to be insensitive to wood locations within the trunk.



#### **DMC-O-05**

## Design and Construction of a Restoring Force Measuring Apparatus for Assessment of Internal Stress Within Kiln-dried Lumber

## Sataporn Jantawee<sup>a,\*</sup>, Satjapan Leelatanon<sup>a</sup>, Prawate Diawanich<sup>b</sup>, Nirundorn Matan<sup>a</sup>

<sup>a</sup> Materials Science and Engineering, School of Engineering and Resources, Walailak University, Thasala district, Nakhon Si Thammarat 80160, Thailand <sup>b</sup> Nakhon Şi Thammarat Seaboard Industrial College, Pakpanang district, Nakhon Si Thammarat 80140, Thailand \*E-mail: sata\_porn@yahoo.com

Keywords: Residual stress, Kiln-dried lumber, Stress measurement, Apparatus

A new approach of a restoring force measurement technique on "half-split" specimens has been proposed to directly assess the level of internal stress within kiln-dried lumber. The equipment consists mainly of a relatively stiff steel frame, two clamping jigs and a load cell. One jig is fixed to the steel frame and another is attached to a steel rod connected to the load cell. While being clamped to the frame, the specimen is half-split at half the thickness for a required length. The restoring force can be then measured online both in a single sawing mode at a particular half-split length and a multiple sawing mode at various half-split lengths. Screw contact area of 24 mm<sup>2</sup> with

An optimal applied torque on each screw of 2-3 N·m is suitable to hold the specimen to the apparatus. Cracks could be developed in the specimen if the screw contact area is too small or the applied torque is too high. The magnitude of the restoring force is proportional to length of the specimen. For the 30 mm thick specimen, the measured restoring force at a particular half-split length is constant if the remaining unsplit length of the lumber is greater than 25 mm. The measured restoring force dramatically decreases below this value. Both distance and angular deviations of cutting away from the half-split line reduce the measured restoring force value. By keeping the distance deviation away from the half-split line to within 1 mm, an error resulting in a reduction in the measured restoring force is less than 5%. The proposed restoring force measuring apparatus together with a suitable set up of the half-split specimen is proved to provide a repeatable measurement of the restoring force of the kiln-dried lumber at various half-split lengths. Interpretation of the restoring force in term of internal stress will be performed in the future work.

#### ENV-I-05

#### Quality Drying of Lumber: From Laboratory to Industry

#### Nirundorn Matan

Materials Science and Engineering, School of Engineering and Resources, Walailak University, Thasala district, Nakhon Si Thammarat 80160, Thailand E-mail: mnirundo@wu.ac.th

Keywords: Lumber, Drying, Internal stress, Kiln controller

Without an online tool to control quality of lumber during drying, the kiln operator is forced to employ a conservative drying schedule which could unnecessarily prolong the drying time and consume more energy. An attempt to reduce the drying time and energy by simply accelerating the drying rate might easily lead to a formation of several defects. Such drying defects mainly arise as a result of the internal stress (IS) built up within the lumber during drying. A new restoring force (RF) technique capable of real-time monitoring IS behavior during drying is presented. Analytical and numerical models have been developed to directly relate the measured RF to the magnitude of IS. In parallel, a semi-automatic kiln control system, *Dry*WooD, has been developed for an effective control of drying in the lumber industry. The system, connected using wire-less links, consists of up to 10 kiln control units, a microcontroller and a control software package. The system has been successfully installed and routinely used in two rubberwood sawmills.

In this talk, the effect of several conventional drying strategies on the development of IS will be discussed and the possible application of the measured RF as a controlling parameter in the drying of rubberwood lumber will be demonstrated.



#### A real-time internal stress controlled drying of lumber

Session: 3-C Timber Drying: Basic and Applied R&D for Optimum Processing and Product Quality (RG 5.04)

#### Division 5 Research Group:

5.04 Wood Processing

#### Abstract:

A wood drying controlled system based on real-time internal stress information obtained from the restoring force (RF) measurement has been developed. The system is capable of controlling the RF magnitude at a set value during a first stage of drying before stress reversal. For a constant dry-bulb temperature drying of rubberwood lumber at 90°C, a schedule of wet-bulb temperature is automatically adjusted by the predetermined RF pattern. Vents are opened or closed if the RF magnitude is smaller or greater, respectively, than its set value and if necessary steam is introduced to increase humidity inside the drying kiln. After stress reversal, the lumber is dried under relatively severe drying condition at wet-bulb temperature of 40°C to accelerate the drying rate. It was observed that the maximum RF value in this second stage of drying strongly correlates with the average rate of RF developing to reach the set RF value during the first stage of drying. By controlling the maximum magnitude and the rate of RF prior to the stress reversal, both surface and internal checking, respectively, could be avoided and the lumber could be dried at the highest possible drying rate without causing these drying defects.

#### Keywords:

Kiln control, Internal stress, Restoring force, Wood Drying, Quality control

#### Authors:

Nirundorn Matan, *Walailak University*Choosak Rittiphet, *Walailak University*Jaipet Tomad, *Walailak University*Sataporn Jantawee, *Nakhon Si Thammarat Rajabhat University* 



Effect of pre-drying on development of internal stress within rubberwood lumber during drying

Session: 3-C Timber Drying: Basic and Applied R&D for Optimum Processing and Product Quality (RG 5.04)

#### Division 5 Research Group:

5.04 Wood Processing

#### Abstract:

A restoring force measurement on a half-split specimen has been performed to investigate the effect of predrying on internal stress development within the 30 mm thick rubberwood lumber during kiln drying. Pre-drying was performed in a controlled chamber at dry-bulb temperature of 30°C and 80% RH until the restoring force reached the negative maximum or the stress reversal (zero force) values. A single-step drying schedule at dry-bulb temperature of 90°C and 26% RH was then employed to dry the lumber. The results revealed that the maximum negative force generated during pre-drying at low temperature is lower than that generated during the drying of lumber at high temperature. Longer pre-drying periods appear to reduce both the maximum negative and the maximum positive forces generated before and after stress reversal, respectively during the drying at high temperature. Pre-drying of lumber therefore, apart from reducing the lumber moisture content, also reduces risks of both surface and internal checking during the kiln drying of lumber at high temperature.

#### Keywords:

Pre-drying, Internal stress, Restoring force, Rubberwood, Kiln-dried lumber

#### Authors:

Sataporn Jantawee, *Nakhon Si Thammarat Rajabhat University* Nirundorn Matan, *Walailak University* Jaipet Tomad, *Walailak University* 

## Appendix 5

Article for press release



## A New Assessment of Internal stress within Kiln-Dried Lumber Using a Restoring Force Technique on a Half-Split Specimen



Matan, N.1\*, Jantawee, S.1, Leelatanon, S.1, Diawanich, P.2, Vannarat, S.3

Materials Science and Engineering, School of Engineering and Resources, Walailak University, Thasala district, Nakhon Si Thammarat 80160, Thailand,
 Nakhon Si Thammarat Seaboard Industrial College, Pakpanang district, Nakhon Si Thammarat 80140, Thailand,
 Internet Innovation Laboratory, National Electronics and Computer Technology Center, Pathumthani 12120, Thailand

E-mail: mnirundo@wu.ac.th

#### 1. Introduction

**Problems:** The drying process always creates internal stress within lumber that continues to exist, even after the lumber is dried. Due to difficulties in determining modulus of elasticity (MOE) of wood, only strain or deflection profiles caused by relaxation of internal stress are normally evaluated for industrial kiln-dried lumber.

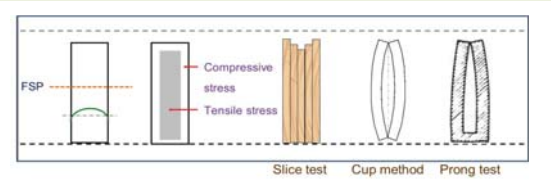
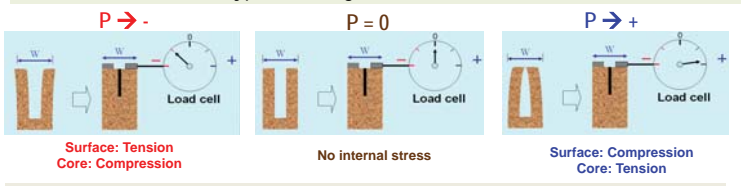


Fig.1 Moisture and internal stress profiles within kiln-dried lumber together with three traditional stress assessment techniques commonly employed in industries.

**Objectives:** We propose a new technique to directly assess the level of internal stress within the lumber without prior knowledge of the MOE of wood.

#### 2. Design of the Restoring Force Measuring Device

**New concept:** A restoring force required to restrain a half-split specimen to an initial configuration prior to sawing is measured. The sign and level of the measured force reflect type and magnitude of the internal stress within lumber.



<u>Fig.2</u> Design concept of the restoring force measurement for an assessment of stress within lumber.

Apparatus: The equipment consists of a stiff steel frame, clamping jigs and a load cell. One jig is fixed to the steel frame and another is connected to the load cell. While being clamped to the frame, the specimen is half-split at half the thickness for a required length. The net force generated as a result of internal stress relaxation is transferred to the load cell.

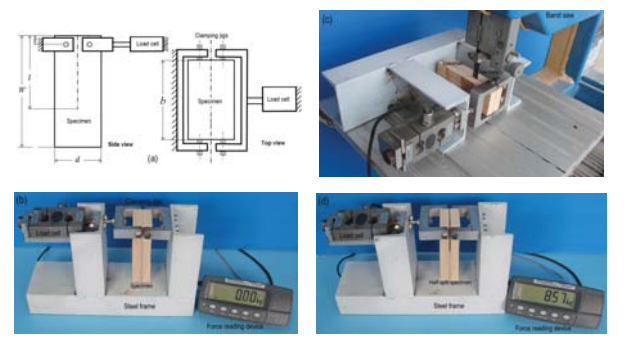


Fig.3 (a) Diagram of the restoring force measuring apparatus and photographs of the specimen installed in the device (b) before, (c) during and (d) after half-split sawing using a band saw.

Force profile: The restoring force abruptly increases and reaches the maximum value then gradually decreases with increasing half-split length.

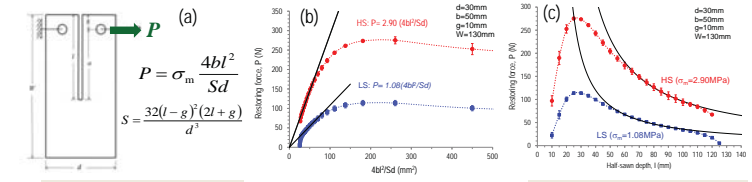


<u>Fig.4</u> Evolution of the detected force on the load cell during half-split sawing at 5 mm intervals. Some values of the derived restoring force are indicated in the graphs.

Acknowledgements: Thailand Research Fund and Walailak University (Grant No. RSA5880025).

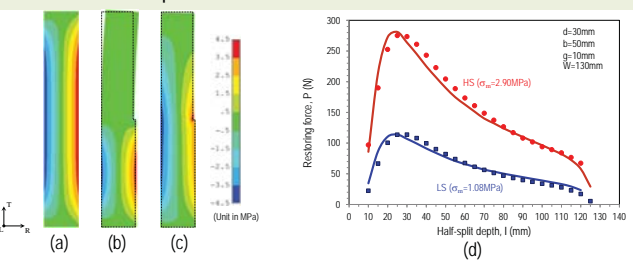
#### 3. Results and discussion

Analytical Model: Within a flexural response regime, an elastic cantilever beam theory has been developed to describe the restoring force behavior and to directly deduce the magnitude of the internal stress.



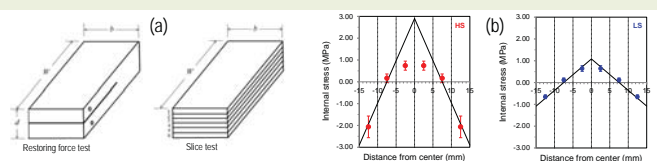
<u>Fig.5</u> (a) Beam model of the half-split specimen, (b) determination of the magnitude of the internal stress and (c) the fitted and experimental restoring force profiles.

**Numerical Model:** Outside the flexural response regime, 3D finite element analysis has been employed to simulate the measured restoring force and to determine the shape factor, S.



<u>Fig. 6</u> Contour plots of the predicted transverse internal stress of (a) the initial specimen and the half-split specimen (b) without restraining and (c) with the restoring force and (d) the simulated (lines) and measured (symbols) restoring force profiles.

**Validation:** The derived magnitudes of internal stress are in good agreement with the ones obtained from the conventional slice test.



<u>Fig.7</u> (a) Specimens for the restoring force and the slice tests and (b) distributions of the internal stresses obtained from the slice test (symbols) and the restoring force test (lines).

**Industrial applications:** The restoring force-internal stress chart has been proposed for a practical use in the lumber industry.

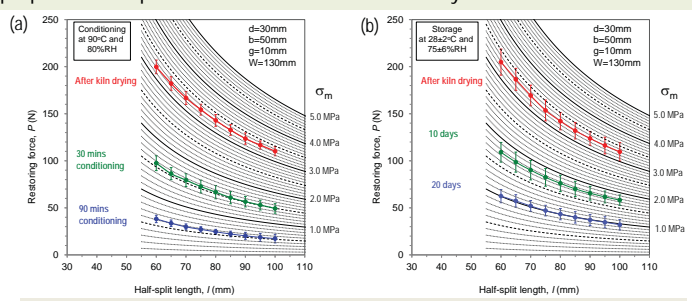


Fig.8 A demonstration has been carried out to follow stress relaxation (a) during conditioning and (b) during storage of industrial kiln-dried rubberwood lumber.

#### 4. Conclusions and future works

The restoring force measurement on a half-split specimen has good potential to replace the three conventional techniques for a reliable and meaningful assessment of drying stress within industrial kiln-dried lumber. Ongoing research focuses on determining the shape factor S for various sizes of commercial kiln-dried lumber.

#### References:

- Jantawee S, Leelatanon S, Diawanich P, Matan N (2016) A new assessment of internal stress within kiln-dried lumber using a restoring force technique on a half-split specimen. Wood Science and Technology 50:1277-1292.
- Jantawee S, Leelatanon S, Diawanich P, Vannarat S, Matan N (2016) Comparison of techniques for quantification of internal stress within industrial kiln-dried lumber. European Journal of Wood and Wood Products (submitted).